

Research and Technology

Annual Report of the
Marshall Space Flight Center

NASA TM-108501



National Aeronautics and
Space Administration

George C. Marshall Space Flight Center
Marshall Space Flight Center, Alabama 35812

November 9, 1998

Introduction

Robert Goddard once said, "It is difficult to say what is impossible, for the dream of yesterday is the hope of today and the reality of tomorrow." The Marshall Space Flight Center has a legacy of extraordinary scientific advancements that make the impossible a reality. With its unique blend of technical and visionary talents, Marshall continues to be a moving force behind many scientific breakthroughs.

As we posture ourselves to meet the challenges and changes that lie ahead, we are committed to sharing our knowledge and further expanding the scope of space-born technologies to enhance the quality of life on Earth. We are essentially creating the future—one in which space exploration and our country's prosperity are closely linked.

Our mission is clear: To create a better world for our children and our children's children. With limitless vision and a staunch refusal to become complacent we will accomplish this goal. Marshall's boundless contributions will propel us toward making our hopes a reality.



A.G. Stephenson
Director
Marshall Space Flight Center



Acknowledgments

The point of contact and coordinator at MSFC for this report is H.C. Stinson, Technology Transfer Office, (CO30/256-544-7239). Members of the editorial committee are William Taylor, director of the Science and Engineering Directorate; Axel Roth, director of Program Development; and Ronald Koczor, associate director for Science and Technology, Space Sciences Laboratory. Detailed editorial support and production assistance were provided by Scientific and Commercial Systems Corporation. The research and technology work at MSFC is a cooperative effort; however, due to space restrictions, it is impossible to list all those involved in the projects described in this report.

To assist the reader, the MSFC contact, office code, telephone number, and e-mail address are included at the beginning of each article. The sponsoring organization and university and industry involvement are given at the end of each article. An abbreviations and acronyms list, an alphabetical index of contacts, and an index of key words are presented at the end of this report.

Table of Contents

Creating the Future

Introduction to Report

viii

Technology Development Programs

Introduction

William Taylor 1

Space Propulsion and Fluid Management

Cryogenic Fluid Management for the Aerospace Industry
Technology Program

Leon J. Hastings 2

Injector Technology for Orbital Maneuvering System
Engine Upgrade

Huu P. Trinh 3

Magnetically Actuated Propellant Orientation

Jim Martin 4

Multipurpose Hydrogen Test-Bed Thermal Control Subsystem
Testing

Leon J. Hastings 6

Shooting Star Solar Thermal Propulsion System

Stephen Tucker 9

Spray-Bar Zero Gravity Cryogenic Vent System Test

Leon J. Hastings 11

Propulsive Small Expendable Deployer System

Judy Ballance 13

Structures and Dynamics

Development of Elliptic Orbit Rendezvous Analytical and
Operational Techniques

Carrie D. Olsen 15

Elastic-Plastic Proof Test Philosophy for Metallic Structures

Charles L. Denniston 17

Life Prediction of Composite Structures Based on Progressive
Damage Analysis

Dr. James B. Min 18

Combining Loads From Random and Sine Excitation Using
Monte Carlo Techniques

Dr. Andrew M. Brown 20

Multidisciplinary Thermal-Fluid Design Optimization Tool

Ten-See Wang 21

Unshrouded Impellar Technology Development

Roberto Garcia 23

Solar Thermal Upper Stage/Shooting Star Experiment

Scott A. Hill 25

Interdisciplinary Testing of Inflatable Structures for the
Shooting Star Experiment

R. Gregory Schunk 26

John O. Lassiter

Robert C. Engberg

Dr. Michael L. Tinker

Jeffrey R. Kegley

On-Orbit Controller Tuning for Robust Pointing Control	Dr. Mark Whorton	28
Microgravity Vibration Control and Civil Applications	Dr. Mark Whorton	29
Automated Rendezvous and Capture Technology Description	Richard Dabney	31
Infrared Fiber-Optic Thermographic Sensor for High-Temperature Applications	Don Bryan	32

Materials and Processes

Laser Induced Impulse on Debris Materials	Jason A. Vaughn	34
Development of Environmentally Compatible Solid Film Lubricants	Phillip Hall	35
Effect of Bearing Cleaning on Long-Term Bearing Life	Tim Jett	36
Comparison of Computed Tomography Data to Actual Physical Density Data for Composite Materials	Dr. Ron Beshears	37
Computed Tomography System Upgrade Provides Improved Imaging Capability	Dr. Ron Beshears	38
Friction Stir Welding Process Development	Jeff Ding	39
Automated Measurement of Weld Shrinkage Recovery	Kirby Lawless	41
High-Strength Aluminum Casting Alloy for Automotive Applications	Jonathan A. Lee	42
Weld Filler Wire Development for Aluminum Lithium 2195 Alloy	Carolyn Russell	43
Vacuum Plasma Spray Forming of Propulsion Components	Frank Zimmerman	44
Material Robustness Testing and Nondestructive Evaluation Methodology Assessment for Liquid Rocket Engine Composite Nozzles—Phase 1 Results	Dr. Raymond G. Clinton	45
Tooling Foam for Structural Composite Applications	Brett H. Smith	47
Space Environmental Effects on Transparent Polymer Lenses for Inflatable and Rigid Space Structures	David Edwards	49
Hot Pressing Yttrium, Copper, and Barium Oxides to Form Bulk-Shaped $\text{YBa}_2\text{Cu}_3\text{O}_{7-x}$ Ceramic Superconductors	Tony Robertson	50
Pressure Controlled Atomization Process for Permanent Magnet Fabrication	Tony Robertson	51

Avionics and Optics

Video Guidance Sensor—Flight Proven	Ricky Howard	54
Signal Conditioning Electronics for Discrete Capacitive Level Sensor Introduction	Randal S. McNichol Kenneth L. Swords Dennis A. Smith	56
Determining the Fractal Dimension of an Image Using Wavelet Analysis	Kenneth Herren	58
Composite Fresnel Lens for Solar Concentration and Alignment	Vinson B. Huegele	62
Rapid Prototyping of Diffractive Optics by Excimer Laser Micromachining	Dr. Helen J. Cole	63
Phase Correction in a Semiconductor Amplifier Array Using Fiber Optics	Kenneth Herren	65
Solar X-Ray Imager X-Ray Detector Calibration	J. Kevin Russell	67
Lightweight Nickel Alloy Mirrors for the Next Generation Space Telescope	John W. Redmon	68
Space-Borne Solar Vector Magnetograph Optical Design	Ron Eng	70
Solar X-Ray Imager Alignment and Focus	Dr. Martin E. Smithers J. Kevin Russell	72
Modeling Optical Pulse Propagation Using Parallel Processing	Andrew S. Keys	74
Electrical Impedance Spectrometer Development and Analysis	Brandon S. Dewberry	76
Diffractive Optics by Direct Write Electron Beam Lithography	Brent L. Beabout	77
Replicated X-Ray Optics Development	William D. Jones	80

Space and Microgravity Science Research Programs

Introduction

A Laboratory Study of the Interaction of Charged Particles With Electron Beams and Ultraviolet Radiation	Gregory S. Wilson	83
A New Ultra-High Resolution Near-Field Microscope for Observation of Protein Crystal Growth	Dr. James F. Spann	84
	William K. Witherow	85

BATSE Observations of Accreting Pulsars	Dr. Robert B. Wilson	87
Characteristics of Thermal Ions in the Topside Auroral Zone as Observed by TOPAZ3/STICS	Victoria Coffey	89
Coronal Heating	Dr. Ronald L. Moore	91
Solar Flares and Coronal Mass Ejections	Dr. Ronald L. Moore	93
Gradient Forming With Magnetic Fluids	Dr. Fred W. Leslie	95
Incorporation of Metal Nanoparticles Into Aerogels for Catalysis Applications	Dr. David D. Smith	97
Large-Scale Organization of Active Region Magnetic Fields	Dr. Mona J. Hagyard	99
Mechanics of Granular Materials Under Very Low Effective Stresses	Dr. Nicholas C. Costes	100
Modeling of Viscous Fluid Flow	Dr. Edwin C. Ethridge	103
The Solar Wind in the Inner Heliosphere	Dr. Steven T. Suess	105
Time-Resolved Fluorescence in Crystallizing Protein Solutions	Dr. David D. Smith	107
Superconductor Interactions with Gravity	Ron Koczor	109

Space System Concept Studies

Introduction

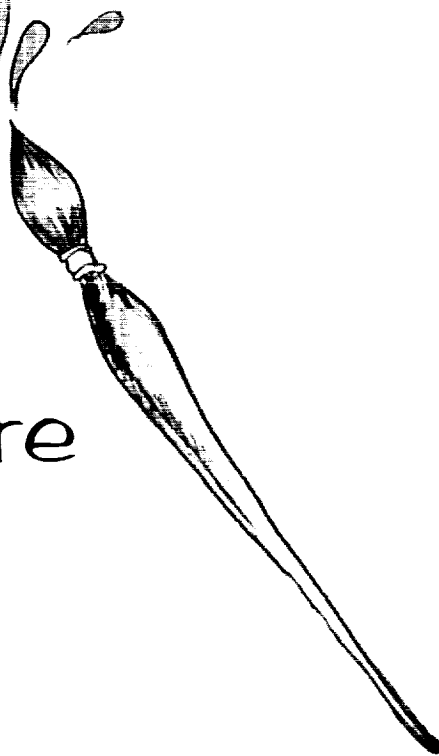
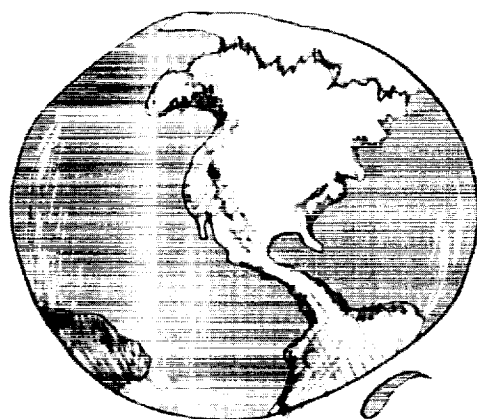
Beamed Energy Research Program for Propulsion and Planetary Defense	Axel Roth	113
Electrodynamic Tether Reboost of the <i>International Space Station</i>	Dr. Jonathan Campbell	114
Improving the Safety of Space Tethers	Les Johnson	115
Space Tether Transportation System	Charles Rupp	117
	Les Johnson	119

Technology Transfer

Introduction

Marshall Center a Partner in High-Tech Business Incubator	Sally Little	121
NASA Computer Imaging Technology Looks Into a Broad Range of Commercial Uses	Benita Hayes	122
NASA "Smart Bolts" Likely to Revolutionize Some Industries	Lisa Hediger	123
Space Code Solves Industries' Identity Crisis	Helen Stinson	124
Small Vibrations in Space Lead to Earthshaking Technology	Bob Lessels	125
	Dr. Mark Whorton	126

NASA Technology Conserves Power and Generates a Successful New Business	William H. Nabors	127
Hair Cleans Up Hairy Oil Spill Problem	Dr. Elizabeth Rodgers	128
NASA Sheds New Light on Cancer	Helen Stinson	129
NASA-Designed Knee Brace Turns Rehabilitation Into a Moving Experience	Steve Jones	130
NASA's Enlightening View on Veins	Dr. Elizabeth Rodgers	131
NASA Funnel Technology to Develop Tornado Warning System	Helen Stinson	132
NASA Technology Helps Zap Mosquitoes Before They Zap You	Steve Jones	133
NASA, USBI Technology Make A Triple Play	Vernotto McMillan	134
NASA Spinoff Helps Golfers Get More Spin on the Ball	Fred Schramm	134
NASA Deep-Space Communications Technology Now Used at NASCAR Race Tracks	Bob Lessels	135
Abbreviations and Acronyms		137
Index of Contacts		139
Index of Key Words		143



creating the future

Since the beginning of time, humans have pondered the future. An innate sense of curiosity creates a wonderment about things yet to come. There are those that revel in others' discoveries—findings that reveal the answers to questions contemplated for years and even centuries.

The Marshall Space Flight Center's reputation is built on a foundation of accomplishments through great strides in research and technology. Marshall houses some of the most talented forward-thinking minds in our country, and it is that talent—combined with a determination to find answers to the questions others only ask—that helps foster the bond between NASA and the American public.

Marshall's capabilities are spread over several areas of research and technology. We are the NASA Lead for Space Transportation Systems Development and Microgravity Research; a NASA Center of Excellence for Space Propulsion; and the Lead for Space Optics Fabrication, Metrology and Testing. MSFC's special areas of expertise allow an intensified focus of effort, thereby allowing us to yield products of unsurpassed quality and ingenuity.

Through the advancement of cutting-edge technology, Marshall maintains its position as the world's leader in Space Transportation Systems Development—one of our primary missions. In this role, Marshall is responsible for the necessary research, technology development, design and integration of space transportation and propulsion systems to take us into the 21st Century. For example, the development of revolutionary reusable launch vehicles, such as the X-33 and X-34, will lead to an economical, safe, and robust launch system to meet the growing needs of placing a diverse range of payloads into orbit. This reusable launch vehicle technology falls under the proud tutelage of the Marshall Center and will significantly reduce the cost of sending people and cargo into space.

With the same determination and vision that put us into space for the very first time, Marshall is facilitating the use of space for the development of commercial products and services. With access to microgravity, the research community is free to study biotechnology, combustion, fluids, fundamental physics, and materials processes and phenomena. An example of research in microgravity is that of protein crystal growth. By growing purer crystals of disease proteins in space, scientists are better able to discern the formation of the crystals, thereby making possible the design of more effective drugs to fight illness and disease here on Earth. The knowledge provided by space-based research also allows researchers to develop stronger metals and alloys, produce materials that conduct electricity better, increase fuel efficiency, improve pollution control, and validate basic theories, to name a few.

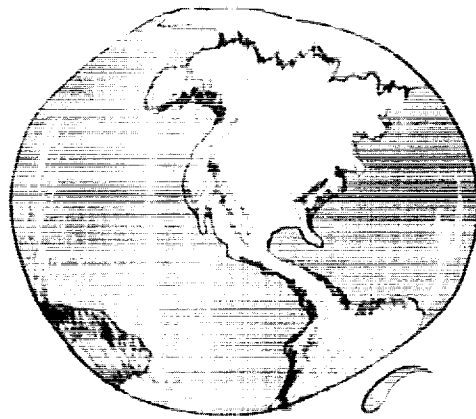
As a NASA Center of Excellence for Space Propulsion, Marshall provides innovative and cost-comparative systems for future access to space. Among our highest priorities are reusable advanced space transportation technology with substantial work in performing technology demonstrations of advanced thermal protection systems, structures, and avionics systems. We are also responsible for developing technologies for high-efficiency, low-cost upper stages, including solar thermal stages, and we reside at the forefront of launch concept definition and architecture studies such as single-stage-to-orbit, two-stage-to-orbit, vertical takeoff, and horizontal landing and takeoff options using air-augmented and rocket-only propulsion. These technological advancements, along with responsibilities that include the Space Shuttle main engines, solid rocket boosters, and the external tank, help us shorten the span between where we are and what lies ahead in the vast mystery of our universe.

As a lead for developing space optics manufacturing technologies, our objective is to provide key enabling contributions to the

Agency's future programs. In performing this role, we will make maximum use of existing resources throughout NASA, other government agencies, industry and academia. We will establish government, industrial and academic consortia which will provide the means for developing and maintaining facilities and equipment critical to the development of the technologies required for NASA's missions in the 21st century. Providing access to these facilities and equipment will serve to augment scarce resources for technology development throughout government, industry and academia, thereby ensuring that our country maintains its pre-eminence in the world scientific community.

Many future missions will require highly sophisticated optical systems. This is especially true in the area of astrophysics, but also holds true for planetary detection, cosmic-ray detection, solar physics, and Earth science remote sensing. Consequently, it is anticipated that early in the next decade, the Agency will be prepared to initiate the development of missions that will require large, lightweight telescopes observing at all wavelengths from gamma ray through infrared. If the scientific requirements are to be met for these missions, it is essential that the United States have the skills and facilities required to produce these telescopes. Therefore, one of the primary objectives of the Marshall optics program is to identify and develop technologies and capabilities required for future missions and to develop and implement plans to overcome any deficiencies.

At the Marshall Center, the future is bright with promise, and we know that it will be what we make it. So we look ahead, using the legacy of our rich and successful past as a guide, plotting a course that will take us to the next Millennium and beyond.



technology development programs

"Those who came before us made certain that this country rode the first waves of the industrial revolution, the first waves of modern invention and the first wave of nuclear power. And this generation does not intend to flounder in the backwash of the coming age of space. We mean to be a part of it—we mean to lead it."

John F. Kennedy

Improvements in technology are some of the most effective engines to drive our country and all of humanity forward. Marshall's history in the technological arena is a legacy of successes for our planet. From our role in the first steps on the Moon, to our Space Shuttle contributions, and science we have conducted on extended visits to the Russian space station *Mir*, we have accomplished scientific leaps and bounds. We need only gaze into our past for confirmation of this, and to understand that there will be other technological gains with the *International Space Station*. Whether it is improved medicines, materials or avionics for Earth-bound transportation, the benefits gleaned from the Space Station and other successfully met challenges over the decades to follow will impact us all.

Marshall is dedicated to help lead the development of those technologies and to assure that the lives of millions are considered when these areas of science are embraced. We invite you to read on so that you will discover more about our work—work in which we attempt to bridge the gap between the successes of our past and the challenges of our future.

William Taylor
Director
Science and Engineering

Space Propulsion and Fluid Management

Cryogenic Fluid Management for the Aerospace Industry Technology Program

Leon J. Hastings/EP63
256-544-5434
E-mail: leon.hastings@msfc.nasa.gov

The solar thermal propulsion concept requires that a number of technologies be matured prior to undertaking full scale development including the subcritical liquid hydrogen (LH_2) storage/feed system. MSFC is participating with an Aerospace Industry Technology Program (AITP) consortium in the design and performance testing of a 2 m^3 LH_2 storage/feed system for the Solar Thermal Upper Stage Demonstrator (STUSTD) program (fig. 1). Elements included are zero gravity venting, capillary screen liquid acquisition device (LAD), pressurization and expulsion, and multilayer insulation (MLI). Basically, the propellant management subsystem concept consists of utilizing the LAD and thermodynamic vent system (TVS) to flow 100 percent vapor to the thruster during burn cycles, i.e., the insulation is configured to match the LH_2 boil-off with the thruster flow rate and mission burn cycle (typically 100 to 200 burns).

The MLI consists of 100 layers of double-aluminized Kapton™ with B4A Dacron™ net spacers to achieve a predicted total heat leak of 20.5 Btu/hr. The TVS includes an active mixer to assure a homogenous distribution of the thermal energy

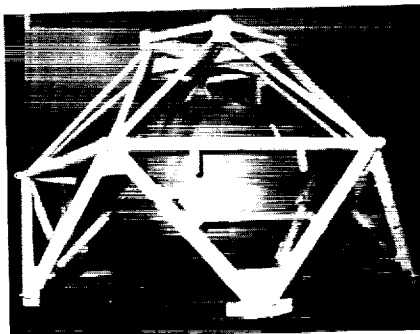


FIGURE 1.—AITP cryogenic fluid management subsystem tank.

within the propellant, and a Joule-Thompson (J-T) expansion valve. The cold fluid from the J-T valve flows through tubing brazed into the apex of the LAD, thereby assuring subcooling of both the LAD liquid and bulk liquid. The LAD consists of four channels spaced at 90 degrees around the tank, with each leg about 1.6 m in length. The LAD/TVS subsystem is designed to feed 0.9 kg/hr (2 lb/hr) to the thruster at 172 kPa (25 psia). Testing will first be conducted to establish the baseline thermal performance (heat leak/ LH_2 boil-off) for the MLI system. The LH_2 feed system will then be operated to simulate a 30-day mission with 140 burns (vent cycles).

The original test article assembly was lost during a checkout test accident in the Fall of 1996. A replacement tank has been fabricated and assembly of internal components at Lewis Research Center was completed in September 1998. Testing will be conducted in the 66-m (20-ft) vacuum chamber at Test Position 301.

Sponsor: Office of Space Access & Technology

Industry Involvement: Boeing Aerospace (Huntington Beach, Huntsville)

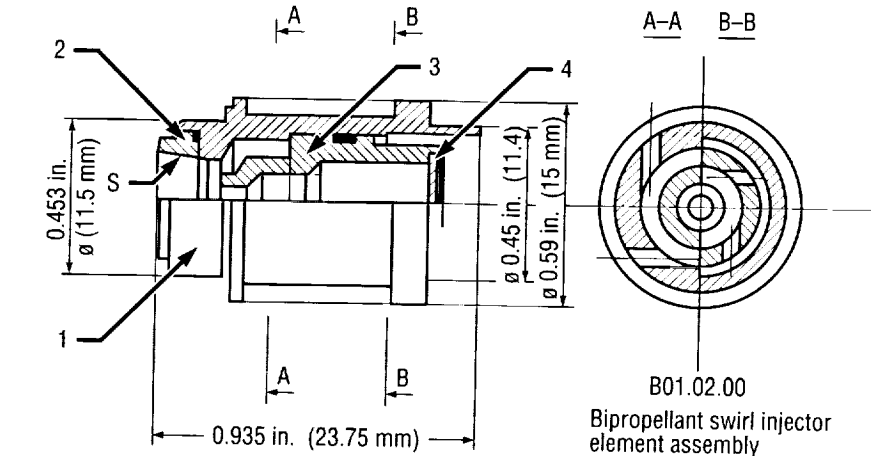
Biographical Sketch: Leon Hastings is currently assigned to the MSFC Propulsion Laboratory. Assignments at MSFC since 1961 have centered on heat transfer, fluid mechanics, and thermodynamics. Hastings has over 15 years of specialized experience in low gravity fluid management and heat transfer. He has often served on Agency level committees to assist in formulating plans/policies for low gravity propellant management research and technology. Hastings has a B.S. in mechanical engineering and an M.S. in engineering science. ▀

Injector Technology for Orbital Maneuvering System Engine Upgrade

Huu P. Trinh/EP62
256-544-2260
E-mail: huu.trinh@mfsc.nasa.gov

MSFC, in conjunction with the Propulsion Research Center of the Pennsylvania State University (Penn State), has been investigating various propellant injection techniques for converting the current propellant injection system for the Orbital Maneuvering System (OMS) engines from a hypergolic to a liquid hydrocarbon (LHC) system. The proposed LHC is ethanol. The results will provide an objective basis for selecting the best injector configuration for the upgraded OMS engines. Three candidate injection schemes—bicentrifugal coaxial swirl, pintle, and jet impinging—have been experimentally evaluated in a unielement optically-accessible combustor. Injector performance characteristics, including combustion efficiency (C^*), stability, and thermal compatibility, will be assessed.

The bicentrifugal coaxial swirler, as shown in figure 2, is an injector of Russian origin. Extensive Russian experience has indicated that the injector provides high combustion efficiency and remarkable reliability. Features of this injector type are high thrust-per-element and stable operation at low injection pressure drops, which result in major weight savings



- Notes: 1. Press part 2 into part 1 with brazing alloy, roll, finish surface S.
2. Place part 4 into part 3, roll, attach brazing alloy.
3. Press part 3 into part 1 with brazing alloy.
4. Braze in neutral media or in vacuum.
5. Check hermeticity of brazed connections.

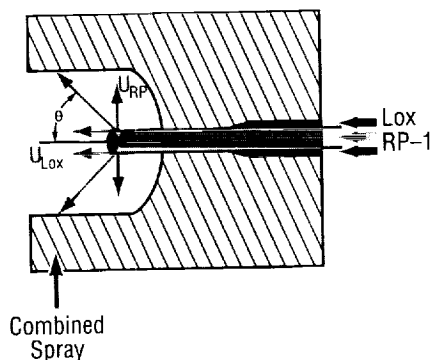
FIGURE 2.—Drawing of a bicentrifugal coaxial swirl injection element.

for pressure-fed applications. In addition, the injector is suited for a liquid/liquid propellant combination, which will be used for the upgraded OMS engines. An initial test series at Penn State has shown that the injector can be operated at a wide range of engine operating conditions where the C^* value ranged from 81 percent to 98 percent.

Pintle injectors provide a large stability margin and a high combustion efficiency when they are well tuned. A scaled pintle configuration for the upgraded OMS engine has been designed. Its schematic and design parameters are shown in figure 3. The LHC fuel is injected vertically from rectangular slots around the tip of the

center pintle, whereas the lox oxidizer exits through the annulus surrounding the pintle. Previous experience has indicated that with the fuel-centered configuration, there are no problems associated with fuel freezing in the center post. The injector configuration, including post diameters, slot sizes, etc., are based on the optimization process of all the design parameters listed in figure 3, and heat transfer and stability considerations. Fabrication of the injector is currently underway at Penn State.

The impinging jet injector to be used for this study is an Aerojet designed splash plate injector, which is a modification of a typical unlike doublet impinger. Aerojet is using its



$$\theta = f(\text{TMR}, \text{BF})$$

$$\text{TMR} = \frac{(\dot{m} \cdot U)_{\text{RP}}}{(\dot{m} \cdot U)_{\text{Lox}}}$$

$$\text{Blockage Factor (BF)} = \frac{\Sigma \text{ Width of Slots}}{\text{Perimeter of Tube}}$$

$$\text{Effective Momentum Ratio (EMR)} = \frac{\text{TMR}}{\text{BF}}$$

FIGURE 3.—Schematic and design parameters of a pintle injector.

in-house research and development funding to design and manufacture the injector. The injector is being fabricated using Aerojet's etched platelet technology, which lends itself to the creation of complex geometries. The splash-plate injector creates unlike fans of partially atomized propellants that impinge on each other for further breakup and mixing. Aerojet will provide Penn State with a full-scale multielement injector suitable for subscale engine tests. The results of this study will be compared with the other injectors in the near future.

Sponsor: Advanced Space Transportation Program Office (ASTP)

University Involvement: Robert J. Santoro, The Propulsion Engineering Research Center of The Pennsylvania State University (PSU)

Biographical Sketch: Huu P. Trinh has worked in the area of liquid rocket engine combustion at MSFC since 1987. He has used computational and analytical models to analyze rocket engine performance. Currently, he monitors a technology project for main chamber and preburner injectors. The effort is conducted under a PSU NRA cooperative agreement to support the Reusable Launch Vehicle program. In addition, he evaluates injector performance of the Fastrac engine and analyzes proposed Bantam main and gas generator injectors. ▀

Magnetically Actuated Propellant Orientation

Jim Martin/EP63
256-544-6054
E-mail: jim.martin@msfc.nasa.gov

In a low-G environment the acquisition and transfer of vapor-free propellant is not as straightforward as similar operations on the ground. The indeterminate location of the bulk liquid within the propellant tank complicates the design of engine feed and transfer systems which rely on proper liquid orientation and an understanding of fluid motion in response to disturbances and imposed accelerations. The methods utilized to solve these problems in the past include the use of screen channel and vane propellant management devices (PMD's) and thruster settling burns. These techniques, however, do have drawbacks. PMD's are typically large, and their reliability with cryogenics is questionable. Moreover, settling burns complicate flight operations and require additional hardware and propellant.

Another approach to these operations is to employ strong magnetic fields which exploit the inherent paramagnetism of liquid oxygen (attractive behavior) and diamagnetism of liquid hydrogen (repulsive behavior). With the advent of lightweight high-temperature superconductors and high-flux density rare-Earth magnets, the use of magnetic fields to control fluid motion in microgravity appears feasible. These magnetic systems, if practical, could replace or augment traditional systems, possibly mitigating many of the issues and problems mentioned previously.

Currently, an evaluation of the feasibility and practicality of magnetically actuated propellant orientation (MAPO) is being studied. A series of low-gravity tests will be performed to examine the attractive forces between a fluid and magnetic field (such as that observed in liquid oxygen). The primary objective is to obtain the experimental data required to validate computational fluid dynamic (CFD) models which will ultimately be used to predict fluid motion in real applications. The test data consists of video footage of the fluid motion supported with corresponding acceleration measurements mounted on the test package.

The low-gravity MAPO experiments were conducted using NASA's reduced gravity workshop (a KC-135 aircraft). The experiments employ a subscale hardware setup which is shown free floating in figure 4.

A noncryogenic ferromagnetic fluid was used to simulate the behavior of liquid oxygen. The ferromagnetic fluid is a water-based commercially available product that contains a suspension of extremely fine ferrous particles. The magnetic solution was diluted and tested at several mixture strengths so that sufficient fluid motion could be generated during the short low-gravity test interval. The test magnet was a rare-Earth type in the shape of a ring with a surface strength of approximately 6,000 gauss.

One objective of the project is the modification of an existing commercially available CFD code to include the body and surface forces arising from the interactions between the fluid and magnetic field. This will provide a more rigorous means of assessing

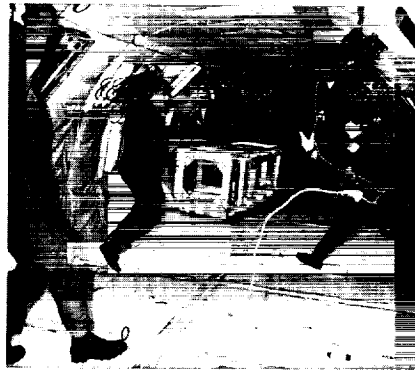


FIGURE 4.—Low-gravity MAPO tests aboard the KC-135.

fluid behavior, and will enable the modeling of more complicated and large geometries. Videotaped recordings of fluid motion and test article accelerations from the low-gravity tests will be used to validate the revised CFD model.

Figures 5 and 6 show experimental data for a baseline water test (no magnetic forces) and a ferromagnetic solution diluted at a 10:1 ratio, respectively. Figure 5 shows the horizontal liquid surface of the nonmagnetic baseline water test transition (after some sloshing) to an ullage bubble surrounded by water as gravity is reduced from 1 gravity to low gravity. This demonstrates dramatically the lowest energy surface shape in an environment dominated by surface tension. Figure 6 illustrates the response of the ferromagnetic mixture (dark and nearly opaque) subject to the same gravity level transition. The ferromagnetic fluid is strongly attracted to the magnet side of the tank where it remains (with some light sloshes due to bumps) for the entire test interval, thus demonstrating that

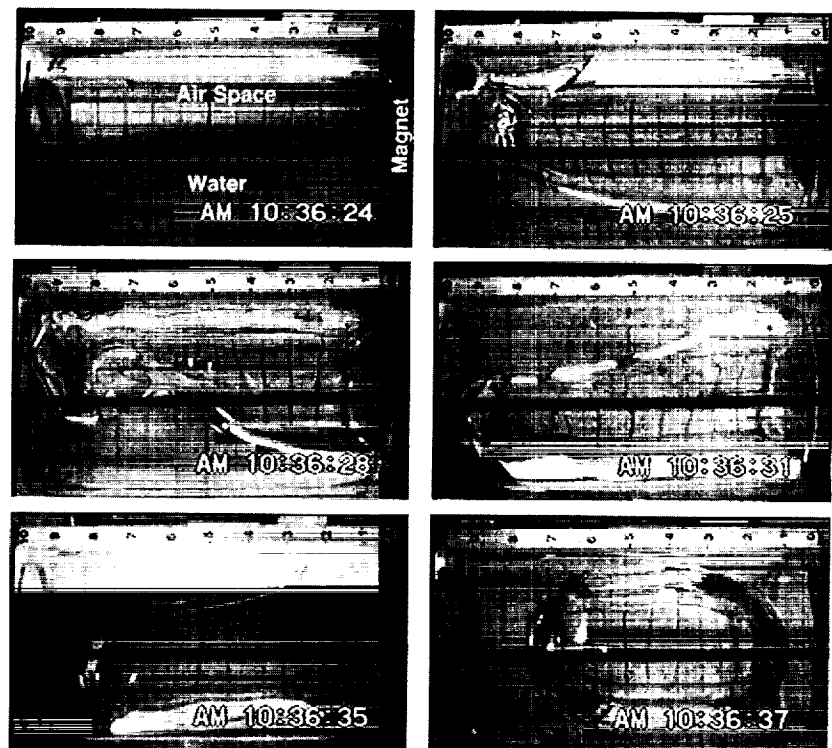


FIGURE 5.—Low-gravity baseline water test.

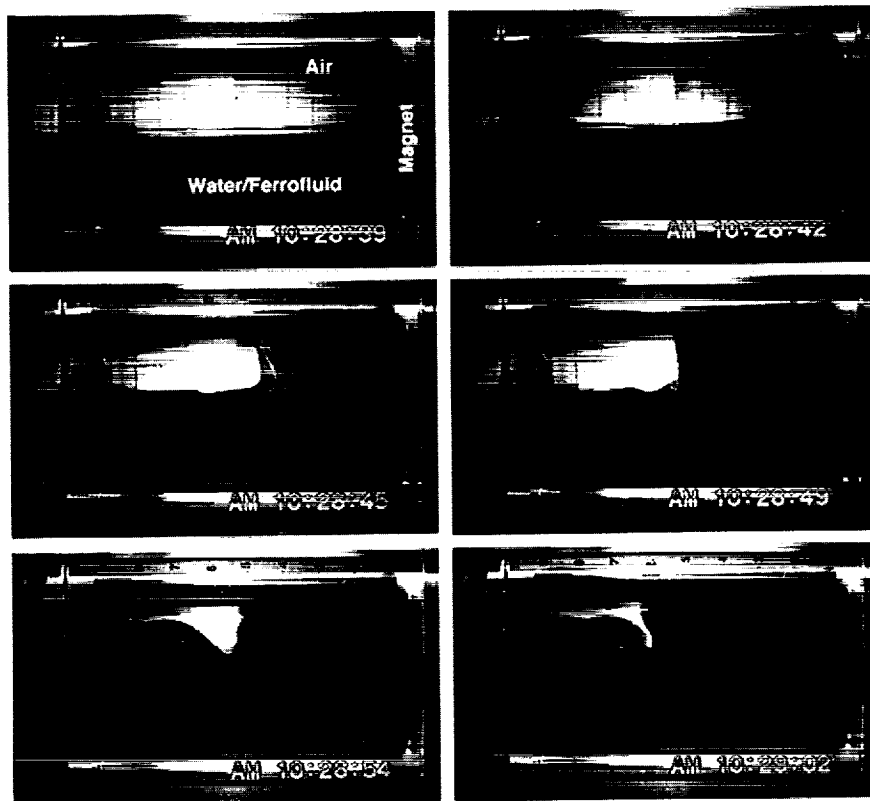


FIGURE 6.—Low-gravity ferromagnetic mixture (10:1 dilution).

the magnetic forces were able to overcome those of the fluid surface tension.

Sponsor: Center Director's Discretionary Fund

Biographical Sketch: James J. Martin is an aerospace engineer in the Space Propulsion Branch of MSFC's Propulsion Laboratory. He received a B.S. and M.S. in aerospace engineering from the University of Missouri at Rolla in 1989. Since 1989, he has been employed by NASA and has accumulated 9 years of experience in the development and testing of cryogenic fluid management system. ▀

Multipurpose Hydrogen Test-Bed Thermal Control Subsystem Testing

Leon J. Hastings/EP63
256-544-5434
E-mail: leon.hastings@msfc.nasa.gov

A system level test-bed termed the multipurpose hydrogen test-bed (MHTB), which is representative (in size and shape) of a fully integrated space transportation vehicle liquid hydrogen propellant tank, has been utilized to evaluate an upper stage cryogenic insulation concept (fig. 7). The MHTB tank is American Society of Mechanical Engineers (ASME) coded, is 3.05 m in diameter by 3.05-m long, has an 18-m³ capacity, and is made from 5083 aluminum. The tank was designed to accommodate updated CFM concepts or alternate versions when they become available. Upper stage studies have often baselined the foam/multilayer insulation (FMLI) combination concept; however, hardware experience with the concept is minimal and it was therefore selected for testing with the MHTB.

The foam element is designed to protect against ground hold/ascent flight environments, and to enable a dry nitrogen purge as opposed to the more complex/heavy helium purge subsystem normally required with MLI in cryogenic applications. The MLI provides protection in the vacuum environment of space and is designed for an on-orbit storage period of 45 days. The foam component consists of an Isofoam SS-1171 layer

bonded to the tank wall. Although only about 1.76 cm of foam were required, the average thickness of 3.53 cm was the minimum that could be robotically applied. The MLI consists of a double aluminized Mylar™ MLI blanket with an average layer density of approximately 25 layers/in., which is composed of 45 radiation shields with coarse Dacron™ net spacer material. Unique features of the MLI concept include a variable density MLI (reduces weight and radiation losses) and fewer but

larger perforations for venting during ascent to orbit. A standard insulation blanket with the same performance would weigh 143 lb, whereas the new MLI with one-quarter-mil Mylar™ would weigh 54 lb, i.e., a weight savings of 89 lb can be achieved. The tank barrel section MLI was installed utilizing a commercially established roll-wrap process. It is estimated that the roll-wrap approach will save about 2,400 man-hours, compared with the standard blanket installation process, on a 10-ft-dia. LO₂/LH₂ tank set. The

process reduces heat leak due to the lack of seams and is less susceptible to structural damage during ascent flight.

Three ground hold tests were performed resulting in average insulation heat leak rates ranging from 2111 to 2225 W (60.7 to 64.0 W/m²). Penetrations contributed a very small fraction of the total heat leak. The environmental shroud GN₂ purge was maintained at a flow rate of approximately 5 kg/min at nearly constant temperature during each test (ranging from 270 to 279 °K). The average heat leak was numerically predicted to be 2172 W (62.5 W/m²) which corresponds favorably with that measured. The spray-on foam insulation (SOFI) successfully prevented purge gas liquefaction except for a small localized area near an odd-shaped penetration peculiar to the MHTB on the lower dome. The foam insulation weight of 45 kg can be reduced to 18 kg in an actual application.

Key items of interest observed during the ascent simulation included both thermal control subsystem (TCS) structural integrity under broadside venting loads, and the time required to achieve TCS thermal equilibrium. During the rapid evacuation (transition from 760 to 35 torr in approximately 120 sec) the roll-wrapped MLI was observed to expand only slightly which is attributed to its seamless robust construction. The heating rate decayed much faster during the second test and reached the 10 W range approximately 1,000 min sooner than in the first test—supporting the idea that increased vacuum exposure is beneficial. Another observation is the temporary heat leak drop due to MLI layer cooling below steady-state values during evacuation. Specifically

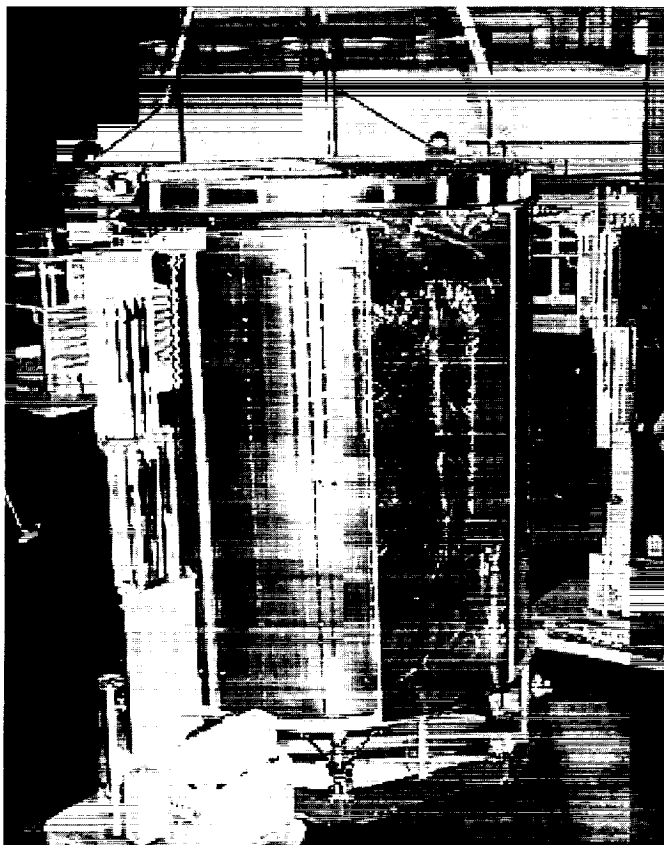


FIGURE 7.—Assembled multipurpose hydrogen test-bed.

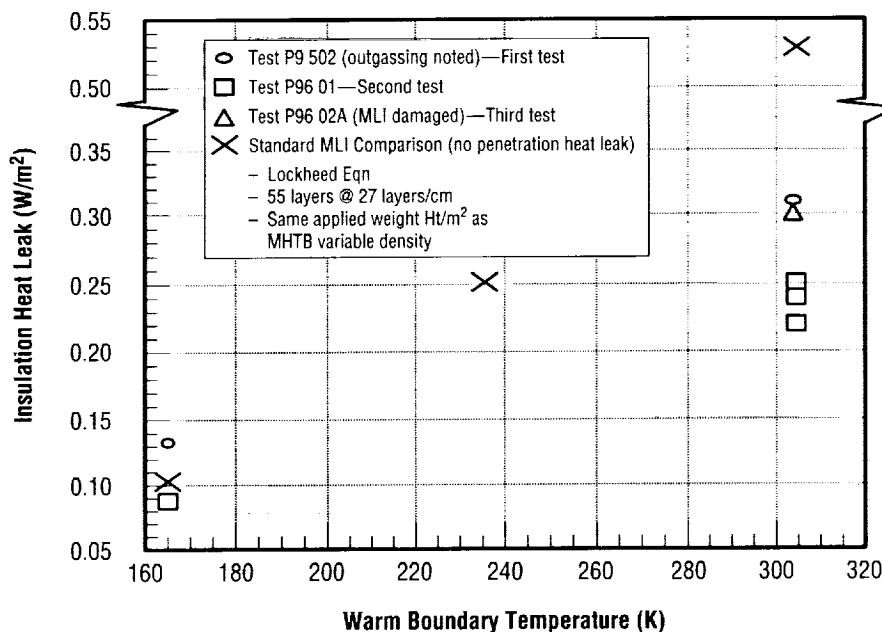


FIGURE 8.—MHTB TCS orbit hold performance.

the rate dropped to approximately 30 percent below the steady-state value at 3,000 min. The heat leak was near steady state in 4,000 to 5,000 min, but about 8,000 min was required to attain complete equilibrium.

The insulation heat leak during the orbit hold tests ranged from 10.93 to 2.98 W (0.31 to 0.085 W/m²) for warm boundaries ranging from 305 to 164 °K. These performance values are illustrated in figure 8 along with the calculated performance of a standard constant density MLI blanket. The variable density MLI outperformed the standard MLI by approximately 50 percent at the highest boundary temperature, and both systems performed equally at the lowest boundary temperature. The second test heat leak was lower than the first test due to decreased outgassing. The third test produced boil-off rates nearly as high as the first test

due to significant MLI damage which occurred at the conclusion of the second test. The two video cameras located within the environmental shroud failed to reveal the damage; however, the incident accidentally demonstrated TCS robustness. In comparison with the best previously measured performance of traditional MLI, a 50 percent heat leak reduction was achieved as shown in figure 8. Boil-off losses of .117 and .16 percent per day were measured with and without heat guards respectively with the warm boundary condition (305 °K). For all tests the vacuum chamber pressure was maintained below the 10^{-6} torr range. The interstitial gas pressure probe results were questionable but typically indicated a pressure level in the mid 10^{-6} torr range or less.

Sponsor: Office of Space Access & Technology

Biographical Sketch: Leon Hastings is currently assigned to the MSFC Propulsion Laboratory. His assignments at MSFC since 1961 have centered on heat transfer, fluid mechanics, and thermodynamics. Hastings has over 15 years of specialized experience in low-gravity fluid management and heat transfer. He has often served on Agency level committees to assist in formulating plans/policies for low-gravity propellant management research and technology. Hastings has a B.S. in mechanical engineering and an M.S. in engineering science. ▀

Shooting Star Solar Thermal Propulsion System

Stephen Tucker/EP63
256-544-0500
E-mail: steve.tucker@msfc.nasa.gov

The desire to reduce launch costs and increase efficiency in future space transportation systems has resulted in increased interest in solar thermal propulsion (STP). The solar thermal engine serves as a high-temperature heat exchanger, collecting concentrated solar radiation into a "black body" cavity and transferring this energy to a propellant causing a significant temperature increase. Propellant gases can be heated to temperatures approaching 4,500 R and expanded in a rocket nozzle, creating low thrust (1–20 lb) with a high specific impulse (I_{sp}) (700 to 900 sec) as shown in figure 9. There are two basic types of solar thermal propulsion, "direct gain" and "thermal storage," both of which have thermodynamic and operational advantages and disadvantages. The direct gain approach simultaneously collects energy, transfers it to a propellant gas, and produces thrusts. A direct gain solar thermal engine for system level ground tests is under evaluation by the Marshall Center through an Aerospace Industry Technology Program (AITP). The thermal storage concept sequentially collects energy, stores it in a thermal storage heat exchanger and then provides thrusts in a pulse mode. A mission level systems trade study is required to establish the preferred concept for a specific application.

The Shooting Star Experiment will demonstrate the feasibility of a solar

thermal upper stage utilizing a thermal storage engine concept. Figure 10 shows the shooting star flight experiment deployed configuration.

The experiment payload is integrated with a Spartan spacecraft for deployment from the Space Shuttle and consists of a Spartan spacecraft, structural module assembly (SMA), an inflation deployed fresnel lens, torus and strut support structure, a sun acquisition and fine pointing system, and a solar thermal storage engine. Because of cost and safety issues, the experiment will use gaseous nitrogen as the propellant. Major engine module components include the engine, engine support structure, thermal control system, and propellant feed and instrumentation lines. A secondary solar concentrator is being considered to increase thermal power to the engine and reduce control requirements. The shooting star engine performance goals and operating parameters are listed below.

Propellant	Nitrogen Gas
Thrust	1.0 lb
I_{sp}	200 sec
Temperature	Variable to 3,000 °F
Thermal Power	1.5 kW
Mass Flow Rate	20 to 60 lb/hr
Thrust Duration	30 sec
Charge Time	30 min

The propellant supply system consists of a nitrogen gas bottle, fill and vent lines and valves, isolation valve, two-stage pressure regulator, and a calibrated orifice for flow rate determination. The feed system is designed to supply GN_2 to the engine

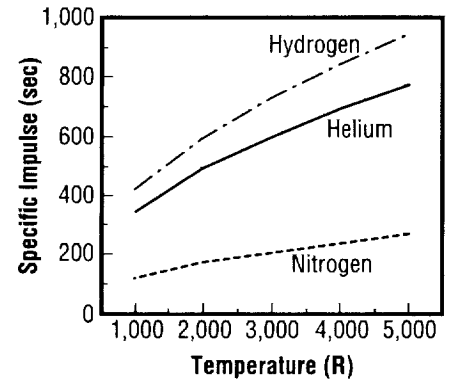


FIGURE 9.—Engine specific impulse versus propellant temperature.

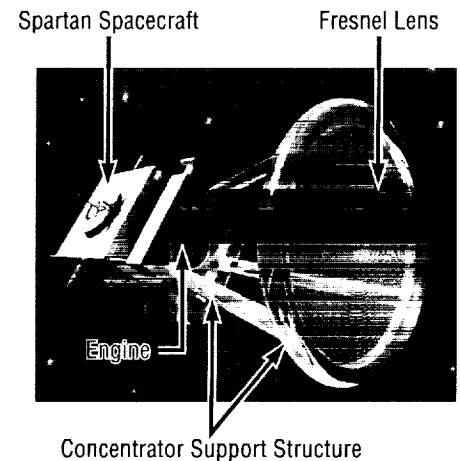


FIGURE 10.—Shooting star flight experiment—deployed.

at a constant inlet pressure of 60 psi, producing a near constant thrust of 1.0 lb. The propellant flow rate decreases with increasing engine temperature from ~ 60 lb/hr to 20 lb/hr, which increases engine I_{sp} . Figure 9 shows engine I_{sp} as a function of temperature for three propellant gases.

The engine consists of an inner shell absorber cavity, thermal storage heat exchanger, outer shell, and nozzle and is fabricated by chemical vapor

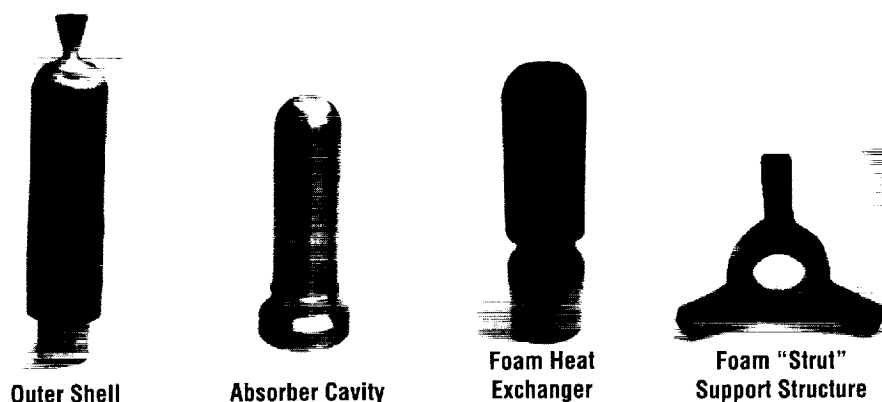


FIGURE 11.—Shooting star engine components.

deposition (CVD) rhenium (Re) onto graphite mandrills to form the desired component configuration.

The absorber cavity is a 1.7-in. dia., 6-in.-long closed cylinder which collects concentrated sunlight and conducts it as heat to the thermal energy storage medium that surrounds the cavity.

The thermal storage heat exchanger material is fabricated from reticulated carbon foam and coated with Re. This material configuration provides thermal energy storage mass and high material surface area for heat transfer. A foam porosity of 45 pores/in. (ppi) is expected to produce uniform flow through the heat exchanger with pressure drops <5 psi. The engine outer shell provides the closure for the propellant flow path, structural support attachments, nozzle, feedline, and instrumentation interfaces. These components are shown in figure 11.

When the engine is heated, the support structure becomes a heat transfer path, reducing engine temperature and imposing unacceptable heat loads on

the spacecraft structure and subsystems. Two engine support structures will be tested and are shown in figure 12.

The "strut" support concept consists of a Re foam hub/strut welded to the engine outer shell and pinned to the SMA. The other is a Re foam disk configuration and is also welded to the outer shell and attached to the SMA with eight rocker arms. The thermal control system employs a combination of materials and design features, including carbon felt and rigidized carbon foam to minimize heat loss.

Engine performance will be determined by temperature, flow rate, and a thrust measurement system using strain gages. Because extreme engine temperatures preclude direct propellant measurements, engine temperature profiles will be calibrated with development engine ground tests and correlated with analytical thermal and fluid models.

The mission profile consists of a number of engine thrust cycles, each at incrementally higher temperatures. Propellant flow is initiated and terminated by a preprogrammed clock and will be calibrated with ground tests.

The shooting star solar thermal propulsion system represents significant scientific and engineering challenges. A successful demonstration of the concept represents a milestone in the development of a new, highly efficient upper stage for small payloads. It will advance the state of the art in high-temperature materials and processes, engine design and operation, as well as high-temperature thermal and optical physics.

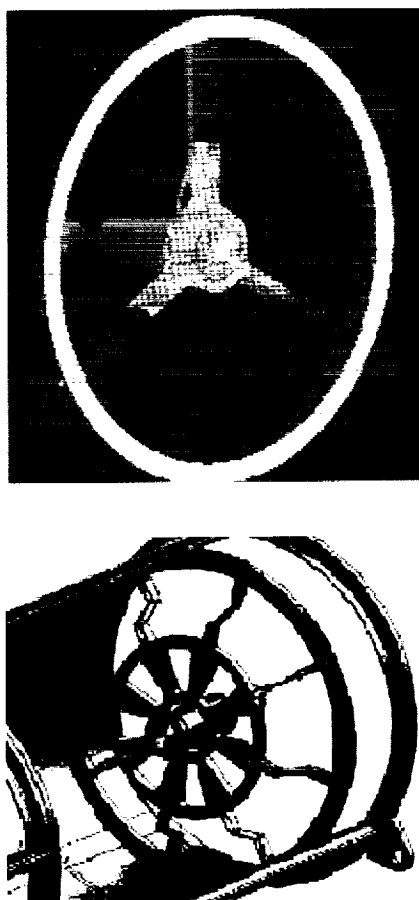


FIGURE 12.—Engine support structures.

Sponsor: The Advanced Space Transportation Program Office

Industry Involvement: Ultramet, of Pacoima, CA, is fabricating the engines and engine support structures.

Biographical Sketch: Stephen Tucker is an aerospace engineer in the Space Propulsion Branch of the Propulsion Research and Technology Division within the MSFC Propulsion Laboratory. He is currently leading a team of engineers responsible for the design, fabrication, and testing of the shooting star solar thermal engine. Tucker has worked at MSFC since 1986 and has a B.S. degree in physics and mathematics from Tennessee Tech University and a B.S. in mechanical engineering from the University of Alabama in Huntsville. ▀

Spray-Bar Zero Gravity Cryogenic Vent System Test

Leon J. Hastings/EP63
256-544-5434
E-mail: leon.hastings@msfc.nasa.gov

A system level test-bed termed the multipurpose hydrogen test-bed (MHTB), which is representative (in size and shape) of a fully integrated space transportation vehicle liquid hydrogen propellant tank, has been utilized to evaluate an upper stage pressure control concept. Thrusters have traditionally been used to settle the liquid prior to orbital tank venting with penalties in performance and operational complexity (Centaur and Saturn/S-IVB). The thermodynamic vent system (TVS) concept enables venting without resettling, but its utilization has traditionally been constrained by a lack of on-orbit

experience. The spray-bar TVS concept selected for testing in the MHTB is more amenable to normal gravity experimentation than other, more traditional, concepts. The MHTB tank is an American Society of Mechanical Engineers coded vessel, 3.05 m in diameter by 3.05 m long, and has an 18-m³ capacity.

The TVS concept evaluated (fig. 13) differs from those previously tested in that the active components (Joule-Thompson (J-T) expansion valve, subsystem pump, and isolation valve) are located external to the tank, as opposed to inside the tank, in a stainless steel cylindrical enclosure which is attached to the bottom of the MHTB tank. Such an approach enables modification or changeout of TVS components without entering the tank. More importantly, in the mixing mode, fluid is withdrawn from the tank by the pump and flows back into the tank through a spray bar positioned along (or near) the tank

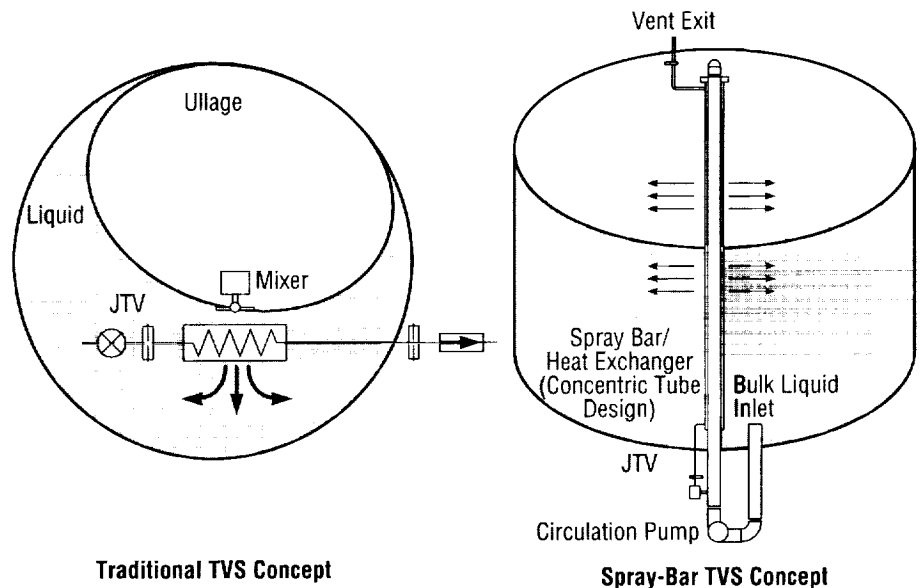


Figure 13.—Zero gravity pressure control spray-bar concept tested in MHTB.

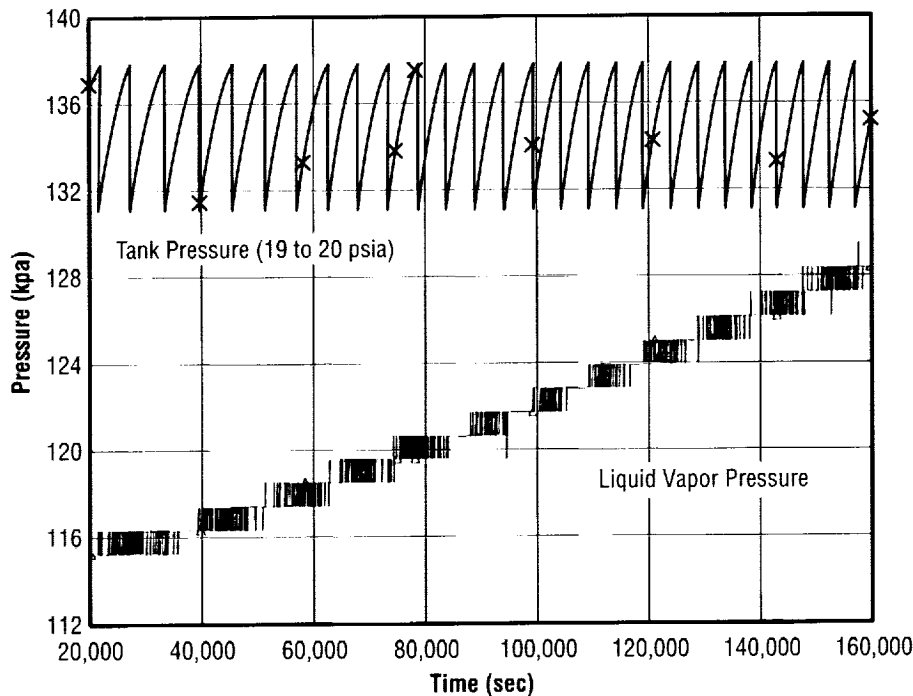


Figure 14.—Spray-bar thermodynamic vent system pressure control performance.

longitudinal axis. The fluid expelled radially into the tank through the spray bar forces circulation and mixing of the tank contents regardless of liquid and ullage position, assuring destratification and minimum pressure rise rate. The spray-bar feature is the key to assuring mixing independent of gravity and liquid/ullage position. When pressure relief eventually becomes necessary, a portion of the circulated liquid is passed through the J-T valve (expanded to a lower temperature and pressure) then through the heat exchanger element of the spray bar, and finally is vented to space. The vented fluid thereby cools the fluid circulated through the mixing element of the spray bar and removes thermal energy from the bulk liquid. In an orbital propellant transfer scenario, the spray-bar concept can also be

utilized to assist tank refill. By filling through the spray bar/heat exchanger, the inflowing fluid can be cooled and used to mix the tank contents, thereby assuring the accomplishment of a "no-vent fill" process.

The zero-G vent subsystem testing successfully demonstrated pressure control within a 6.89 kPa (1 psi) operating band (131 to 137.8 kPa or 19 to 20 psi) for 75 h (fig. 14). The TVS mixer performance was excellent, and complete destratification of the liquid and ullage at fill levels of 90 percent, 50 percent, and 25 percent was achieved. Apparently, the spray atomization and condensation was better than expected, resulting in TVS operating times of 1 to 2 min versus 3 to 10 min predicted. The TVS heat exchanger flow rate was slightly

higher than predicted resulting in a heat rejection rate of 1371 W (1.3 Btu/sec) versus 1266 W (1.2 Btu/sec) predicted. The heat absorbed by the vented gas was 180 Btu/lb or 94 percent of the available heat of vaporization. Optimization of the heat exchanger can enable 100 percent vaporization in future designs.

Additionally, it was demonstrated that the TVS could reduce the liquid hydrogen saturation pressure from 19 to 10 psi in 2 h at the 25 percent fill level. Also, preliminary testing with helium in the ullage indicated that ullage pressure decay was slower due to decreased hydrogen condensation rates. Although it was demonstrated that tank pressure could be maintained with helium in the ullage, the TVS was not designed to accommodate that condition and further testing will be conducted. Future tests include the evaluation of a point source mixer/TVS concept for Lewis Research Center beginning in March 1998.

Sponsor: Office of Space Access & Technology

Biographical Sketch: Leon Hastings is currently assigned to the MSFC Propulsion Laboratory. Assignments at MSFC since 1961 have centered on heat transfer, fluid mechanics, and thermodynamics. Hastings has over 15 years of specialized experience in low gravity fluid management and heat transfer. He has often served on Agency level committees to assist in formulating plans/policies for low gravity propellant management research and technology. Hastings has a B.S. in mechanical engineering and an M.S. in engineering science. ▀

Propulsive Small Expendable Deployer System

Judy Ballance/EE61
256-544-6042
E-mail: judy.ballance@msfc.nasa.gov

The Propulsive Small Expendable Deployer System (ProSEDS) space experiment will demonstrate the use of an electrodynamic tether propulsion system. ProSEDS, which is planned to fly in the year 2000, will use the flight proven small expendable deployer system (SEDS) to deploy a tether (5-km bare wire plus 15-km spectra) from a Delta II upper stage to achieve ~0.4 N drag thrust, thus deorbiting the stage. The experiment will use a predominately "bare" tether for current collection in lieu of an endmass collector and insulated tether approach used on previous missions. ProSEDS will utilize tether-generated current to provide limited spacecraft power. In addition to the use of this technology to provide orbit transfer of payloads and upper stages from LEO to higher orbits, it may also be an attractive option for future missions to Jupiter and any other planetary body with a magnetosphere.

The ProSEDS flight experiment will demonstrate electrodynamic propulsion (through drag thrust) in space. From theoretical analyses and preliminary plasma chamber tests, bare tethers appear to be very effective anodes for collecting electrons with relatively short tether lengths. A predominately uninsulated (bare wire) conducting tether, terminated at one end by a plasma contactor, will be

used as an electromagnetic thruster. A propulsive force is generated on a spacecraft/tether system when a current from electrons collected in space plasma flows down a tether length, due to the electromotive force (emf) induced in it by the geomagnetic field (fig. 15).

The main advantage of electrodynamic tethers is that they can be used as propellantless space propulsion systems. Tethers take advantage of the natural plasma environment and sunlight to provide thrust and power. For example, if solar arrays and an external power supply are used, an

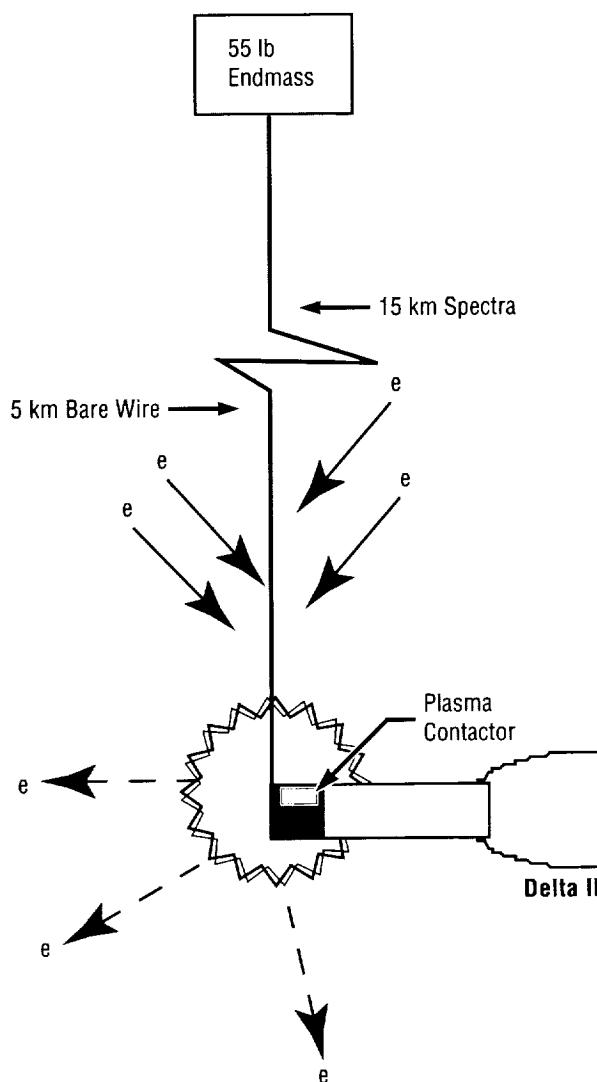


FIGURE 15.—Geomagnetic field exerts thrust proportional to current at each point along tether.

emf can be generated in the tether such that current collected from the ionosphere produces thrust rather than drag. This thrust can then be used to raise the orbit of the system or change its inclination, all without propellant or rocket engines. It is envisioned that this type of propulsion could be used on a reusable upper stage to provide a low recurring cost alternative to chemical stages. Another application of electrodynamic tethers is for deorbiting spent stages at the end of their lifetime. A small tether system could be carried to provide end-of-life drag thrust for satellites and upper stages. Instead of carrying additional propellant to perform this task, the tether could be deployed to provide this deorbit maneuver.

The ProSEDS flight experiment is planned to validate the performance of the bare electrodynamic tether in space and demonstrate its capability to produce thrust. ProSEDS will be placed into a 400-km circular orbit as a secondary payload from a Delta launch vehicle. Once on orbit, the flight-proven SEDS will deploy 15 km of Spectra tether attached to an endmass, followed by 5 km of bare wire tether. Upward deployment will set the system to operate in the generator mode, thus producing drag thrust and electrical power. The drag thrust provided by the tether with an average current of 0.5 A will deorbit the Delta II upper stage in approximately 17 days, versus its nominal >6 months lifetime. Approximately 100 W of electrical power will be

extracted from the tether to recharge mission batteries and to allow extended measurements of the system's performance. A plasma contactor will be attached to the Delta II to complete the circuit and emit electrons back into space. Performance and diagnostic instruments mounted on the Delta II will be used to correlate the propulsive forces generated by the electrodynamic tether with the existing plasma conditions. These instruments will measure plasma density, temperature, energy, and potential. ProSEDS will be the first tether mission to produce electrodynamic thrust, use a bare wire tether, and recharge mission batteries using tether generated power.

Sponsor: Advanced Space Transportation Program Office

University/Industry Involvement: Tethers Unlimited; Tether Applications Company; Smithsonian Astrophysical Observatory; Triton Systems; University of Alabama in Huntsville (UAH); University of Michigan

Biographical Sketch: Judy Ballance is the chief engineer of the ProSEDS flight experiment. She works in the Space Transportation Programs Chief Engineer's office and supports the Advanced Space Transportation Program. Judy has been employed with NASA at the Marshall Center since 1989. She has worked on various projects including Spacelab and the X-Ray Calibration Facility. She holds a bachelor's of science in electrical engineering from UAH. ▀

Structures and Dynamics

Development of Elliptic Orbit Rendezvous Analytical and Operational Techniques

Carrie D. Olsen/ED13
256-544-2271
E-mail: Carrie.Olsen@msfc.nasa.gov

The objective of this research is to develop the strategies and capabilities needed to accomplish highly elliptic orbit rendezvous in future mission designs. Theoretical and numerical approaches are being employed to categorize and evaluate various options for elliptic rendezvous, and to develop and recommend operationally efficient elliptic rendezvous procedures.

Rendezvous of two spacecraft in orbit began in the Gemini and Apollo programs and has become almost commonplace in the Shuttle era. Its continued importance to our space program is illustrated by the Shuttle-Mir missions as these flights continue to prepare us for the *International Space Station* era. Through these programs, rendezvous between two vehicles in nearly circular orbits has become a predictable, highly standardized procedure. However, not all spacecraft occupy nearly circular orbits, and rendezvous in elliptic orbits presents a whole new set of problems. The two spacecraft's velocities vary with position in the orbit (true anomaly) and thus the relative motion is more complex. One example of such relative motion is depicted in figure 16. While many works appear in the literature which address various aspects of the elliptic relative motion problem, mostly in a theoretical vein,

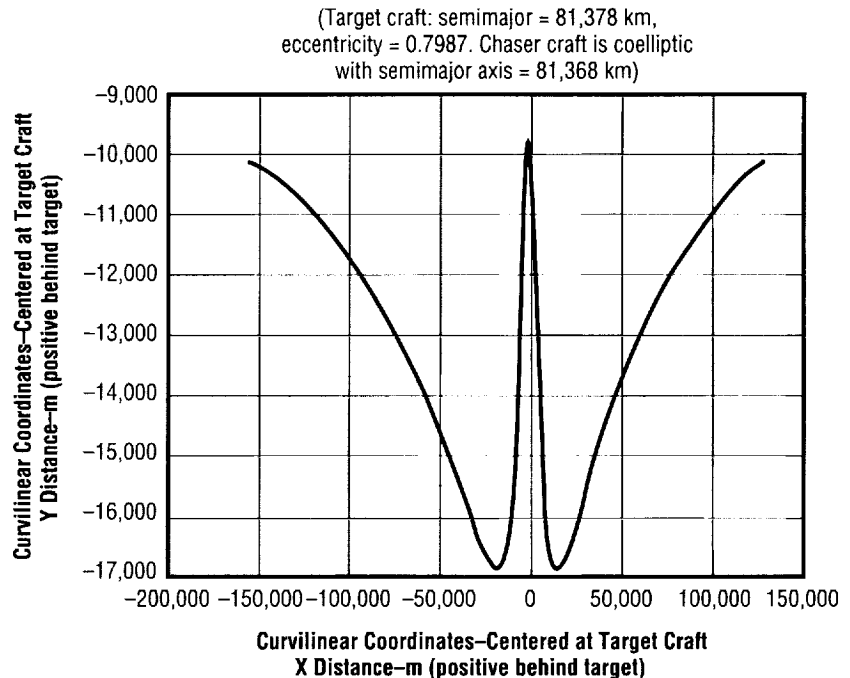


FIGURE 16.—One orbit revolution of motion: chaser spacecraft relative to target spacecraft.

there remains an immense gap in knowledge where practical targeting algorithms and operationally feasible rendezvous planning is concerned. This research seeks to narrow that gap.

The approach being used involves four interrelated tasks. The first is literature research. Through this research the principal investigator (PI) is discovering what efforts have already been made in the field and which findings and methods lend themselves to modification and extension for this project. Literature research also provides results to which the PI may compare her ongoing investigations. The second, and perhaps the largest task, is the development of computer programs that facilitate the study of elliptic rendezvous. These include, but are not limited to, routines to propagate the motion of two vehicles in a

suitable relative coordinate system, to calculate necessary changes in velocity (ΔV 's) to move the vehicles from one relative state to another, and methods to evaluate which rendezvous scenarios are "best." The third task is to use the software developed to study and evaluate options for accomplishing elliptic rendezvous. Then, in the fourth task, the results are analyzed and strategies for efficient, operationally desirable rendezvous will be formulated.

At the time of this report, the literature study task is almost complete. Periodic checks for new papers on elliptic rendezvous continue to be made, and references dealing with genetic algorithms are being collected. A genetic algorithm is a type of optimization scheme that works in a way that is analogous to the natural

processes of genetics and evolution. This type of scheme is being evaluated by the PI as a possible means for sorting through the overwhelming number of parameter combinations that could be used in elliptic rendezvous to identify "optimal" rendezvous scenarios.

In the area of computer code development significant progress has been made. Relative motion targeting and propagation programs have been created which accept inputs and provide outputs in curvilinear and local vertical-local horizontal (LVLH) relative coordinates, as well as in absolute Cartesian coordinates and orbital elements. In addition, the propagator was upgraded to handle nonspherical Earth gravity terms (J2-J4) and solar and lunar perturbations. The targeting scheme engine is a universal formulation of Lambert's equations based on the work of Klumpp and Battin.

Work on the parametric studies task is progressing. Relative motion in coelliptic and scaled elliptic orbits for some candidate orbits has been studied and found to closely duplicate unpublished work done by Kachmar, Shepperd, and Chu of Draper Laboratories. Also, a number of terminal rendezvous studies have been done, some with orbits similar to those the Advanced X-Ray Astrophysics Facility (AXAF) spacecraft will occupy over its 10-yr lifetime, to characterize the effects of initial true anomaly and transfer time selections. Also, since the capability to model perturbations has been added to the relative motion propagator, some studies have been done to determine which perturbations can be neglected

and in what cases. In addition, with the inclusion of perturbing forces, variations in the "out of plane" orbital elements (inclination, right ascension of the ascending node and argument of perigee) come into play, providing even more control parameters in this optimization problem. Some preliminary work in studying the effects of these elements has been done.

Some preliminary results from the project are as follows. Candidate final rendezvous maneuvers from 20 km behind and 10 km below a target vehicle to 1 km behind a vehicle in an AXAF-type orbit reveal favorable approach paths and velocities when initiated at apogee and completed over half a revolution of orbit travel. However, these transfers are very long

(approximately 32 h in an AXAF-type orbit). These extremely long terminal rendezvous maneuvers would represent a significant departure from circular orbit rendezvous procedures and could present operational difficulties. Also, long transfers are subject to significant perturbation effects—especially if the orbits involved have a low perigee altitude. Figure 17 illustrates chaser vehicle approach paths for various transfer times from a representative starting point.

Transfers with more typical transfer times (45–90 min) exhibit approach paths that seem operationally feasible yet constitute dramatic departures of the chaser vehicle from its natural relative motion in the phasing orbit, thus increasing the Delta-V of the

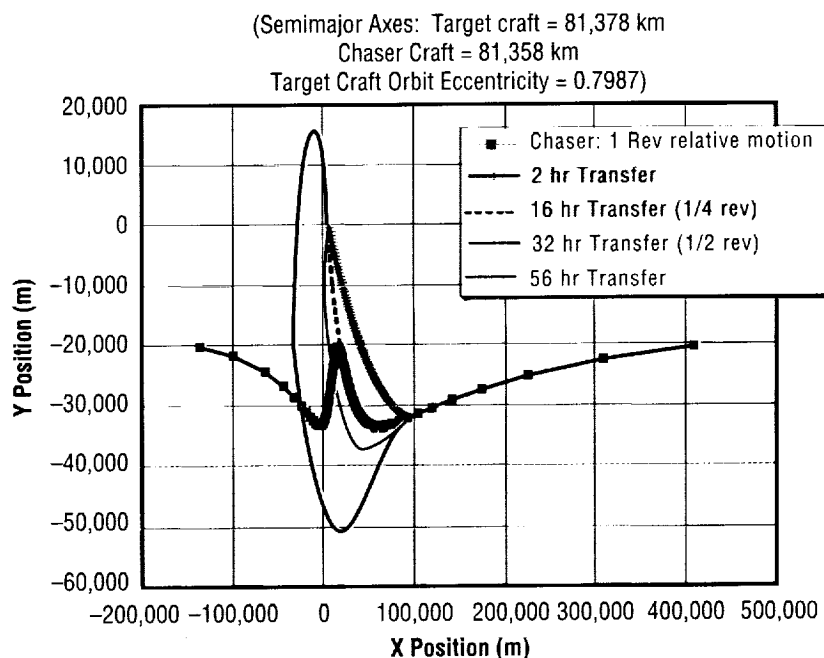


FIGURE 17.—Rendezvous transfers of various durations from a representative coelliptic chaser orbit.

maneuver. It is hoped that further parametric studies and optimization work will reveal combinations of orbital and rendezvous parameters that will produce terminal rendezvous maneuvers of reasonable duration, approach path, and propellant usage.


Future plans call for continuation of parametric studies with the software that has been developed to date and with genetic algorithm and calculus of variations-based optimization methods. These studies should lead to better understanding of the relative motion of elliptical orbit rendezvous and how it can best be undertaken operationally. The final product should be the identification and description of families of operationally optimal rendezvous scenarios, as well as a battery of computer programs for their planning and evaluation. Some more development and evaluation of analytical targeting and propagation methods may be done although, at this time, this avenue does not appear particularly promising.

Battin, R.H.: *An Introduction to the Mathematics and Methods of Astrodynamics*, American Institute of Aeronautics and Astronautics, Inc., 1987.

Klumpp, A.R.: "Universal Lambert and Kepler Algorithms for Autonomous Rendezvous," AIAA Paper, AIAA-90-2883.

Sponsor: The Center Director's Discretionary Fund

Biographical Sketch: Carrie Olsen has over 10 years of experience in

orbital mechanics, trajectory analysis, and mission planning at the Marshall Center. She has worked on such projects as Spacelab mission planning and operations, collision avoidance maneuver logic and software development for the Automated Rendezvous and Capture project and trajectory planning for the X-33 program. Olsen holds B.S. and M.S. degrees in aerospace engineering from Mississippi State University and is currently a Ph.D. candidate in the University of Texas at Austin's Department of Aerospace Engineering and Engineering Mechanics. 

Elastic-Plastic Proof Test Philosophy for Metallic Structures

Charles L. Denniston/ED25
256-544-7248
E-mail: charles.denniston@msfc.nasa.gov

The Southwest Research Institute has finished the final report for the Proof Test Philosophy to State-of-the-Art Technology Contract (Contract Number NAS8-39380). In this report, Southwest Research developed a proof test guidelines report for the Durability Analysis Branch of the Marshall Center. This report describes an elastic-plastic fracture mechanics (EPFM) issue-based approach for planning a proof test of thin metallic structures. This new approach allows mitigation of issues that NASA-SP-8040 currently does not address. Among these are the following:

- Crack tip plasticity
- Stable tearing before fracture
- Cracks at geometric discontinuities
- Plastic constraint
- Net section yielding
- The interaction between primary and secondary stresses.

The fracture mechanics parameter upon which much of this report's analytical approach was based is the J-Integral. Resistance curves based on the J-Integral (or J-R curves) are also used to predict tearing before fracture. Many of the analysis procedures for predicting fracture and tearing in this report are implemented by means of failure assessment diagrams (FAD's).

Combining Loads From Random and Sine Excitation Using Monte Carlo Techniques

Dr. Andrew M. Brown/ED23
256-544-1584
E-mail: andy.brown@msfc.nasa.gov

Structures in many environments experience both random and harmonic excitation. A program has been written at MSFC to generate a consistent design value for the combination of the loads resulting from these simultaneous excitations. The standard method, which adds the amplitude of the sine load to three times the root mean square (rms) of the random load using simple hand calculations, yields unnecessarily over-conservative values because it assumes the sine peak value always occurs simultaneously with the peak random value, which is unrealistic. The value obtained with this new program removes this extra conservatism, which can be critical for lightweight aerospace components. It also quantifies the load value obtained with a consistent reliability value, unlike the traditional technique. Because of the flatness of the cumulative distribution function (CDF) at high reliability levels, the design value is extremely sensitive to the reliability level chosen, so the choice of a consistent value is extremely important. Finally, because of the tremendous advances in computing power in recent years, the calculation of the combined load using this Monte Carlo technique is as fast as the older method.

In general, the dynamic response analysis of structures for random and harmonic cases are performed

separately, and the results are then combined to obtain a design load. For random excitation only, standard practice in industry is to assume the random response has a Gaussian distribution and to use the 3σ value for this load, where σ is the root mean square output value. This value exceeds 99.86 percent of the responses as defined by the CDF of the response.

Since a sine wave is not a random signal, though, it has always been unclear how to combine the results from the harmonic input with output from random excitation to obtain a design load. Standard practice has been to sum the maximum amplitude of the harmonic response with the 3σ random response. This value is not tied to a particular probability level, although it is extremely conservative since it assumes the peak random level always occurs at the same instant as the peak of the sine wave. This value will always exceed the 99.86 percent level. In reality, the random peaks can occur at the same time as any portion of the sine wave.

A more consistent approach is to find the actual level that exceeds 99.86 percent of the responses for the combined excitation, defined here as the "equivalent 3σ " value. This program performs a Monte Carlo simulation to obtain this value. The random load is first simulated by generating a vector of points $\{r\}$ that falls within a Gaussian (or Normal) distribution of mean zero and standard deviation equal to the input rms value. This can be expressed as $\{r\} \sim N(0.0, \sigma_{\text{random}})$. The vectors representing the sine load are then generated. This program can account for multiple independent harmonic excitations $\{y\}_i$, $i=1, \dots, n$. Since the

frequencies of each sine wave are different and the relative phasing is unknown, each sine wave can combine with the random signal and every other sine wave at any equally likely point along the wave. Therefore, vectors representing each wave are separately created using the formula $\{y\}_i = A_i \sin(2\pi \{x\}_i)$, where $\{x\}_i$ are vectors of uniformly distributed points $\{x\} \sim U(0,1)$. The summation of all the harmonic signals and the random signal is performed for each sample to create a new vector $\{z\}$, which is equal to a sample set of total responses of the structure to the multiple simultaneous excitations. The CDF of $\{z\}$ is then generated. The program obtains and prints the value that is greater than 99.86 percent of the responses, the "equivalent 3σ " value. For comparison, the value obtained using the standard approach is also calculated and printed. As expected, test results for a large variety of combinations of random and sine show that the standard method can substantially overpredict the "equivalent 3σ " value.

The user is given a wide variety of options when using this program. User specification of the number of combinations, the number of samples used in the Monte Carlo analysis, and the number of independent sine waves to be combined with the random excitation is provided. In addition, the user can specify a different CDF level for output for any combination. The entire CDF (in x-y format) of the final random-sine combination set is printed into a separate output file for plotting. A sample CDF for a combination of a sine load of amplitude 10 with a random load of rms 10 is shown in figure 18.

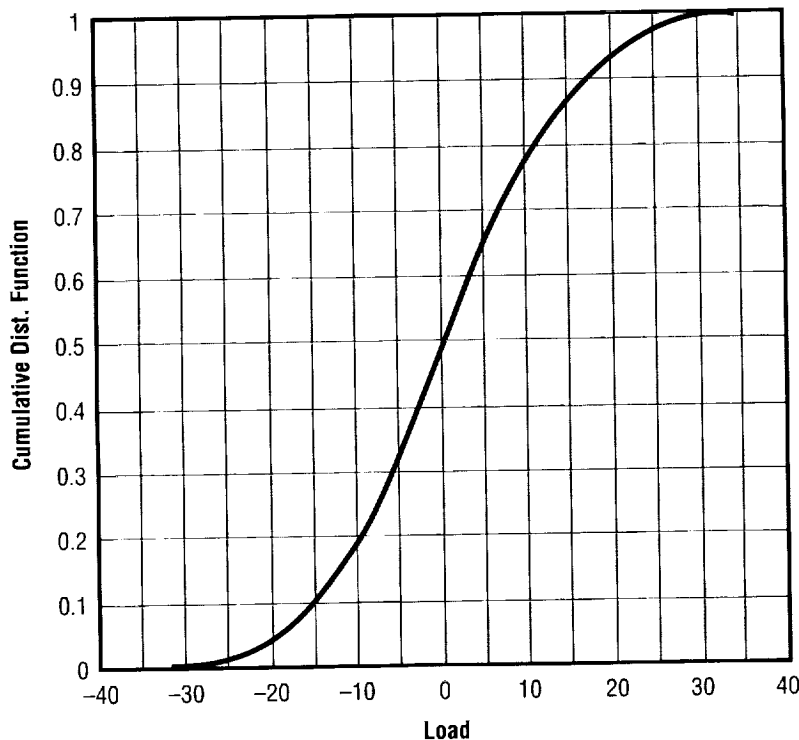


FIGURE 18.—Sample CDF output for total load due to random rms=10, sin amplitude=10.

The main source of error when using this program is in the sample size chosen for the Monte Carlo simulation. This error decreases as the sample size is increased. This error is also somewhat sensitive to the number of simultaneous signals that are combined. For a combination of several signals, it is recommended that the largest sample size possible for use with the program, 100,000, be used. This maximum size can be easily altered in the source code if further accuracy is desired.

This program was designed to stand alone without any additional subroutines and is able to be executed on any computer carrying FORTRAN 90. It has been installed in the NASA software library at COSMIC, and is available for general use.

Sponsor: X-34 and Technology Transfer

Biographical Sketch: Andrew Brown is an aerospace engineer in the Structural Dynamics and Loads Branch of the Structures and Dynamics Laboratory. His duties at Marshall include evaluating the vibrational response of the Space Shuttle main engine, analyzing new propulsion systems for excessive vibration, and performing research to develop new tools to analyze these systems. Brown received his undergraduate degree from Duke University and his Ph.D. in mechanical engineering from the Georgia Institute of Technology. ▀

Multidisciplinary Thermal-Fluid Design Optimization Tool

Ten-See Wang/ED32
256-544-0503
E-mail: Ten-see.Wang@msfc.nasa.gov

Two engineering design analysis tools have been successfully merged into a unified multidisciplinary thermal-fluid prediction model. On one hand, the Systems Improved Numerical Differencing Analyzer (SINDA) code is a thermal analysis software for simulating solid components energy balance using a method of conductor-capacitor networks. It also includes other models such as wall radiation heat transfer and one-dimensional fluid flow models. On the other hand, many practical applications in rocket engine flow analysis require computational fluid dynamics (CFD) models, such as the Finite-Difference Navier-Stokes (FDNS) code, for better predictions of the flow fields which cannot be modeled properly with the simplified method used in SINDA.

Merger of these two disciplines into one unified analytical model enhances the prediction capability and efficiency of the thermal-fluid design tool. A parallel computing algorithm, using parallel virtual machine library has been developed, to provide a boundary conditions passing mechanism to provide solution interaction automation and computational efficiency. Each model is operated within its own computational environment. And the current interface model, with conservative formulations for general patched interfaces, is running

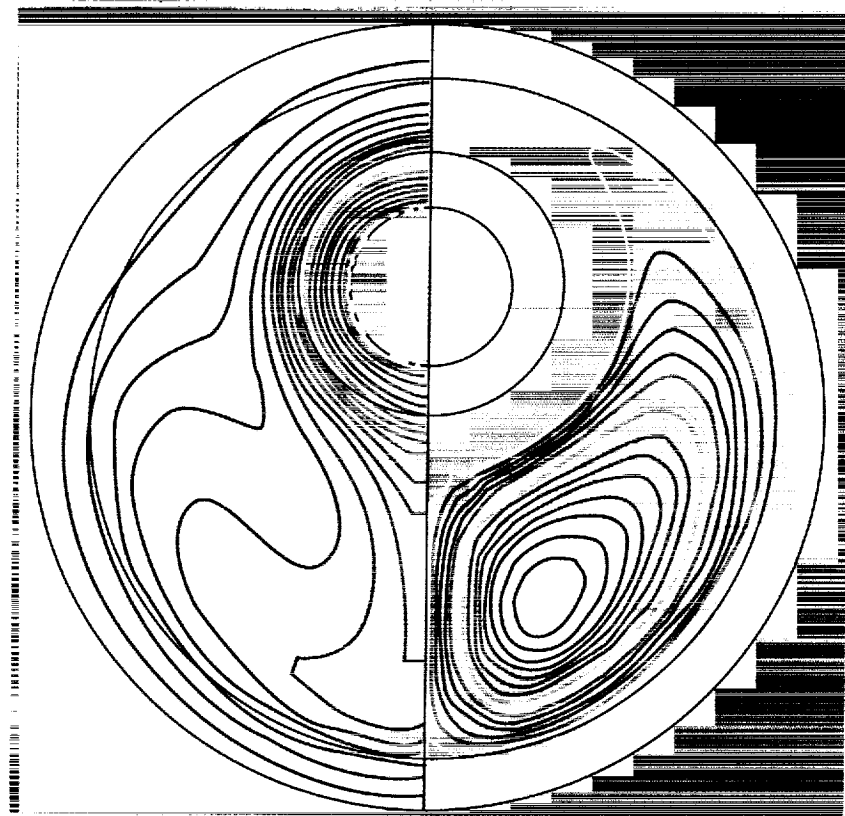


Figure 19.—Thick-walled eccentric tubes thermal-fluid analysis: temperature (right) and streamline (left) contours.

concurrently to manage the data transfer through the solid-fluid boundaries. The benefit of the parallel computing method in thermal-fluid analysis is not only that each model can be operated on separate machines, but that several flow models can be activated simultaneously to cut down the computational time for the CFD model. The net outcome is a greatly increased efficiency in performing the analysis.

Two-dimensional and three-dimensional benchmark validation cases were investigated during the phase I project. A cross-sectional plot of the

temperature and streamline contours of two thick-walled eccentric tubes with natural convection is illustrated in figure 19. The predicted results are in good agreement with the test data (fig. 20). The final goal of the phase II research project is to develop an engineering tool that can be used to model and solve complex thermal-fluid design problems in a single analysis such that it will be accepted as a robust design tool for the propulsion system design community and the thermal-fluid analysis industry.

Sponsor: Small Business Innovative Research Program

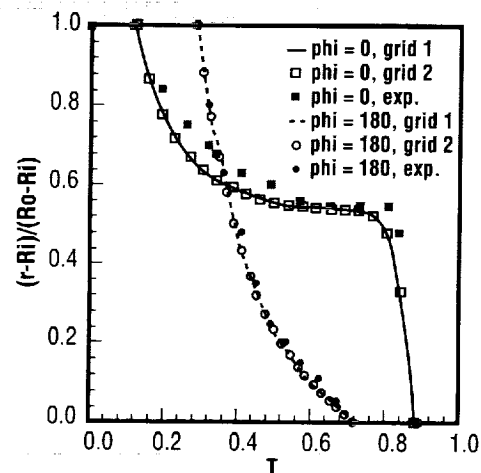


Figure 20.—Thick-walled eccentric tubes thermal-fluid analysis: data comparisons.

Industry Involvement: Engineering Sciences, Inc.

Biographical Sketch: Dr. Ten-See Wang is currently a team leader of the Computational Analysis Team in the Fluid Dynamics Analysis Branch. He received his Ph.D. from Louisiana State University in 1980. He had previously been affiliated with SAIC, Continuum, SRA, and SECA, Inc. His recent work has been applying CFD methods for propulsion system and launch vehicle plume-induced environment. ▀

Unshrouded Impeller Technology Development

Roberto Garcia/ED32
256-544-4974
E-mail: robert.garcia@msfc.nasa.gov

Future reusable launch systems will require higher thrust-to-weight (T/W) ratio engines than currently available. One of the key technologies that will enable significant improvements in T/W ratio is advanced unshrouded impeller technology. Unshrouded impellers have been used in rocket engines in the past primarily because they can be manufactured less expensively than shrouded impellers. However, unshrouded impellers also have a structural advantage over shrouded impellers. The use of unshrouded impellers allows for higher tip speeds and, hence, higher stage loading resulting in the reduction of turbopump size and weight. Table 1 illustrates the benefits of the increased stage loading possible with the use of high head coefficient, high efficiency unshrouded impellers. Note that there is a potential weight savings of 500 lb to the Space Shuttle main engine (SSME) alternate turbopump (ATP) high-pressure fuel turbopump (HPFTP) if advanced unshrouded impellers are used.

The goal of the present program is to evaluate advanced unshrouded impeller concepts, cold flow test the most promising concepts, and perform a hot-fire verification of the best concept. In order to achieve these goals, three major tasks have to be performed. The first task involves making improvements to the grid generator TIGER. TIGER is an

efficient turbomachinery components grid generator developed under NASA/LeRC sponsorship. However, TIGER lacks the capability to generate grids for impellers containing partial blades. Under this program TIGER has been enhanced by Engineering Sciences, Inc. (ESI) to overcome this shortcoming. Grids previously requiring 1 to 3 days to generate can now be generated with the upgraded version of TIGER in 3 to 4 h. Additional improvements are being made to TIGER to facilitate the grid generation in the tip-clearance region.

The main thrust of this program is to evaluate unshrouded impeller concepts using computational fluid dynamics (CFD) analysis and experimental techniques. Pratt & Whitney in Florida is designing the various concepts being evaluated, and MSFC is performing the CFD analyses. Nine impeller cases have been analyzed and their predicted performance and flow features compared. Figure 21 shows typical results obtained thus far. The results have been scaled to the same tip speed as the SSME ATP HPFTP for comparison. The definitive

TABLE 1.—Weight savings potential for the SSME ATP HPFTP.

	Shrouded	Unshrouded
Pump Efficiency (%)	78.6	76.3
Pump Horsepower	75,670	78,600
Impeller Tip Speed (ft/sec)	1,890	2,321
Head Coefficient	.558	.552
Stage Loading (Feet of Head)	61,145	92,390
Pump Stages	3	2
Turbopump Weight (lb)	990	490

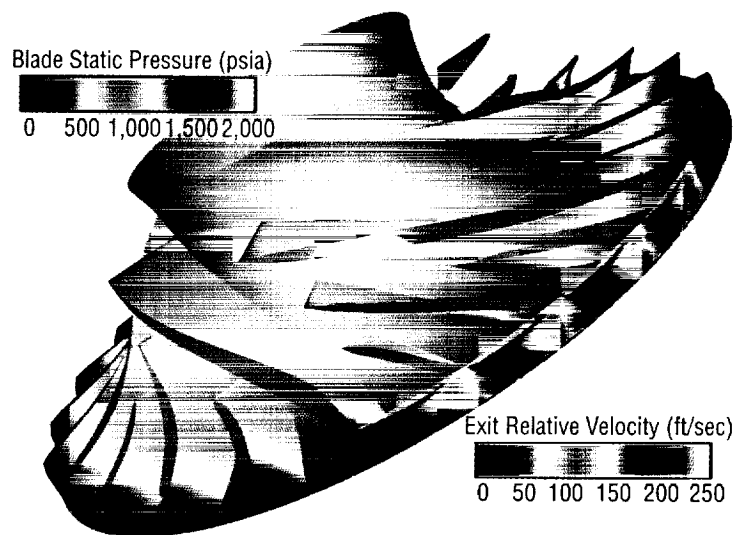


FIGURE 21.—Sample CFD analyses results in support of the unshrouded impeller development. Shown is the static pressure distribution on the blade surfaces and velocity magnitude at the impeller exit plane.

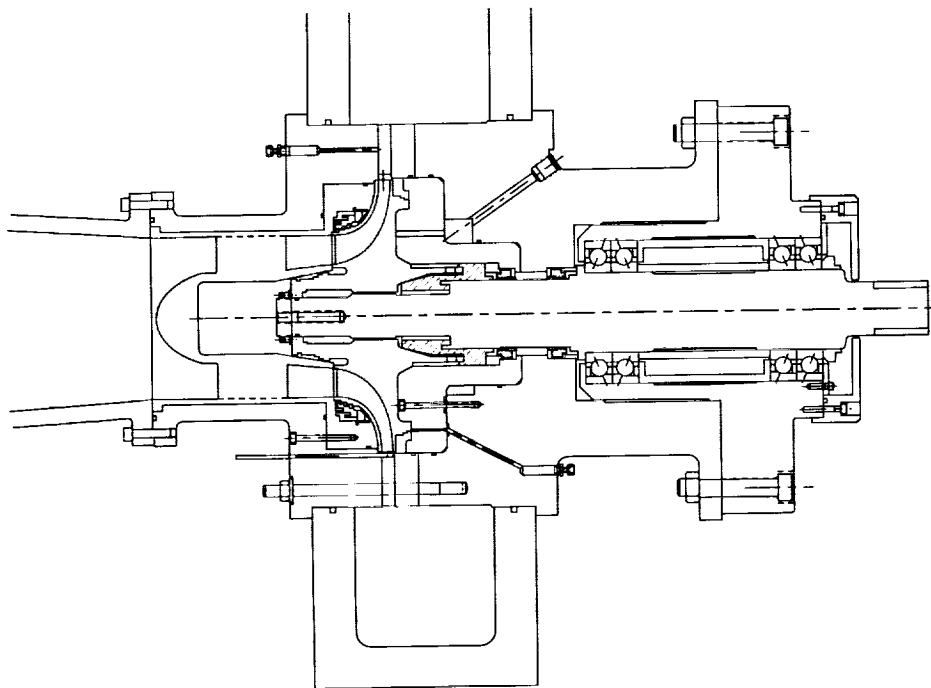


FIGURE 22.—Cutaway view of the unshrouded impeller technology water flow rig.

unshrouded impeller will operate at approximately 22 percent higher tip speed. The analyses performed thus far have been performed using a nominal tip clearance of 3 percent of the impeller blade trailing edge height. Based on these initial results, the goal of achieving 95,000 feet of head with an efficiency comparable to that of the SSME HPFTP is attainable.

Three to four more impeller cases will be evaluated prior to selecting the best design for testing under simulated conditions in water. The water rig is being designed by Microcraft, Inc. and will be tested at the Marshall Center's pump test equipment (PTE) facility. The design of the water rig (fig. 22) is 90 percent complete and only requires final determination of the impeller

design for completion. The rig is designed to be easily assembled and disassembled to facilitate testing the impeller under various tip clearances. Allowance has been made in the rig design for the testing of the impeller with or without a vaned diffuser, for testing of impellers of various profile shapes, and for testing with various inlet velocity profiles. The rig is extensively instrumented such that the performance of the impeller can be measured directly rather than having to rely on the more common flange-to-flange performance measurements.

Testing of the selected impeller is scheduled to occur during the summer of 1998. The products of this program will include validated design tools, unshrouded impeller design databases,

and verified advanced hardware designs that will significantly increase the T/W ratio over current engine systems.

Sponsor: Long Term/High Payoff Technologies—part of the Reusable Launch Vehicle Technologies Program.

Industry Involvement: Engineering Sciences, Inc.—TIGER grid generator enhancements; Pratt & Whitney, Florida—Unshrouded impeller designs; Microcraft, Inc.—Water flow rig design

Biographical Sketch: Roberto Garcia received a bachelor of science degree in aerospace engineering from the University of Florida in 1986. Since obtaining his degree he has been employed by NASA at the Marshall Center. He works in the Fluid Analysis Branch of the Fluid Mechanics Division in the Structures and Dynamics Laboratory. His primary duty is to perform CFD analyses of rocket engine components in support of NASA's rocket propulsion programs. ▀

Solar Thermal Upper Stage/Shooting Star Experiment

Scott A. Hill/ED52
256-544-4106
E-mail: scott.hill@msfc.nasa.gov

The purpose of the Shooting Star Experiment (SSE) is to prove the feasibility of a solar thermal upper stage utilizing new technology such as inflatable structures, thin film optics, and thermal storage engines. By proving the feasibility of these technologies, the design and manufacture of future upper stages would have low launch volumes, thus allowing larger payloads to be carried to orbit.

The SSE is designed to be integrated inside a Spartan spacecraft bus developed by Goddard Space Flight Center. The Spartan spacecraft will provide power, gaseous fluids (for inflation and propulsion), and pointing control for the experiment. The SSE consists of four major subsystems: The inflatable structure containing the thin film fresnel lens; the fluid distribution system; the thermal storage engine including the secondary concentrator; the avionics including the sunlight centering system; and the structural module assembly (SMA) that integrates all the subsystems into the Spartan spacecraft. The inflatable structure consists of three struts tied at one end to the SMA and the other end to a torus assembly containing the thin film fresnel optic. The thermal storage engine consists of two chemical vapor deposition (CVD) rhenium shells sandwiching a CVD rhenium foam

heat exchanger. This assembly is in turn welded to a CVD rhenium foam flange that acts as a structural member to connect to the SMA. The secondary concentrator is a refractive optic consisting of a magnesium oxide crystal that is being developed by Lewis Research Center.

The SMA configuration, shown without skin panels or engine insulation, (fig. 23) depicts the crank rocker mechanism used to support both the secondary concentrator and thermal storage engine, the orientation of the secondary concentrator to the thermal storage engine, and the three-point mounting system used to integrate the experiment in the Spartan spacecraft. The fresnel optic contained in the inflatable structure focuses sunlight onto the spherical surface of the secondary concentrator. This light then exits the secondary concentrator's "light pipe" within the cavity of the

engine's inner shell. The inner shell absorbs this energy and conducts it to the engine's heat exchanger and outer shell. When the engine reaches the operating temperature of $\sim 3,500^\circ\text{F}$, the fluid distribution system activates to allow gaseous nitrogen to flow through the engine's heat exchanger. This allows the nitrogen to absorb the stored energy and cool the engine. The nitrogen flows out through the engine's outer shell nozzle that in turn provides a propulsive force of ~ 1 lb.

The crank rocker mechanism used on both the secondary concentrator and the thermal storage engine serves two purposes. It's first responsibility is to react all the loads resultant from launching the vehicle into orbit. The second is to provide a structure that will accommodate the large thermal deflections in those elements while maintaining them in their proper alignment to receive the collected light focused by the fresnel optic.

Sponsor: Office of Aeronautics and Space Transportation Technology

Biographical Sketch: Scott Hill is a senior design engineer in the Structural Development Branch of the Structures and Dynamics Laboratory and has been employed with NASA at the Marshall Center since May of 1989. During his 9 years at MSFC, Hill has had a wide variety of tasks ranging from hypervelocity impact simulation using state-of-the-art hydrocodes to designing and developing MSFC's 5-ft-dia. Cryostat Test Facility. Hill holds a bachelor of science degree in mechanical engineering from Mississippi State University. ■

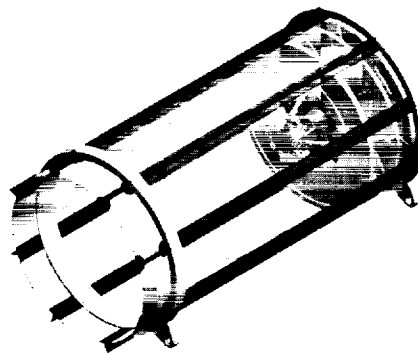


FIGURE 23.— View of the structural module assembly (SMA) containing the secondary concentrator and thermal storage engine. (Several skin panels have been removed for view clarity.)

Interdisciplinary Testing of Inflatable Structures for the Shooting Star Experiment

R. Gregory Schunk/ED63
256-544-7221
E-mail: richard.schunk@msfc.nasa.gov

John O. Lassiter/ED73
256-544-3022
E-mail: john.lassiter@msfc.nasa.gov

Robert C. Engberg/ED73
256-544-9348
E-mail: robert.engberg@msfc.nasa.gov

Dr. Michael L. Tinker/ED23
256-544-4973
E-mail: mike.tinker@msfc.nasa.gov

Jeffrey R. Kegley/EL72
256-544-2291
E-mail: jeff.kegley@msfc.nasa.gov

The Shooting Star Experiment (SSE) is a solar thermal propulsion demonstrator for the MSFC Aeronautics and Space Transportation Technology Transfer Program. Solar thermal propulsion utilizes sunlight to heat a working fluid to provide thrust at an increased specific impulse. The thrust is produced by expanding the heated fluid through a nozzle in the solar thermal engine. The SSE will be integrated with a Spartan spacecraft and, once on orbit, deployed from the Space Shuttle using the orbiter's remote manipulator arm. After release of the experiment, pyrotechnics will be used to open the inflatable structure container allowing the inflation

sequence to begin. Figure 24 shows the SSE in the on-orbit deployed configuration. The inflatable concentrator assembly consists of a thin film Fresnel lens for focusing sunlight, a torus ring that supports the lens, and three struts that support the torus and attach to the Spartan.



FIGURE 24.— Shooting Star Experiment and Spartan carrier.

A series of development tests have been performed to evaluate the structural dynamic and thermal behavior of prototype inflatable structures for the SSE. The tests have been conducted to measure the response of individual struts, as well as the combined dynamic and thermal behavior of complete inflatable structures (torus, struts, lens) under ambient pressure (Pathfinder I) and under vacuum (Pathfinder II and Pathfinder III).

Initially, modal tests were performed for individual struts in a vibration lab at atmospheric pressure. The potential damping effect of air was to be evaluated in subsequent tests. In the tests, a single strut was oriented vertically in both a free-free and cantilevered boundary configuration.

Foam plugs were used at each end of the strut to seal it and at the upper end to provide an opening for the pressure line. Soft supports were used to simulate a free-free condition, and shaker excitation was applied at the lower end of the strut. Testing was done at various pressures for two different thicknesses of the polyimide film material. It was found that the natural frequency varies as a function of both the film thickness and pressure inside the structure. Data from these tests were valuable for determining the applicability of simple beam theory for modeling inflatable beam-like structures constructed of highly nonlinear materials. Measured mode shapes showed the general characteristics of a free-free and cantilevered beam.

Modal testing of a prototype concentrator assembly, consisting of a torus, lens simulator, and three tapered struts, was also performed at ambient pressure. Excitation was provided with a shaker attached to the support plate at the top of the inflatable assembly. It was determined during pretest investigations that excitation could not be applied directly to the surface of any of the inflatable components to obtain acceptable response. Modal tests were run at three different inflation pressures, 0.25, 0.50, and 1.0 psig. Considerable variation in the measured frequencies and mode shapes was observed for the three different pressures. Correlation of finite element models to the test data is in progress. It is yet to be determined if the nonlinear variation of material modulus properties is as critical for modeling of the inflatable assembly as it is for a single strut.

Thermal vacuum testing of the SSE Pathfinder III inflatable was conducted in the MSFC X-Ray Calibration Facility (XRCF) thermal vacuum chamber as shown in figure 25. The development testing was divided into two phases—thermal cycle/balance/gradient and modal survey. The primary objective of the thermal vacuum testing was to characterize the structural deformation of the SSE inflatable under extreme thermal environments. During the thermal phase of testing, the Pathfinder III inflatable was cycled twice between -120°F and $+75^{\circ}\text{F}$ under vacuum and exposed to horizontal and vertical temperature gradients as induced by the chamber shroud and by an array of lamps located underneath the test article. No adverse effects were observed from the thermal cycling, and leakage rates remained constant throughout the test. Six theodolite measurements were made to measure thermally induced static deflections in

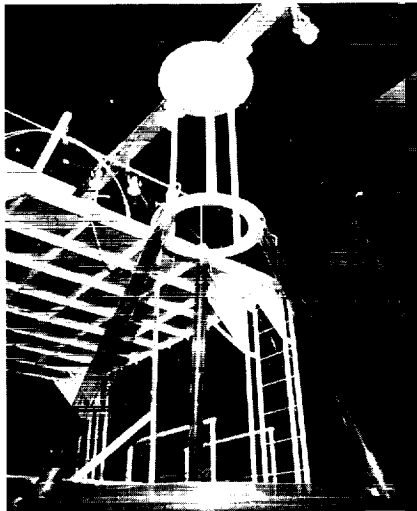


FIGURE 25.—Pathfinder III inflatable inside the XRCF.

the inflatable structure under varying pressures and temperatures.

Modal testing the dynamics of the inflatable structure within the vacuum chamber was complicated by several factors. Because of the structure's lightweight and thin (<4 mils) polyimide Kapton™ material, conventional accelerometers were not feasible for use, especially inside a thermal vacuum chamber. As a result, noncontacting measurement techniques, such as the use of a laser vibrometer and video camera, were used to measure the dynamic response of the structure. The results showed highly damped and closely coupled modes.

Data from the thermal vacuum tests will be used by dynamic, stress, and thermal analysts for math model correlation and to aid in establishing pointing and alignment error budgets for the SSE/Spartan spacecraft. Pressure measurements of the inflatable structure made throughout the thermal vacuum tests will aid designers in establishing control schemes for the pressure management of the inflatable on orbit, as well as to budget the quantity of gas required. Static deflection measurements made at the beginning, throughout, and at the conclusion of the thermal vacuum tests may reveal permanent changes in the inflatable, resulting from temperature or pressure cycling.

In addition to achieving the stated objectives, the tests demonstrated an in-house capability at MSFC to perform complex interdisciplinary thermal and dynamic testing of an

inflatable structure. Special provisions were made to make static deflection and dynamic response measurements of the inflatable structure while mounted inside the XRCF vacuum chamber. Handling procedures and special test fixtures for the inflatable were developed in support of the testing. A special purpose low-flow gas system was adapted to inflate and deflate the test article as required during the tests.

One of the most important findings from the thermal vacuum tests may be the demonstrated capability to construct an inflatable that exhibits minimal leakage after being subjected to the thermal extremes that will likely be encountered on orbit. Mathematical model correlation of data from the modal survey tests is significant in showing that linear finite element analysis can be useful in the modeling of inflatable structures. Verified mathematical models of the concentrator assembly will eventually be used in on-orbit dynamic and thermal simulations in support of the SSE design.

Sponsor: Advanced Space Transportation Programs Office

Biographical Sketches: Greg Schunk is an aerospace engineer in the Thermal Engineering and Design Branch involved in the analysis and design of space vehicles and systems. He received a B.M.E. from the Georgia Institute of Technology in 1983.

John Lassiter is an aerospace engineer in the Dynamics Test Branch involved in experimental modal testing and

vibration control. He received a B.S.A.E. from the University of Alabama in 1978, and an M.S.A.E. from the U.S. Air Force Institute of Technology in 1980.

Robert Engberg is an aerospace test engineer in the Dynamics Test Branch involved in planning, preparation, performing, and analyzing results of vibration, modal, and dynamic control systems tests. He received a B.I.E. from Auburn University in 1994.

Dr. Mike Tinker works in the Structural Dynamics and Loads Branch, performing modal analysis, structural dynamic modeling, pretest analysis, model correlation, and loads analysis. He is also involved in research of improved modal test techniques. He received his Ph.D. in aerospace engineering from Auburn University in 1989.

Jeff Kegley is an aerospace test engineer in the Vacuum Engineering Test Branch involved in the thermal vacuum testing of space vehicles and systems. He received a B.S.M.E. from the Tennessee Technological University in 1987 and a M.M.E. from Auburn University in 1991. ▀

On-Orbit Controller Tuning for Robust Pointing Control

Dr. Mark Whorton/ED12
256-544-1435
E-mail: mark.whorton@msfc.nasa.gov

A primary difficulty with control of flexible space structures is that accurate models of the on-orbit system are not available a priori. Meeting stringent pointing requirements often necessitates a high-performance pointing control system. However, to account for modeling errors, compensators for orbiting vehicles must be designed with a high degree of robustness which limits achievable performance. One solution is to trade robustness for increasing performance, which requires integration of system identification and control system design in a form that facilitates iterative redesign, or "tuning," of the control system.

For many spacecraft, to obtain high performance pointing control on orbit requires closed-loop system identification and controller tuning. A methodical process for on-orbit tuning for flexible spacecraft must consist of five steps: 1) Empirical or analytical model development for initial control design, 2) low authority control design for robust stability, 3) closed-loop system identification to improve knowledge of the on-orbit plant dynamics, 4) controller refinement to increase control authority and improve performance, and 5) performance assessment. Steps 3-5 may be iterated until the desired controller performance is obtained. The critical elements in this process are system identification and controller refinement.

Under this technology development activity, advancements have been made which provide a fruitful paradigm for the on-orbit control redesign problem. These advancements include mixed-norm optimal control synthesis and a new procedure for closed-loop system identification which are merged in a realistic procedure for on-orbit control system redesign. With regard to closed-loop system identification, a procedure has been developed which utilizes closed-loop response data to refine a state-space model in a minimal realization. This new technology is an extension of a technique developed for open-loop system identification which exploits the structure of the closed-loop system when the system is realized in canonical form. Using a least-squares prediction error approach, the open-loop system parameters are estimated such that the closed-loop time response error is minimized.

The controller tuning technology utilizes a continuous homotopy algorithm to generate a continuous deformation of the dynamic compensator parameters.¹ This deformation may be optimized for changing plant parameters such as in tuning the controller based on a refined plant model as well as for performance versus robustness trades. Using the homotopy algorithm to synthesize mixed H_2/H -infinity controllers is especially significant in the controller tuning application. Mixed H_2/H -infinity control theory allows dynamic compensators to be designed which maximize performance for a prescribed set of inputs/outputs using the H_2 norm, and guarantees robust stability using the H -infinity norm for another set of inputs/outputs.

The technology is a significant step toward a unified on-orbit controller tuning process. The system identification process is a realistic on-orbit model refinement tool. Using the mixed H_2/H -infinity homotopy algorithm is an effective means for controller tuning based on the refined plant model and provides an explicit means of trading robustness for increasing performance based on improved confidence in the refined model. Further details on both the system identification and control design aspects are available in reference 2.


1. Whorton, M.S.; Buschek, H.; and Calise, A. J.: "Homotopy Algorithm for Fixed Order Mixed H_2/H -infinity Design," *Journal of Guidance, Control, and Dynamics*, Vol. 19, No. 6, pp. 1262–1269, November–December 1996.
2. Whorton, M.S.: "High-Performance, Robust Control of Flexible Space Structures," Ph.D. Thesis, The Georgia Institute of Technology, August 1997.

Sponsor: Center Director's Discretionary Fund

University Involvement:

Dr. Anthony Calise, School of Aerospace Engineering, The Georgia Institute of Technology

Biographical Sketch: Dr. Mark S. Whorton is an aerospace engineer in the Precision Pointing Systems Branch of the Control Systems Division, NASA/Marshall. Whorton received B.S. (with honors) and M.S. degrees in aerospace engineering from The University of Alabama in 1987 and

1989 and a Ph.D. from The Georgia Institute of Technology in 1997. Dissertation research was in the area of robust control for flexible space structures. Recent work assignments have included control design and analysis for microgravity vibration isolation systems such as STABLE and the Boeing Active Rack Isolation System. 

Microgravity Vibration Control and Civil Applications

Dr. Mark Whorton/ED12
256–544–1435
E-mail: mark.whorton@msfc.nasa.gov

Controlling the vibration of structures is essential for both space structures as well as terrestrial structures. Due to the ambient acceleration levels anticipated for the *International Space Station*, active vibration isolation is required to provide a quiescent acceleration environment for many science experiments. Technology developed for vibration control of flexible space structures may also be applied to control of terrestrial structures such as buildings and bridges subject to wind loading or earthquake excitation. Recent developments in modern robust control for flexible space structures provide good structural vibration control while maintaining robustness to model uncertainties. Results of a mixed H_2/H -infinity control design for a benchmark problem in earthquake engineering for building structural control have demonstrated the fruitful application of technology developed for space to civil use.

Traditional methods for mitigating vibrations of structures include adding structural mass to stiffen the structure. However, the cost of launching payloads to orbit renders this option unfeasible for flexible space structures. Instead, active control must be used to mitigate vibrations of flexible space structures. Active control may be thought of as a means to effectively stiffen a structure (such as with

position feedback) or effectively increase its structural mass (such as with acceleration feedback). Actuators may be used to actively cancel disturbance forces applied to a structure. However, in many cases adding structural mass may not be sufficient for ground structures either. In those cases, technologies that have been developed for space application can be fruitfully applied to the problem of controlling vibrations in civil structures such as buildings, bridges, and towers.

While robust control provides performance in the presence of uncertainties, the performance is often defined by an H-infinity norm measure, which may not be well suited to the performance objectives. To minimize the mean-square vibration response of a structure, the H_2 -norm is a better measure of performance. However, it is well known that H_2 design at high control authority levels has very poor robust stability properties. These issues are addressed in the mixed H_2 /H-infinity design method. Mixed H_2 /H-infinity design seeks to minimize the H_2 -norm of one transfer function while satisfying an overbound constraint on the H-infinity norm of another transfer function. Using this approach allows one to design for H_2 nominal performance while maintaining the robust stability provisions of H-infinity design.

There are various design approaches for the problem of structural vibration control which achieve nominal performance only (H_2), robust performance (H-infinity or μ -synthesis), and nominal performance/robust stability (mixed H_2 /H-infinity or mixed H_2/μ). The challenge is to achieve the highest attainable level of

mean-square performance for a specified bounded set of uncertainties. For a more thorough treatment of the underlying control theory, uncertainty modeling and control design results, reference is made to reference 1. This reference compares these controller design techniques and applies the design approach to a benchmark problem in structural control of buildings using the three-story tendon controlled structure at the National Center for Earthquake Engineering Research.²

The results of this work show that while considering nominal mean-square performance, robust stability is a necessary design consideration. Robust stability requires the closed-loop system to remain stable for bounded model errors. A significant difference in performance exists between the H_2 and μ designs since the μ designs achieve a given level of output performance at a higher control cost than the H_2 designs. However, the mixed H_2 /H-infinity designs effectively recover the mean-square performance of the H_2 designs while providing the same level of robust stability as the μ designs. The mixed H_2/μ design procedure provides performance comparable to H_2 design while overcoming the major shortcoming of H_2 design, namely a lack of stability robustness. An evaluation model was used with the Simulink model provided with the benchmark problem to generate time responses for the controller designs.

1. Whorton, M.S.: "High Performance, Robust Control of Flexible Space Structures," Ph.D. Thesis, The Georgia Institute of Technology, Atlanta, GA, August 1997.

2. Spencer, B.F. Jr.; Dyke, S.; and Deoskar, H.: "Benchmark Problems in Structural Control," *Proc. 1997 ASCE Structures Congress*, Portland, OR, April 13-16, 1997.

Sponsor: Center Director's Discretionary Fund

University Involvement: Dr. Anthony Calise, School of Aerospace Engineering, The Georgia Institute of Technology

Biographical Sketch: Dr. Mark S. Whorton is an aerospace engineer in the Precision Pointing Systems Branch of the Control Systems Division, NASA/Marshall. Whorton received B.S. (with honors) and M.S. degrees in aerospace engineering from The University of Alabama in 1987 and 1989 and a Ph.D. from The Georgia Institute of Technology in 1997. Dissertation research was in the area of robust control for flexible space structures. Recent work assignments have included control design and analysis for microgravity vibration isolation systems such as STABLE and the Boeing Active Rack Isolation System. ▀

Automated Rendezvous and Capture Technology Description

Richard Dabney/ED13

256-544-1473

E-mail: richard.dabney@msfc.nasa.gov

In the past, all U.S. rendezvous and docking operations have been piloted or ground-controlled, but autonomous rendezvous and capture (AR&C) has become an enabling technology for expendable resupply of Space Station and planetary sample return missions. Significantly reduced operations cost, increased repeatability, reliability, and safety are but a few of the benefits AR&C offers. Although the Russian docking system is available, it is not fully autonomous during all mission phases, requiring ground radar tracking and command for rendezvous, producing high contact velocities, and has experienced significant technical difficulties during recent missions. The current NASA MSFC

AR&C project has completed all flight software development and achieved a successful test flight of its video guidance sensor (VGS) on the Shuttle; test facility upgrades are complete and system integration is well underway. AR&C requires no real-time human commanding of the resupply vehicle, allows automated mission design prior to flight, and fully automates vehicle operations, incorporating onboard mission/trajectory updates from real-time navigation data.

A typical AR&C mission flight profile, with the chase vehicle docking from behind, is shown in figure 26; approaches from ahead of and below the target are also supported. A complete system block diagram is included in reference 3, which describes in more detail the guidance, navigation, and control algorithms used in each phase of the mission.

Maturity of the AR&C system will be proven upon completion of the ongoing ground demonstration project and planned test flights, including

verification and documentation of AR&C specific hardware and software. Another Shuttle flight of a VGS is planned late this summer to better evaluate its performance at longer range (up to 130 m) and establish reliability and repeatability of measurements. Extensive system integrated ground testing will be performed to validate and verify performance of the complete system, followed by closed-loop flight (if funding permits) of a complete automated rendezvous and docking experiment as a payload on the Shuttle or on an expendable vehicle to identify any unexpected problems. At that point, the AR&C system will be ready for use by customer programs.

Further research is being conducted on methods of improving system performance, including a weighted least-squares inverse perspective implementation, which extracts near-optimal relative attitude and position measurements from available VGS data, and better methods for determining target image centroids within the

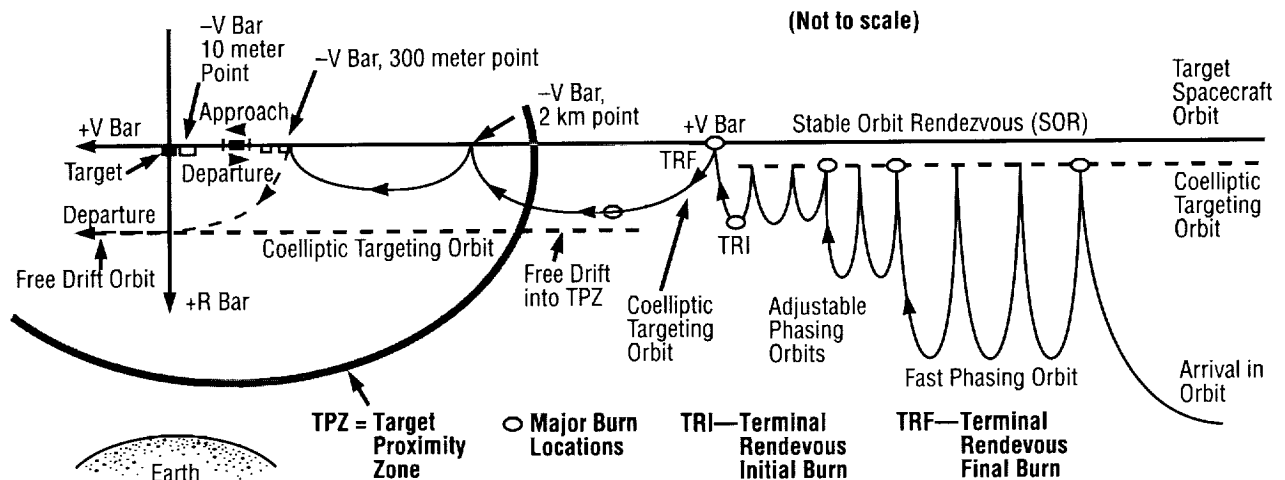


FIGURE 26.— Typical AR&C mission flight profile.

VGS. Ongoing relative GPS algorithm development is making significant progress in reducing measurement noise induced by multipath and "selective availability." Together, these advances will make possible docking with spacecraft with unusual requirements, such as tumbling rates or large appendages, which require high bandwidth and measurement accuracy, as well as further increasing overall system performance and reducing fuel consumption.

1. Dabney, R.W.: "Application of Neural Networks to Autonomous Rendezvous and Docking of Space Vehicles," AIAA Space Programs and Technology Conference, Huntsville, AL, March 24-27, 1992.
2. Dabney, R.W.; and Howard, R.T.: U. S. Patent Nos. 5,109,345, "Closed-Loop Autonomous Docking System," April 28, 1992.
3. Dabney, R.W.: "Automated Rendezvous and Capture Technology Description," *Research and Technology 1995 Annual Report of the Marshall Space Flight Center*, NASA TM-108501, pp. 107-110.
4. Calhoun, P.; and Dabney, R.W.: "A Solution to the Problem of Determining Relative 6-DOF State for Spacecraft Automated Rendezvous and Docking," SPIE International Symposium on Aerospace/Defense Sensing & Control and Dual-Use Photonics, April 1995.

Sponsor: MSFC AR&C Demonstration Program Office

Biographical Sketch: Richard W. Dabney has been involved with MSFC's AR&C work since 1981, and has extensive experience with the design of piloted and automated transfer vehicles, including the Orbital Maneuvering Vehicle and Cargo Transfer Vehicle. He has received three U.S. patents, two for AR&C system components and one for an energy-saving electric motor controller. Dabney has a B.S.E.E. degree from the University of Kentucky and is currently pursuing an M.S.C.S. degree at the University of Alabama in Huntsville. ▀

Infrared Fiber-Optic Thermographic Sensor for High-Temperature Applications

Don Bryan/ED63
256-544-4265
E-mail: donald.bryan@msfc.nasa.gov

Infrared fiber-optic thermography (IRFOT) technology for use by NASA's Marshall Center has been developed under a Phase II SBIR contract by SRS Technologies. This technology allows thermal imaging via infrared (IR) fiber optics. The initial prototype's minimum sensed temperature is 650 °F while the maximum is near 2,000 °F if the probe is cooled adequately. The follow-on system is projected to sense temperatures down to approximately 300 °F (IRFOT 2). The probe itself can sustain temperatures up to 500 °F without active cooling. Actively cooled probes are also being designed.

Standard imaging fiber-optic materials and manufacturing methods have traditionally precluded the use of the best IR fiber materials. Innovative signal processing and manufacturing techniques developed by SRS allow for cost-efficient fiber-optic bundle designs using materials suitable for transmission of the IR energy. In particular, significant cost savings are achieved by using an incoherent fiber-optic bundle coupled with a sophisticated signal processing system rather than the much more expensive coherent bundles. Shown in figure 27 is the prototype IRFOT 1 fiber-optic system. Not shown is the image processing computer.

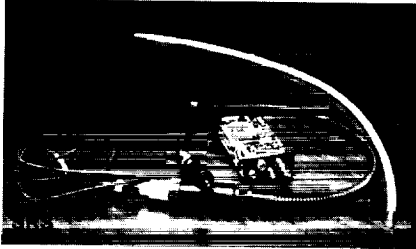


FIGURE 27.—Prototype fiber-optic probe, sensor, and fiber-optic bundle.

NASA and SRS are developing this technology to enable internal monitoring of high-temperature rotating machinery such as liquid hydrogen and oxygen turbopumps. The initial IRFOT prototype will be installed in a supersonic hot gas wind tunnel at the Marshall Center to undergo testing and be used as part of the wind tunnel instrumentation to control surface heating of test articles.

The basic IRFOT system consists of the IR fiber optics, image acquisition IR focal plane and associated electronics, PC image acquisition card and image processing software. The system works with a PC, or a fully integrated system can be supplied (recommended). System requirements are a dual Pentium 166 or faster with WindowsNT and 64 Mb of RAM with at least one available PCI slot.

Sponsor: Small Business Innovative Research Program

Industry Involvement:
Hill Roberts/SRS Technologies
205-971-7000
E-mail: hroblib@aol.com

Biographical Sketch: Donald Bryan is an aerospace technologist—heat transfer, for the Marshall Center. His duties include developing new

methods of measuring the temperatures of aerospace components at high temperatures and severe environments. He has worked in the Thermal Engineering and Design Branch for 6 years. He has also worked for Safety and Mission Assurance and the Propulsion Laboratory. He has a B.S.M.E. from the University of Wisconsin—Madison. ▀

Materials and Processes

Laser Induced Impulse on Debris Materials

Jason A. Vaughn/EH12
256-544-9347
E-mail: jason.vaughn@msfc.nasa.gov

Lasers have been used for a wide range of applications from delicate microsurgery to targeting for missiles. As part of the MSFC Advanced Propulsion Technology (APT) Program Office at the Marshall Center, lasers are being examined for potential use in new propulsion technology. One of several areas of interest in the APT program is the potential use of lasers to clean the low-Earth orbit (LEO) environment of debris particles. The Engineering Physics and Environmental Effects Branch in the Materials and Processes Laboratory at MSFC was tasked with measuring, while in an LEO vacuum environment, the impulse a laser would impart into typical debris materials by vaporizing part of the surface material. The objective of this task was twofold—first, to determine if the laser could impart sufficient momentum to be detected, and, second, to quantify the impulse caused by hitting various materials as a function of laser energy densities. The data from this test would be used to determine if a laser on the ground could deliver a high enough energy density to a debris particle in space, causing a momentum change large enough to sufficiently lower part of its orbit, thus causing it to burn up upon re-entering Earth's atmosphere.

The feasibility of making impulse measurements using a high-powered laser at a low cost to the APT Program was evaluated as an initial step. The

evaluation included determining what type of hardware was available and what type of hardware had to be purchased. The most important task, however, was designing a method to measure, in vacuum, the micro-Newton impulse from the laser. The laser induced momentum balance (LIMB)—which transfers the linear momentum produced when the laser heats and vaporizes material at the target sample surface into angular momentum—was used to make direct angular momentum measurements from target samples “shot” with the laser. The LIMB is simply a double arm mechanism stretched from both the top and bottom between two taut pieces of 0.01-cm-dia. tungsten wire. The angular displacement caused by the laser “shot” on one side of the double arm mechanism was monitored through a video system. The sensitivity of the angular measurement of the system depended directly on the wire material and diameter.

A complete test system (fig. 28) was developed by modifying in-house hardware to support the laser, provide

for laser alignment through the vacuum chamber window to the target sample on the LIMB, position the LIMB within the vacuum chamber, and transmit a very short pulse or “shot” of high energy laser light to the target sample. The heart of the system was a 3-J-pulsed ruby laser with a pulse duration of 35 ns. A typical laser spot size was 1.0 cm in diameter, producing an energy density at the samples of about 110 MW/cm. The laser passed through a focusing lens which allowed the energy density at the target sample surface to be varied. The ruby laser was lined up with the target sample by sighting a small helium-neon (HeNe) laser through the ruby laser and the focusing lens onto the target. The laser was set up to fire single pulses using a remote control system.

The angular momentum of the LIMB was measured by monitoring the angular displacement of the sample fixture relative to a fixed reference scale using a video camera and a remote mirror system (fig. 28). The video recording of the laser impact

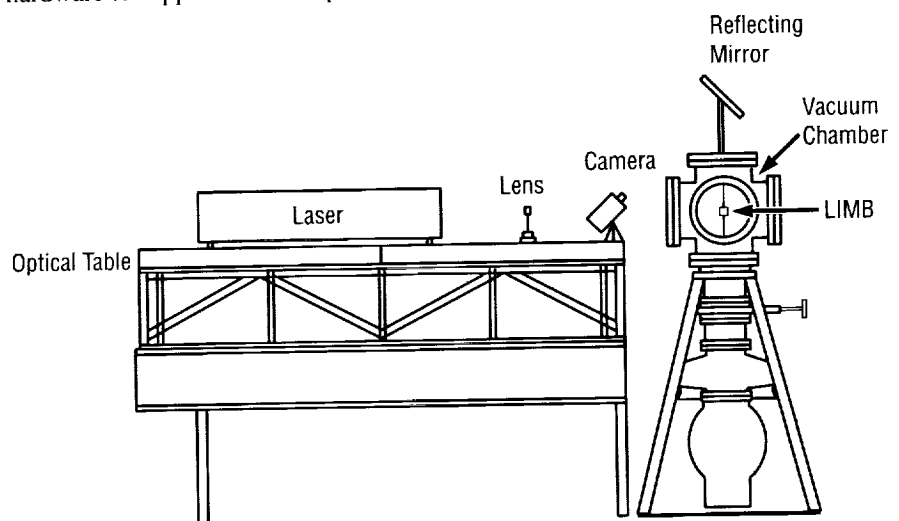



FIGURE 28.— Laser impulse on orbital debris test system.

provided slow motion replay for measuring the angular displacement as a function of time to within 3 degrees.

Two typical target materials were tested with the main objective of demonstrating the capability of measuring impulse in a vacuum of 10^{-7} torr. The two target materials were aluminum foil coated with a black polyurethane paint and plain aluminum foil for comparison. The first coating had very high absorption in the visible light region compared to the plain aluminum foil. The LIMB system performed better than expected, resulting in an angular displacement for the black coated aluminum foil of approximately 165 degrees peak-to-peak and of the aluminum foil at near 20 degrees peak-to-peak. Ongoing evaluations are being performed to quantify the change in momentum that can be obtained from various debris type materials as a function of energy density from the 3 J ruby laser.

Sponsor: Advanced Propulsion Technology Program Office

Biographical Sketch: Jason Vaughn is a senior engineer in the Physical Science and Environmental Effects Branch in the Materials and Processes Laboratory. Vaughn is responsible for developing and conducting tests systems for simulating the effects of the space environment. Vaughn has a master's degree in mechanical engineering from Colorado State University. 

Development of Environmentally Compatible Solid Film Lubricants

Phillip Hall/EH13
256-544-2525
E-mail: Phillip.Hall@msfc.nasa.gov

Multibody launch vehicles require the use of solid film lubricants (SFL's) to allow for unrestricted relative motion between structural assemblies and components during lift-off and ascent into orbit. The Space Shuttle solid rocket booster (SRB), uses a dual coat, ceramic-bonded high-temperature SFL in several locations such as restraint hardware between the SRB aft skirt and the mobile launch platform (MLP), the SRB/external tank (ET) attach struts, and the forward skirt SRB/ET attach ball assembly. A family of environmentally compatible nonlead/antimony bearing alternative SFL's for use on transportation equipment, all types of lubricated fasteners, and energy related equipment have been developed. The new SFL's trade name is Boosterlube™ which is a family of single layer thin film (0.001 in. (.025 mm) maximum) coatings that are a unique mixture of nonhazardous pigments in a compatible resin system that allows for low temperature curing (450 °F (230 °C)). Significant savings in energy and processing time as well as elimination of hazardous material usage and disposal will result from the nontoxic one-step SFL application. A compatible air-dry field repair SFL was also developed called Perma-Slik RMG™ to be used to eliminate disassembly of launch vehicle restraint hardware

during critical time-sensitive assembly operations. At this time Perma-Slik RMG™ and Boosterlube™ are commercially available from E/M Corporation.

MSFC/EH13 in conjunction with USBI/Kennedy Space Center (KSC) has completed the qualification plan to implement Boosterlube™ and Perma-Slik RMG™ on the SRB system. The qualification plan consisted of six different areas which included tribological testing, coating adhesion, fluid compatibility, corrosion protection, flammability, and aging stability. Tribological testing included monoball high-load tests, Falex block on ring tests per ASTM D 2714, and Falex pin and Vee-block tests per ASTM D 2625 A/B for endurance and load capacity. Coating adhesion tests were completed per ASTM D 2510 procedure A. The fluid compatibility tests were completed per ASTM D 2510, procedure C.¹ Corrosion protection testing was completed at KSC by exposing coated samples to the ocean environment for 6 months and comparing these to uncoated samples exposed the same amount of time. Flammability testing was done to NHB 8060.1 at ambient temperatures. Aging stability testing was completed at KSC using monoball high-load test samples exposed to the ocean environment for 3 and 6 months, than ran using the normal high-load test procedure.

The result of the qualification plan showed that Boosterlube™ and Perma-Slik RMG™ are an acceptable replacement for the present lubrication system now being used. The only anomaly found during testing was the aging stability tests which indicate that the Boosterlube™ binder system

degraded during exposure to the ocean environment. This was caused by the ultraviolet radiation degrading the epoxy binder system. The SRB parts scheduled to be coated with this new lubrication system will not experience this type of exposure. Because of the positive results of this qualification plan, Boosterlube™ is scheduled to be implemented in the spring of 1998.

1. Annual Book of ASTM Standards, Vol. 05.02, "Petroleum Products and Lubricants," ASTM, Philadelphia, PA, 1992

Sponsor: Solid Rocket Booster Program

Biographical Sketch: Phillip Hall is an engineer in the Nondestructive Evaluation and Tribology Research Branch at Marshall. Currently he evaluates solid film lubricants for space use, conducts research in traction testing in liquid oxygen, and reviews/troubleshoots designs for tribological problems. He has a bachelor's in science in materials engineering from Auburn.

Acknowledgment: Thanks to Howard L. Novak of USBI/KSC for supporting this program and seeing it to completion. ▀

Effect of Bearing Cleaning on Long-Term Bearing Life

Tim Jett/EH13
256-544-2514
E-mail: Tim.Jett@msfc.nasa.gov

For many years chlorofluorocarbon (CFC) based solvents, such as Freon™ and tetrachloroethane (TCA), were used as bearing cleaning solvents for space mechanisms. The 1995 ban on the production of ozone depleting chemicals (ODC) such as CFC's has resulted in a change to new ODC-free cleaners for the precision cleaning of bearings. With this change the question arises, "What effect if any do these new cleaners have on bearing life and performance?" Many space mechanisms require long-life bearings and lubrication. These new ODC-free cleaners may have a negative effect on the long-term life and performance of these space mechanisms.

These ODC-free cleaners may modify bearing surfaces differently than CFC-based cleaners. Performance anomalies may occur due to wetting differences or changes in surface reactivity resulting in shorter bearing life. There is evidence to suggest some new aqueous cleaners are detrimental to bearing operation. These cleaners may actually clean the bearing surface better than the CFC-based cleaners. This could leave a reactive surface and contribute to lubricant degradation. It is also possible the detergent used for aqueous cleaners is not completely rinsed which might lead to a reduced bearing life. These new cleaners need to be carefully evaluated to determine

the effects that they may have on long-term bearing life.

MSFC initiated a study to evaluate the effects of these new ODC-free cleaners on long-term bearing life. Two in-house tests are being performed. The first test involves a 1-yr-long bearing test. For this test, 60 small electric motors are being evaluated in a Marshall Center High Vacuum Test Facility. We have tested the long-term performance of space-compatible greases for many years using this high vacuum facility which consists of a high vacuum manifold that is connected to two 10-in. diffusion pumps. These pumps are capable of maintaining pressures in 1E-6 torr range during test operation. This manifold has 12 vacuum bell jars attached to it. For this testing, three bell jars are being used with 20 test motors in each.


Each motor contains two small angular contact bearings. The bearings are R-4 size (0.635 c. I.D. by 1.59 cm O.D.). These bearings are AISI 440c steel bearings with ribbon type stainless steel cages. Motors are run continuously for 1 yr at 90 °C at approximately 1E-6 torr pressure. The motors are loaded to maintain a 22.2 N thrust load with no radial load. The bearings operate at 3,600 rpm, and this results in a fully developed elastohydrodynamic film being formed. Four cleaners and three space compatible greases are being evaluated. These cleaners are Freon™, Brulin 815 GD, Turco, and supercritical carbon dioxide. The three space compatible lubricants are Braycote 601EF grease, Vackote 48822, and Rheolube 2001. Mass measurements of the lubricated

bearings are made both, pre- and post-test. Along with mass loss measurements, a profilometer trace will be taken of the inner race to determine posttest wear of the bearings. In addition, the bearings will be visually examined and analyzed using an optical microscope. This 1-yr testing should be completed in March 1998. After this, a 5-yr test is planned.

The second in-house test involves the evaluation of bearings used in controlled moment gyroscope (CMG) motors. For this test CMG bearings are cleaned with an ODC-free cleaner Turco, Brulin, carbon dioxide or Freon™. The bearings are being tested in *Skylab* vintage CMG motors. These motors use two 107H size (35-mm bore) angular contact bearings that utilizes a phenolic cage. Prior to testing, these cages are vacuum oil-impregnated with either Braycote 815Z oil or Pennzane 2001A oil. A CMG motor is mounted in a bell jar work station and run under a high vacuum environment (1E-6 torr). The CMG motor runs at 7,800 rpm with a 178 N axial load. This results in a fully developed elastohydrodynamic film. During testing, motor and bearing temperatures are continuously monitored via a strip chart recorder. The motors run continuously until a failure occurs. Failure is determined when the motor torque increases enough to cause an in-line 0.75-A fuse to blow. This CMG testing should be completed in late 1998.

Sponsor: *International Space Station*

Biographical Sketch: Tim Jett is a materials engineer in the Nondestructive Evaluation and Tribology Research Branch at Marshall where he

performs research and development on space compatible oils and greases. In addition, he performs quasi-static and dynamic analysis and computer modeling of bearings for use on space mechanisms and high-speed turbomachinery. Jett earned his B.S. in materials engineering from the University of Alabama in Birmingham in 1982, and an M.S. in materials engineering from University of Alabama in Birmingham in 1991. 

Comparison of Computed Tomography Data to Actual Physical Density Data for Composite Materials

Dr. Ron Beshears/EH13
256-544-2550
E-mail: ron.beshears@msfc.nasa.gov

Computed tomography (CT) inspection produces cross-sectional images of inspected components. This method generates images that accurately depict the location and geometry of defects in materials by detecting differences in density and x-ray absorption between nominal and flawed regions. Without known density standards, CT is capable only of detecting relative density differences between such regions.

The application of the CT system to inspection of composite nozzles and test cylinders for the Advanced Space Transportation Program (ASTP) Fastrac engine development project has provided an unprecedented opportunity to advance the system's capability to detect and diagnose defects in selected composite materials. The material testing phase of the Fastrac nozzle development project involves intensive CT inspection and destructive analysis of test cylinders and nozzles fabricated from silica phenolic and graphite epoxy. Separations in the bond line between the two composite materials in the nozzles and cylinders can be detected by CT inspection, but in those cases where the separated area is filled with adhesive or resin residuals, it is often

difficult for CT to determine the exact nature and mechanism of the bond line separation. By comparing the destructive analysis data with CT image data and CT density profile measurements, the Center's Nondestructive Evaluation team is developing a database that allows correlation of CT image data profiles to physical density data. This will allow more accurate detection and diagnosis of bond line anomalies in composite materials than is currently possible using only nondestructive inspection techniques.

Sponsor: Advanced Space Transportation Program/Fastrac project

Biographical Sketch: Dr. Ron Beshears is a Materials Engineer and has coordinated computed tomography work at MSFC for 6 years. In addition, he serves as a specialist on numerous Agency programs and failure investigations. He holds a NASA Level III certification for radiographic testing and B.S., M.S., and Ph.D. degrees in physics. ■

Computed Tomography System Upgrade Provides Improved Imaging Capability

Dr. Ron Beshears/EH13
256-544-2550
E-mail: ron.beshears@msfc.nasa.gov

The computed tomography (CT) system in building 4707 was upgraded to a new Unix-based operating system during FY97. The upgraded system features better image resolution and improved data analysis and management capabilities. One of the benefits of the improved data handling capability is that data can now be presented in a much more intuitive fashion than before. The upgraded system is currently supporting the Advanced Space Transportation Program (ASTP) Fastrac engine development project.

The CT system was specifically designed to detect flaws in composite materials and has proven effective at inspection of the composite materials in the Fastrac 60K nozzles. The nozzle consists of a silica phenolic liner that is bonded to a graphite epoxy overwrap. The CT system is capable of detecting radial cracks in the liner material, an example of which is shown in figure 29. The crack in this nozzle was open to the inner surface of the nozzle but was difficult to see because it was obscured by charred liner material after the nozzle had been used in a test firing.

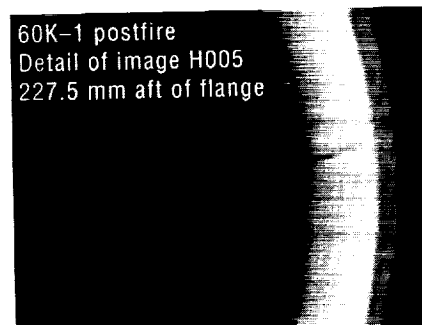


FIGURE 29.—This is a cross-sectional image of a Fastrac 60K nozzle taken in the forward chamber of the nozzle, showing a crack in the liner material.

The upgraded system can export image data in a format that can be read into commercial image processing software. This allows 3D reconstruction of sets of individual cross-sectional CT images collected at successive intervals throughout the nozzle, producing a model of the nozzle that more clearly shows the nature and extent of the crack. Figure 30 is a 3D model of the forward chamber of the same nozzle as was shown in figure 29, showing that the crack runs from the forward end of the nozzle through the throat of the nozzle.

The 3D reconstruction was generated using T3D™, a product of Fortner Research LLC. This program imports the CT images and stacks them sequentially to produce accurate 3D representations of the inspected component. This capability can be used to provide a much more intuitive image of the crack in the nozzle. By allowing export of CT images in

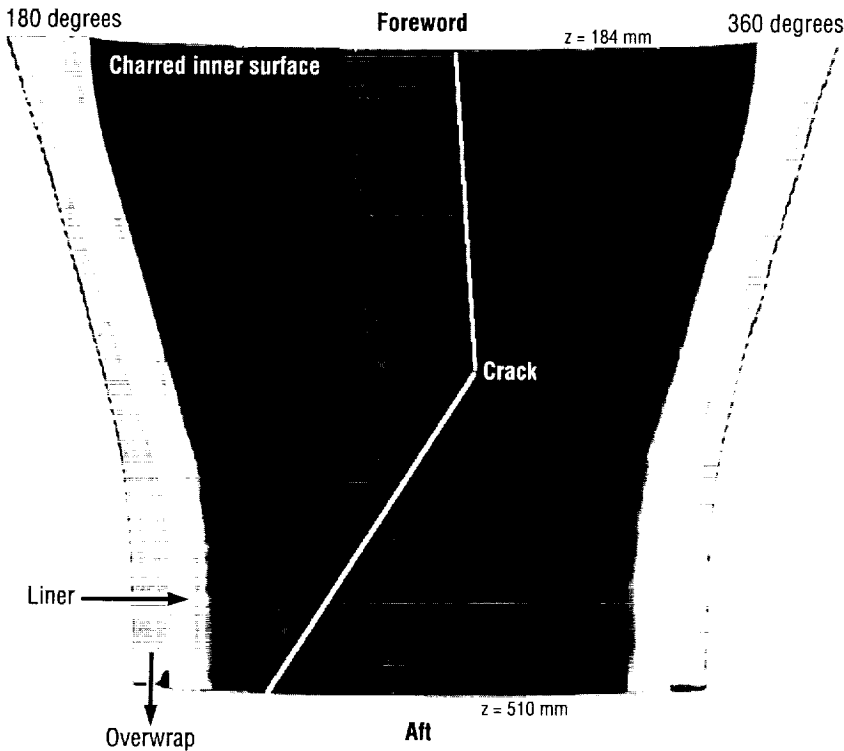


FIGURE 30.—This is a 3D reconstruction of a set of CT slices (like the one shown in fig. 29) collected throughout the forward chamber of the same Fastrac 60K nozzle, showing that the crack in the liner runs throughout the forward chamber and throat of the nozzle.

common image file formats, the CT system upgrade provides a more understandable presentation of nondestructive evaluation data.

Sponsor: Advanced Space Transportation Program/Fastrac project

Biographical Sketch: Dr. Ron Beshears is a materials engineer and has coordinated computed tomography work at MSFC for 6 years. In addition, he serves as a specialist on numerous Agency programs and failure investigations. He holds a NASA Level III

certification for radiographic testing and B.S., M.S., and Ph.D. degrees in physics. **D**

Friction Stir Welding Process Development

Jeff Ding/EH23
256-544-2700
E-mail: jeff.ding@msfc.nasa.gov

Engineers at the Marshall Center have advanced the friction stir welding technology for use on the manufacturing floor. A friction stir welding system has been integrated with a 4.5-m (15-ft) tall vertical weld tool in the Productivity Enhancement Complex at the Center. This is the first production oriented friction stir welding system of this magnitude to be installed in this country (fig. 31). The vertical weld tool is similar to production tooling found at the Michoud Assembly Facility in New Orleans, LA, where the Space Shuttle external tank is fabricated. The tooling at the Michoud Assembly Facility, however, is dedicated to the current weld system used to fabricate the external tank, Variable Polarity Plasma Arc Welding. The first hardware planned for fabrication using the Marshall friction stir weld system is an 8.4-m (27.5-ft) diameter, 4.5-m (15-ft) high simulated hydrogen barrel section from the Space Shuttle external tank. The barrel section is comprised of 9 curved panel sections that are joined by 10 longitudinal welds. It is made out of a new aluminum-lithium alloy 2195 material, specially made for the external tank program. The weld joint material thickness has both constant thickness and tapered thickness areas. The tapered weld thickness changes from 8 mm to 16.5 mm (0.320 in.-0.650 in.)



FIGURE 31.—Vertical weld tool.

thick. The capability to weld tapered material thicknesses is made possible by a product of Marshall Center research. Engineers have designed, manufactured and patented a special device called a retractable pin-tool, which will effectively join a tapered weld joint configuration (fig. 32).

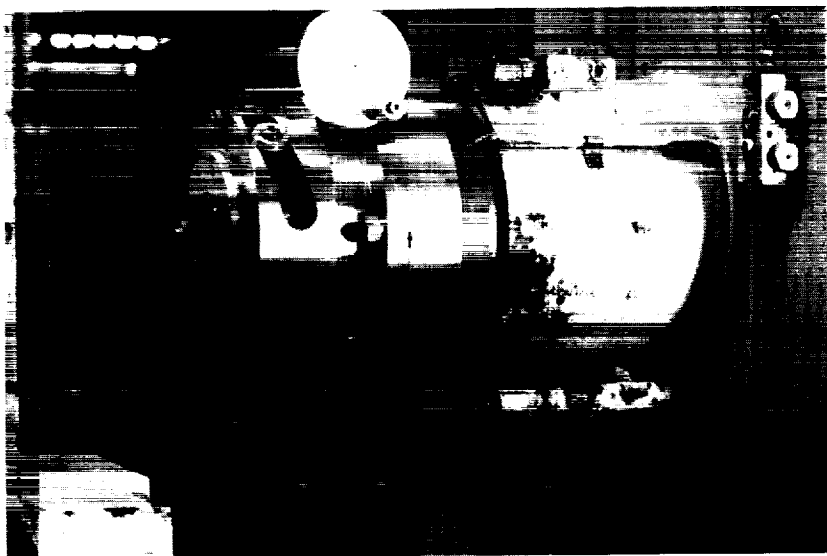


FIGURE 32.—Retractable pin-tool.

Friction stir welding is a revolutionary new weld process invented and patented by The Weld Institute of Cambridge U.K. It is a solid state process, in which the material being welded does not melt. This nonmelting attribute is very significant for high-performance aluminum alloys in that the resultant material properties of the weld are significantly higher in comparison to weld properties of the same material completed with a fusion weld process. A friction stir weld is formed by plunging a rotating shouldered pin tool, with a probe length less than the weld depth required, into the faying workpiece faces, until the tool shoulder is in intimate contact with the work surface. The rotating shoulder heats the metal (via frictional heating characteristics) as the probe inside the weld joint produces a plasticized tubular column of metal around the probe. As the pin tool is moved in the direction of welding, the leading face of the probe, assisted by a special profile, crushes and forces plasticized

material to the back of the probe, while applying a substantial downward mechanical forging force. This force consolidates the weld metal into the weld joint at the trailing edge of the tool.

Sponsor: Office of Aeronautics and Space Transportation Technology

Industry Involvement: Rocketdyne Division of Boeing North American, Inc.; Lockheed-Martin Manned Space Flight Systems

Biographical Sketch: Jeff Ding is a welding engineer for the Materials and Processes Laboratory at the Marshall Center. He came to Marshall in June 1986, working in the area of welding process development on Space Shuttle main engine and external tank applications. Ding is the lead engineer for friction stir welding process development. He earned his B.S. degree in biology at Bowling Green State University, Bowling Green, OH, 1976; his B.S. degree in welding engineering from Ohio State University, Columbus, OH, in 1986; and an M.S. degree in engineering from the University of Tennessee in 1993. ▀

Automated Measurement of Weld Shrinkage Recovery

Kirby Lawless/EH23

256-544-2821

E-mail: kirby.lawless@msfc.nasa.gov

The Marshall Center has directed a coordinated effort to bring advanced sensor technology to Shuttle manufacturing operations in order to provide fast and accurate measurements of weld shrinkage during planishing. The planishing operation is a peening process in which the weld bead is compressed with mechanical blows on one side of a particular part, while being restrained by an anvil from the part's backside (fig. 33). It is used to relieve residual stresses induced when weld repairs are made in the Shuttle's



FIGURE 33.—Planishing operations.

super lightweight tank. Weld shrinkage and recovery of it by planishing is a key parameter determining weld quality and is typically measured using calipers placed into punch marks on either side of the weld.

Origin technologies developed a vision system in order to improve the accuracy of these shrinkage measurements, remove operator measurement error, eliminate data entry errors and speed the measurement operation. Marshall and Lockheed-Martin have provided validation testing, feedback for design improvements, and implementation efforts for the Shuttle external tank manufacture.

The system (fig. 34) utilizes a handheld camera and edge detection software routines to determine the distance between scribe lines placed on both sides of a weld or weld repair. As the sensor calculates the scribe line distances, it either displays the output measurements or transmits them to standard personal computer spreadsheet processing.

Benefits gained by the sensor implementation include an 8:1 gain in

measurement speed over handheld calipers, a greater than 50 percent measurement accuracy improvement, elimination of operator error, and elimination of operator transcription error.

The system has been tested on external tank flight hardware and is currently undergoing factory implementation trials at NASA's Michoud Assembly Facility. At the Marshall Center, it is currently being used for ongoing welding development activities and is the instrument of choice by lab technicians.

Sponsor: Office of Space Flight

Industry Involvement: Origin Technologies, Inc.; Lockheed Martin Michoud Space Systems

Biographical Sketch: Kirby Lawless is an engineer at the Marshall Center. He earned a B.S. degree in metallurgical engineering at the University of Alabama in 1976. He came to MSFC in 1989, working in the area of welding process automation development for external tank applications. Since then he has been extensively involved in welding automation and implementation of aluminum-lithium alloy weld development at MSFC. **D**

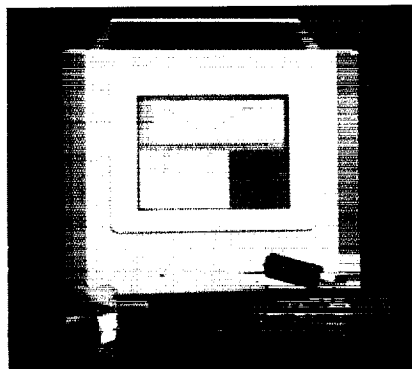


FIGURE 34.—Automated shrinkage measurement tool.

High-Strength Aluminum Casting Alloy for Automotive Applications

Jonathan A. Lee/EH23
256-544-9290
E-mail: jonathan.lee@msfc.nasa.gov

A new hypereutectic aluminum-silicon (Al-Si) alloy has been successfully developed at MSFC to have significant improvement in tensile and fatigue strengths at elevated temperatures of 315 °C (600 °F). The new alloy has the same high wear resistance, low thermal expansion properties as the commercial 390 alloy series, and it could withstand more heat than most conventional aluminum cast alloys. An automotive engine using the new piston alloy can improve the gas mileage and may produce less air pollution. This alloy was developed specifically to meet the U.S. automotive legislative requirements for low hydrocarbon engine emissions. The material projected cost is less than \$1 per pound, and it will allow automotive components to be cast at high production volume, high reliability, and at low fully accounted cost.

It is well known that most traditional aluminum casting alloys acquire their strength by the use of a small amount of alloying elements such as Cu, Mg, Si, Ni, and Ti. These elements strengthen the aluminum alloy by solid solution, precipitation or dispersion strengthening mechanisms which often involve the formation of aluminum intermetallic compounds. However, the effectiveness of these

major strengthening mechanisms are limited by high temperature and will decrease with time as the cast alloy is exposed to service temperatures over about 350 °F. For this reason, most commercial state-of-the-art aluminum alloys are unable to meet a constant demand for higher mechanical strengths at temperatures of above 400 °F. If such a low-cost aluminum alloy were available, it would help solve many of the high-temperature materials-related problems facing NASA, and particularly the automotive industry. It must be recognized that low cost is an important factor for mass production in commercial and automotive industries. It is undeniable that some advanced aerospace materials such as carbon-carbon metal matrix composites all have outstanding mechanical properties. However, unless they meet the automotive requirements for supplier infrastructure, high reliability and low material cost for mass production capability, such aerospace materials stand very little chance of making it into commercial production. One technical approach is to use high-strength ceramic fibers and particulates to reinforce conventional cast aluminum alloys which are called aluminum metal matrix composites (MMC's). Although some MMC's have reached the demonstrator stage, high production cost is still a major issue in the highly competitive automobile industry. It must be recognized that production cost includes not only raw materials, but also processing, labor, capital and energy.


This program objective is to develop a low cost, high wear resistance, low thermal expansion and castable Al-Si alloy for pistons to operate at high

temperatures in the range of 500 °F to 600 °F. Specifically, the objective of this program is to create a new monolithic castable aluminum alloy with significant improvements in high cycle fatigue strength of at least 30 percent higher than conventional aluminum alloy, which is rated at 10 million cycles at 600 °F. This goal will be accomplished through a combination of better casting process, new heat treatment schedule and/or development of a new castable aluminum alloy. Low material and processing cost will also be the primary goal of this program. Several commercial potential applications from this new alloy are listed below:

- High-performance automotive engine parts and heavy duty diesel engines
- Aircraft pistons, connecting rods, gear and generator housings
- Applications requiring high strength and wear resistance at elevated temperatures
- High strength, lightweight aluminum castings for the aerospace industry
- Internal combustion engine pistons, blocks, manifolds and cylinder heads
- Outboard motors, snowmobiles and recreational combustion engine parts.

Sponsor: Center Director's Discretionary Fund

Biographical Sketch: Jonathan Lee is a metallic materials researcher at Marshall's Materials & Processes laboratory. He worked as a materials consultant for the BDM Corporation prior to joining MSFC in 1989 as a program manager for the Geostationary Earth

Observatory Satellite. Lee has written a book on MMC's which has been in print and sold to the public since 1987 through Noyes Data Publisher in Park Ridge, NJ. His involvement in the development of graphite-magnesium MMC was selected by the NASA Technology Utilization Office in 1993 as one of the significant NASA technology transfers of the year. In 1995, he headed a joint program with Ford Motor Company of Dearborn, MI, to develop a new high-strength aluminum piston alloy. Lee received his M.S. degree in mechanical engineering from the University of Alabama in Huntsville in 1984. 

Weld Filler Wire Development for Aluminum Lithium 2195 Alloy

Carolyn Russell/EH23
256-544-2705
E-mail: carolyn.russell@msfc.nasa.gov

Aluminum lithium (Al-Li) alloy 2195 has been used to replace 2219 aluminum on the external tank. The 2195 alloy, although readily weldable, is very sensitive to heat input and therefore displays a propensity for cracking during repair welding activities. To overcome the difficulty in successfully repairing 2195 welds, 4043 filler wire was chosen for both the initial variable polarity plasma arc welds and the manual gas tungsten arc repairs. While 2195 is an aluminum-copper alloy (Al-Cu), 4043 filler wire is an aluminum-silicon (Al-Si) alloy enabling better repairability, but lower weld strengths.

The objective of this program was to identify an aluminum-copper based filler wire for use in fusion welding 2195 which would overcome the repair weld cracking experienced with 2319 filler wire and result in higher weld strengths compared to the 4043 welds. To accomplish this, a test matrix was used to quantify the influence that eight alloying elements had on the properties of a 2195 plasma arc weld. The elements evaluated were copper (Cu), lithium (Li), silver (Ag), magnesium (Mg), zinc (Zn), manganese (Mn), vanadium (V) and titanium (Ti). Six additional chemistries were

evaluated to provide a more focused investigation of specific elements which have been shown in the past to be beneficial in a filler alloy.

For each of the 14 filler wire chemistries, tensile, fracture, stress corrosion cracking resistance, and weld microstructure data were evaluated. Also, both qualitative and quantitative assessments were made of the propensity of repair weld cracking for each of the chemistries. The filler wire chemistries were ranked using a 75 percent weldability and 25 percent mechanical properties weighting.

Results of the tests showed that filler wires containing higher Cu and no Li additions were the least susceptible to weld cracking, while still maintaining good mechanical weld properties. Though interactions between the majority of the elements were observed, the most significant positive factors found were Cu, Ag, Mg, Zn and Ti. The most negative factor was Li. Ag and Mg together form a strengthening phase in the as-cast weld structure.

The test matrix and the approach to element evaluation were successful in determining the influence of elements on the as-welded ultimate and yield strength, and elongation. From these results a confirmation chemistry as well as three other chemistries were determined for further evaluation. The four new chemistries, containing Cu, Ag, Mg, Zn, and Ti additions have shown promising results in decreasing the propensity for repair weld cracking while maintaining higher weld strengths than comparable welds made with 4043 filler wire on 2195 Al-Li.

Bjorkman, G.; Cho, A.; Sisk, D.:
"Filler Wire Development for 2195
Aluminum Lithium," Part 1 Report,
Contract No. NAS839929, Decem-
ber 1996.

Sponsor: Office of Space Flight

Industry Involvement: Lockheed
Martin Astronautics and Michoud
Space Systems; Reynold Metals
Company

Biographical Sketch: Carolyn Russell
is a welding engineer at the Marshall
Center. She came to Marshall in 1984,
working in the area of welding process
development for the Space Shuttle
main engine and external tank
programs. Since then she has built
extensive experience in aerospace
welding on a variety of materials using
several different welding techniques.
Russell earned a B.S. degree in
welding engineering at the Ohio State
University in 1983 and an M.S. degree
in materials engineering at Auburn
University in 1989. ▀

Vacuum Plasma Spray Forming of Propulsion Components

Frank Zimmerman/EH23
256-544-4958
E-mail: frank.zimmerman@msfc.nasa.gov

The Vacuum Plasma Spray Laboratory
at the Marshall Center has developed
and demonstrated a fabrication
technique using the vacuum plasma
spray process to form structural
components from tungsten and a
tungsten rhenium alloy. These
materials were selected for their high-
temperature ($>2,500^{\circ}\text{C}$) strength. The
components were assembled to form
the absorption cavities (fig. 35) of two
fully functioning ground test units for
solar thermal propulsion engines.
These engines are deliverables to the

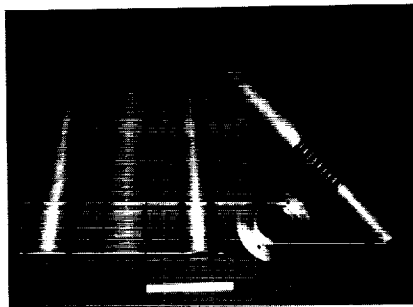


**FIGURE 35.—Vacuum plasma spray-formed
solar thermal engine
components.**



**FIGURE 36.—Assembled solar thermal
engine absorber.**

Advanced Industrial Transportation
Program consortium.

The absorber (fig. 36) functions as a
heat exchanger. Sunlight is concen-
trated and focused in the absorber,
raising the temperature to over
 $2,500^{\circ}\text{C}$. Each absorber cavity com-
prises three vacuum plasma spray-
formed coaxial shells with two
double-helical flow passages through
which the propellant gas flows. As the
gas flows through the helical channels,
it absorbs energy, expands, and exits
the nozzle. Through this process, solar
energy is converted to kinetic energy
and thrust. The test units built at MSFC
are designed to produce 2 to 2.5 N of
thrust using hydrogen as the propellant.

Vacuum plasma spray is a thermal
spray process conducted in a low-
pressure inert atmosphere within a
vacuum chamber. Plasma is generated
by flowing an inert gas through a
direct current arc. The gas ionizes,
forming a high-temperature plasma,
and exits through a nozzle into the
low-pressure (nominally 20,000 Pa)
environment. The material to be
deposited is injected into the plasma
as a fine powder, heated, and accel-
erated toward the substrate. Material is
deposited until the desired thickness is
achieved.

The engine components are formed
by depositing refractory metal onto a
graphite mandrel of the desired shape.
The mandrel acts as a male mold,
forming the required contour and
dimensions of the inside surface of the
deposit. Tungsten and tungsten/25
percent rhenium alloy were used in the
development and production of
absorber cavities for two test engines.
Two additional shells were spray
formed and used to refine the machin-
ing techniques for the test engines.

After the metal has been deposited to the desired thickness, the sacrificial graphite mandrel is removed. This is done by bead basting using a plastic medium, such as acrylic, which erodes the soft graphite leaving the sprayed deposit unaffected. If necessary, a "starter" hole can be machined into the graphite to provide access for the bead blast nozzle.

McKechnie, T.M.; Zimmerman, F.R.: "Metallurgy and Properties of Plasma Spray Formed Material," Proceedings of the International Thermal Spray Conference, Orlando, FL, pp. 839-845, May 1992.

Zimmerman, F.R. et al.: "Thermal Spray Forming of Refractory Metals and Ceramics for Space Furnace Containment Cartridges," Journal of Thermal Spray Technology, pp. 143-144, June 1995.

Sponsor: Advanced Systems and Technology Office

Industry Involvement: Rocketdyne Division of Boeing North American, Inc.

Biographical Sketch: Frank Zimmerman is a metallurgist at the Marshall Center. He came here in 1987 working in the area of welding process development on Space Shuttle main engine and external tank applications. Since then he has built extensive experience in thermal spray technology and in the development of vacuum plasma spray forming. Zimmerman earned a B.S. degree in metallurgical engineering at the University of Notre Dame in 1986. **D**

Material Robustness Testing and Nondestructive Evaluation Methodology Assessment for Liquid Rocket Engine Composite Nozzles—Phase I Results

Dr. Raymond G. Clinton Jr./EH32
256-544-2682
E-mail: corky.clinton@msfc.nasa.gov

Recent studies examining areas of opportunity to increase performance for the next generation of liquid rocket engines have identified the significant potential to increase the thrust-to-weight ratio for such engines by developing lightweight components. Weight reduction can be achieved by innovative design, in some cases, or through utilization of advanced materials. High-temperature composite materials offer one approach for weight reduction and cost savings relative to conventional regeneratively cooled metallic nozzles. The Materials and Processes Laboratory, with support from the Long-Term/High-Payoff technologies project of the Reusable Launch Vehicle (RLV) Program, initiated a project to address critical technologies required for the development of high-temperature composite nozzle extensions. A materials screening task and a second task to assess nondestructive evaluation (NDE) methodologies applicable to these material systems and component geometries were selected as critical technologies after discussions with Government and industry

organizations. A summary of the objectives and a brief overview of each of these tasks may be found in the 1996 MSFC Research and Technology Report.

For the materials screening task, relative to the material systems described in the prior report,¹ one material system has been added and one material system slightly modified. The complete list of material systems to be evaluated under this task is provided in table 2. The additional material, a coated carbon-carbon, was provided by Ceramic Composites Incorporated (CCT) and is shown as item 9 in the table. The modified material system is shown as item 8 in the table. Previously, the coating for this carbon-carbon composite was to have been applied by Amercom. Synterials, which acquired the coating technology from Amercom, applied the coating system.

Results of tensile strength tests conducted by Southern Research Institute (SRI) at room temperature, nominal use temperature, and elevated use temperature are provided in figure 37 for seven of the nine material systems. Tests of the remaining two materials have been delayed due to significant scheduling difficulties at B.F. Goodrich. The carbon fiber-reinforced silicon carbide matrix composites from DuPont Lanxide composites (DLC) exhibited the greatest high-temperature strength retention, and comparable performance between the two materials. The Hi-Nicalon reinforced materials from DLC and Dow exhibited comparable performance with expected loss of strength at the higher temperatures. The lower strength exhibited by the Synterials-coated materials is curious,

TABLE 2.—Nozzle material descriptions for robustness testing task.

Item	Material	Manufacturer	Yarn	Yarn HT	Fiber Architecture	Yarn Ends	Interface Coating	Matrix	Densification	Oxid. Inhib.	Coating
1	Enhanced C-SiC	Dupont Lanxide	1K T-300	1,700 °C	2D Plain	19/in	Yes	SiC	Isothermal CVI	Yes	Yes
2	Standard C-SiC	Dupont Lanxide	1K T-300	None	2D Plain	19/in	Yes	SiC	Isothermal CVI	No	Yes
3	Carbon-SiC	BFG	1K T-300	1,800 °C	2D Plain	19/in	Yes	SiC	Isothermal CVI	Yes	Yes
4	Coated C-C	CCAT	1K T-300	1,700 °C	2D Plain	30/in	Yes	C	Phen. Impreg	No	Yes
5	Hi Nic. SiC	Dupont Lanxide	1K Hi Nicalon	None	5 HS	17/in	Yes	SiC	Isothermal CVI	Yes	None
6	Hi Nic. SiNC	DOW	.5K Hi Nicalon	None	2D Plain	16/in	Yes	SiNC	PIP	Yes	None
7	Coated SiC-C	BFG	.5K Hi Nicalon	None	2D Plain	16/in	Yes	C	Isothermal CVI	No	Yes
8	Coated C-C	CCAT/Synterials	1K T-300	1,700 °C	2D Plain	30/in	Yes	C	Phen. Impreg	No	Yes
9	Coated C-C	CCI	1K T-300	None	2D Plain	19/in	Yes	C	Pulsed CVI	No	Yes

considering that the substrate carbon-carbon is the same as for the CCAT test articles. The CCI-coated carbon-carbon material system also exhibited a surprising loss of strength at the higher temperatures in comparison to the CCAT test results. An investigation of the microstructures of these materials is currently in progress in an attempt to learn the cause of strength

reductions. Fatigue results, to date, are provided in figure 38. Tests were conducted in air at nominal use temperature, with a mean stress above the predicted mean stress in the use environment. As can be seen, for these test conditions, the DLC-enhanced carbon fiber-reinforced silicon carbide and the CCAT carbon-carbon outperformed the other materials by a

substantial margin. The Hi-Nicalon reinforced materials performed poorly under these test conditions. Tests at lower mean stress levels will also be conducted to complete the fatigue assessment. Remaining testing for all materials is expected to be completed during FY98, pending resolution of B.F. Goodrich scheduling difficulties, and summary results will be provided in the Research and Technology 1998 report.

The initial phase of NDE methodology assessment is nearing completion at SRI. For this task, standard specimens were designed containing prescribed flaws representative of naturally occurring and critical defects. Descriptions of these specific defects produced in CCAT-coated carbon-carbon and DLC carbon fiber-reinforced silicon carbide are provided in last year's report.¹ Techniques utilized by SRI include ultrasonic spectroscopy, classical pulse echo ultrasonics, and radiography. Samples will subsequently be inspected at Argonne National Laboratory using air coupled ultrasonics, a technique amenable to full-scale article inspection, and two

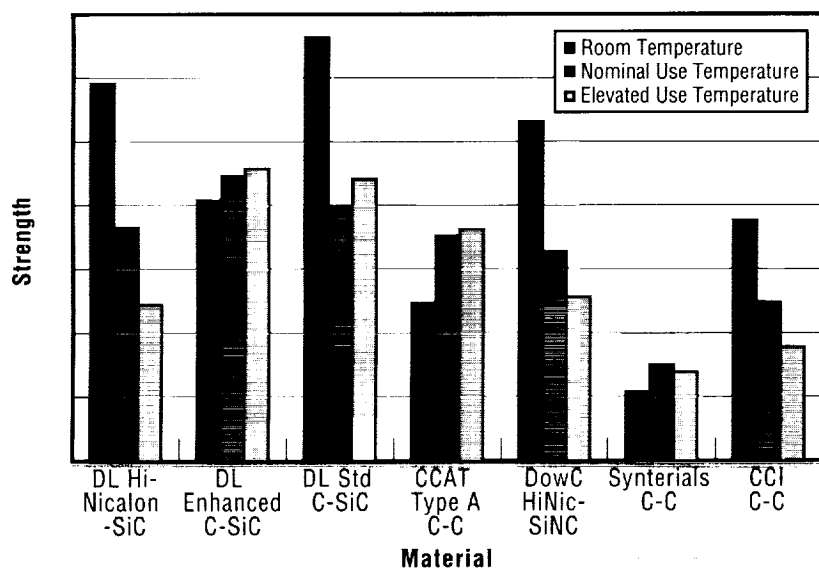


FIGURE 37.—Strength of nozzle candidate materials at various temperatures.

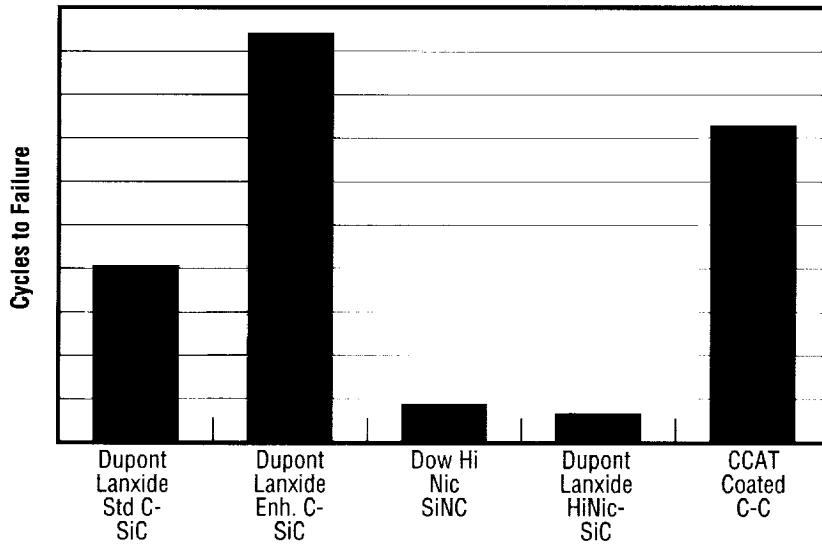


FIGURE 38.—Average cycles to failure in fatigue for nozzle candidate materials at 2,650 °F in air.

variations of thermography. The specimens will also be inspected at NASA Lewis Research Center (LeRC) before returning to MSFC for evaluation. Techniques to be used at LeRC include microfocus ultrasonics and computed tomography. Results of these basic efforts are expected to be presented in July 1998 at the Fifth International Congress of Composite Engineers in Las Vegas. A summary of the results and conclusions of the NDE methodology assessment task will be provided in the Research and Technology 1998 report.

1. Clinton, R.G., Jr.: "Material Robustness Testing and Nondestructive Evaluation Methodology Assessment for Liquid Rocket Engine Composite Nozzles," Research and Technology, 1996.

Sponsor: RLV Long-Term/High Payoff Technologies Program

Industry Involvement: Rocketdyne; Pratt & Whitney; Aerojet; Southern Research Institute; DuPont Lanxide Composites, C-CAT; Dow; B.F. Goodrich; Synterials; Ceramic Composites Incorporated; Argonne National Laboratory.

Biographical Sketch: Dr. Raymond Clinton is a supervisory aerospace materials engineer with NASA's Materials and Processes Laboratory at the Marshall Center, specializing in nonmetallic materials development and evaluation for rocket engine applications; composite materials (polymer matrix, carbon matrix, and ceramic matrix) selection, processing, material property characterization testing, performance evaluation and verification testing; development of material property databases for design and analysis; and program planning. He holds a Ph.D. in aerospace engineering from the Georgia Institute of Technology. ▀

Tooling Foam for Structural Composite Applications

Brett H. Smith/EH33
256-544-7036
E-mail: brett.smith@msfc.nasa.gov

Tooling technology applications for composite structures fabrication have been expanded at MSFC's Productivity Enhancement Complex. A tooling foam, MARCORE™, was developed in MSFC's Thermal Protection Systems Materials Research Laboratory for use in composite materials processing and manufacturing. In comparison with other tooling foam materials, this foam exhibits superior thermal and mechanical properties. Most tooling foam materials have a tendency to dissolve during autoclave conditioning, but MARCORE™ shows a much higher resistance to chemical degradation. A shelf life of at least 6 months is easily maintained when the components are stored between 50 and 70 °F. This tooling foam is compatible with most prepregged composite resins, such as epoxy, bismaleimide, phenolic and their associated cure cycles.

The MARCORE™ tooling foam system is a two-component, urethane-modified polyisocyanurate, high-density rigid foam that is environmentally friendly with zero ozone depletion potential. MARCORE™ also can be tailored to meet the requirements for composite processing of parts with unlimited cross-sectional area. Because of its processability, MARCORE™ is excellent for applications requiring

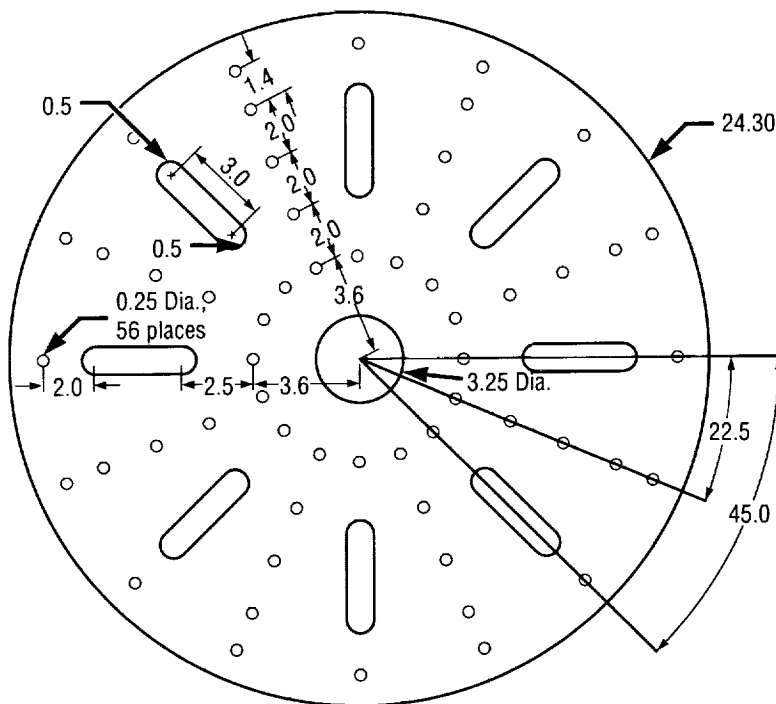


Figure 39.—Vent hole and stress relief slot configuration.

either integral or removable tooling and can be removed with a portable, 2,000 lb/in² pressure water system. This readily machinable, lightweight tooling foam is ideal for composite structures fabrication and is dimensionally stable at temperatures up to 350 °F and pressures up to 100 lb/in². The thermal stability of the foam is critical when parts are subjected to more than one autoclave cure cycle. The thermal stability capability can be increased when vent holes and stress relief slots are machined into the foam. These minor modifications help to reduce the foam's internal pressure by allowing trapped gases to escape,

thus providing a more even heat-up rate for the tool.

Prototype part fabrication includes mandrels for subscale composite cryogenic tank development activities and stiffener core fillers for tank wall simulation specimens. One challenge in working with this material is that although MARCORE™ is a closed-cell foam, it often exhibits voids along the mandrels surface after machining operations. This presents a manufacturing processing dilemma. To eliminate the voids and improve the surface finish of the composite part, a two-part silicone rubber mixture,

Silastic-E, has been applied with a low-pressure siphon feed paint gun. To date, MARCORE™ has proven to be an invaluable, cost-effective source of tooling technology and has reduced the intensive labor efforts associated with fabricating tooling for composite hardware.

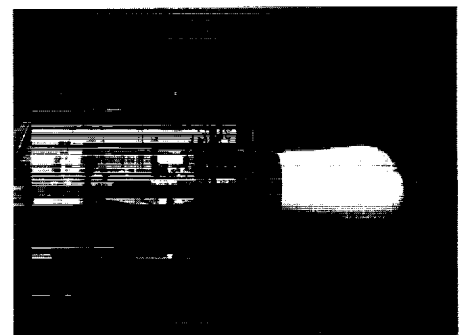


Figure 40.—MARCORE™ foam mandrel coated with Silastic-E.

Sponsor: Office of Space Access and Technology, and X-33 Task Agreement EH-09

Industry Involvement: Lockheed Martin Michoud Space Systems—MSFC Operations

Biographical Sketch: Brett H. Smith is a structural materials engineer in the Nonmetallic Processes Branch where he works with composites processing technology applications. He earned the bachelor of science degree in mechanical engineering from Southern University and A&M College in Baton Rouge, LA. ▀

Space Environmental Effects on Transparent Polymer Lenses for Inflatable and Rigid Space Structures

David Edwards/EH12
256-544-4081
E-mail: David.Edwards@msfc.nasa.gov

Transparent polymer films are currently considered for use as solar concentrating lenses for spacecraft power and propulsion systems. These polymer lenses concentrate solar energy onto energy conversion devices such as solar cells and thermal energy systems. Conversion efficiency is directly related to the polymer transmission. Space environmental effects will decrease the transmission and thus reduce the conversion efficiency.

Recently, much emphasis has been placed on the concentration of solar energy for spacecraft propulsion and electrical power systems. Increasing interest in lightweight structures that possess small stowage space and deploy on orbit are driving development towards flexible solar concentrators.

Transparent polymer usage as a solar concentrating lens is dependent on the ability of the polymer to maintain optical integrity while in the space environment. These flexible polymer lenses offer a number of distinct advantages from both the power system cost and manufacturability perspectives. Even with these advantages, these materials must demonstrate


long-term optical performance in the relevant space environment.

A large number of commercially available transparent polymers have been investigated to determine the effect of various simulated space environmental exposures on the polymer transmission. A method was developed to calculate the solar transmissivity over the wavelength range from 300 nm to 1,000 nm. This method allows the polymers to be ranked according to the tolerance of the space environmental exposure. A technique was also developed that demonstrates the effect of transmission degradation on the power output of a standard gallium arsenide (GaAs) solar cell. This technique can be used first to choose an optimum polymer/solar cell pair and second, to determine the solar cell surface area needed to maintain spacecraft power requirements throughout the mission lifetimes.

The results obtained in this study provide a small, but significant contribution to the database necessary to further the development and implementation of transparent polymers for space. Continued material development and quantitative testing are expected as the applications for these materials continue to expand.

Edwards, D.L., et al.: "Space Environmental Effects on the Properties of Selected Transparent Polymers," Proceedings of the International Solar Energy Conference, Solar Engineering, 1997.

Sponsor: Office of Space Flight

Biographical Sketch: David Edwards is a senior engineer in the Physical Science and Environmental Effects Branch in the Materials and Processes Laboratory. He is responsible for developing test systems which simulate the space environment, conducting space environmental effects tests on materials and characterizing the response of the materials to the space environmental exposure. Edwards has a master's degree in physics from Auburn University and is completing a Ph.D. in materials engineering from Auburn University. 

Hot Pressing Yttrium, Copper, and Barium Oxides to Form Bulk-Shaped $\text{YBa}_2\text{Cu}_3\text{O}_{7-x}$ Ceramic Superconductors

Tony Robertson/PS05
256-544-7102
E-mail: Tony.Robertson@msfc.nasa.gov

The Marshall Center is currently investigating several advanced space transportation systems which need magnetic confinement of various combustion gases and plasmas. Magnetic confinement in some cases will need bulk-shaped superconductors to allow for magnetic field compression at reduced weight compared to coil magnets.

The procedure for making the $\text{YBa}_2\text{Cu}_3\text{O}_{7-x}$ (Yttrium (Y), Barium (Ba), Copper (Cu), and Oxygen (O)) superconductor powder currently used to produce bulk ceramic superconductors involves a complex task of mixing the appropriate raw materials, which are calcined in a furnace at temperatures varying between 850 °C and 950 °C.¹ The resulting $\text{YBa}_2\text{Cu}_3\text{O}_x$ material is ground into powder form by hand or ball-milled in some cases up to 24 hr. The powder may be recalcined and reground to improve properties. The final powder is then sifted to ensure that individual particle sizes are in the millimeter range. To make the bulk-shaped $\text{YBa}_2\text{Cu}_3\text{O}_{7-x}$ ceramic superconductors, the $\text{YBa}_2\text{Cu}_3\text{O}_x$ powder is either cold or hot pressed into shape and sintered at temperatures up to 950 °C to promote

grain growth, typically for 12 hr (longer in some reported cases). It is then annealed in oxygen (or air) during cool down between 600 and 500 °C to maximize the absorption of oxygen, producing the $\text{YBa}_2\text{Cu}_3\text{O}_{7-x}$ structure.

As can be seen by the aforementioned procedure, it would be simpler to make bulk-shaped $\text{YBa}_2\text{Cu}_3\text{O}_{7-x}$ ceramic superconductors directly from a mixture of the raw materials. This research study is investigating the production of $\text{YBa}_2\text{Cu}_3\text{O}_{7-x}$ superconducting ceramic from the raw oxides using a hot press technique. The technique involves mixing the raw materials and pressing the mixture under various pressures and temperatures. This study utilizes a 300-ton hot press to form a solid 2-in.-dia. disk from approximately 70 g of the raw material. The same furnace is used for both sintering and oxygen annealing of the samples. The procedure for sintering and annealing is as described above.

The initial investigation started with barium nitrate ($\text{Ba}(\text{NO}_3)_2$) mixed with yttrium oxide (Y_2O_3) and copper (II) oxide (CuO) sifted to ensure a well-mixed mixture. This mixture performed well in the hot press. However, the nitrogen in the barium nitrate formed copper nitrate during the sintering cycle and melted into the silicon carbide plate that was being used to support the samples. This destroyed the sample and the silicon carbide plate. A procedure which raised the temperature slowly and holding for several hours at 650, 750, and 950 °C prevented the formation of the copper nitrate. However, no sample was produced from the oxygen annealing process that exhibited

superconductor properties during liquid nitrogen cooling.

The second mixture under study contains barium carbonate (BaCO_3) instead of the barium nitrate. Barium carbonate is typically the raw material used in the production of the $\text{YBa}_2\text{Cu}_3\text{O}_x$ powder. This mixture performed well in both the hot press and sintering cycles. A failure with one of the furnace's thermocouples allowed the sample to cool in air. And when placed in liquid nitrogen, the sample levitated a small magnet indicating that it was in a superconductive state. Oxygen annealing was not accomplished due to the malfunction in the furnace. However, other samples produced the same way and exposed to air cooling exhibited superconducting properties. Further investigating of the samples indicated that the densities of the ceramic disks were relatively low (approximately 4 g/cm² after sintering) compare to theoretical (6.3 g/cm²).

One cause for the low density is the outgassing of the carbon during sintering which leaves voids in the sample. Therefore, barium oxide (BaO) was used in the third mixture instead of the barium carbonate. This new mixture, however, formed a eutectic that caused the mixture to liquefy when exposed to temperatures above 500 °C and pressures above 2,500 lb/in². The liquefied mixture then seeped out of the die destroying the sample. A procedure, which involved cold pressing the mixture and then lowering the pressure to 1,500 lb/in² while the temperature was raised slowly to 550 °C, prevented the mixture from totally liquefying. Samples that were held overnight (about 14 to 16 hr) at 550 °C had a

density after sintering of approximately 5 g/cm^2 . This is a significant increase over the samples with barium carbonate. Due to the furnace malfunction, a different sintering furnace was used for these samples. This furnace does not allow air or oxygen cooling. Therefore it was no surprise that no sample exhibited superconductor properties in liquid nitrogen.

Plans are to conduct more tests on the samples with barium carbonate and barium oxide once the annealing furnace is repaired. Once a suitable mixture and procedure are established, doping of the mixture with various materials like silver (Ag) and tin (Sn) will be conducted. These doping materials have been shown to increase the superconductor properties of the $\text{YBa}_2\text{Cu}_3\text{O}_{7-x}$ Superconductor ceramics.^{2 3}

1. Salama, K.; Ravi-Chandar, K.; Selvamanickam, V.; Lee, D.F.; Reddy, P.K.; and Rele, S.V.: "The Influence of Fabricating Technologies on the Structure and Properties of $\text{YBa}_2\text{Cu}_3\text{O}_{7-x}$," *Journal of Metals*, pp. 6-10, August 1988.
2. Monot, I.; Higuchi, T; Sakai, N.; and Murakami, M.: "Possibility of Tc and Jc Enhancement in 10% BaSnO_3 - Doped MPMG - Processed YBCO," *Supercond. Sci. Technol.* 7, pp. 783-786, Printed in the UK, 1994.
3. Dayt, M.J.; Sutton, S.D.; Wellhofer, F.; and Abell, J.S.: "The Microstructural and Critical Current Properties of Melt-Processed YBCO + Ag Thick Films," *Supercond. Sci. Technol.* 6, pp. 96-105, Printed in the UK, 1993.

Sponsor: Advanced Space Transportation Research

Biographical Sketch: Tony Robertson is an aerospace engineer in the Advanced Concept Office at MSFC. He serves as the project integration manager for the newly developed Advanced Space Transportation Research Facility, which supports various research experiments in the areas of fusion, fission, magnetohydrodynamics (MHD), and gravity shielding. He is also the MHD and magnetics technical lead. Tony earned a B.S. in physics and mathematics from the University of North Alabama in Florence, AL, 1982. He earned a master's in operation research from the University of Alabama in Huntsville (UAH), 1993, and will soon complete a second master's in engineering management from UAH. He also plans to seek a Ph.D. in engineering management. ■

Pressure Controlled Atomization Process for Permanent Magnet Fabrication

Tony Robertson/PS05
256-544-7102
E-mail: Tony.Robertson@msfc.nasa.gov

The Marshall Center is currently investigating several advanced space transportation systems which need magnetic control of various conductive gases, including combustion gases and plasmas. In some cases, there will be a need to easily fabricate thin layers of high-field permanent magnets to allow for control of the conductive gases at reduced weight (compared to coil and bulk permanent magnets). The pressure controlled atomization process (PCAP) is a thermal spray process that may allow for such an application.

The PCAP has been developed by MSE-Technology Applications in Butte, MT. PCAP is a unique thermal spray process because it starts with the metal being sprayed in a liquid form rather than the solid wire or powder form of most thermal spray processes. This situation places a minimum of superheat into the liquid metal, and when the metal is sprayed as fine droplets of approximately 10μ dia., they can be rapidly cooled to form a metallic glass. The formation of a metallic glass is a necessary step in the fabrication of isotropic FeNdB (Iron (Fe), Neodymium (ND), and Boron (B)) magnetic materials. As the liquid droplets strike a substrate at high speed, they form a structure of interlocking splats that has signifi-

cantly higher mechanical strength than that of adhesively bonded powder materials. The droplets can be sprayed into a cooled mold of a specific desired shape to form a net shape magnet or as a magnetic coating on a part. The ability to fabricate the magnets in this manner can significantly reduce the steps to a finished product that will have a relatively high mechanical strength.

A schematic of the process is shown in figure 41. The PCAP consists of flowing a heated inert gas through a converging/diverging nozzle that contains an orifice in the nozzle throat.

Attached to the orifice is a tundish that contains a liquid metal. The tundish is pressurized with an inert gas. When the pressure on the liquid metal is greater than the gas pressure at the nozzle throat, the metal will flow through the orifice into the gas stream flowing through the nozzle, where it is atomized and given direction and momentum. This atomized liquid metal plume can then be deposited as a coating on a suitable substrate, or be built up layer by layer as a near net shape solid object. The pressurization of the tundish allows control of the liquid metal flow rate into the nozzle orifice.

Initial testing of the FeNdB material has demonstrated that it can be sprayed. The material is quite reactive and easily wets the hexagonal boron nitride material used to make the nozzle and tundish. This condition has made it difficult to obtain spray deposit consistency from test to test. MSE-Technology Applications is now in the process of looking for an alternate nozzle and tundish material that will not be wet by the FeNdB material.

Plans are for MSE to deliver to MSFC samples of the sprayed FeNdB magnetic material for characterization.

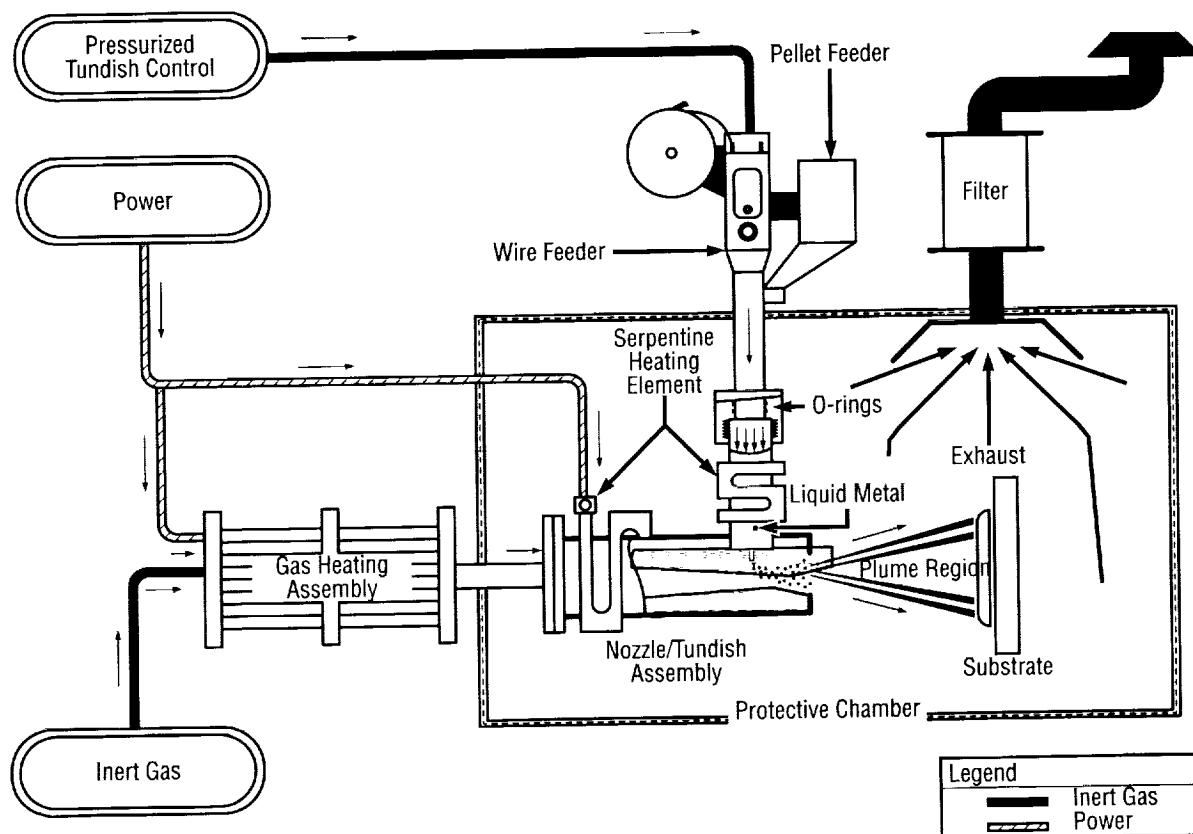



FIGURE 41.—Pressure controlled atomization process.

Sponsor: Advanced Space Transportation Research

Industry Involvement: Principal Investigator Ronald Glovan/MSE-Technology Applications. Glovan has both bachelor's and master's degrees in metallurgical engineering, and is a registered professional engineer. He has been associated with the development of PCAP since its inception at MSE-Technology Applications in 1989. Phone: 406-494-7416, fax 406-494-7230, e-mail: rglovan@in-tch.com.

Biographical Sketch: Tony Robertson is an aerospace engineer in the Advanced Concept Office at MSFC. He serves as the project integration manager for the newly developed Advanced Space Transportation Research Facility, which supports various research experiments in the areas of fusion, fission, magnetohydrodynamics (MHD), and gravity shielding. He is also the MHD and magnetics technical lead. Tony earned a B.S. in physics and mathematics from the University of North Alabama in Florence, AL, 1982. He earned a master's in operation research from the University of Alabama in Huntsville (UAH), 1993, and will soon complete a second master's in engineering management from UAH. He also plans to seek a Ph.D. in engineering management. 

Avionics and Optics

Video Guidance Sensor—Flight Proven

Ricky Howard/EB44
256-544-3536
E-mail: ricky.howard@msfc.nasa.gov

The video guidance sensor (VGS) has been under development at the Marshall Center for approximately 10 yr. During this time, it has progressed from a short range sensor (out to 10 m) that operated at 2 Hz, to a sensor that operates from 150 m to dock and outputs data at a 5-Hz rate. The latest version of the VGS flew on STS-87 in November 1997. The VGS target was mounted on the SPARTAN spacecraft, and the VGS sensor was mounted in the orbiter's cargo bay. The flight experiment was a success. The VGS acquired and tracked its target during tests performed with the Shuttle remote manipulator system (RMS). Due to an anomaly that occurred during the SPARTAN deployment, no long-range data were gathered during this flight experiment. The SPARTAN and the VGS are scheduled to fly again on STS-95 in October 1998.

The VGS consists of two major portions—a sensor and a target. The target is approximately 1-m wide and consists of filtered corner cubes arranged in patterns to allow tracking of two different sets of reflectors at different ranges. The sensor consists of two parts: the sensor head (with a camera, laser diodes, heaters, and thermoelectric coolers (TEC's)) and the electronics module (with a frame grabber, processors, and control electronics for the camera, laser diodes, and TEC's). The VGS works by taking two pictures of the target,

using the lasers to illuminate the reflectors in one picture and the background in the other, subtracting the background picture from the foreground picture and processing the results, and calculating the relative positions and attitudes between the target and the sensor. This relative position and attitude data covers all six degrees of freedom (x , y , z , pitch, yaw, and roll).

Figure 42 shows the VGS mounted on the SPARTAN flight support structure in the orbiter bay.

During the flight experiment, the SPARTAN with its VGS target was moved by the orbiter's RMS to 16 different positions relative to the sensor. At each of the 16 positions, the VGS took data while the RMS was

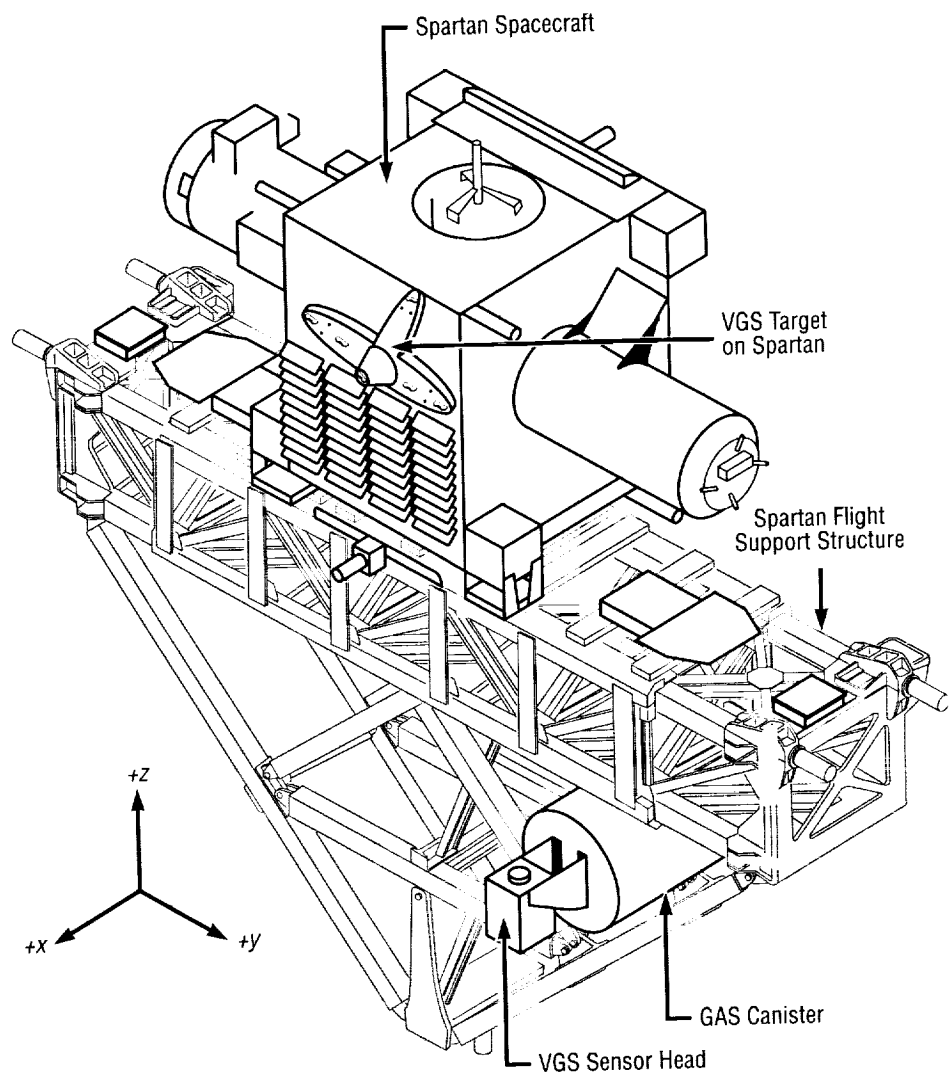


FIGURE 42.—The VGS mounted in the flight experiment configuration.

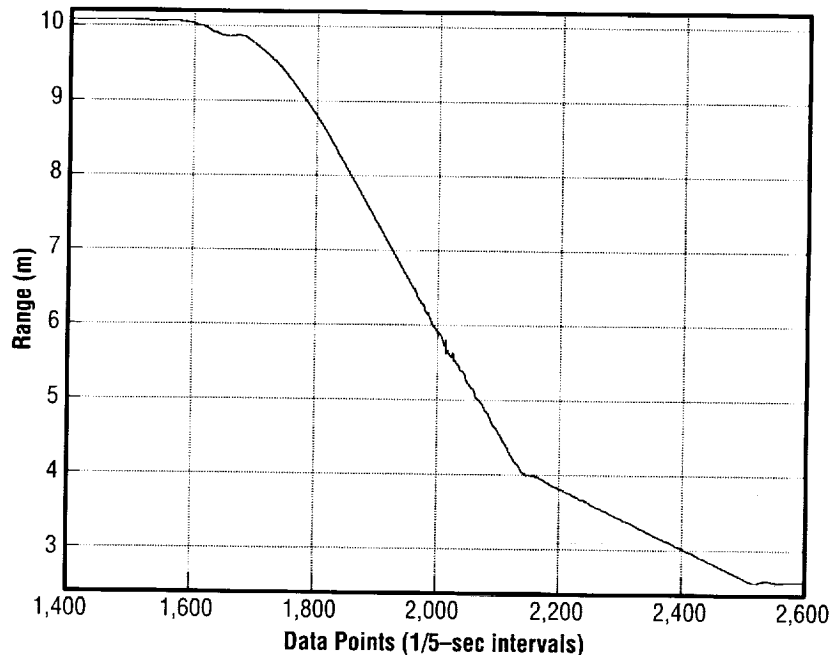


FIGURE 43.—Range from sensor to target while moving the RMS.

stationary, and then for most of the positions, the RMS rotated the target to generate varied pitch and yaw data for the VGS. Prior to the first position, the target was moved to a starting location of 10 m by the RMS. The sensor tracked the target as it was brought in from 10 m down to the first position at a range of 2.5 m. This plot is shown in figure 43.

The VGS is a part of the Automated Rendezvous and Capture (AR&C) program at MSFC. The AR&C program is developing all of the technologies necessary to perform automated spacecraft docking, and will demonstrate the complete system using closed-loop testing in the Flight Robotics Laboratory at MSFC. The VGS is the close-range sensor (110 m to dock) of the AR&C system.

Howard, R.; Bryan, T.; Book, M.; and Jackson, J.: "Active Sensor System for Automatic Rendezvous and Docking," SPIE Laser Radar Technology and Applications II Conference Proceedings, Vol. 3065, pp. 106–115.

Howard, R.; Cole, H.; Jackson, J.; Kamerman, G.; and Fronek, D.: "Automatic Rendezvous and Docking System Test and Evaluation," SPIE Laser Radar Technology and Applications II Conference Proceedings, Vol. 3065, pp. 131–139.

Sponsor: The Office of Space Flight sponsored the AR&C Ground Program. The MSFC Center Director sponsored the flight experiment.

Biographical Sketch: Richard Howard has worked at MSFC for over 16 years, starting as a cooperative education employee in 1981. He is currently working in the Orbital Systems and Robotics Team in the Astrionics Laboratory as the Responsible Design Engineer for the Video Guidance Sensor. This work involves overseeing the design of the VGS systems—optical, electronic, and mechanical; programming one of the embedded processors; and performing testing and integration of the components as well as analysis of all of the relevant data from the flight experiment. Howard graduated from the University of Alabama in Huntsville (UAH) in 1986 with a bachelor of science in electrical engineering. He then earned a master's degree in electrical engineering, majoring in control theory, in 1992, also from UAH.

Signal Conditioning Electronics for Discrete Capacitive Level Sensor Introduction

Randal S. McNichol/EB23
256-544-0907
E-mail: Randy.McNichol@msfc.nasa.gov

Kenneth L. Swords/EB23
256-544-3674
E-mail: Kenneth.L.Swords@msfc.nasa.gov

Dennis A. Smith/EB23
256-544-3531
E-mail: Dennis.A.Smith@msfc.nasa.gov

This document details the operation of the engine cutoff (ECO) signal conditioning electronics. The ECO electronics will be used on the Low-Cost Boost Technology (LCBT) Program propulsion test article one (PTA-1) at Stennis Space Center (SSC). The electronics were designed to provide a cut signal to the propulsion system controller (PSC) to cut the rocket engine in the event that the rocket propellant fuel (RP-1) or liquid oxygen (lox) tank(s) goes empty during testing. This is a ground-based test only; therefore, there are no flight ratings required on the electrical parts.

In addition to conditioning the ECO sensors in the PSC, the ECO signal conditioning electronics were designed with the capability to operate a capacitive sensor while not communicating on the Versa Module Eurocard (VME) data bus. This was accomplished by bringing the necessary communication signals and sensor status signals to unused/undedicated pins on the P2 connector of the ECO

signal conditioning electronics. This mode of operation is the basis for which the ECO card will be used for making facility measurements in the lox tank which is used for level indication of the "fill" tank (i.e., no control functions performed with "fill" tank sensors—used for indication of level only).

The ECO sensor signal conditioning electronics is a slave board in a VME bus chassis which comprises the PSC (fig. 44). There are two ECO sensor boards, one dedicated to the lox tank and another dedicated to the RP-1 tank. Each ECO sensor electronic board is comprised of three channels which interface with three separate

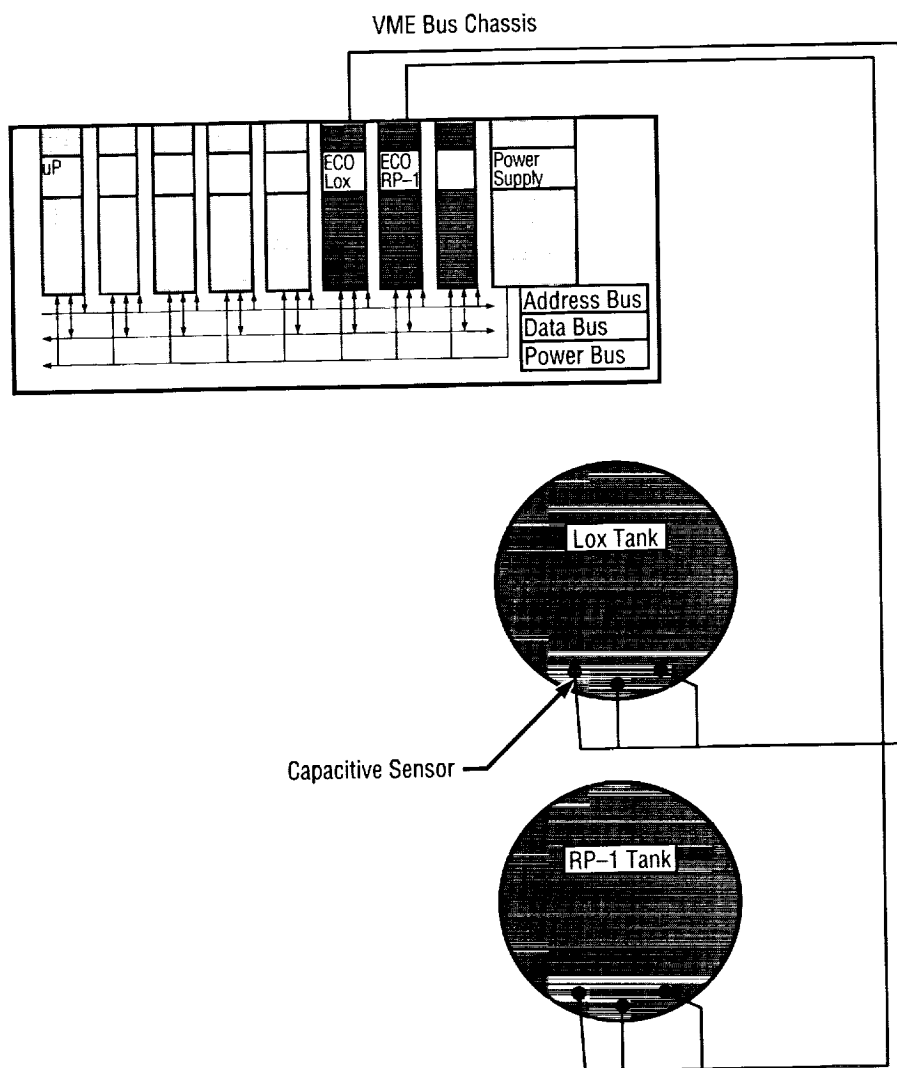


FIGURE 44.—Propulsion system controller.

capacitive sensors. Capacitive sensors mounted at the bottom of the tanks indicate wet or dry status signals to the ECO sensor electronics. A sensor cover by lox or RP-1 gives a "wet" signal, while a sensor exposed to only air gives a "dry" signal to the electronics. Wet or dry sensor status is then sent on to the master controller in the PSC.

The master controller or central processing unit (CPU) in the VME bus controls the exchange of information to and from the slave boards via the use of the address bus and the data bus. The master controller initiates data transfer bus cycles while a slave board detects bus cycles generated by masters. The address bus allows the master controller to access a particular board on the bus for communication while the data bus allows the exchange of data between the master controller and slave boards.

The status word is periodically sampled by the master controller and thus obtains sensor status information. The status word is comprised of a 16-bit word with each bit assigned a function to indicate sensor status—sensor wet or dry, sensor open or shorted, and whether the ECO sensor signal conditioning electronics is in calibration mode for each of the three sensors in each system tank.

Additionally, a command word is utilized by the master controller to command/control specific functions on the ECO sensor electronics board. The command word allows the master controller to electronically command the instrument to automatically calibrate itself and other test functions. The command word is also 16 bits in length.



FIGURE 45.—ECO board in VME bus chassis for operational checkout with liquid nitrogen.

The purpose of this instrument is to measure the discrete liquid level in a tank, i.e., a sensor covered by fluid is an "ON" (wet) signal and a sensor not covered by a fluid is an "OFF" (dry) signal. The sensor used in this design is a capacitive sensor. A capacitive sensor works by measuring the change in the dielectric between the plates of the capacitor as defined by the equation below:

$$C = \frac{\epsilon_0 A}{D}$$

Where: C = capacitance in farads

ϵ_0 = dielectric constant

A = area of the plates of the capacitor

D = distance between the plates of the capacitor

As can be seen from the above equation, as the dielectric constant changes (i.e., the medium or fluid that

the sensor experiences), so does the capacitance of the sensor. When the sensor is not covered by a fluid or substance it (i.e., sees only air across its plates as a dielectric) has a certain capacitance value. When the sensor is wetted by a fluid it experiences a different dielectric across its plates and has a different capacitance value. When the sensor is in AIR, the capacitance of the sensor is 5.45 picofarads (pf) and when the sensor is in lox, the capacitance of the sensor is 7.76 pf. In fact, this instrument was designed to measure a change in capacitance of only 2 pf at the end of a long coaxial cable (300 to 400 ft in distance).

To be able to measure such a small capacitance value, a circuit was developed that nulls out any induced stray capacitance from cables, solder traces and pin contacts. Stray

capacitance from cables and solder traces attenuates the measurement signal by providing another current path to ground. To alleviate this problem, a circuit was developed that adds an inductor in parallel with the system stray capacitance. By doing this, a parallel resonant circuit is formed with the stray capacitance and the effects of the stray capacitance are eliminated. The parallel resonant circuit formed from the system stray capacitance and inductor looks like an infinite impedance to the measurement system and eliminates a small leakage current-to-ground which originally attenuated the signal.

NASA Tech Brief MFS-31195.

Equipment Specification MSFC-PROC-2726.

Operations Procedure MSFC-SPEC-2724.

Sponsor: MSFC Low-Cost Boost Technology Program

Biographical Sketches: Randal S. McNichol is an electronics engineer in the Control Electronics Branch at MSFC. He is responsible for the design and development of electronic control systems and electrical instruments. He has a B.S. in electrical engineering from Memphis State University, May 1988.

Kenneth L. Swords is an electronics engineer in the Control Electronics Branch. He is responsible for the design and development of electronics systems/instrumentation signal

conditioning. He has a B.S. electrical engineering from the University of Mississippi, December 1983.

Dennis A. Smith is an electronics engineer in the Control Electronics Branch at Marshall. He is responsible for the design and development of electronic control systems, instrumentation and signal conditioning. Smith has a bachelor's degree in engineering with electronics and computer engineering major from the University of Alabama in Huntsville, May 1983. ▀

Determining the Fractal Dimension of an Image Using Wavelet Analysis

Kenneth Herren/EB52

256-544-4261

E-mail: Kenneth.A.Herren@msfc.nasa.gov

A technique for determining the fractal dimension has been explored recently (see, for instance, Argoul, et. al., 1989, Arneodo, et. al. 1992 or Jones, 1996a). This method uses the wavelet transform to pick out the singularity strength at each discontinuity in the scene. These researchers have shown that the wavelet transform is related to the fractal dimension for points of discontinuity in the image.

Given a fractal set, B , with mass support, $\mu(B(x, \epsilon))$, the equation for the increase of the mass with decreasing size, ϵ , is given by:

$$\mu(B(x, \epsilon)) = \int_{B(x, \epsilon)} d\mu(y) \sim \epsilon^s.$$

Note that $\mu(B(x, \epsilon))$ is just the portion of the total mass contained in a ball of radius ϵ centered at x . In most cases the fractal measure will scale differently from point to point and will exhibit a multifractal measure. In these cases the exponent s will then be replaced with a scaling function of the form, $\alpha(x_0)$, which defines the pointwise dimension, or singularity strength at location x_0 . The smaller the exponent, α , the more singular the measure around x and the "stronger" the singularity (Arneodo, et. al., 1995).

Then the equation for the pointwise dimension is given by:

$$\alpha(x) = \lim_{\varepsilon \rightarrow 0} \alpha(x, \varepsilon) = \lim_{\varepsilon \rightarrow 0} \frac{\log \mu(B(x, \varepsilon))}{\log \varepsilon}.$$

The scaling behavior of the mass density (with scale factor λ) at a particular point x_0 in the scene is just,

$$\mu(B(x_0, \lambda\varepsilon)) - (\lambda\varepsilon)^{\alpha(x_0)} = \lambda^{\alpha(x_0)} \varepsilon^{\alpha(x_0)} - \lambda^{\alpha(x_0)} \mu(B(x_0, \varepsilon)).$$

The strength of a singularity of a function is usually defined by the *Holder exponent* (e.g., Falconer, 1990, chapter 2). If f is a function such that $f(x)=y$ for domain x and range y and if:

$$|f(x) - f(y)| \leq c |x - y|^\alpha \quad (x, y \in X)$$

for a constant c , then f is known a Holder function of exponent α . Taking the Taylor series expansion of f at the point x_0 up to order n gives an n^{th} order polynomial. Replacing $f(y)$ by this polynomial gives the following,

$$|f(x) - f(x - x_0)| \leq c |x - x_0|^{\alpha(x_0)}.$$

If $\alpha(x_0)$ is contained in the open interval $(n, n+1)$ then it is clear that f is n times, but not $n+1$ times differentiable at the point x_0 . So, $\alpha(x_0)$ measures the irregularity of the function f near the point x_0 .

If the analyzing wavelet $h_{a,b}(x)$ has $m > \alpha(x_0)$ vanishing moments, then the local behavior of $\alpha(x_0)$ is mirrored by the wavelet transform which locally

behaves like the following (Mallat and Hwang, 1992):

$$W_h(a, x_0) \sim a^{\alpha(x_0)}$$

in the limit as $\varepsilon \rightarrow 0^+$. So the exponent can be extracted using a log-log plot of the wavelet transform amplitude versus scale parameter.

It has been shown by Holschneider (1988) that in the limit as $\lambda \rightarrow 0^+$ and for a wavelet, $h(x, y, a, b)$, that decays sufficiently fast at infinity, the wavelet transform scales like the following (Freysz, 1990):

$$W_h(\lambda a, x_0 + \lambda b) \sim \lambda^{\alpha(x_0)} W_h(a, x_0 + b).$$

This last equation mimics exactly that governing the fractal dimension, and is now popularly known as the wavelet transform modulus maxima (WTMM) method. Arneodo, et. al., (1992) have used an experimental arrangement to perform the convolution optically in order to calculate the values of the dimension. Their results showed that the dimension can be determined but the measurement suffered from the low dynamic range of devices used in the optical system. The fractal array size grows by the ratio of a^2 in each step of the formation of the fractal, and their imaging system was limited to $<1024 \times 1024$.

Jones (1996a) has used this technique to determine the dimension of fungal colonies grown on newspaper using various levels of nutrients. He reports that the fractal dimension of bacteria grown on newspaper alone is 1.406 ± 0.124 versus a dimension of 1.501 ± 0.076 for the same colony on newspaper with 2 percent cellobiose

added. The added cellobiose encouraged bacterial growth which produced more branching and resulted in the higher dimension.

Arrault, et. al., (1997) have used the WTMM technique to calculate the multifractal spectrum of 2D images, both random walk Brownian surfaces as well as Landsat images. These calculations produce a characterization of the roughness of fractal surfaces in the study of cloud models and satellite data.

Fractal sets rarely occur in nature independent from other forms of information. The image of a fractal-like tree line will most probably contain a very nonfractal barn, and the fractal noise in a communication system will have lots of real signal around it in the transmission. The techniques for determining the fractal dimension spectrum that have been discussed have used only purely fractal images. It is the intent of this research to investigate the dimension spectrum of fractal and fractal-like sets in the presence of nonfractal sources. The work will center around the obvious image processing context, but is general enough to fit any fractal process.

In any real image there will be some areas that contain 2D regions as well as some areas that might contain fractal-like clutter. Construction of the dimension versus image position for fractal only images will be done and then simple nonfractal objects will be inserted into the images and the resulting changes in the dimension map will be investigated.

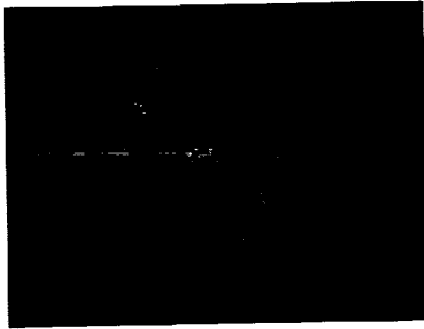


FIGURE 46.—The twindragon fractal.

The wavelet transform using the Mexican hat wavelet acts as an edge detection scheme for any solid 2D area in an image, so that the WTMM method will produce an array of zeros for the dimension of that area and some nonzero values around the edge pixels. The WTMM only calculates the value of the dimension at the discontinuities in the scene. This will help reduce the computation time since only those points where discontinuities occur are of interest. But the areas of zeros will contribute in a negative way to the value of the dimension spectrum for points near a solid object, but not so much for those points that are remote to the areas. The properties of other wavelets can be exploited to explore the characteristic values of the calculated fractal dimension of filled areas.

For a line of dimension one, the WTMM using the Mexican hat wavelet will return a value of one if the point is on the line and rapidly approaches zero elsewhere. Other wavelets will produce varying widths of values for the dimension near the line, but at the discontinuity (the line) the value of the dimension is always one. Thus, simple 1D nonfractal clutter will produce an obvious signature that can be used to eliminate

TABLE 3.—WTMM results.

Method		Dimension of Edge of Twindragon Fractal	
WTMM	Near Image Center	1.279	1.560*
	Near Image Edge	1.280	1.560
Sandbox		1.464	1.810
Theoretical		1.556	

*excluding low-scale values

those elements if the element is not "too near" its neighbors.

Figure 46 is the twindragon fractal. This is a well known set which is

fractal along the edges. The WTMM method was used to determine the fractal dimension at points along the edge of this fractal. The results are given in table 3.

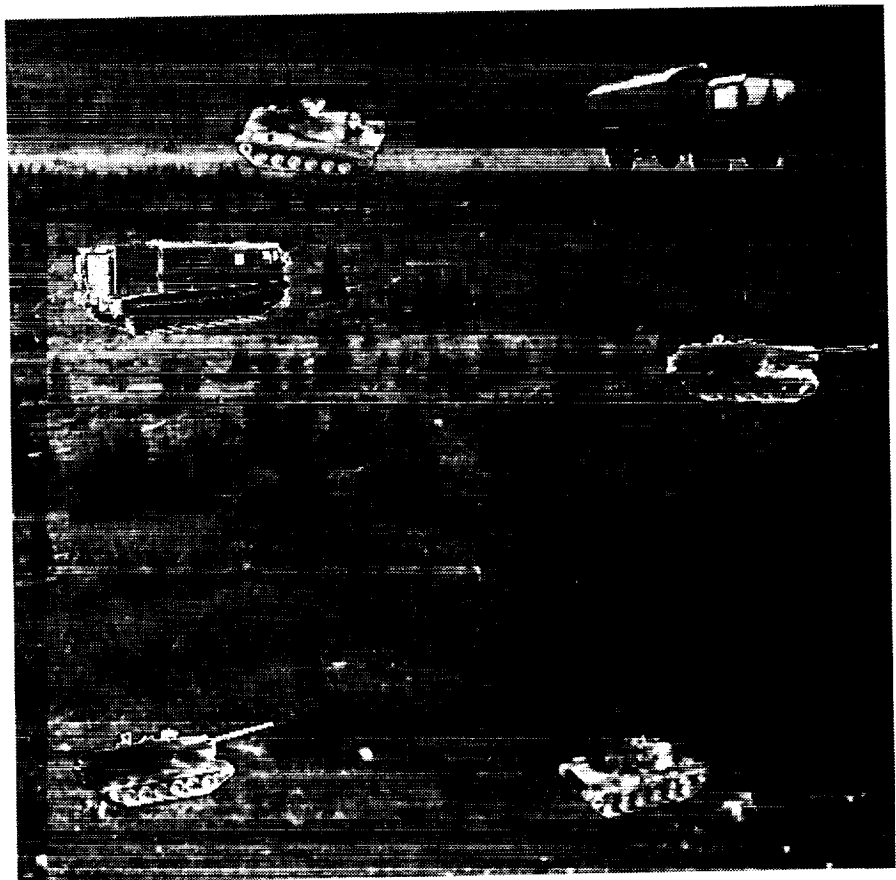


FIGURE 47.—Input image showing objects of interest.

Figure 47 shows a real scene containing objects of interest in a cluttered field. This image was used in the WTMM method, and the fractal dimension at every point in the field was computed. Figure 48 shows this result. It is obvious that the areas in figure 47 that contain the highest density of contours correspond to the objects of interest in the twin dragon fractal.

Argoul, F.; Arneodo, A.; Elezgaray, J.; Grasseau, G.; and Murenzi, R.: "Wavelet Transform of Fractal

Aggregates," *Phys. Lett. A*, Vol. 135, No. 6, 7, p. 327, March 1989.

Arneodo, A.; Argoul, F.; Muzy, J.F.; Pouligny, B.; and Freysz, E.: "The Optical Wavelet Transform," Y. Meyer ed., *Wavelets and Their Applications*, Springer-Verlag, Berlin 1992.

Arneodo, A.; Bacry, E.; and Muzy, J.F.: "The Thermodynamics of Fractals Revisited with Wavelets," *Physica A*, Vol. 213, pp. 232-275, 1995.

Arrault, J.; Arneodo, A.; Davis, A.; and Marshak, A.: "Wavelet Based Multifractal Analysis of Rough Surfaces: Application of Cloud Models and Satellite Data," *Phys. Rev. Lett*, Vol. 79, No. 1, 7, pp. 75-78, July 1997.

Falconer, K.J.: *Fractal Geometry, Mathematical Foundations and Applications*, John Wiley, Chichester, 1990.

Jones, C.L.: "2D Wavelet Packet Analysis of Structural Self-Organization and Morphogenic Regulation in Filamentous Fungal Colonies," Complex Systems Conference-From Local Interactions to Global Phenomena, July 14-17, 1996, Charles Sturt University, Albury, Wodonga, Australia, URL ref: <http://www.swin.edu.au/chem/bio/cs96/camjones.htm>.

Sponsor: MSFC Internal Research

University Involvement: The University of Alabama in Huntsville

Biographical Sketch: Kenneth Herren earned his B.S. and M.S. in physics from the University of Alabama in Huntsville. **D**

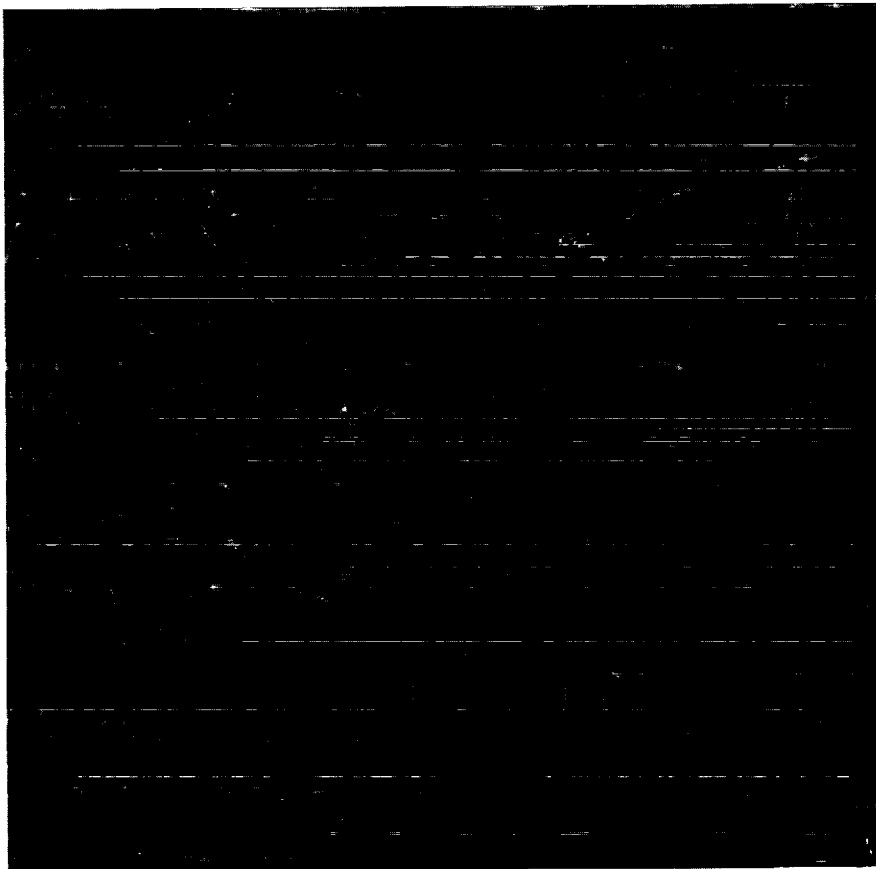


FIGURE 48.—Plot of fractal dimension versus position.

Composite Fresnel Lens for Solar Concentration and Alignment

Vinson B. Huegele/EB52
256-544-3475
E-mail: vinson.huegele@msfc.nasa.gov

MSFC is studying thin membrane fresnel lenses for use in deployable solar concentrators for thermal propulsion. A solar concentrator lens that faces the Sun to receive and focus the light also blocks any direct sight of the Sun to an alignment detector behind the lens on the spacecraft structure. A fresnel lens has been developed to both concentrate energy into a thermal cavity and relay solar orientation information to a detector.

While orbital telescopes maintain their target alignment by intercepting a beam from the primary optic near the focal plane, the focused energy of a solar concentrator would melt regular photosensors and thermal couples. No detectors can survive the thermal environment around the heat exchanger for the fine alignment of the solar spot. A divergent ray element was incorporated in the primary optic to direct sunlight to photodetectors placed away from the high temperature area around the heat exchanger.

The fresnel lens focuses light with a series of small concentric circular refractive or prismatic wedges instead of a continuous curved surface. This allows the lens to be very thin. At the location of the Sun-centering annulus (which is the series of groove rings that focuses light to the detector), the wedge angles have a different slope and direction than the adjacent

concentrator grooves. The light from these grooves is focused to a completely different path. A corresponding glass spherical lens design would have drastic surface discontinuities and could not be reasonably fabricated. The fresnel design allows a dual focus from a single lens without significantly altering the manufacturing procedures.

The composite design concentrates sunlight into a heat exchanger and provides an optical pick-off for maintaining alignment to the Sun. Instead of a point, the Sun-centering annulus focuses sunlight into a ring onto four symmetrically placed detectors at 90-degree increments about the optical axis. Each detector has a cylindrical lens that reduces the size of the solar disk.

The alignment optical path starts from the annulus on the fresnel lens. The solar alignment optics for one of the four optical paths is shown in figure 49. The detector location is at the ray's endpoint. Light travels from the Sun-centering annulus to a neutral density filter, then to a glass cylinder lens and finally through a bandpass filter to the detector. The cylinder lens condenses the Sun's image to a much smaller spot to fit on the detector. Each rectangular detector's length extends radially from the axis. As the Sun goes out of alignment, this spot appears to move directly toward or away from the optical axis on any detector on which it registers. A detector traces the Sun a little over 2.5 degrees and has an accuracy of ~ 0.01 degree over the first 1.0 degree. This provides a total field of view of at least 5.0 degrees.

Composite Fresnel Lens

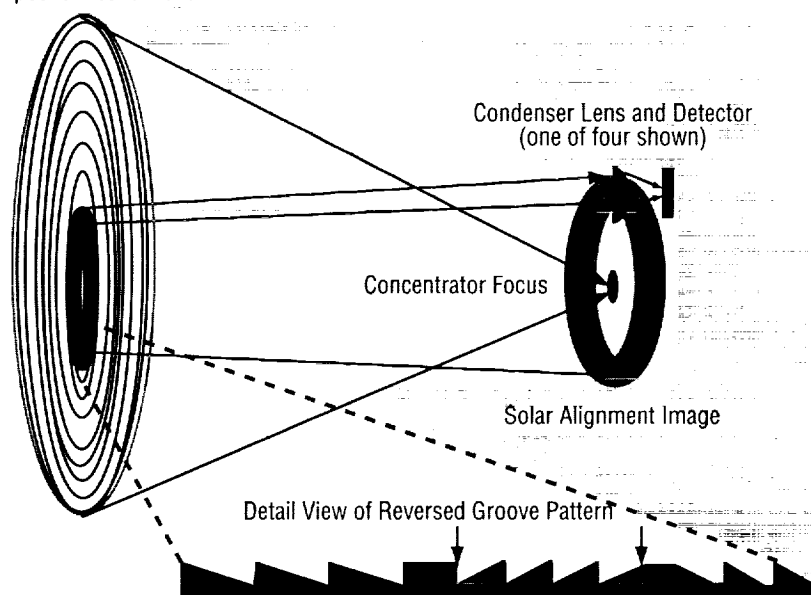


FIGURE 49.—Ray trace of the composite solar concentrator fresnel lens.

The composite lens was designed on CODE V optical design software. CODE V simulates a fresnel lens as a set of grooves, and refracts a ray at the surface by obtaining the local slope of the fresnel lens based upon the derivative of the standard CODE V sag equation for a high-order aspheric surface. Optical designs were obtained by employing sixth and eighth order aspheric coefficients, the conic constant, and the paraxial curvature.

The optical prescription for a model of the fresnel lens was designed and converted into a groove pattern compatible with the diamond turning machine at the MSFC Optics Branch. A mandrel was made by cutting the groove pattern into an aluminum blank with the machine. The polyimide membrane was cast on the mandrel to produce a fresnel lens.

The finished lens was illuminated by a collimated beam, and the focused images were observed and compared to the design values. The composite lens produced the expected alignment ring centered around the focus of the concentrator spot. Additional testing is planned with the detectors to measure the actual assembly performance.

By designing and producing a composite thin membrane fresnel lens, this research has improved the understanding of the technology to make functional fresnel solar concentrators. Innovative solutions are necessary to advance space deployable optics into actual flight hardware.

Sponsor: Office of Space Access and Technology

Industry Involvement: Micro Craft, Inc.

Biographical Sketch: Vinson Huegele is an optical physicist in the Optics Branch and has been with MSFC since 1980. He received his B.S. in physics from David Lipscomb University and his M.S. in engineering from the University of Tennessee Space Institute. ■

Rapid Prototyping of Diffractive Optics by Excimer Laser Micromachining

Dr. Helen J. Cole/EB53
256-544-6790
E-mail: helen.cole@msfc.nasa.gov

Advances in semiconductor processing techniques have made diffractive optical elements (DOE's) a viable technology that provides optical system designers with new degrees of freedom that can be used to drive future commercial as well as photonics-in-space technologies needing advanced sensors, high-speed data transmission, real-time information processing, high-density data storage, high-resolution displays and adaptive telescope aberration correction. Standard fabrication methods are often complex, expensive and time consuming. This effort demonstrates the use of a tabletop excimer laser micromachining workstation and optical surface profiler to prototype practical DOE's (having a relief pattern in flat or curved surfaces), in a matter of minutes to hours. This work was performed by Potomac Photonics, Incorporated of Landam, MD, and supported by Small Business Innovative Research (SBIR). In 1997, this technology was named by *Laser Focus World* magazine as a winner of their Commercial Technology Achievement Award for the year.

Figure 50 illustrates the ultraviolet (UV) laser micromachining workstation developed for this work. Beam size and shape are selected under computer control from an array of apertures, and imaged onto the

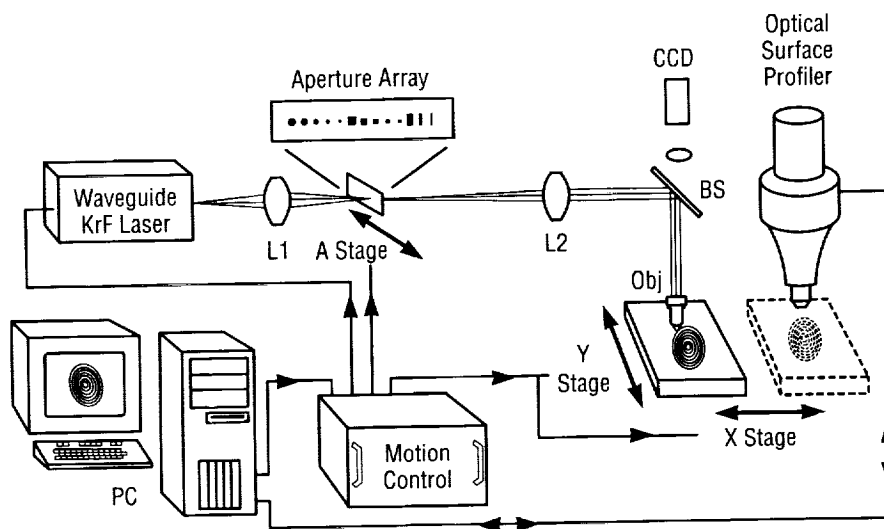


FIGURE 50.—The UV laser micromachining workstation and optical surface profiler.

workpiece. Controlled ablation of spin-coated poly(imide) films or direct ablation of polycarbonate lens materials is performed to create the diffractive surface relief structures. The UV objective (Obj) with camera allows through-the-lens real-time monitoring. The integrated optical

surface profiler permits rapid characterization and refinement of the micromachining process. Diffractive elements can be designed and fabricated at a single workstation. Typical write speeds for DOE fabrication are on the order of 200–5,000 $\mu\text{m}/\text{sec}$.

The fabrication of binary, multilevel, and blazed diffractive structures using the system developed here has been demonstrated¹ and applied in commercial test-bed optical systems.² An example of a multilevel diffractive element fabricated with the UV laser workstation is shown in figure 51. A three-dimensional contour plot of a detail of a four phase level bitmapped computer generated hologram (CGH) machined into polyimide is displayed in figure 51. The pixel size is 5 μm . White areas are unablated. The CGH has a $256 \times 256 \times 4$ -level unit cell that is repeated in a 2×2 array. Overall DOE size is 2.56-mm^2 . The optical reconstruction of the diffractive optical element is shown in figure 52. A 633-nm wavelength laser was used to reconstruct the diffractive element.

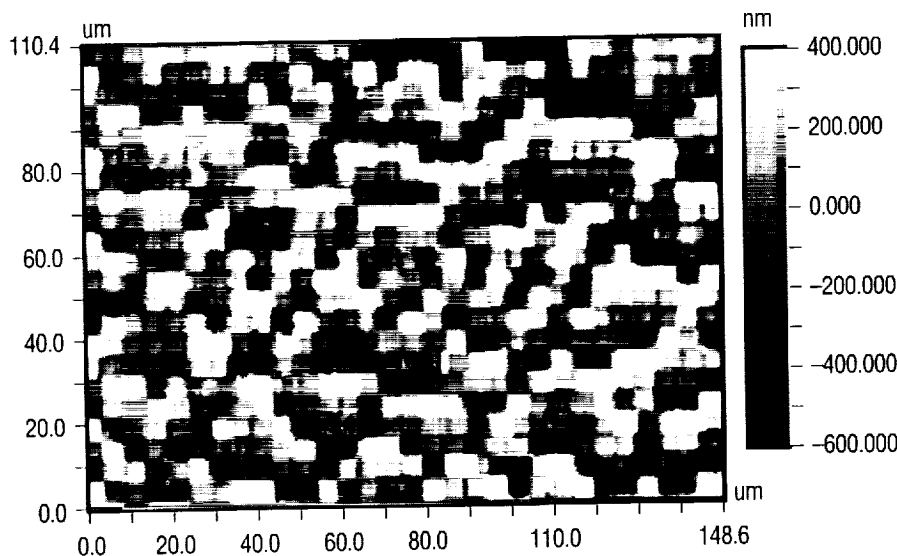


FIGURE 51.—Three-dimensional image of a detail of a four-phase level bitmapped CGH machined into polyimide.

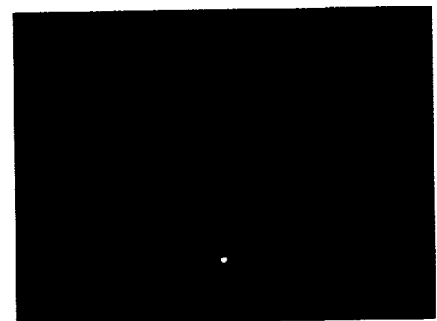


FIGURE 52.—An image of the reconstruction of the diffractive element shown in figure 51.

Plans for commercially funded developments in this area include methods to produce DOE's within materials other than poly(imide). Pattern transfer techniques are under study which use the polyimide written structure as a mask in a selective reactive ion processing process.

1. Behrmann, G.P.; Duignan, M.T.: "Excimer Laser Micromachining for Rapid Fabrication of Diffractive Optical Elements," *Applied Optics*, Vol. 36, pp. 4666-4674, 1997.
2. Johnson, E.G.; Brasher, J.D.; Gregory, D.; Erback, P.; Duignan, M.; Behrmann, G.; Lee, S.H.; Daschner, W.; Long, P.: "Optical Recognition of Phase-Encrypted Biometrics," *Optical Engineering*, 37, 1, pp. 18-26, 1998.

Sponsor: NASA MSFC SBIR Phase II contract No. NAS8-40572

Industry Involvement: Dr. Michael Duignan, Potomac Photonics, Inc., 4445 Nicole Drive, Lanham, MD 20706, telephone: 301-459-3031, fax: 301-459-3034, e-mail: mduignan@potomac-laser.com

Biographical Sketch: Dr. Helen J. Cole is an optical physicist in the Electro Optics Branch of the Astrionics Laboratory. She has worked in the Astrionics Laboratory since 1991 and is responsible for the development of diffractive optics technologies and their application to future space optical system requirements. Cole holds a B.S. in mechanical engineering from the University of Wisconsin, and a Ph.D. in mechanical engineering from the University of Alabama in Huntsville. ■

Phase Correction in a Semiconductor Amplifier Array Using Fiber Optics

Kenneth Herren/EB52
256-544-4261
E-mail: Kenneth.A.Herren@msfc.nasa.gov

Continuing investigations of new propulsion methods for space vehicles are beginning to include technologies for beaming energy from the ground to space. In one concept under consideration, an intense laser beam is converted into electrical power by a photovoltaic array, typical of those used on spacecraft today. While this is not currently used in space missions, demonstrations of the technologies needed to complete such a power beaming system are being accomplished. Earth-based power beaming could be used to power orbital transfer vehicles, geosynchronous orbit satellites, or *International Space Station*. Conversion efficiency from coherent laser light to electrical power is twice that possible in converting sunlight. Also, there is less waste heat generated in the array with laser light, making possible higher power incident beams. This could allow a 10-fold increase in converted power. Converted power could be used on board space vehicles for propulsion or payload operations.

Earth-based optical power beaming requires a high-intensity source and a system to address beam phase and location. A synthetic aperture array of phase locked sources can provide the necessary power levels as well as a means to correct for phase errors. A fiber optic phase modulator with a

master oscillator and power amplifier (MOPA) using an injection-locking semiconductor optical amplifier has proven effective in correcting phase errors as large as 4π in an interferometer system. Phase corrections with the piezo electric fiber stretcher were made from 0-10 kHz, with most application oriented corrections requiring only 1 kHz. The amplifier did not lose locked power output while the phase was changed; however, its performance was below expectation. Results of this investigation indicate that fiber stretchers and amplifiers can be incorporated into a MOPA system to achieve successful Earth-based power beaming.

Using fiber optics and a Canadian Instrumentation and Research Ltd. model 915 fiber stretcher, the phase of one beam was changed over 4π using OPD modulation (fig. 53).

The induced piston error changed the phase of one beam traveling through the fiber stretcher with respect to a beam that just went through fiber. The piston error was created by changing the OPD in one arm of a Mach-Zehnder fiber interferometer with the 915 fiber stretcher. The other fiber arm was kept at a constant OPD, and served as a reference path length. The fiber stretcher could create OPD changes of over four waves with modulation frequencies from 0-10 kHz.

Fringe movement in the interference pattern indicated a phase shift caused by fiber OPD change when the actuator stretched the fiber. Phase correction can be monitored using a feedback system, performing corrections to the OPD using the fiber stretcher with up to a 10 kHz frequency.

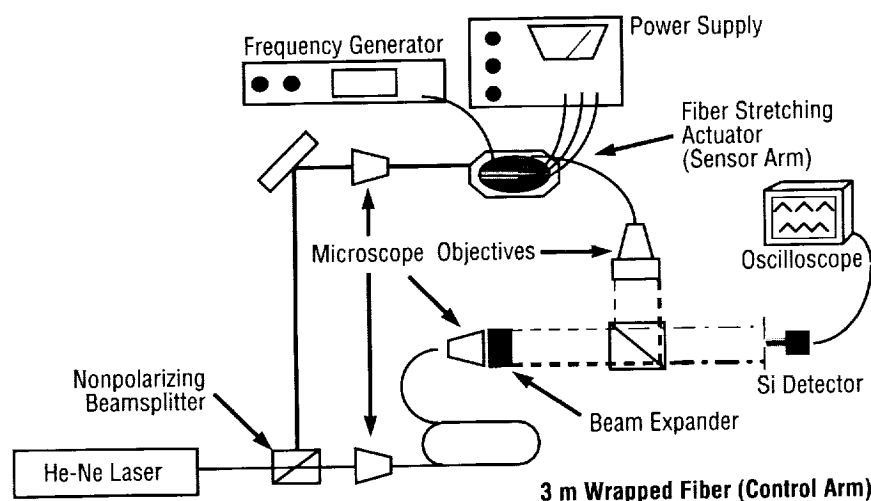


FIGURE 53. Experimental arrangement for phase correction.

In order to phase match beam paths across an array, the out of phase beams need a maximum π phase correction. This is a half-wave of induced piston error, which is easily attained with the CIR 915 fiber stretcher. Once the phase of a beam is sampled and corrected to a reference path in a feedback system, it can be amplified by an injection-locking semiconductor amplifier which boosts the output intensity. An array of optical amplifiers with fiber-coupled injection placed in a synthetic aperture geometry could provide correctable, steerable, coherent power. Injection-locked amplifiers that are locked in to their source signal preserve the phase and mode of the injected beam, and can amplify the locking beam while the phase is changing. These tests and experiments demonstrated amplification of a laser beam from an injection-locking optical amplifier loaned by Phillips Laboratories PL/LIDA group. The amplified emission from the amplifier was observed while the phase was changing in the sensor arm of the interferometer.

Investigation of a fiber optic phase modulator for an array of diode lasers has demonstrated that a fiber-stretching actuator can correct phase differences in an array of sources. An array using a MOPA system with fiber stretchers in the fibers leading to the injection-locking optical amplifiers can create a high-power coherent beam. The phase of each emitted beam is correctable, and the semiconductor devices are reliable and efficient for supplying high power over a long lifetime. An array of sources is not likely to have total power shutdown, and small angle beam steering is possible using phasing across the array instead of using a steering mirror. These advantages make the MOPA system with fiber optic phase modulators a possible solution for a laser power beaming source.

Further research work would be beneficial in advancing the principles found from the investigation and results of this work. Customized, single channel, one-pass, multiple quantum well injection-locking

amplifiers need to be obtained to replicate an actual array emitter. Knowing the true dimension, power characteristics, and cooling requirements is crucial to effectively model the output from these devices. The Phillips Laboratory model amplifier was suitable for technology demonstration, but not for actual system characterization because of difficulty in locking in the amplifier and lower than expected amplification results. The new amplifier should be manufactured to amplify an 835-nm injected signal, since this is a very good wavelength for transmission through the atmosphere. It is a good choice for conversion efficiency with satellite photovoltaic detectors, and ease of obtaining the master laser since 835 nm is a common diode laser wavelength.

Sensing electronics to fit a system for sensor fiber interferometers, such as a sampling Fabry-Perot interferometer, could incorporate feedback and correction to test the modulation frequency of the fiber stretcher with phase detection and correction at the target. This would also require fiber couplers and beamsplitter to be added into the amplifier fibers. Collimating optics such as lenslet arrays or small diffractive optics would provide high throughput and a collimated beam for test bench power measurements and far-field beam steering capabilities with a phased array of two or more amplifiers.

Feedback systems from the target could provide spot size and power distribution information usable by a feedback and correction loop at the source aperture itself. Propagation distortions and beam misshaping caused by atmospheric conditions can

be corrected with spatial light modulators, providing a method to test phase information from the target to correct piston errors and produce optimal spot size and power.

These additions to the current system and further research would facilitate progress toward system characterization with scaled down system modeling and bench testing. Completion of a system this size requires comprehensive technical and experimental test data, both of which would be greatly improved by adding these recommendations to the current system and continuing the scope of research.

The results of from this investigation conclude that a piezo electric fiber stretcher can reliably serve as a phase modulator. The CIR 915 fiber stretcher used in this experiment accurately changed the OPD in the fiber, using both a change in refractive index and fiber path length to create an observable phase shift in a fiber-based Mach Zehnder interferometer. The fiber stretcher proved to change the phase of one arm of the interferometer at least 4π radians over an operating range of 10 kHz modulation frequency. This fiber stretcher can be controlled using a servo board, and can be incorporated into a corrective loop system to correct for phase errors in propagating light.


The injection locked amplifier used in this research proved that it can amplify injected light that matched its design wavelength, within a temperature tuned bandwidth. Operation of the amplifier is very similar to diode lasers, and is a possible source for use in a MOPA system when combined with several other amplifiers in an array. The locked in operation of the

amplifier was not affected by the fiber stretcher changing the phase of the injected beam; therefore, a combination of the two could be used to emit near infrared light with a controllable phase angle.

The fiber stretcher and injection locking amplifier used in series in this experiment has demonstrated the ability to rapidly and reliably change the phase of an amplified output beam. The combination of a large number of phase controlled beams could be constructed as a phased array of semiconductor amplifiers in order to deliver very intense light to a detector target far away. Phase errors in propagation could be corrected at the array with the fiber stretchers using a correction and feedback loop.

Industry Involvement: Paul D. Burke, Nichols Research, Huntsville, AL, phone: 256-890-6276

Sponsor: Center Director's Discretionary Fund

Biographical Sketch: Kenneth Herren earned his B.S. and M.S. in physics from the University of Alabama in Huntsville. 

Solar X-Ray Imager X-Ray Detector Calibration

J. Kevin Russell/EB52
256-544-1168
E-mail: kevin.russell@msfc.nasa.gov

The objective of this work was to characterize and calibrate the Solar X-Ray Imager (SXI) soft x-ray imaging detector. The detector is based upon a microchannel plate (MCP) intensifier/converter, a charged coupled device (CCD), and a phosphor-coated fiber optic.

The Marshall Center developed an x-ray imaging detector for the SXI project. The SXI is an x-ray telescope designed to generate full disk, soft x-ray (6 Å to 60 Å) images of the Sun and will be flown on the Geostationary Operational Environmental Satellite (GOES)-M. The detector has three major components—an MCP, a phosphor-coated fiber optic, and a 512×512 -CCD. The incident x rays striking the walls of the 8-μ MCP pours create an electron avalanche. The electrons are accelerated into the phosphor coating on the fiber optic. The emitted light is channeled through the fiber optic and is detected by the CCD.

The calibration tasks were divided into two groups, x-ray sensitivity and spacial characterization. The goals were to 1) derive a relationship between incident x-ray flux and MCP voltage, and recorded CCD average digital number, 2) determine the single photon detection quantum efficiency, 3) derive the detector point spread function (PSF), 4) derive the

focal plane scale and, 5) characterize any spacial nonlinearities in the imaging system.

The instrument was calibrated in the MSFC detector calibration laboratory. The calibration facility was design and fabricated for soft x-ray detector calibration. The facility consists of a 2.4-m pipe, an x-ray generator, and beam monitoring flow proportional counters. Computer hardware and software were provided/developed for data archiving and analyses.

More than 1,200 images were acquired at aluminum (1.49 keV) and carbon (0.277 keV) energies during detector sensitivity calibration. Plots showing the detector response as a function of incident flux and MCP voltages were derived and utilized for telescope calibration. Incident radiation varying from 0.1 to 50 photons per pixel was readily observed. Also plots of the detector single photon detection quantum efficiency at these two energies were derived.

An etched nickel spatial resolution mask was placed in direct contact with the MCP surface for spatial resolution testing. This U.S. Air Force resolution chart consist of a series of closely spaced slit patterns of known width, length and spacing. By exposing the detector, with resolution mask, to a near parallel beam of x rays, the detector PSF and focal plane scale were determined.

The spacial linearity characterization test used a uniformly spaced pinhole array mask to measure any spatial distortions and to verify plate scale over the focal plane on the camera system. These data were utilized to

verify the detector gross and/or shear distortion effects of the fiber optic expander.

The detector was installed in the SXI telescope following successful characterization and calibration. The telescope was subsequently calibrated and shipped for integration into the GOES-M spacecraft.

Sponsor: Code Y, Earth Sciences

Industry Involvement: New England Advance Research Laboratory

Biographical Sketch: J. Kevin Russell is an optical physicist in the Optics Branch at MSFC and is the SXI Astrionics chief engineer. He has a B.S.E.E. degree from The University of Alabama. ■

Lightweight Nickel Alloy Mirrors for the Next Generation Space Telescope

John W. Redmon/EB52
256-544-9297
E-mail: john.redmon@msfc.nasa.gov

Engineers at MSFC and the University of Alabama in Huntsville Center of Applied Optics (UAHCAO) are working on a technology that will allow space-based telescopes to be bigger, better, and less costly than ever before. This technology involves the manufacture of large, lightweight nickel and nickel alloy mirrors using a novel technique known as electrolytic deposition, or electroforming. Mirrors made by this process are lighter and stronger than conventional glass mirrors and are not prone to catastrophic failure (brittle fracture). Further, manufacturing economy is exploited since the process does not involve grinding and polishing the optical substrate from thick sections.

In this process, nickel or a nickel-based alloy is electrolytically deposited onto a highly polished mandrel (cathode) which is submerged in a carrier media (aqueous nickel sulfamate); see figure 54. A deposition rate of approximately 0.2 mm/hr is achieved for a current density of 75 amps per square meter of cathode. Once the desired thickness (approximately 1 mm) is attained, the nickel shell (or mirror substrate) is removed from the bath, and released from its mandrel leaving a lightweight, high-quality mirror surface. This shell can then be laminated onto a lightweight

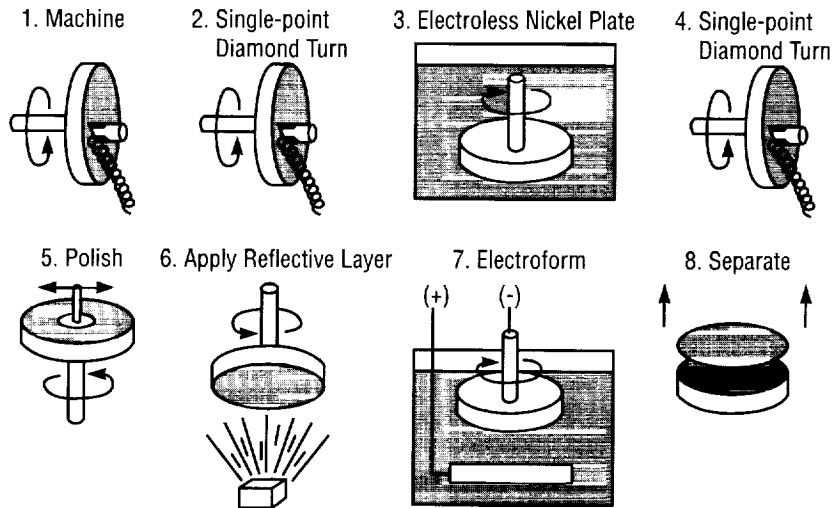


FIGURE 54.—Electroforming process.

composite structure thus producing a mirror that is 10 times lighter than those of conventional manufacture (i.e., grinding and polishing to shape). Since the mandrel (or master) can be reused, multiple mirror segments can be produced in a short time, thus further exploiting the economy of this technique. An example of this is shown in figure 55, the multisegmented Next Generation Space Telescope (NGST). Here, a very large telescope mirror is composed of an assembly of smaller mirrors which are easier to handle and produce, and are more readily available from conventional manufacturers/optical shops.

Space telescope performance is enhanced with an increase in the collecting area (area of the primary mirror). However, as the collecting area (and weight) increases, mission economy suffers. Therefore, to be better, future space telescopes must be bigger and lighter than the current state of the art; the proposed NGST is

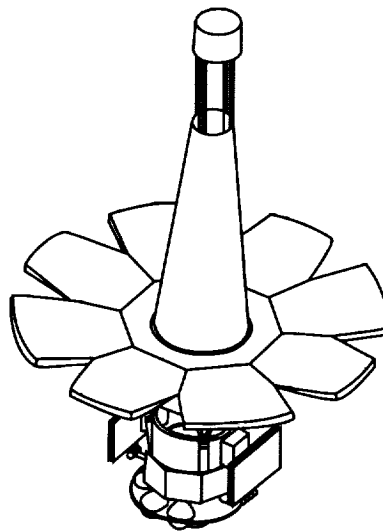


FIGURE 55.—The Next Generation Space Telescope.

designed to accomplish that. The NGST is an 8-m circular aperture, segmented telescope scheduled for deployment in the 2005–2010 time-frame. The NGST is a novel approach

to space astronomy predicated on substantial improvements to both the performance and economy of a large, space-based system. For one, the telescope must be deployed to its final configuration once in space, since a launch vehicle large enough to transport the primary mirror to orbit does not exist. Further, the optical telescope assembly (OTA) weight is not to exceed 1,000 kg; this equates to an areal density of around 15 kg/m^2 of collecting area (in contrast, the Hubble space telescope has a 2.3-m aperture and an areal density approximately 10 times greater). Robust, lightweight optics such as those produced from nickel or nickel alloys hold the promise for satisfying the NGST requirements; space telescopes that are larger, lighter, and less costly than ever before, are a step closer to reality due to this promising new mirror manufacturing technique.

Research is focused on the production of one-half-meter prototype mirrors to be used in structural, environmental, and optical testing. As of February 1998, several such mirrors have been produced (fig. 56). Current work involves optimization of the electroforming parameters so as to insure that no residual stress is plated into the substrate and that a uniform deposit is applied. Other work involves varying the composition of the electroforming bath with organic and/or metallic additives; this has been shown to markedly increase the strength of the deposit, and thus improve the precision yield point of the material. Also, methods to attach the optical substrate to an adjacent structure are under study; this involve electrojoining and bonding techniques in order to mitigate the effects of “print-thru” or “quilting” from differing thermal



FIGURE 56.— Prototype mirror for the Next Generation Space Telescope.

expansion rates. Once these parameters are tuned, optical testing will follow. It is expected that 1998 will bring the first successful interferometric optical test of these mirrors with cryogenic optical testing soon to follow.

Sponsor: Office of Space Science

University Involvement: Darell Engelhaupt, senior research scientist, University of Alabama in Huntsville Center of Applied Optics (UAHCAO)

Biographical Sketch: John Redmon is an optomechanical design engineer in the Optical Fabrication Branch of the Astrionics Laboratory at Marshall. ▀

Space-Borne Solar Vector Magnetograph Optical Design

Ron Eng/EB52
256-544-3603
E-mail: ron.eng@msfc.nasa.gov

The dark spots on the Sun are sunspots, and solar activity increases with the number of sunspots. These sunspots are sources of solar flares; their sudden release of energy is enormous and the effects can be damaging to human and electronic instruments in space and on Earth. The radiation dosage from the high-energy particles can be hazardous for astronauts working in Space Shuttles and Space Station, and can cause irreversible damages to satellite components. Solar flares are known to disrupt radio communications, navigation systems, electric power distribution on Earth, and satellite operations in space. The Sun has an approximately 11-yr cycle of solar flare activity. The next predicted solar activity peak is around year 2001.

The changes on the Sun's magnetic field that lead to the explosive release of energy in solar flares can be observed with a solar vector magnetograph. The front end of the solar vector magnetograph instrument is a Cassegrain telescope with series of optical filters, beamsplitters, imaging lenses and large array detectors or charge coupled devices (CCD) to spatially, spectrally, and temporally resolve the changing structures on the Sun's surface. Ground-based solar vector magnetographs suffered from

the Earth's atmospheric disturbances. A space-borne magnetograph will eliminate the Earth's atmospheric seeing fluctuation, which removes the optical transfer function of the polarized and unpolarized information of the Sun.

Space-borne optical instruments can lead to another set of engineering problems normally not encountered for ground-based optical instruments. Space-borne optical instruments must be able to survive the launch environment with high random vibration level and shock. Once in space, the optical components will cycle through extreme temperature in a short period of time. The combination of temperature excursion and random vibration can cause optical components to shatter and misalign. During instrument operation, spacecraft components can outgas and deposit onto critical optical surfaces. The space radiation will gradually darken most optical glasses over the lifetime of the instrument. The combination of outgassing and radiation darkening of glasses can lower the optical transmission of the instrument and lower the signal to noise ratio over time. In order to solve these engineering problems, special efforts must be taken into consideration during the initial design phase of the instrument design. The choice of optical materials used in the design involves trade off consideration for optical performance, thermal, structural contamination, weight, power, and cost.

Since the magnetograph instrument will be in a Sun-synchronous polar orbit for an instrument lifetime of 5 yr, the instrument will be exposed to

a moderate amount of particles associated with ionizing radiation, which include electrons, trapped radiation belt particles, and solar flare protons. The effect of a radiation dose above 1,000 rads on nonradiation resistant optical glasses will cause the optical throughput to attenuate dramatically over its operational lifetime. Radiation resistant optical glasses or Cerium doped glasses are necessary to allow the glass to stabilize against discoloration due to ionizing radiation.

The first order layout of the solar magnetograph optical system was analyzed with the CODE V optical design code to establish packaging requirements, and first order design specifications. The magnetograph optical system consists of the following key components: 1) A 60-cm diffraction limited Cassegrain telescope with a full aperture heat rejecting prefilter; 2) a highly sensitive polarimeter assembly consists of a rotating Glan-Thompson prism and polarizer; 3) a correlation tracker for accurate image pointing and tracking; 4) a high-resolution spectral filter of the Fabry-Perot etalon type; and 5) a large CCD array (2048×1024), with 22- μ pixels for a field of view of 8.5 by 4.3 arc min with 0.25 arc sec resolution across the entire field of view.

After the system components were defined, radiation resistant optical glass elements were inserted to meet various optical parameters. The 50-mm-dia. beam traversing the polarimeter must be collimated to minimize the field of view effect. In order to match the spectral width of

the Fabry-Perot etalon, the 150-mm-dia. beam traversing the etalon must be telecentric with 20 arc min of marginal ray angle. The final imaging lens has to match the 50.6 mm active image area. An aspheric optical element was used to minimize the image distortion. With all the optical parameters satisfied, the design spot size is 10 μ on axis, less than the 22 μ pixel size. The root mean square (rms) wavefront error is 0.025 waves on axis and 0.039 waves at the corners of the CCD.

An optical tolerance analysis was performed to see whether the system could be built with standard optical shop practice. Prototype optical shop tolerance was used for both linear and angular optical tolerance analysis. Some of the linear tolerance parameters are lens thickness, air spacing, radius of curvature, and index of refraction. Some of the angular tolerance parameters are optical element tilt and decenter within its optical mount, and optical wedge due to manufacturing errors. The rms wavefront error with tolerance is 0.076 waves on axis and 0.1 waves at the corners of the CCD. It is still within the system requirements.

This preliminary optical design would serve as a good starting point for any future space-borne solar vector magnetograph instrument design.

Sponsor: Center Director's Discretionary Fund

Biographical Sketch: Ron Eng is an optical design engineer at the Optical Branch at MSFC. He worked on the wide-field angle lenses for the

lightning imaging sensor and optical transient detector, technology mirror assembly realignment for the AXAF program, and the solar vector magnetograph. He received a B.S. degree in optics from the University of Rochester, and took additional graduate courses at the University of Rochester and the University of Alabama in Huntsville. ▀

Solar X-Ray Imager Alignment and Focus

Dr. Martin E. Smithers/EB52
256-544-3477
E-mail: martin.smithers@msfc.nasa.gov

J. Kevin Russell/EB52
205-544-1168
E-mail: kevin.russell@msfc.nasa.gov

The objective of this work was to align the Solar X-Ray Imager (SXI) detector charged coupled device (CCD) and to verify the alignment and focal position of the SXI. This was done using both an ultraviolet (UV) collimator and an x-ray source. Images were taken with the instrument CCD detector. The images were analyzed to determine the alignment and focus.

SXI is an x-ray telescope designed to generate full disk, soft x-ray images of the Sun and will be flown on an Geostationary Operational Environmental Satellite-M (GOES-M). The SXI instrument is an in-house project of the Marshall Center. It was built for the National Oceanic and Atmospheric Administration through NASA Goddard Space Flight Center which manages the development of the GOES spacecraft. The telescope mirror was built by joint effort between United Technology Optical Systems and Marshall.

The SXI mirror is a Wolter type I design (consisting of a paraboloid-hyperboloid pair) with the two approximately cylindrical grazing-incidence mirrors made from a single zerodur substrate and coated with



FIGURE 57.—SXI UV test set-up.

nickel. Nickel was chosen as the mirror coating to enhance the reflectivity for low-intensity low x-ray energy solar features. The flat detector surface was moved from the principal focus toward the mirrors in order to improve the imaging at large field angles.

The UV collimator test-bed was used to provide a baseline for telescope alignment and to verify that the alignment did not change significantly following environmental testing. Tests were conducted on the SXI telescope to determine the optical axis centering, the roll of the detector relative to the telescope mount, the tilt of the detector, alignment of the SXI mirror optical axis to the high accuracy Sun sensor optical axis and alignment of the SXI mirror optical axis to the telescope alignment reference. Testing was also conducted to check for changes in these quantities after environmental testing.

In the UV collimator tests, images produced by SXI were taken both on- and off-axis. At each field position, defocused images (rings) were taken and the ring radii and centroids were calculated. Also the focal positions were calculated by using the angle of convergence of the beam determined from the x-ray tests. These calculated values were then used to determine the various alignment parameters. This approach was used rather than looking directly at focused images because the SXI telescope could not be brought to an accurate focus in this configuration.

The x-ray focus tests were conducted in the MSFC Stray Light Facility. The purpose of the focus test was to determine the focal distance of SXI

measured from the position of the detector with the flight spacers inserted. The test was performed at various thermal conditions, including those expected on orbit. The results of the test were used to select the finite source shims needed to achieve the desired location of focus in the telescope characterization test (in front of focus to improve off-axis resolution at the expense of on-axis resolution). After environmental testing of SXI, the focus test was repeated (the focus verification test) to check for any change in the focal distances and to run various other thermal cases.

In the focus test, images were taken on-axis with flight spacers inserted between the mirror and the detector. Flight spacers are used to bring the telescope to the desired focus on orbit for an infinite source distance. Because of the finite source distance in the x-ray tests, the images produced were out of focus rings. Various shims were also inserted to shift the relative focal position and produce rings of different diameters. The diameters of the rings were calculated. Using the diameters with the different shims inserted, and knowing the thicknesses of the shims, a calculation of the linear projection of the ring diameters to zero yields a determination of the in-focus position with the finite source distance. Knowing the finite source distance, the expected focal position on orbit could then be calculated.

The final result was that in the UV tests no significant changes in the alignment and focus of SXI after environmental testing were observed. In the x-ray tests, the focal distances of the telescope were determined in various thermal cases, and these

distances were used to set focus. Also, no significant change in focus was observed after environmental testing.

Sponsor: Code Y, Earth Sciences

Industry Involvement: Staffan B. Persson/SVERDRUP, 205-961-0098, e-mail: staffan.persson@msfc.nasa.gov

Biographical Sketches: Martin E. Smithers is an optical physicist in the Optics Branch at MSFC. He does optical design and analysis. He has a Ph.D. degree in physics from Washington University.

J. Kevin Russell is an optical physicist in the Optics Branch at MSFC and is the SXI Astrionics chief engineer. He has a B.S.E.E. degree from the University of Alabama. ■

Modeling Optical Pulse Propagation Using Parallel Processing

Andrew S. Keys/EB53
256-544-8038
E-mail: andrew.keys@msfc.nasa.gov

Research performed by the author as a participant in the Marshall Center's Full-Time Study Program and by researchers at the University of Alabama in Huntsville (UAH) studies the evolution of ultra-short optical pulses as they propagate through multilayered stacks of dielectric material exhibiting a frequency-dependent photonic band gap. Of particular interest is the ability of these resonant transmissive structures to act as delay line elements in agile optical phased array technologies.¹ To assist in the study of pulse propagation within these structures, an existing numerical method has been used as the basis for a new simulation tool written to execute on a parallel processing computer platform.

Pseudospectral methods, sometimes referred to as finite or fast Fourier transform (FFT) methods, are often used to numerically describe the diffractive effects of propagating optical fields.² However, the standard FFT beam propagation method (FFT-BPM) assumes a slowly varying pulse envelope with respect to time. In the case of a multilayered resonant transmissive structure, the large discontinuities in refractive index between dielectric layers along the direction of pulse propagation violate the standard FFT-BPM's assumptions. Fortunately, modifications to the standard FFT-BPM have been made

to handle not only the rapid pulse envelope variation caused by large refractive index changes at each material interface, but to also handle the pulse's reflections and transmissions incurred at each interface.³ The modified FFT-BPM uses spatially-dependent functions to describe the pulse and structure profiles as opposed to using time-dependent functions, allowing a clear visualization of the pulse and structure interaction along the pulse propagation axis.

For accurate results, the distance over which the pulse is propagated with each iteration of the modified FFT-BPM algorithm must be small when compared to the wavelength of the pulse's carrier wave or the feature size of the resonant transmissive structure. This accuracy requirement implies the need for a large number of points to describe both the pulse and resonant transmissive structure within one computational window. FFT algorithms require the number of points within the computational window be equal to a power of two. Simulation runs using computational windows of 32,768 individual data points are common for this research. Additionally, depending on the chosen propagation step size, thousands of iterations may be required to propagate the pulse an appreciable distance through the computational window.

The ability to handle a large number of points per computational window combined with the numerous algorithmic iterations required for one simulation run necessitates the use of formidable computational resources. The MasPar MP-01 meets the computational needs for this research. The MasPar is a massively parallel processing computer platform utilizing

4,096 processing elements (PE's) in a modified single instruction multiple data (SIMD) approach to data processing. This type of system architecture allows a single set of program instructions to be executed on an array of potentially thousands of active PE's, with each PE maintaining a unique set of data values for designated program variables. Adapting the modified FFT-BPM for execution on the MasPar MP-01's parallel processing architecture allows a significant reduction in simulation time when compared to the same algorithm executing on a conventional, single processor computer platform.

Two sets of figures are included to illustrate the pulse propagation simulation as computed on the MasPar MP-01.

The three sequential frames of figure 58 show the evolution of a propagating pulse as it encounters a resonant transmissive structure configured to act as a dielectric mirror for the pulse's carrier frequency (defined to be 300 THz). The structure consists of 29 alternating simulated dielectric layers, 15 layers with a defined index of refraction equal to two interspersed by 14 layers with a defined index of refraction equal to one. The thickness of each layer is equal to one quarter of the pulse's carrier frequency's wavelength as measured within the material of that layer. This particular configuration is often referred to as a "quarter-wave stack" and serves to create a resonant transmissive environment characterized by a photonic band gap centered on the pulse's carrier frequency. Constructive and destructive resonances caused by the numerous transmissions and reflections within the structure result in a

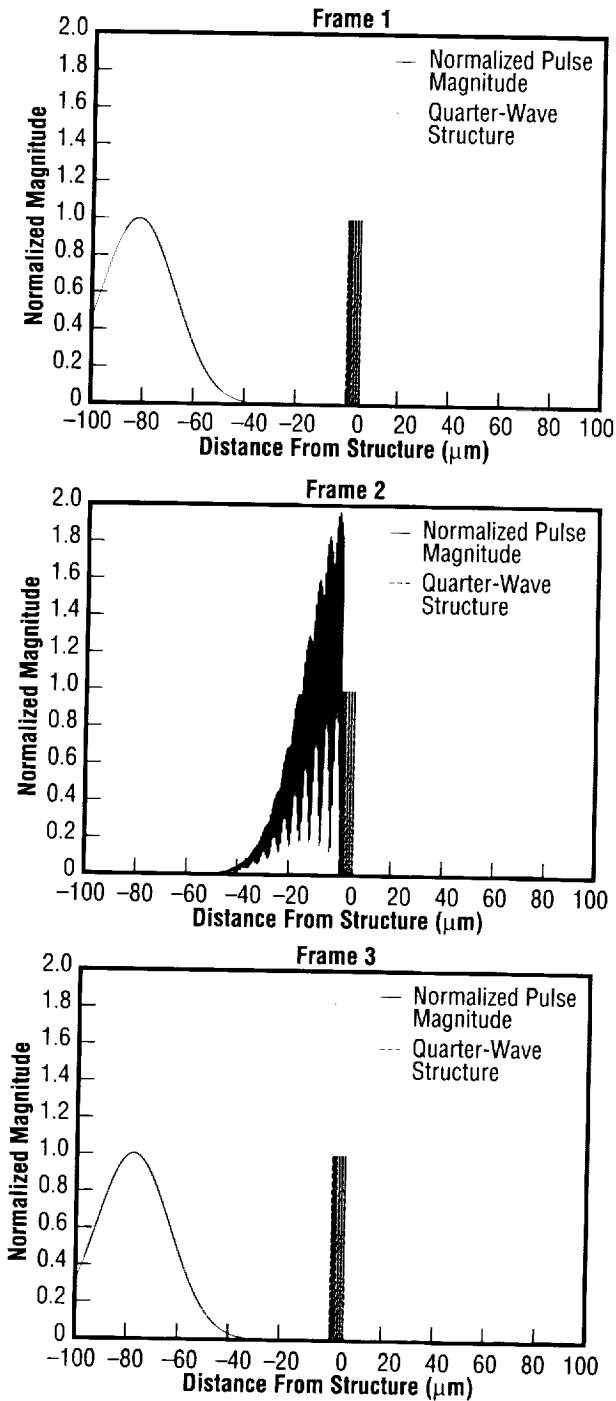


FIGURE 58.—A series of frames illustrating the evolution of a pulse encountering a "quarter-wave stack" of dielectric materials.

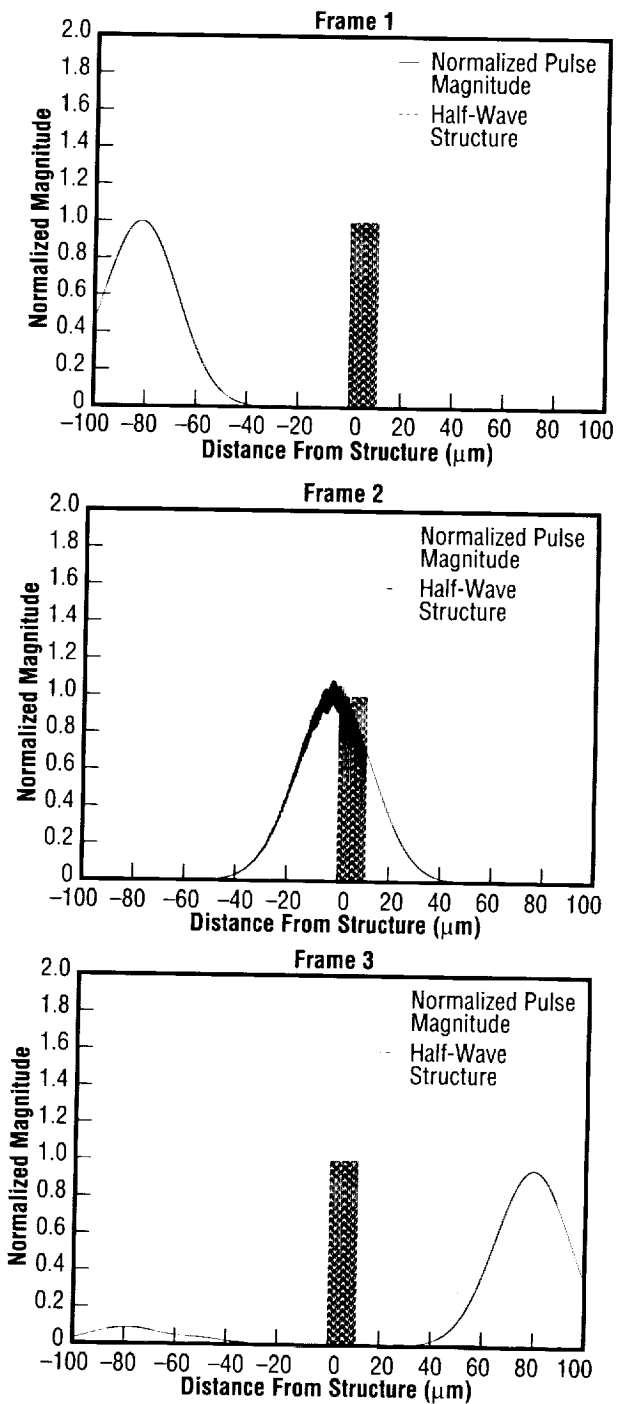


FIGURE 59.—A series of frames illustrating the evolution of a pulse encountering a "half-wave stack" of dielectric materials.

reflection of most of the pulse's frequency components.

The three sequential frames of figure 59 show the evolution of a propagating pulse as it encounters a resonant transmissive structure configured to act as a transmitting resonator for the pulse's carrier frequency (again defined to be 300 THz). For this case, the layer thicknesses of the structure described in the preceding paragraph are doubled, creating a "half-wave stack." When this stack is encountered by the propagating pulse, constructive and destructive resonances occur to cause a transmission of most of the pulse's frequency components.

The implementation of the modified FFT-BPM algorithm on the MasPar MP-01 computational platform serves as a valuable simulation tool for investigations into the intrinsic properties of resonant transmissive structures. A complete understanding of the interactions of the pulse envelope and the resonant transmissive structure provides the foundation for the creation of a unique and new class of optoelectronic devices, with application in agile optical phased arrays, optical switching, and optical modulators.

1. Fork, R.L.; Riasati, V.R.; Jones, D.K.; Jones, M.W.; and Dimmock, J.O.: "Physics of Excitations of a Small Number of Quanta in Microresonators," International Society for Optical Engineering (SPIE) Proceedings, Vol. 2994, pp. 287-299, 1997.
2. Feit, M.D.; and Fleck, J.A., Jr.: "Light Propagation in Graded-Index Optical Fibers," Applied

Optics, Vol. 17, no. 24, pp. 3990-3998, December 15, 1978.

3. Scalora, M.; and Crenshaw, M.E.: "A Beam Propagation Method That Handles Reflections," Optics Communications, Vol. 108, pp. 191-196, June 1, 1994.

Sponsor: Office of Human Resources and Education

University Involvement: Richard L. Fork/UAH; Darryl K. Jones/NASA Graduate Student Researcher Program (GSRP)

Biographical Sketch: Andrew S. Keys is an electronics engineer within the Electro Optics Branch of MSFC's Astrionics Laboratory where he is investigating optical phased array technologies. Keys earned a B.E.E. degree from Auburn University in 1988 and an M.S. degree in electrical engineering from Auburn University in 1990. He is currently working on the research portion of a Ph.D. in electrical engineering from the University of Alabama in Huntsville. ▀

Electrical Impedance Spectrometer Development and Analysis

Brandon S. Dewberry/EB23
256-544-4247
E-mail: Brandon.Dewberry@msfc.nasa.gov

The purpose of this investigation is the development of state-of-the-art electrical impedance spectrometry measurement and parameter identification techniques. Specific goals include increase in measurement accuracy and time resolution (speed) of acquisition with parameter identification. These techniques can be applied to many areas of science. Areas of interest to NASA include estimation of furnace material resolidification characteristics through electrical impedance spectra modeling, and measurement of changes in intracellular and extracellular fluid volumes in biological tissue, thus enabling investigations into many fundamental processes during adaptation to weightlessness.

In reference to figure 60, any dielectric fluid or solid material, including biologic tissue, acts as an RC equivalent circuit, with intracellular resistance, R_i , cell membrane capacitance, C_m , and extracellular resistance R_e . At low frequencies (<5 kHz) current flows mostly through extracellular fluid around cells. At high frequencies (>1 MHz) current flows through intracellular and extracellular fluid. An equivalent circuit model shown in figure 61 expresses the electrical impedance $Z(\omega)$ as a function of R_e , ω , C_m , and R_i . In actual dielectric

material or tissue, a distribution of time constants occurs resulting in a more complex model.

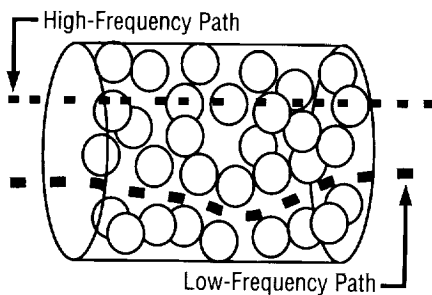


FIGURE 60.—Illustration of electrical current pathways with associated equivalent circuit.

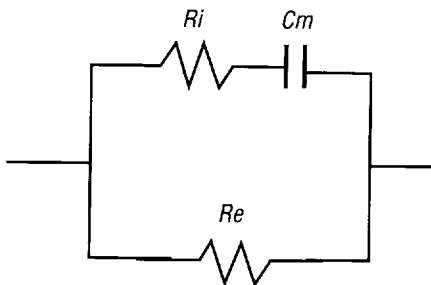


FIGURE 61.—An equivalent circuit model.

A tetrapolar (four electrode) system is used. A constant rms sinusoidal wave of 1 mA excitation current is imposed through outer electrodes, and the resulting voltage is measured across inner electrodes in order to minimize electrode impedance effects. Analog circuitry measures the phase difference between excitation and measurement waveforms. Analog signal conditioning rectifies, gains, offsets and smoothes the voltage and phase signals. The phase and voltage signals are digitized and stored on the PC using a multiplexing analog-to-digital converter. Excitation frequency can

be altered using a digital to analog converter and a voltage-controlled function generator. An optically isolated parallel port interface circuit was derived for safely interfacing to the personal computer. C code and a mathematical analysis package is used to archive, plot, and identify basic parameters of the model.

Sponsor: Center Director's Discretionary Fund

Biographical Sketch: Brandon Dewberry is an aeronautical engineer in the Instrumentation and Control Division of Marshall's Astrionics Laboratory. His duties include the development of instrumentation and control electronic systems for flight and ground-based systems. He earned his bachelor's degree in computer engineering at Auburn University in 1987 and completed a master's degree in electrical engineering at the University of Alabama in Huntsville in 1996. He is currently pursuing a doctorate in engineering at Vanderbilt University. ▀

Diffractive Optics by Direct Write Electron Beam Lithography

Brent L. Beabout/EB53
256-544-3611
E-mail: brent.beabout@msfc.nasa.gov

Researchers are currently investigating diffractive optics from several perspectives. Diffractive optics holds the promise of greater design freedom, lighter weight and more compact optics. Diffractive optics is directly applicable to integrated optic devices, micro-optic devices and traditional optic systems. Design and modeling tools are being developed to allow development of microlens and complex diffractive designs. Fabrication techniques are being investigated include photo-lithography, direct write electron beam lithography and laser writing. The characterization of the direct write electron beam lithography system fabrication techniques to produce small scale diffractive elements is the primary emphasis. Masters for diffractive elements have been fabricated using the electron beam system. Replica optics have been made and tested. Efforts are being made to modify the patterning software of the electron beam system allow for direct exposure control of geometric elements of a pattern. This facilitates easier implementation of complex phase functions of a diffractive optic element. This will reduce or totally eliminate the need for repeat exposures and the inherent alignment problems. A majority of these efforts have been in support of a Technology Reinvestment Program (TRP) with various members of private industry diffractive optics technology consortium.

This research is being conducted as a joint effort between the Marshall Center and the U.S. Army Air and Missile Command Weapons Sciences Directorate Research, Development, and Engineering Center. The research is currently supported by MSFC via the Center Director's Discretionary Fund and partially reimbursable space act agreement funds from the TRP. The prime contractor for the TRP is Rochester Photonics Corporation.

In order to fabricate diffractive optic devices it is necessary to be able to form structures on the order of a fraction of the wavelength of light being manipulated. Fabrication technologies used by the microelectronic industry can be adapted to create submicron structure sizes necessary to produce visible wave-

length diffractive optics. Direct write electron beam lithography techniques are being characterized to determine the best processes, capabilities and limitations of this technology to produce diffractive optics.

The initial goals were to establish exposure dose versus depth characteristics of polymethylmeth-acrylate (PMMA), and operational characteristics of the electron beam system. A test pattern

consisting of a series of binary gratings with 1- to 32- μ feature sizes was developed. Each set of these gratings was written at seven different dose levels by writing or overwriting each pattern up to seven times. Each write was done using the same dwell time and current density. Figure 62 shows the result of these calibration patterns.

Also generated was a microlens array. The lens design specification called for a 225- μ m-dia. f/3 lens (fig. 63). This design was implemented using a four-step binary approximation with 16 zones. Unlike the previous exposures, the different write depths were achieved by using different dwell times. An exposure file was required for each exposure level. This multiwrite process was necessary due

to original limitations in direct dose control in the original pattern generation software.

These initial results (fig. 64) show good promise for applying a direct write e-beam system to produce diffractive optics elements. The lens was also examined using an atomic force microscope (fig. 65).

The next step taken was to modify the pattern generation software to use the variable dwell capability inherent in the hardware design of the electron beam system. The original intended use of this system was production of microelectronic devices, and hence the pattern generation software was designed for two-dimensional pattern generation. Depth was irrelevant. However with diffractive optics, direct control of write depth of each fundamental element is highly desirable. Due to the variable flash sizes used for writing and to allow for proximity effect compensation, dynamic control of the dwell times and hence write depth is implemented in the figure generation hardware. But this was not directly controlled by the input pattern files. In the original software, dwell times for flashes in a subfield were derived from the beam current density, the critical dose parameter and the proximity correction control. Direct dwell time control was only supported for box shapes, not for polygon or arcs. Modification of the pattern software is being implemented to provide for the direct control of dwell time for these primitives. This supports direct control of the pattern depth of each fundamental elements (arc, polygon, or box) of a diffractive optic structure. More than 128 discrete exposure dose levels at any given beam current density are available

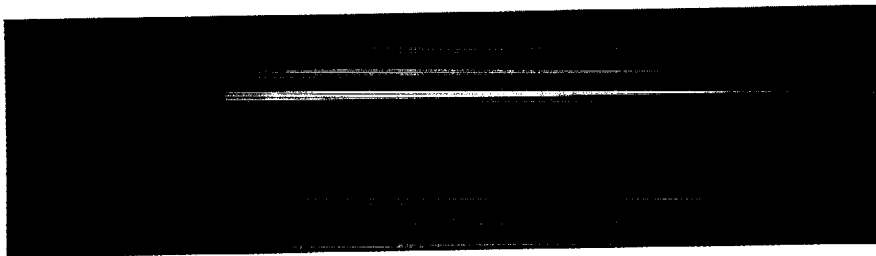


FIGURE 62.—Exposure calibration binary grating.

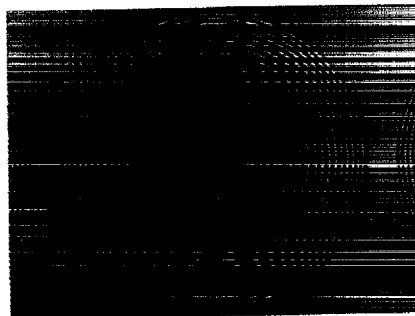


FIGURE 63.—225- μ m-dia. f/3 microlens.

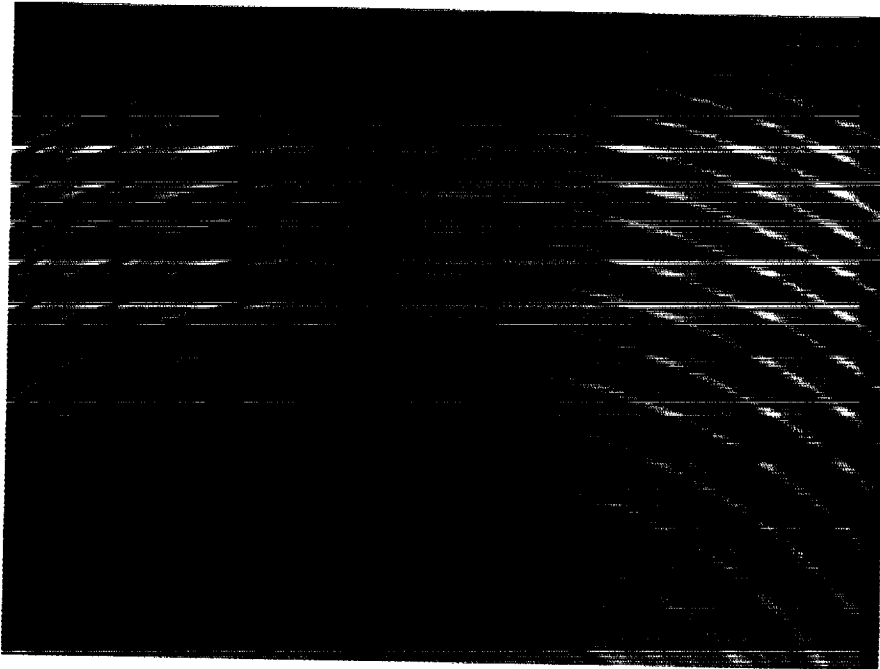


FIGURE 64.—Outer zones of microlens.

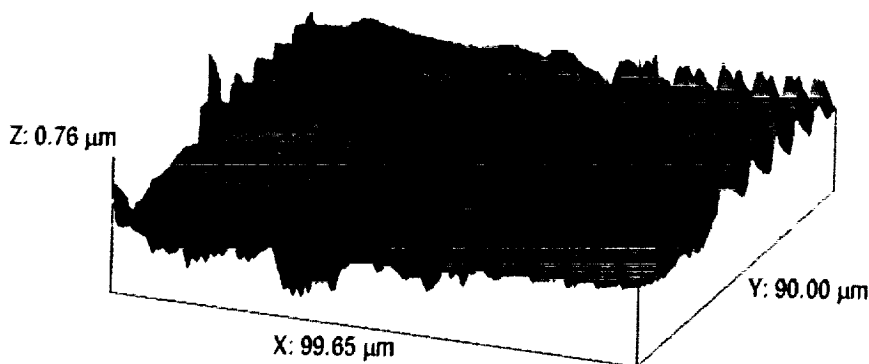


FIGURE 65.—Atomic force microscope view of microlens.

with this technique. Dynamic beam current variations, shape-dose nonlinearities and resist exposure latitude limitations are other issues that must be considered when determining actual exposure control resolution.

A 16-level blazed grating was fabricated using the direct dwell time extension to control exposure dose. This was delivered to Rochester Photonics for replication and testing.

Continued refinement of exposure curves will be done. Test structures to verify smallest feature size capabilities are planned. Test designs of microlens arrays and other diffractive elements will be fabricated. An alternate gray scale electron beam sensitive material characteristics will be studied.

Sponsor: Center Director's Discretionary Fund; Space Act Agreement, MSFC-RFC-106 with Rochester Photonics Corporation

Other Involvement:

- Joseph Grant/EB53, Electro Optics Branch, 256-544-3457, e-mail: joseph.grant@msfc.nasa.gov
- Dr. Helen J. Cole/EB53, Electro Optics Branch, 256-544-6790, e-mail: helen.cole@msfc.nasa.gov
- Dr. Paul Ashley, U.S. Army Air and Missile Command, Weapons Sciences Directorate, and Engineering Center, 256-876-7484
- Dr. David Lanteigne, U.S. Army Air and Missile Command, Weapons Sciences Directorate, and Engineering Center, 256-876-6418

Biographical Sketch: Brent Beabout works in the Electro Optics Branch at MSFC. He has a B.S.E.E. from Auburn University and an M.S.E. from the University of Alabama in Huntsville. ▀

Replicated X-Ray Optics Development

William D. Jones/EB52
256-544-3479
E-mail: william.d.jones@msfc.nasa.gov

During FY97, development of replicated optics for the Constellation X-Ray Mission (CXM) continued. This approach to optics manufacture utilizes a precisely shaped and polished mandrel to impart the correct shape to an optic which is formed over the outside of the mandrel and subsequently removed. It is well-adapted mass production since the mandrel can be reused after the optic is removed (fig. 66).

Two small mirrors (62-mm-dia.) were successfully tested in January 1996, demonstrating approximately 15 arc second half-power diameter (HPD) x-ray resolution. For the Constellation X-Ray Mission, much larger mirrors will be required, ranging in diameter from 352 mm to 1,300 mm. MSFC has selected an incremental approach to demonstrating mirrors of this size. First, a 250-mm- (quarter-meter) diameter mirror will be designed, fabricated and tested. Using knowledge gained during this activity, a 500-mm- (half-meter) diameter mirror will be designed, fabricated and tested. The final stage will be a 1,000-mm- (1-m) diameter mirror. At the same time, the infrastructure needed for this activity will be put in place. Significant progress toward these goals was made during the year.

The design for quarter-meter mirror mandrels was finished during FY96. This design was somewhat novel in that the parabola and hyperbola were made as two separate parts, then

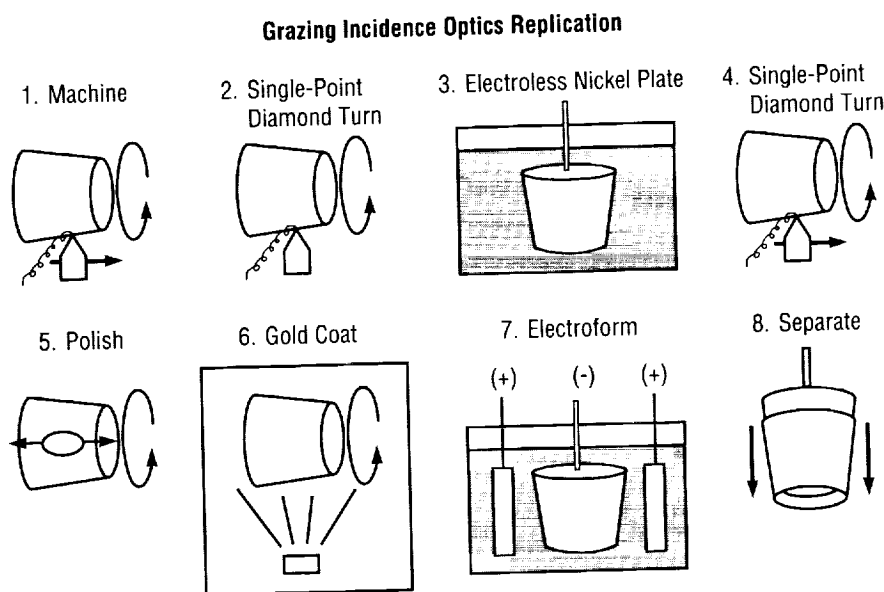


FIGURE 66.—Replication process flow.

joined later in the manufacturing process. During FY97 conventional machining for two complete mandrels was completed. The first set of mandrels was diamond-turned at the Marshall Center. This initial manufacturing step establishes the optical figure ("prescription") that enables the finished optic to focus x rays correctly. Following this operation, the mandrel was plated with electroless nickel (nickel-phosphorus or alloy) to provide a hard, polishable surface. Normally the mandrel would be diamond-turned a second time following plating to establish the final optical figure; however this was not possible since the diamond turning machine was being repaired. Consequently loose abrasive grinding was used for preliminary figuring of the mandrel. Final figuring and polishing was done using a pitch lap and aluminum oxide polishing slurry (fig. 67). Although this alternate process is more time consuming than diamond turning (because of the need for additional metrology), it

successfully demonstrated the feasibility of loose abrasive grinding as a "fallback" option in the event of equipment failures. In addition, the opticians gained valuable experience with the grinding and polishing machine and refined many of the

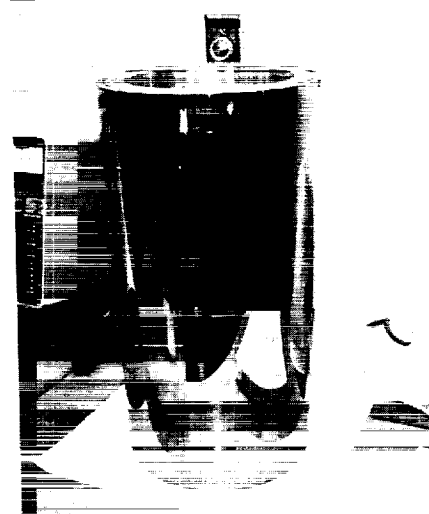


FIGURE 67.—Polished and figured 0.25-m mirror mandrel.

procedures that will be needed for larger mandrels to follow, and developed a better understanding of the capabilities and limitations of the metrology equipment and devised useful techniques to cross-check the accuracy of the equipment.

While repairs were being made to the diamond turning machine, the second quarter-meter mandrel was shipped to Oak Ridge National Laboratory (ORNL) for diamond turning.

A design for a half-meter mirror mandrel, which had been started in FY96, was finished in early FY97. Fabrication of two mandrel sets was completed, using aluminum forgings purchased earlier. These components were delivered in FY97 (fig. 68) and will be diamond turned when repairs and upgrades to the diamond turning machine are complete.

In addition to work on the quarter-meter and half-meter mandrels, modifications were begun to adapt an

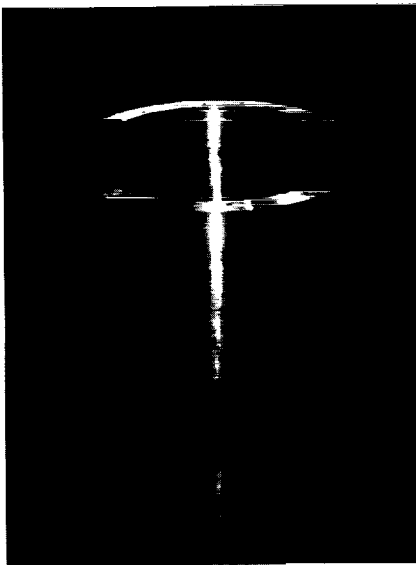


FIGURE 68.—0.5-m mirror mandrel blank.

automatic cylindrical grinder/polisher (ACG/P) (originally used to polish the inner diameter of the AXAF-I optics) to polish the outer diameter of x-ray mirror mandrels. This work was still in progress at the end of FY97. These modifications will allow mandrels up to 1.3 m in diameter to be polished under automatic control.

Fabrication of a fixture to support the completed replicated x-ray mirror and guide it away from the mandrel without damage was begun and continued through the end of FY97. This fixture can accommodate mandrels and mirrors up to 0.5 m. It also has provisions for cooling the mirror mandrel assembly, using liquid nitrogen as a coolant, and for purging with dry air to prevent contamination of the optical surfaces due to condensation of moisture.

One of the great challenges in this activity is meeting the stringent weight budget (250 kg for a 90-mirror assembly) while simultaneously maintaining the optical resolution. Meeting this goal will require reducing the weight by six times and will require that the mirrors have very thin walls, especially if a relatively dense material such as nickel is selected. Consequently, an effort was started in FY97 to examine alternate materials as potential replacements for nickel. Some materials under consideration at the end of FY97 were nickel with additives to reduce the grain size and nickel alloys (nickel-cobalt and nickel-iron). Both these efforts build upon work previously done. Also under consideration are ceramic materials such as silicon carbide, aluminum oxide (alumina), silicon nitride and titanium diboride, and composite materials such as fiber-reinforced cyanate esters. Each of these materials

has some advantage (superior elastic modulus, low density, etc.) but techniques to form thick sections with the required accuracies are not well-established. This work will continue into FY98.

A related difficulty created by the thinness of the mirror walls is excessive stress in the mirror as it is removed from the parent mandrel. This problem is exacerbated if the mirror becomes "stuck" to the mandrel. Consequently a series of experiments were started to quantify the adhesion of the mirror to the parent mandrel using flat, electroless nickel plated aluminum discs. Concurrently, an effort was started to calculate the stresses in the mirrors during separation using a finite element structural model; results are expected to become available in FY98.

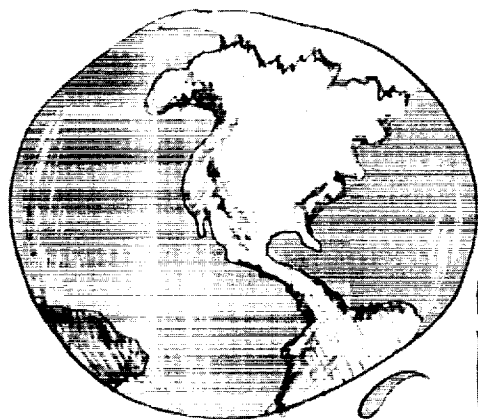
Sponsor: Code S, Office of Space Science

University/Industry Involvement:

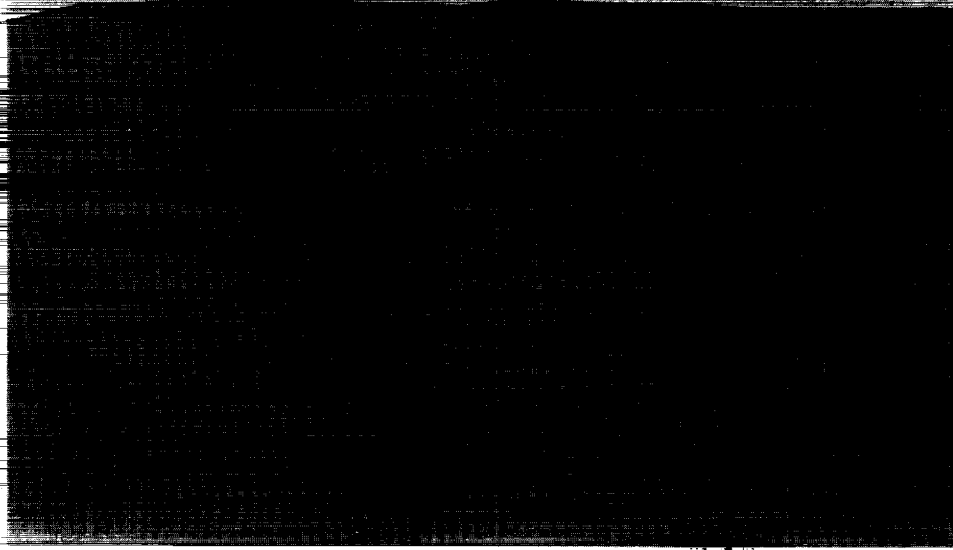
University of Alabama-Huntsville, Huntsville, AL; Morton Advanced Materials, Woburn, MA; Composite Optics, Inc., San Diego, CA; Smithsonian Astrophysical Observatory (SAO), Harvard University, Cambridge, MA; Oak Ridge National Laboratory (ORNL), Oak Ridge, TN; Penn State University (PSU), State College, PA.

Biographical Sketch: William D.

Jones, a senior optical physicist in the Optics Branch at the Marshall Center, is chief technologist for the Replicated X-Ray Optics Development Program. He has a bachelor of science in engineering science from the University of South Florida and has studied optics and electrical engineering at the University of Alabama in Huntsville.



space and microgravity
science research programs



"Man's mind and spirit grow with the space in which they are allowed to operate."

Kraft A. Bracke
Rocket Pioneers

NASA and the Marshall Center continue to lead the way to keep the American spirit of exploration alive. The missions we are planning, the technology we are developing, and the science we are performing are vital to fulfilling the American dream. Twenty-five years ago, our exploration led us to a new world. Now, we are at the eve of a new millennium and the challenges before us are great. We cannot even imagine what our world will be like a hundred years from now, but we do know that the research being done today by the scientists and engineers in NASA will form an indispensable foundation for that future.

The following articles describe some of the research being performed here at the Marshall Center. As you read through them, envision where each of them could lead and how they support a better life for our people and for all humanity. This research springs from the imaginations and skills of some of the most talented people in the country. Their goal is to make space just another environment for human activity and to bring the benefits of that activity home to Earth. Join us in the excitement of this quest!

Gregory S. Wilson
Director
Space Sciences Laboratory

A Laboratory Study of the Interaction of Charged Particles With Electron Beams and Ultraviolet Radiation

Dr. James F. Spann/ES83
256-544-5339
E-mail: James.F.Spann.Jr@msfc.nasa.gov

The purpose of this experiment is to probe the charging mechanisms of dust grains by measuring the equilibrium charge under different space-like conditions.

Small dust grains are prevalent throughout regions of space. Most often these grains are electrically charged and are immersed in a field of charge particles such as electrons, protons and ions. This agglomeration is called a dusty plasma. Dusty plasmas affect many regions of space including the Earth's upper atmosphere, the Earth's magnetosphere (that region in space where the Earth's magnetic field dominates the interactions of particles), the planetary rings around Saturn and Uranus, comet tails, and interstellar regions of space. It is important to understand how dusty plasmas are formed and how they affect these regions. In order to do that, it is required that a full understanding of the charging mechanisms of the dust grains be achieved.

One of the unique aspects of this dusty plasma experiment is the use of an electrodynamic balance. Instead of using a group or cloud of dust grains in the experiment, a single dust grain will be studied at a time. In addition, the dust grain will be in a stable or

equilibrium condition, not flying by so that it is probed only momentarily. Using this approach repeated measurements can be made under varying conditions on the same dust grain. In this way, the microphysics of the charging mechanism will be probed. Light scattering and viscous drag measurements will be employed to determine the dust grain size.

This year has been a productive one. The electrodynamic balance has been assembled and tested. A liquid particle generator has been fabricated which has allowed us to trap particles with a size of $\sim 2 \mu$ in diameter. We are in the process of checking out the electron beam gun. Based on the efforts expended thus far in this Center Director's Discretionary Fund project, a proposal was submitted in response to NRA 97-OSS-08 to study the infrared extinction cross sections of interplanetary dusty particles. The dusty plasma experiment will be featured in an upcoming episode of the syndicated PBS show "Bill Nye the Science Guy." The crew of the show spent one morning filming the episode highlighting the likelihood of being able to study a real dust grain captured in a comet tail. A very interesting web page has been constructed and is in use which describes the dusty plasma experimental work. The URL is <http://www.ssl.msfc.nasa.gov/ssl/pad/sppb/dusty/>.

Sponsor: Center Director's Discretionary Fund

Biographical Sketch: Dr. James Spann is an astrophysicist in the Space Sciences Laboratory at Marshall, a position he has held since 1986. Prior to his position here, he was an Oak Ridge Associated Universities

Postdoctoral Fellow at the U.S. Department of Energy in Morgantown, WV. His current research focuses on developing space imaging instrumentation. His work with the International Solar Terrestrial Project polar ultraviolet imager has contributed to the acquisition of observations of the aurora in the ultraviolet previously unmeasured and of fundamental significance to the discipline of space plasma and magnetospheric physics. He is also recognized for his innovative laboratory work with aerosol chemistry and the interaction of intense radiation with particles. Spann has a B.S. degree (physics and mathematics), Cum Laude, from Ouachita Baptist University in Arkadelphia, AR, 1979, and earned his Ph.D. in physics at the University of Arkansas, Fayetteville, in 1984. ▀

A New Ultra-High Resolution Near-Field Microscope for Observation of Protein Crystal Growth

William K. Witherow/ES76
256-544-7811
E-mail: bill.witherow@msfc.nasa.gov

The primary objective of this Advanced Technology Development (ATD) is to build and test a new optical method for observing protein crystals as they nucleate and grow. The new technique will be based on a tapered fiber probe in a near-field scanning optical microscope (NSOM). Standard microscopy is typically limited to about 1- μ resolution while the NSOM is capable of resolving 12-nm objects. A state-of-the-art NSOM will be built and then used to visualize individual molecules in a protein crystal growth solution. Labeling the proteins with a fluorescent material and polarization techniques should allow determination of the molecules' orientation both in the solution and on a crystal surface with the NSOM. We will design and fabricate new probes to improve the capabilities of NSOM. The new probe designs may improve the resolution or may eliminate the need for scanning.

The project will take place at the Marshall Space Flight Center (MSFC) with assistance provided by the University of Alabama in Huntsville. Both groups have experience in designing and constructing optical systems, while the group at MSFC has extensive experience in protein crystal growth (PCG). A commercial NSOM

has been constructed at MSFC. A fiber puller has been purchased to construct tapered fiber probes. The first probes will be standard tapered fiber probes built according to current techniques.

Coating the fibers with aluminum will take place in a vacuum sputtering system located at MSFC. The tapered fiber probe will be immersed directly into a protein crystal growth solution.

Tunneling near-field optical microscopy will also be examined for possible applications to observing protein crystal growth. As each improvement is made in the NSOM systems under development, it will be evaluated through use in PCG experiments. From the results of the experiments the NSOM system will be refined and improved to further enhance its performance.

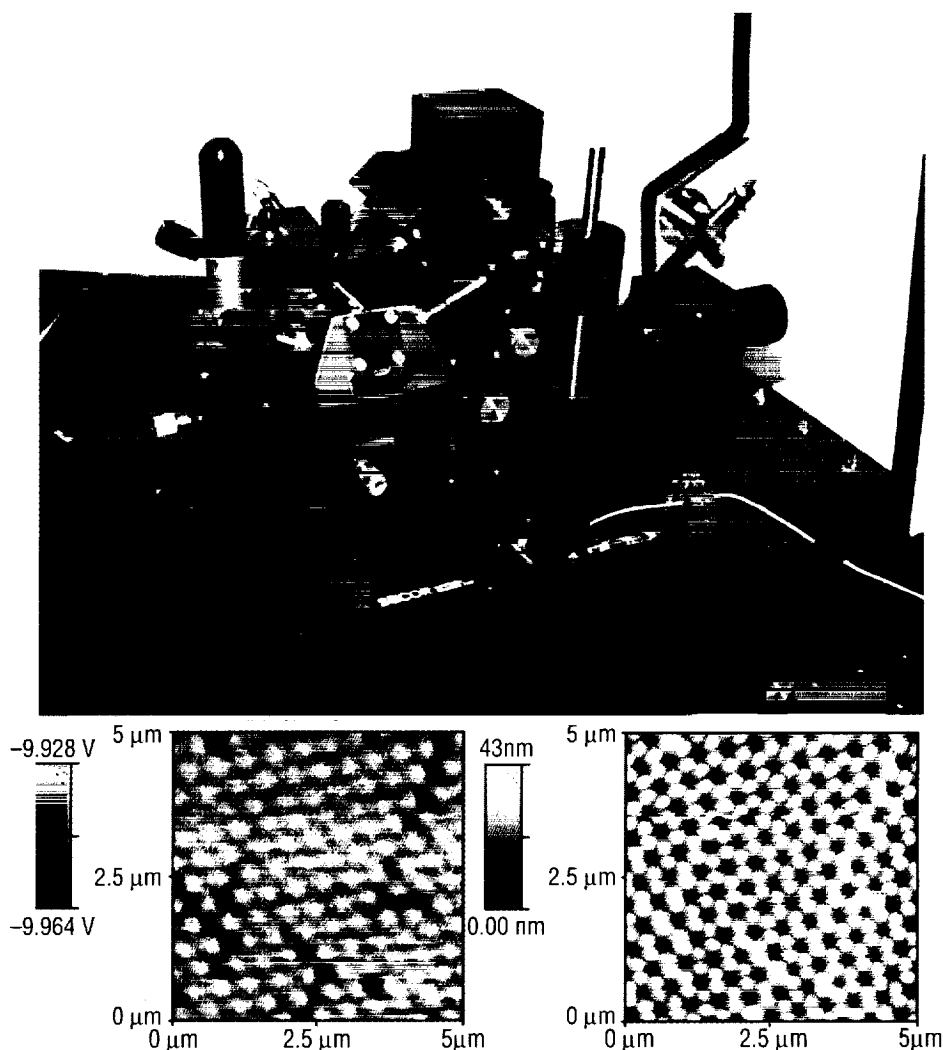


FIGURE 69.—NSOM apparatus, (top); NSOM image of aluminum deposition, (lower left); topography of aluminum deposition, (lower right).

Recently, we have succeeded in incorporating the fluorescent probe lucifer yellow into the substrate binding cleft of chicken egg white lysozyme. The covalently modified protein crystallizes with the same habit (tetragonal) as the unmodified protein, and from this we conclude that the probe is apparently not interfering with the crystal growth process. The bound lucifer yellow retains its fluorescence. Thus, we now have a suitable fluorescent derivative of the most commonly used model material in protein crystal growth studies. Having suitably labeled molecules and a functional NSOM, the following types of experiments can be done: Flow effects, aggregate sizing, cluster formation on crystal surfaces, and poisoned surfaces.

We will attempt to improve the quality of the tapered fiber probe by experimenting with fiber pulling and coating techniques. We will also investigate making novel fiber probes. Experiments involving polarization detection to determine the orientation of protein molecules on protein crystal surfaces will be possible with even a low resolution NSOM. We anticipate that several flight experiments will develop from this ATD.

We have synthesized at least 11 different fluorescent derivatives of lysozyme to date. There are two reasons for making multiple derivatives. First, different probes have different changes in their fluorescent behavior between free in solution and covalently bound. We are looking for those which have the highest fluorescence signal in the bound state. Second, the probes are generally not rigidly bound, i.e., they have a motion which is independent of the proteins.

When doing polarization studies, it is important that the probe absolutely determines the underlying proteins orientation. This can only be done if the probe is rigidly bound. We have only just recently made a derivative that, on the basis of the initial characterization results, appears to be rigidly bound.

The closest analogy to NSOM is AFM, which has rapidly become a valuable research tool in many areas of science and technology. While NSOM technology will be developed for a protein crystal growth use in this proposal, it is anticipated that many other areas of science will have an immediate use for this technology. The utility of NSOM technology should also extend past that of imaging surfaces to allow the "imaging" of small volumes of solutions. In a suitably designed system, this will allow the direct counting and sizing of aggregate species present, eliminating the problems in resolving such information from polydisperse solutions by methods such as light scattering. Both topics, surface studies and particle sizing of solutions, represent areas of high commercial potential with the development of suitably improved instrumentation or methods.

Sponsor: Headquarters Program Office, Advanced Technology Development Program; ATD Manager is Isabella Kierk

University Involvement: Chandra Vikram, University of Alabama in Huntsville

Biographical Sketch: William K. Witherow is an AST, Basic Properties of Materials. Currently, he designs and

fabricates optical data acquisition systems for various experiments including protein crystal growth, immiscible fluid studies, and crystal growth. His work also includes image analysis, and he serves as project scientist for the Observable Protein Crystal Growth Facility. Witherow has a bachelor of science in engineering physics with honors from the University of Tennessee in Knoxville, March 1977, and a master's in physics from the University of Alabama in Huntsville, August 1981. ▀

BATSE Observations of Accreting Pulsars

Dr. Robert B. Wilson/ES84

256-544-7695

E-mail: Robert.B.Wilson@msfc.nasa.gov

The Burst and Transient Source Experiment (BATSE) has been observing the entire sky (except for Earth blockage) since the launch of the Compton Gamma-Ray Observatory (CGRO) in April 1991. Data are available at a 1-sec time resolution, so that pulsed sources with periods above a few seconds can be monitored during the entire time they are above the Earth's horizon, in the energy range 20 keV (thousand electron volts) to 1 MeV (million electron volts). The pulsations are due to accretion of matter onto the magnetic polar regions of a neutron star. The matter flows from a normal star about which the pulsar orbits. The systems can be categorized primarily by the nature of this companion object. Systems with a low mass companion (less than the mass of our Sun) tend to be small systems, enabling mass transfer from the companion in a direct stream ("Roche lobe overflow"). Systems with massive companions can accrete matter in a direct stream or from the strong stellar wind of the companion. Systems with companions that are massive and rapidly spinning on occasion produce high-density equatorial winds, leading to transient outbursts when the neutron star in an elliptical orbit is closest to its companion. BATSE has observed members from each class of objects, and gained a new understanding of the behavior of these systems. A review of results obtained by a collaboration of MSFC, University of Alabama in Huntsville,

Universities Space Research Association, and Caltech have recently been published by Bildsten, et al., in *Astrophysical Journal Supplements*, Vol. 113, p.367, 1997. BATSE has observed 20 of the 44 known accreting pulsars to date, including 5 which it discovered.

The rate at which the rotation periods of these objects changes is highly variable, due to variations in the mass accretion rate, and in the manner in which the infalling matter interacts with the neutron star magnetic field. Examples of four systems we have observed are shown in figure 70.

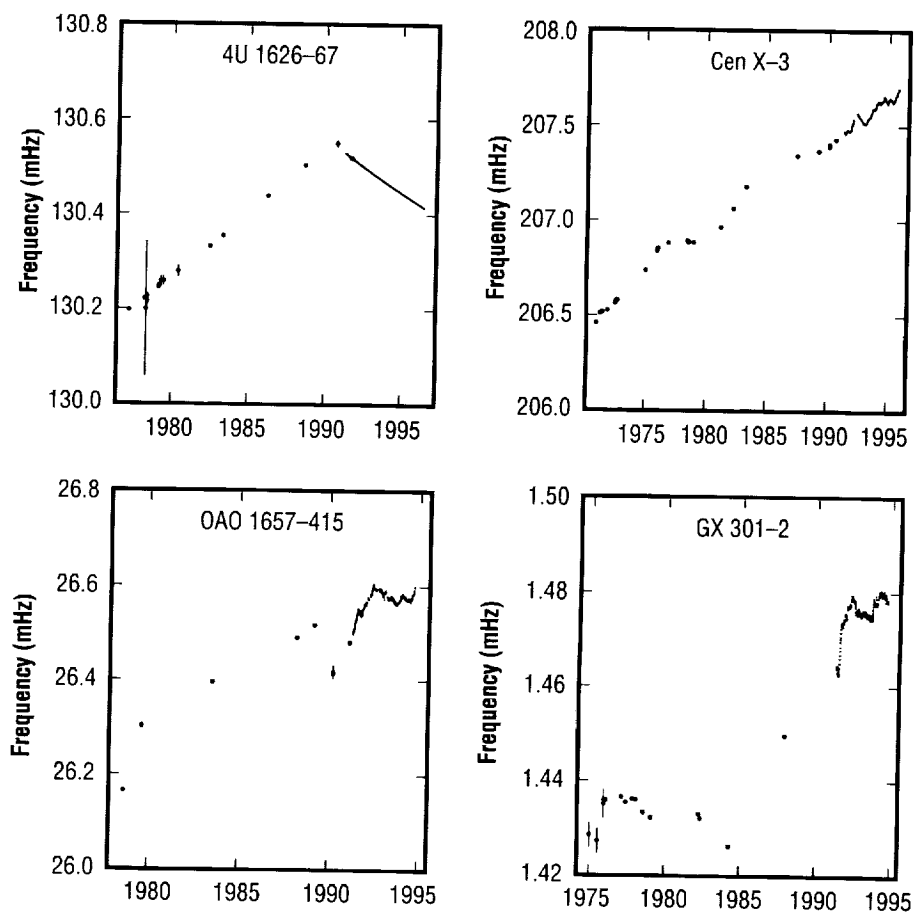


FIGURE 70.—Frequency histories obtained for four sources observed by the BATSE experiment on the Compton Gamma-Ray Observatory. For each source, all observations ever made are plotted. The observations become nearly continuous after April 1991, due to the continuous monitoring capability of BATSE. The frequency unit is milliHertz (mHz), which is 0.001 cycles/second. The rapid changes from spin-up (increasing frequency) to spin-down (decreasing frequency) observed for Cen X-3 and OAO 1657-415 were not known prior to these data. The rapid frequency increase near the beginning of the history for GX 301-2 constitutes evidence for a transient accretion.

The infrequent observations made by pointed instruments prior to BATSE make it difficult to identify the time scales on which the rotation rate is changing. The source 4U 1626-67, discovered to be a pulsar in 1977 by the SAS-3 spacecraft, had been increasing its spin frequency at all times prior to the launch of CGRO. Surprisingly, the spin frequency was found to be slowing down from the beginning of the BATSE observations. The rate of change is about the same for both the times of spin-up and spin-down. This switching behavior is also observed in Cen X-3, but instead of spending 10 or more years in one state, this source changes at intervals of 10's to 100's of days. Another important discovery of BATSE is notable in the frequency history of GX 301-2. This wind-fed system, with a chaotic variation of rotation history characteristic of such systems, shows intervals of rapid spin-up which is an indicator of accretion from a disk. The presence of these transient accretion disks was not identified before BATSE due to the very infrequent observations.

Transient outbursts of the "Be" systems have been observed previously to be of two types. "Giant" outbursts are found to start after the time of closest approach, last in many cases for longer than one full system orbit, and produce large changes in the neutron star spin rate. "Normal" outbursts occur just at times of closest approach, and thus recur at multiples of the orbital period. BATSE has found that giant outbursts tend to occur during a sequence of normal outbursts. Figure 71 shows a plot of the times of outburst from the transient systems BATSE has observed. The

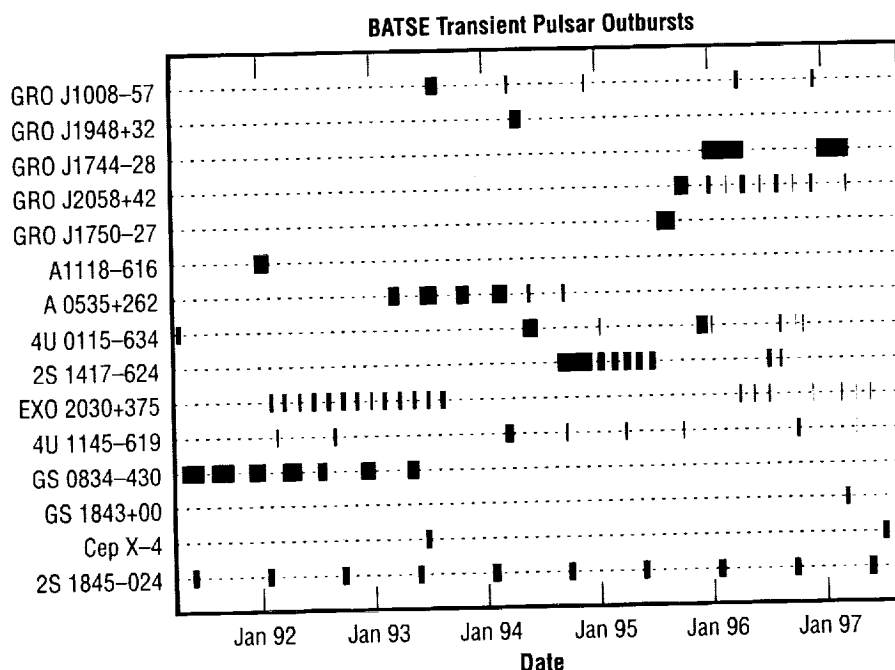


FIGURE 71.—Outburst history of transient sources observed by BATSE since April 1991. The upper five sources were discovered by BATSE. The continuous viewing by BATSE ensures that the characteristic time scales of outbursts for these sources are intrinsic to these objects. Many sources show repetition at regular intervals, a result suggested by previous data, and strongly evident in these results. The outbursts occur near periastron (closest approach to the companion star).

continuous viewing by BATSE ensures that the occurrence frequency displayed here is in fact characteristic of these systems.

Sponsor: Office of Space Science, Structure & Evolution of the Universe

University Involvement: Mark H. Finger/Universities Space Research Association, 256-544-6256, e-mail: Mark.Finger@msfc.nasa.gov

Biographical Sketch: Dr. Robert B. Wilson is an astrophysicist in the Space Sciences Laboratory of MSFC. He shares the responsibility for pulsar

studies of the gamma-ray astronomy group with Dr. Mark Finger. Dr. Wilson's primary research has been in gamma-ray astronomy. He is a co-investigator for the BATSE experiment on the Compton Gamma-Ray Observatory. Dr. Finger, a researcher employed by Universities Space Research Association, has been responsible for development of many of the analysis techniques used to produce the results reported here. ▀

Characteristics of Thermal Ions in the Topside Auroral Zone as Observed by TOPAZ3/STICS

Victoria N. Coffey/ES83
256-544-7635
E-mail: victoria.coffey@msfc.nasa.gov

Solar wind plasma was thought to be the dominant source of magnetospheric plasma until the discovery of O^+ which was clearly of ionospheric origin in the hot magnetospheric plasma. Subsequently, satellite observations of large upward fluxes of heavy (O^+ and He^+) and light ions (H^+) led to the suggestion that a substantial fraction of the magnetosphere was of ionospheric origin. But the source of these outflows was observed to be very cold and having insufficient energy to escape the gravitational field of the Earth. Questions naturally arose as to what were the physical processes responsible for the acceleration and transport of these ionospheric ions.

Ion heating in the topside ionosphere provides the necessary energy to the heavy ions so that they can achieve heights where they can be further accelerated. This heating is observed to be perpendicular to the magnetic field and is seen in different forms of bulk characterization of the plasma, the flux peaks of hot tails, and ion conics. Ion conics are formed by perpendicular heating which allows the ions to surge upward through the gradient magnetic field force. They gain parallel energy at the expense of

their perpendicular energy and gradually become more field aligned. Due to the adiabatic motion they have a cone-shaped distribution in velocity space.

Sounding rocket experiments have the best opportunity to probe the altitudes where transverse accelerated ion (TAI) heating commences and to identify the particle-wave interactions. A rocket flight called TOPAZ 3 was proposed to observe and identify processes responsible for the transfer of energy to the cool ionospheric plasma,

leading to heated or nonthermal ion and electron distributions, and to evaluate the significance of the resulting ion transport. This rocket was launched February 12, 1991, at 0911:54 Universal Time on a Black Brant XII sounding rocket from Poker Flat Research Range, Fairbanks, AK. It had a geographic northward and slightly westward trajectory, reaching the apex at 1,068 km, and landed in the Arctic Ocean after an 18-min flight. The Scanning Thermal Ion Composition Spectrometer (STICS) was designed at the MSFC Space

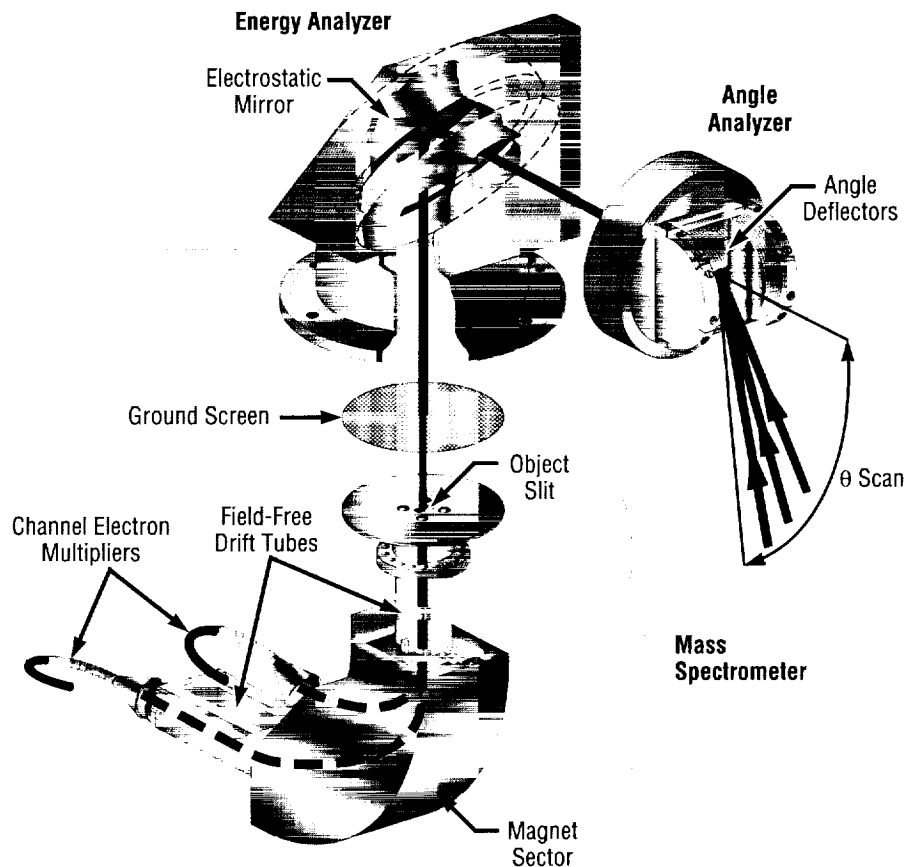


FIGURE 72.—Scanning thermal ion composition spectrometer (STICS).

Sciences Lab to measure three-dimensional velocity distributions in the ionospheric thermal energy range, and was provided as part of the plasma diagnostic instrumentation in support of the TOPAZ 3 sounding rocket payload.

STICS consists of three major components: A pair of electrostatic deflection plates for the polar selection of the particle arrival angle; an electrostatic focusing mirror for selection of ion energy; and a conventional magnetic sector analyzer that allows for the simultaneous detection of two mass species with a mass to charge (m/q) separation of 4:1. The instrument also has its associated stepping power supplies, preamplifiers, counters, and a programmable sequencer that stores and executes the flight program for stepping of the power supplies. An artist's drawing of the sensor, shown in figure 72, illustrates an optimal path of an ion trajectory as it is transmitted through the angle analyzer, the energy analyzer, and finally the mass spectrometer to the detectors.

High time resolution instruments on the payload measured bursty transverse oxygen heating within localized regions of lower hybrid wave events called spikelets. These measurements were made on the order of 100 msec. In correlation with the wave events were density depletions on the order of 10–50 percent with the larger depletions associated with the more intense spikelets. In 85 percent of the cases, there was a one-to-one correspondence between the TAI's and the wave event. Figure 73 shows TAI's in the top panel and spikelets in the second panel. The three bottom panels show the O^+ temperatures derived

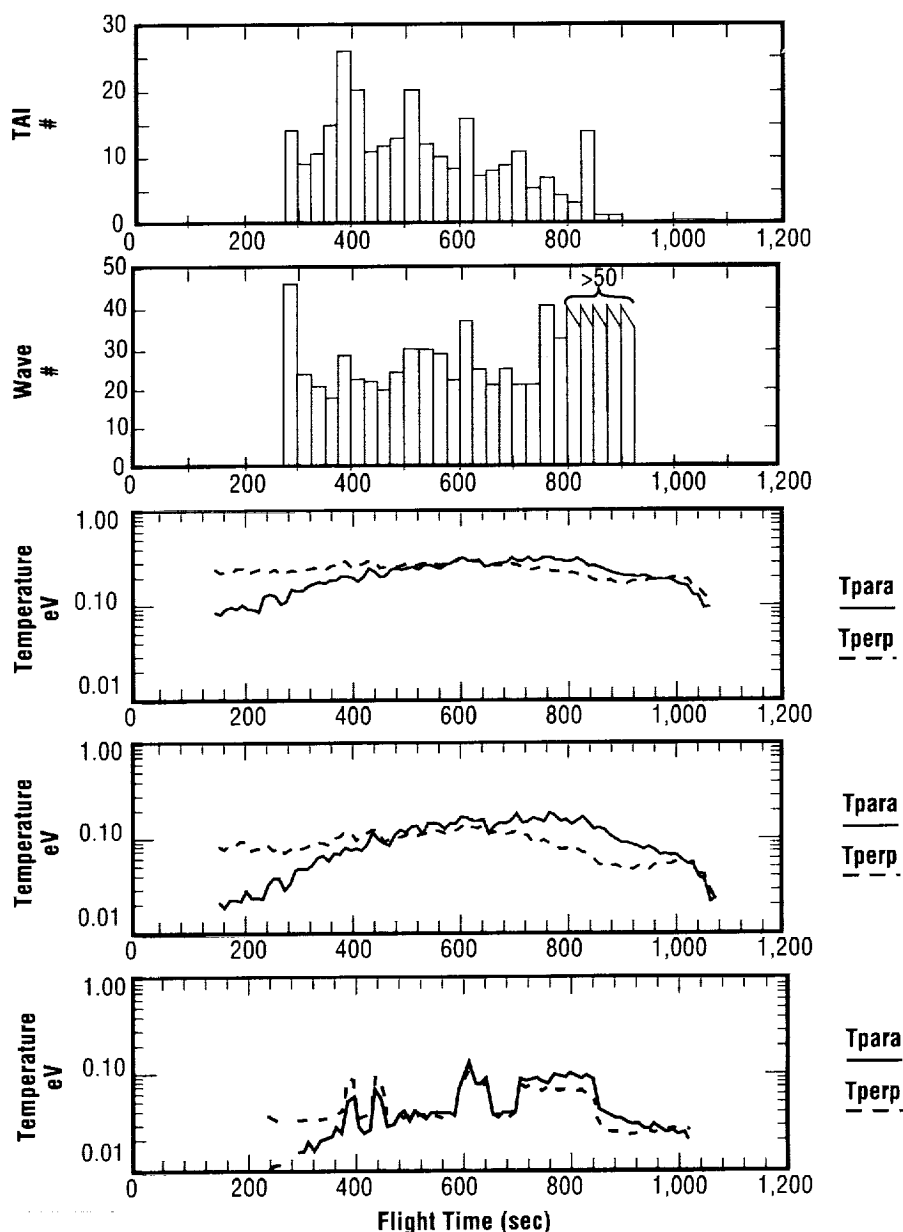


FIGURE 73.—Comparison of temperatures with wave and TAI events.

from the STICS data set that were measured with a resolution of about 10 sec. The third panel shows parallel and perpendicular temperatures of approximately 0.3 eV at apogee which are considered to be representative temperatures for the topside ionosphere. The second and third panel show these same measurements after restricting the velocity integration to the range of energies of 0.3 to 1.8 eV and 0.3 to 1.5 eV respectively. As the integrated velocity bins are reduced to lower energies, small-scale heating events appear at approximately 400, 600, and 800 sec in the bottom panel which correlate with the TAI's and spikelets in the first and second panel. This correlation of heating events with the TAI and wave events show that macroscopic 10-sec measurements can possibly be a good indicator of the microphysical 100 msec events.

Sponsor: This work was supported at MSFC by NASA RTOP 435-11-00-19

Biographical Sketch: Victoria N. Coffey supports the flight instrument programs in the Space Physics Branch. She optimizes instrument designs for particle throughput, tests and calibrates instruments before flight, and analyzes flight data to study ionospheric transport processes. She received her master's degree in physics from the University of Alabama in Huntsville in 1997. ▀

Coronal Heating

Dr. Ronald L. Moore/ES82
256-544-7613
E-mail: ron.moore@msfc.nasa.gov

The Sun keeps its outer atmosphere, the corona, heated to million-degree temperatures. Because it is so hot, the corona glows in x rays and is unbounded, continually expanding and escaping from the Sun (fig. 74) to become the super-Alfvenic solar wind that forms the heliosphere, reaching far beyond the planets. While it has been established for decades that the corona and solar wind owe their existence to coronal heating, the heating process remains unknown other than in broad outline. Determination of the specifics of the heating, the main drivers and mechanisms, is a major quest of solar astrophysics.

It is known that coronal heating is an aspect of the Sun's magnetic activity. X-ray and extreme ultraviolet images together with magnetograms plainly show that on the overall scale of active regions and larger ($>10^5$ km), coronal heating is generally stronger where the magnetic field is stronger, the strongest heating occurring in active regions, which are sites of the strongest magnetic fields found on the Sun. However, within active regions it is seen that different areas of the same field strength differ greatly in strength of coronal heating. So, it is clear that the strong coronal heating in active regions is a result of the strong magnetic field, but depends on more than the field strength alone.

Over the past few years, solar scientists at MSFC have explored the magnetic origins of coronal heating in active regions by registering Yohkoh

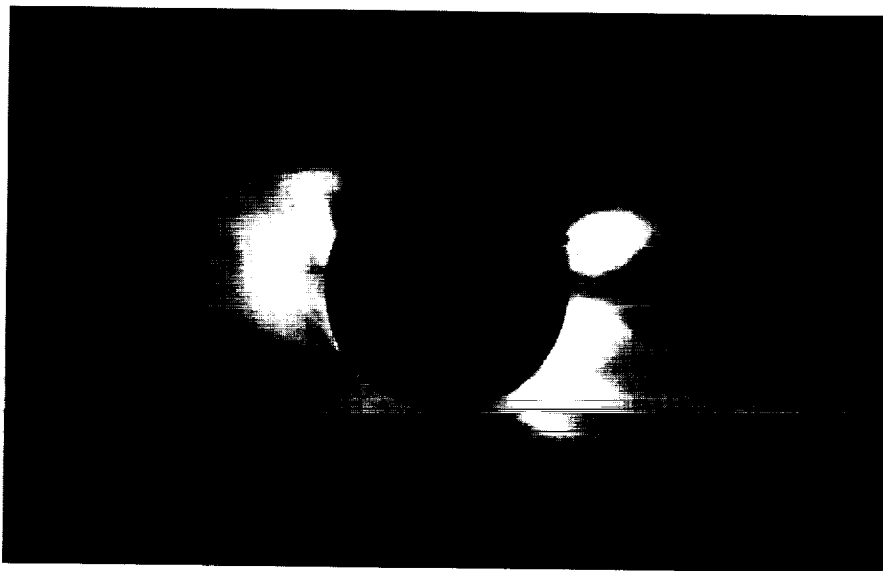


Figure 74.—The solar corona and solar wind.

coronal x-ray images with MSFC vector magnetograms and examining the magnetic roots of the bright coronal features.^{1, 2} In their sample of ~100 bright coronal features, they found that nearly all were rooted near a neutral line (polarity dividing line) in the photospheric magnetic flux. These bright coronal features were found to be of two basic types: core features and extended loops. A core feature resides within the core magnetic field, a field closely enveloping a neutral line. An extended loop is rooted, at one end, in or around the core field of a neutral line, but extends well away from this neutral line and core field. Each bright coronal feature rooted near a neutral line either was one of these two types or was a combination of these two elements. In a large majority of cases, the core field that was at the foot of an extended loop and/or held a core feature was strongly sheared. Furthermore, substructures within the core features continually changed in form and brightness (microflared) on time scales of a few minutes, whereas the extended loops evolved more gradually. From these results, Falconer et al.² concluded that 1) the source of much of the strong coronal heating in active regions—both in the core features and in the extended loops—is the core field low along the neutral lines; and 2) this heating is driven by microflaring activity in the core field, and the microflaring and coronal heating are more probable and usually stronger when the core field is more strongly sheared, hence holding a larger store of free magnetic energy that might be released to drive the coronal heating.

During the past year, these scientists have extended their study of coronal

heating to quiet regions, i.e., to all areas not in active regions.³ The heating of the extended corona in quiet regions is the main driver of the solar wind. The magnetic origins of coronal heating in quiet regions were examined by combining Fe XII coronal images from the Solar and Heliospheric Observatory with magnetograms from the National Solar Observatory. Spatial filtering of the coronal images showed a network of enhanced structures of the scale of the magnetic network in quiet regions. Superposition of the filtered coronal images on maps of the magnetic network extracted from the magnetograms showed that the coronal network does indeed trace and stem from the magnetic network. Network coronal bright points, the brightest features in the network lanes,

were found to have a highly significant coincidence with neutral lines in the network magnetic flux, and often were found to be at the feet of enhanced coronal structures that stem from the network lanes and reach out over the cells of the network. These results indicate that, similar to the close linkage of neutral-line core fields with coronal heating in active regions, low-lying core fields encasing neutral lines in the magnetic network often drive noticeable coronal heating within themselves (the network coronal bright points) and on more extended field lines rooted around them. This behavior favors the possibility that active core fields in the network are the main drivers of heating the bulk of the corona, on scales much larger than the network lanes and cells (fig. 75).

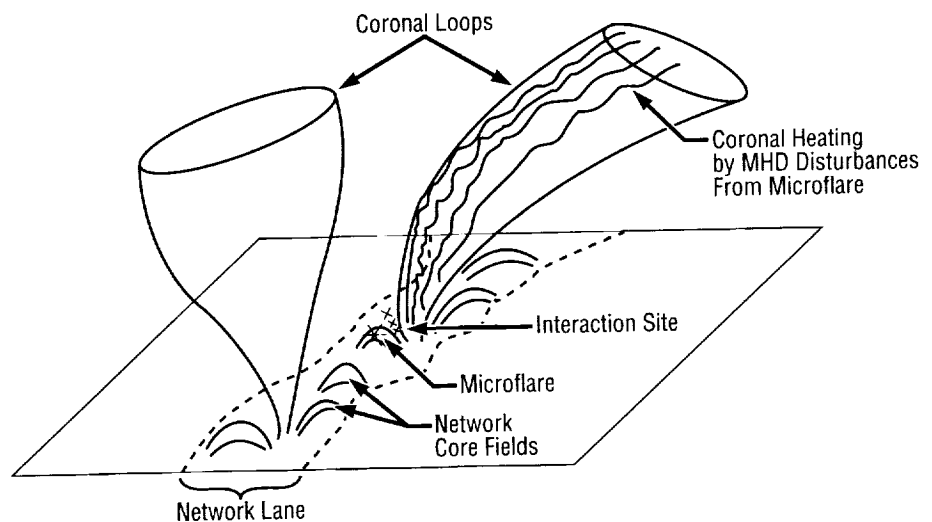


Figure 75.—Scenario for coronal heating by active core fields in the magnetic network.

1. Porter, J. G.; Falconer, D. A.; Moore, R. L.; Harvey, K. L.; Rabin, D. M.; Shimizu, T.: "Magnetic Roots of Enhanced High Coronal Loops," in *Magnetohydrodynamic Phenomena in the Solar Atmosphere—Prototypes of Stellar Magnetic Activity*, ed. Y. Uchida, T. Kosugi, and H. S. Hudson (Kluwer: Dordrecht), p. 429, 1996.
2. Falconer, D. A.; Moore, R. L.; Porter, J. G.; Gary, G. A.; Shimizu, T.: "Neutral-Line Magnetic Shear and Enhanced Coronal Heating in Solar Active Regions." *Astrophysical Journal*, 482, p. 519, 1997.
3. Falconer, D. A.; Moore, R. L.; Porter, J. G.; Hathaway, D. H.: "Network Coronal Bright Points: Coronal Heating Concentrations Found in the Solar Magnetic Network." *Astrophysical Journal*, in press, 1998.

and was a Research Fellow with the Caltech Solar Astronomy group (1972 through 1980). ▀

Solar Flares and Coronal Mass Ejections

Dr. Ronald L. Moore/ES82
256-544-7613
E-mail: ron.moore@msfc.nasa.gov

Solar flares and coronal mass ejections are explosions of large internally contorted bipolar magnetic bubbles in the solar atmosphere. In the most powerful of these events, the rates of heating and mass expulsion transiently exceed those of the entire nonflaring corona and solar wind. These events are the greatest explosions in the solar system, blasting out through the solar wind and disrupting the magnetospheres and ionospheres of the planets. A large Earthward-directed magnetic explosion can deliver a blow to the Earth's magnetosphere severe enough to both knock out electrical power grids on the ground and expose humans and electronics in orbit to lethal doses of particle radiation.

A twisted magnetic filament, impregnated with plasma visible in chromospheric and/or coronal images, typically rides in the core of the exploding magnetic bubble. For hours, even days, before the explosion, the filament is visible in the core of the magnetic bubble, traces the magnetic field in which it is held, and thereby shows that the core field is greatly sheared and twisted. Hence, in the explosion, the erupting filament is a tracer of the exploding field's core. If the core field is strong enough (100 G to 1,000 G), the field eruption and launching of the coronal mass ejection produces intense particle acceleration and plasma heating so that the event is seen as a bright flare in thermal and nonthermal radiation

Sponsor: Office of Space Science

University/Industry Involvement: University of Tokyo; National Solar Observatory; Naval Research Laboratory

Biographical Sketch: Dr. Ronald L. Moore is an internationally recognized solar scientist. He joined the MSFC Solar Physics branch in 1981 where he developed and continues to lead a research program on observed solar magnetic fields and their effects in the solar atmosphere. Moore has published over 100 solar research papers and articles in refereed journals, conference proceedings, books, and encyclopedias. He received his Ph.D. from Stanford University in 1972,

across the entire spectrum from radio to gamma rays. If the field is weaker (~ 10 G), the particle acceleration and heating are much weaker and the flare brightening is weak or undetectable, but a large coronal mass ejection can still be produced. Apparently, regardless of the field strength, all of these ejective events are the same kind of magnetic explosion, and so all are appropriately called either ejective flares or flaring coronal mass ejections.

Basic unresolved questions about ejective flares/coronal mass ejections include: Why do these magnetic bubbles explode and what triggers the explosion? The answers depend directly on the three-dimensional field configuration of the bubble before and during the explosion. Progress in certifying and improving a three-dimensional magnetic picture proposed nearly 20 yr ago for these events was achieved during the past year by MSFC solar scientists in collaboration with others in the United States and France.¹

This research team combined ground-based chromospheric images and space-based coronal x-ray images of a large ejective flare observed during its long-lasting decay phase. The x-ray images were from the soft x-ray telescope (SXT) of the Japan/U.S. Yohkoh orbiting solar observatory. Managed by MSFC, the SXT was built for NASA by Lockheed and tested in MSFC's X-Ray Calibration Facility. From the chromospheric and coronal images together, it was found that the three-dimensional magnetic field configuration late in this flare was similar to that at and before the

onset of such large ejective bipolar flares. The sheared core field running under and out of the flare arcade was S-shaped, and at least one elbow of the S looped up into the low corona. From previous observations of large ejective flares, it was concluded that such core-field coronal elbows, though rarely observed, are probably a common feature of the three-dimensional magnetic field configuration late in large ejective flares. The rare circumstance that apparently resulted in a coronal elbow of the core field being visible in chromospheric images of our flare was the occurrence of a series of subflares low in the core field under the late-phase arcade of the large flare. These subflares probably produced flaring arches in the northern elbow, thereby rendering this elbow visible in chromospheric emission.

The deduced late-phase three-dimensional field configuration in this flare, together with the recent sheared-core bipolar magnetic field model of Antiochos, Dahlburg, and Klimchuk,² and recent Yohkoh SXT observations of the coronal magnetic field configuration at and before the onsets of large

ejective flares, supports the three-dimensional model proposed by Moore and LaBonte³ as sketched in figure 76. The present study confirms 1) that the preflare magnetic field is closed over the filament-holding sheared core field as in figure 76, and 2) that the preflare core field has the shape of an S (or backward S) with coronal elbows. In addition, the present study reveals the presence of a field component not shown in figure 76—the core field has a lower part that does not erupt in the explosion but remains closed throughout the flare and can have coronal elbows similar to those of the upper part of the core field that does erupt. In this improved picture, the rest of the core field, the upper part (the part shown in fig. 76), does erupt and open along with the preflare arcade envelope field in which it resides. The flare arcade is formed as shown in figure 76 by reconnection that begins in the middle of the core field at the start of the eruption and progresses from reconnecting the closed core field early in the flare to reconnecting the "opened" envelope field late in the flare.

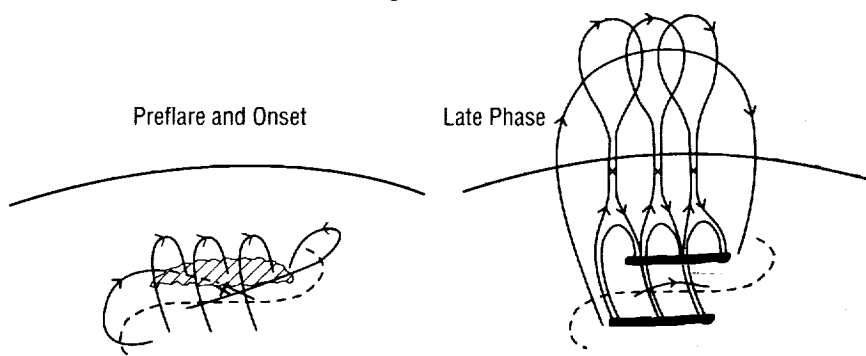


Figure 76.—A three-dimensional configuration of the magnetic field in ejective flares/coronal mass ejections.

1. Moore, R. L.; Schmieder, B.; Hathaway, D. H.; Tarbell, T. D.: "3D Magnetic Field Configuration Late in a Large Two-Ribbon Flare." *Solar Physics*, 1998, in press.
2. Antiochos, S. K.; Dahlburg, R. B.; Klimchuk, J. A.: "The Magnetic Field of Solar Prominences." *Astrophysical Journal*, 420, L41, 1994.
3. Moore, R. L.; LaBonte, B. J.: "The Filament Eruption in the 3D Flare of July 29, 1973: Onset and Magnetic Field Configuration." In *Solar and Interplanetary Dynamics*, ed. M. Dryer and E. Tandberg-Hanssen (Reidel: Dordrecht), p. 207, 1980.

Sponsor: Office of Space Science

Industry Involvement: Meudon Observatoire de Paris; Lockheed Palo Alto Research Laboratories

Biographical Sketch: Dr. Ronald L. Moore is an internationally recognized solar scientist. He joined the MSFC Solar Physics branch in 1981 where he developed and continues to lead a research program on observed solar magnetic fields and their effects in the solar atmosphere. Moore has published over 100 solar research papers and articles in refereed journals, conference proceedings, books, and encyclopedias. He received his Ph.D. from Stanford University in 1972, and was a Research Fellow with the Caltech Solar Astronomy group (1972 through 1980). ■

Gradient Forming With Magnetic Fluids

Dr. Fred W. Leslie/ES71
256-544-1633
E-mail: fred.leslie@msfc.nasa.gov

A great number of crystals grown in space are plagued by convective motions which contribute to structural flaws. The character of these instabilities is not well understood but is associated with density variations in the presence of residual gravity (g-jitter). As a specific example, past HgCdTe crystal growth in space indicates radial compositional asymmetry in the grown crystals. In the case of HgCdTe, the rejected component into the melt upon solidification is HgTe which is denser than the melt. The space-grown crystals indicate the presence of three-dimensional flow with the heavier HgTe-rich material clearly aligned with the residual gravity (0.55–1.55 μg vector). This flow stems from multicomponent convection, namely, thermal and solutal buoyancy driven flow in the melt. A model experiment to study this problem in space requires the rapid development of a concentration (density) gradient which is difficult to establish in the absence of a stabilizing gravitational field. An important objective of this study is to evaluate the feasibility of using a magnetic fluid to study this phenomenon. Once the effectiveness of a magnetic field in stabilizing the concentration gradient is established, the developed techniques can be utilized in the design of a space experiment to study the crystal growth instability problem.

Artificial ferrofluids are typically colloidal suspensions of extremely small ferrite particles that have been treated with a surfactant to prevent clumping and settling. Although a multiphase mixture at the microscopic scale, the nearly uniform dispersion of very small particles permits ferrofluids to be well represented by a continuum model. The fundamental hydrodynamic equations describing the flow of a ferrofluid have been developed and highlight the primary phenomena arising from the coupling between an imposed magnetic field and the fluid flow.

The primary objective of this effort is to develop a novel method for quickly producing an exponential gradient to be used in future space experiments. By demonstrating this technique on the ground using a strong magnetic field to overcome gravity, we can be assured that this method would be applicable to space systems using a substantially weaker field. A gradient former essentially consists of a dual syringe system, with one syringe containing pure solvent and the other the solute solution of the required maximum concentration in the experiment. By deploying two liquids at variable speeds into a mixing chamber and eventually into the test cell, precise gradients ranging from linear to exponential can be realized within minutes. This mechanism works in terrestrial setups aided by gravity. In low gravity, however, the gravity force is significantly attenuated and an alternate means is required. It would be ideal to "switch gravity on" while deploying the gradient and then turn it off before

the experiment starts. Although this is not possible, an analog using magnetism is considered.

One novel way of realizing the required solute gradient is by using a magnetic fluid and a controlling magnetic field to provide the required body force in the gradient former deploys into the test cell a solution of increasing concentration of the paramagnetic salt or ferrofluid as the supply syringe is depressed. The magnetic field—due to a controllable electromagnet—provides the body force that interacts with the varying solution magnetism much like gravity allows the set up of a solute gradient due to solution density variations.

In our ground-based experiments, ferrofluid EMG-909 (Ferrofluids Corp., New Hampshire) was used in a magnetic field of strength up to 3.5 kG. This fluid consists of subdomain magnetic particles in a light mineral oil carrier fluid. The fluid has a saturation magnetization value of 200 G and absolute viscosity of 5 cP. Because this fluid is very opaque, it was diluted with the carrier mineral oil to a concentration of 0.5 percent by volume to allow viewing the concentration gradients with a camera. The magnetic field was mapped out in two dimensions using a hall probe. The lower part of this field where the vertical gradient is uniform is the region where the experiments were conducted. The resulting gradient is 0.3 kG/cm.

Figure 77 shows two snapshots of the experiment cell with a deployed ferrofluid gradient without and with an imposed magnetic field. When the

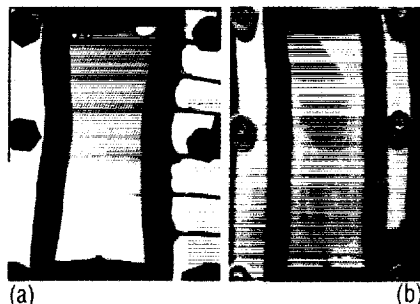


FIGURE 77.—Gradient deployment experiment: (a) With a magnetic field of 3.0 kG (the deployed gradient is stabilized); (b) without a magnetic field (sedimentation of the heavier fluid is visible).

experiment commences, the gradient former deploys fluid of increasing concentration which translates to fluid of increasing density. With no applied magnetic field, sedimentation of the heavier fluid is clearly seen in figure 77b as a distinct plume. The water-ferrofluid interface is also visible in this figure. When the magnetic field is applied however, the field gradient leads to a stabilization of the deployed concentration gradient as evidenced in figure 77a. Since the ferrofluid is deployed through a small tube at the top, essentially as a jet, some inertia effects are evident during the run. These effects are, however, damped out as the deployment is completed and the experiment is allowed to equilibrate. Thus in this case, the magnetic force on the ferrofluid is able to overcome the gravitational force. The ensuing gradient was found to be very stable and repeatable. If the magnetic field is now switched off, a collapse of the gradient field is observed. The upper bound for this time delay is dictated by the diffusion time scale which is rather long in this case.

Future work in this project will be focused on a thorough quantification of the experiment results and comparison with developed theoretical predictions. This will be pursued by nonintrusive (optical) and intrusive (magnetization) measurements. For use in the latter tests, the experiment cell has been modified to permit the extraction of small samples for testing. The magnetization measurement technique will be further refined and tested. A calibration sequence is presently in progress. Similarly, optical diagnostics will be further developed and tested.

Sponsor: MSFC Center Director's Discretionary Fund

University Involvement: Dr. N. Ramachandran, Universities Space Research Association

Biographical Sketch: Dr. Leslie is a research scientist in the Space Sciences Laboratory working in the area of microgravity fluid dynamics. He was a payload specialist on STS-73 where he spent 16 days in space conducting a number of experiments in fluid dynamics, materials processing, biotechnology, life science, and combustion. ▀

Incorporation of Metal Nanoparticles Into Aerogels for Catalysis Applications

Dr. David D. Smith/ES76
256-544-7778
E-mail: david.d.smith@msfc.nasa.gov

We have fabricated aerogels containing silver nanoparticles for gas catalysis applications.¹ Silver aerogels, for example, may be used for lightweight filtration systems in hospitals, airplanes, or space vehicles to prevent bacterial, viral, or fungal contamination. By applying the concept of an average or effective dielectric constant to the heterogeneous interlayer surrounding each particle, we extend the technique of immersion spectroscopy to heterogeneous or porous media. Specifically, we apply the predominant effective medium theories for the determination of the average fractional composition of each component in this inhomogeneous layer. Hence, the surface area of metal available for catalytic gas reaction is determined. The technique is satisfactory for statistically random metal particle distributions but needs further modification for aggregated systems.

Surface plasmon resonance imaging has in the past been applied to the characterization of thin films.² In this study we apply the surface plasmon technique—not to determine macroscopic spatial variations—but rather to determine average microscopic information. Specifically, we deduce

the dielectric properties of the surrounding gel matrix from the visible absorption characteristics of colloidal metal nanoparticles contained in silica aerogel pores, a process known as immersion spectroscopy. This deduction is possible because the dielectric constant of metal nanoparticles is linked to that of the host matrix at the surface plasmon resonance of the metal. Hence, any change in the dielectric constant of the medium surrounding the metal particles results in a shift in the surface plasmon wavelength observable with standard UV-visible spectroscopy. Immersion spectroscopy is usually applied to the characterization of continuous host media.³ However, by applying the concept of an average or effective dielectric constant, we extend the immersion spectroscopy technique to inhomogeneous materials characterized by spatially dependent dielectric constants, such as aerogels.

Now since the material surrounding the metal particle in fact consists of two separate materials in separate phases, we must treat it as a composite medium. The concept of an average or effective dielectric constant may be used to relate the refractive index of this surrounding medium to that of its constituents (i.e., the silica and solvent). Two common effective medium theories are that of Maxwell Garnett (Maxwell Garnett, 1904; 1906) and that of Bruggeman (Bruggeman, 1935). Maxwell Garnett's theory describes small concentrations of isolated spherical inclusion particles. Bruggeman's theory, on the other hand, describes a worm-like geometry in which both materials are present in similar

concentrations. For these silica aerogel composites, Bruggeman's theory might be expected to yield better results since the concentrations of silica and solvent (or air) are comparable at the surface of the metal particle.

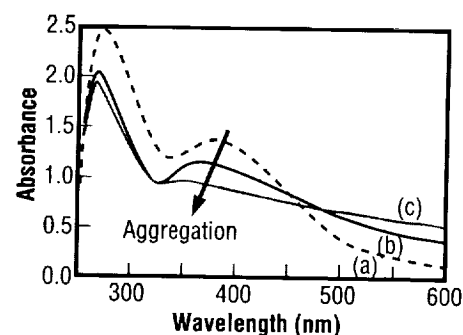


FIGURE 78.—Shift in absorption as a function of Ag aggregation. The spectra are for (a) yellow, (b) green/brown, and (c) silver-colored gels.

Silver particles incorporated into the solgel recipe displayed a strong surface plasmon resonance which shifted to shorter wavelengths upon supercritical solvent extraction (formation of the aerogel), with the blue-shift depending on the degree of aggregation as shown in figure 78. Not shown is the plasmon peak for the initial alcogel samples which was observed at 401 nm. The blue-shift occurs because the coherence of the gel is maintained during supercritical extraction so that the substitution of air for ethanol results in a lower refractive index in the heterogeneous layer surrounding each particle. The aerogels appeared yellow, greenish-brown, and silver in color. Note that there is a broad increase in long

wavelength absorption and that the blue-shift of the plasmon is greater for more highly aggregated systems. The average fraction of metal surface area covered by silica f was then calculated from the various blue-shifts. The results obtained from four different models (Newton, Landau/Lifschitz, Maxwell-Garnett, and Bruggeman) for the yellow, brown, and silver-colored aerogels, as well as for the initial silver colloid/prehydrolyzed TEOS mixture (alcosol) are summarized in table 4.

calculated for the brown and silver-colored aerogels are therefore not representative of the actual composition of the interlayer, but are provided simply to demonstrate that the presence of aggregation undermines the statistical disorder necessary for the application of effective medium theories.

By applying effective medium theory to the heterogeneous interlayer between the clusters and the matrix, we have extended the immersion

disorder and results in cluster-cluster interactions which prevent the proper determination of f using standard effective medium theories.

TABLE 4. —Application of effective medium theories to aerogels containing Ag clusters.

			N.	L./L.	M.G.	B.
Sample	$\lambda_s(\text{nm})$	ϵ_{layer}	$f(\%)$	$f(\%)$	$f(\%)$	$f(\%)$
Alcosol	401	1.87	16	17	17	17
Yellow	382	1.46	40	46	48	46
Brown	366	1.13	11	14	15	15
Silver	348	0.78	<0	<0	<0	<0

The broad increase in long wavelength absorption for the silver-colored sample of figure 78 indicates the formation of percolation paths and the onset of bulk behavior. Hence, the absorption profiles in figure 78 suggest the occurrence of coalescence, rather than simply coagulation of the clusters. Note in table 4 that f is larger in the yellow sample than it is in the more highly aggregated samples. In fact the effective medium calculation loses meaning with aggregation because it ignores the electrodynamic coupling between clusters. The values

spectroscopy technique to porous or heterogeneous materials and determined the fractional composition of each component in this interlayer. Hence the fraction of metal surface area available for catalytic gas reaction is determined. For random isolated silver particles in an aerogel host, we found that the average fraction of metal particle surface area covered by silica was $f=(46 \pm 5)$ percent. We have found that this technique is most applicable for statistically random metal particle distributions. Aggregation undermines statistical

1. Smith, D.D.; Sibille, L.; Cronise, R.; Noever, D.A.: "Surface Plasmon Resonance Evaluation of Colloidal Silver Aerogel Filters," Fifth International Symposium on Aerogels, Montpellier, France, September 1997, *Journal of Non-Crystalline Solids*, accepted for publication.
2. Knobloch, H.; Szada-Borrowski, G.V.; Woigk, S.; Helms, A.; and Brehmer, L.: *Applied Physics Letters* 69, 2336, 1996.
3. Kreibig, U.; and Vollmer, M.: *Optical Properties of Metal Clusters*, Springer, Berlin, 1995.

Sponsor: MSFC Center Director's Discretionary Fund; MSFC Space Products Development Office.

University Involvement: Laurent Sibille, Universities Space Research Association, ES76, 205-544-5221, e-mail: laurent.sibille@msfc.nasa.gov

Biographical Sketch: Dr. David D. Smith is a research scientist who develops microgravity research programs by performing novel theoretical and experimental research in advanced materials. He also serves as a project scientist for flight projects, and promotes technology transfer of relevant research. Dr. Smith has a bachelor's in optics from the University of Rochester, and a Ph.D. in physics from the University of Alabama in Huntsville. ■

Large-Scale Organization of Active Region Magnetic Fields

Dr. Mona J. Hagyard/ES82
256-544-7612
E-mail: mona.hagyard@msfc.nasa.gov

Both observational data and theoretical considerations lead us to believe that the magnetic fields observed at the surface of our Sun are subject to a large-scale organization. The topological property of magnetic helicity h_m can be used to characterize these large-scale patterns: $h_m = \mathbf{A} \cdot \nabla \times \mathbf{A}$, where \mathbf{A} is the vector potential of the magnetic field. This parameter describes the twisting and linkage of the magnetic fields and consequently can be used as a measure of the complexity of the magnetic field in solar active regions.

Observations for a number of years have provided evidence for large-scale helical patterns in the Sun. Famous solar astronomers noted early on that the outer filamentary structures of sunspots exhibited a hemisphere-dependent vorticity such that left-handed spiral structures of sunspots were dominant in the northern solar hemisphere with the opposite result for right-handed spiral spots. Filaments seen in spectroheliograms taken in the light of the $H\alpha$ (spectral line (656.3 nm) generally appear to have helical structures with opposite helicity in northern and southern hemispheres. Recently, measurements of the vector magnetic field at the surface of the Sun have been used to calculate the average helicity of the fields of solar active regions and determine whether they also follow

the hemispherical rule. In this case the results have been less convincing since a significant fraction of the regions analyzed violated this rule. But these studies covered only a very few active regions and these were from only one solar cycle (the last cycle that had its maximum in 1991).

The MSFC vector magnetograph has produced a vast amount of data on solar active regions, covering the period from 1980 to present and thereby spanning more than one 11-yr solar cycle. This database is unique because the Marshall instrument acquired more data in the 1980–1990 timeframe than any other vector magnetograph in existence. Such a large database presents an excellent resource to study the magnetic helicity in the many active regions that have been on the Sun from 1980 to the present time. Consequently, we began a research program in 1997 based on this archived data to find answers to the following questions:

- Is there a global pattern of helicity?
- Do active regions have a predominant helicity?
- Does magnetic flux emerge at the surface already with a predominant helicity?
- What is the relation between flare activity and helicity?
- Are there recurrent patterns of helicity and what are their cyclical characteristics?

To date we have analyzed the helicity of five active regions and in each case the hemispherical rule has been validated. In the case of two of these regions the archived data covered most of their disk transit so we could calculate the helicity over several days to look for changes; these changes

seemed to fall within the noise levels of the measurements. The archived data for these regions generally contained several observations taken very close in time (within minutes) so we were able to derive quantitative values for the noise level in the calculation of helicity. We found an unexpected result in the analysis of 57 data sets taken over a 6-hr period for an active region on the Sun on June 10, 1991—there was a pronounced linear change in helicity over the 6 hr. We found a similar result for a different active region observed September 9–16, 1980. While we are still investigating the source of these changes, we believe they are the result of a slight misalignment of the vector magnetograph telescope that causes a drift in the image throughout the observing period. One further result from our analyses so far—the values of helicity calculated from observations taken at different spectral settings of the magnetograph's filter for a single active region all agree within the measurement error. This result is significant because it means the effects of Faraday rotation are not important in the calculation of helicity, and we can therefore select a single spectral setting to evaluate the helicity rather than calculating it at several spectral settings.

Sponsor: Office of Space Science, Sun-Earth Connection, Solar Physics

University Involvement: This research is a cooperative effort with solar scientists at Montana State University, Bozeman, Montana, under grant NAG8-1399.

Biographical Sketch: Dr. Mona Hagyard joined the Space Science Laboratory at the Marshall Center in

September of 1967 and has been associated with that laboratory since that time. Her main areas of research include the interpretation and analysis of solar vector magnetograph data, radiative transfer with magnetic fields, and modeling of solar magnetic fields. Dr. Hagyard has been associated with the MSFC vector magnetograph project since its inception in 1968 and in 1980 she was appointed Team Leader of the MSFC Solar Observatory. As team leader, she directs the day-to-day operations of the Observatory, planning coordinated observing programs with solar space mission experiments and with other ground-based observatories around the world. Dr. Hagyard received the Ph.D. degree in physics from the University of Kentucky in 1967. ▀

Mechanics of Granular Materials Under Very Low Effective Stresses

Dr. Nicholas C. Costes/ES71
256-544-1637
E-mail: Nicholas.C.Costes.Dr@msfc.nasa.gov

The constitutive behavior of uncemented granular materials such as strength, stiffness, and localization of deformations are to a large extent derived from interparticle friction between solid particles and particle groups. Interparticle forces are highly dependent on gravitational body forces. At very low effective confining pressures, the true nature of the Mohr envelope, which defines the Mohr-Coulomb failure criterion for soils, as well as the relative contribution of each of nonfrictional components to soil's shear strength, cannot be evaluated in terrestrial laboratories. Because of the impossibility of eliminating gravitational body forces on Earth, the weight of soil grains produces interparticle compressive stresses which mask the true constitutive behavior in cohesionless granular materials, even in the smallest samples. The microgravity environment induced by near-Earth orbits of spacecraft provides unique experimental opportunities for testing theories related to the mechanical behavior of terrestrial granular materials in the absence of gravitational body forces. Such materials may include cohesionless soils, industrial powders, crushed coal, etc. Therefore, a microgravity experiment designated as Mechanics of Granular Materials (MGM) was designed, fabricated, and flown on missions STS-79 and STS-89 to investigate

the behavior of such materials in a microgravity environment.

The objective of the MGM microgravity experiment is to develop a quantitative understanding of the constitutive properties and deformation behavior of uncemented granular materials at very low confining pressure (effective stress) levels. A total of nine constant displacement triaxial (axisymmetric) compression tests were performed to achieve the science objectives. The first three tests (F1) were performed on dry, medium-dense silica sand specimens during the STS-79 Shuttle-Mir mission in September 1996. All tests were performed successfully under 0.05 kPa, 0.52 kPa, and 1.30 kPa confining pressures, and were subjected to quasi-static axial loading/unloading profiles. The subsequent six tests (F2 and F3) were performed on dry, loose specimens during the STS-89 Shuttle-Mir mission in January 1998 under the same confining pressures. F2 experiments were subjected to quasi-static axial loading/unloading whereas F3 experiments were subjected to cyclic loading.

The axial strain versus the nominal deviator stress responses for the three experiments performed during STS-79 mission are shown in figure 79. The five unloading-reloading cycles are indicated in all three experiments. The three stress-strain traces, which display substantial elastic stiffness, are characterized by distinct periodic oscillations in stress of similar frequency, amplitude and pattern, as inelastic deformations dominate the response. The 1.30 kPa experiment displays more pronounced oscillations of slightly greater amplitude than the other two experiments,

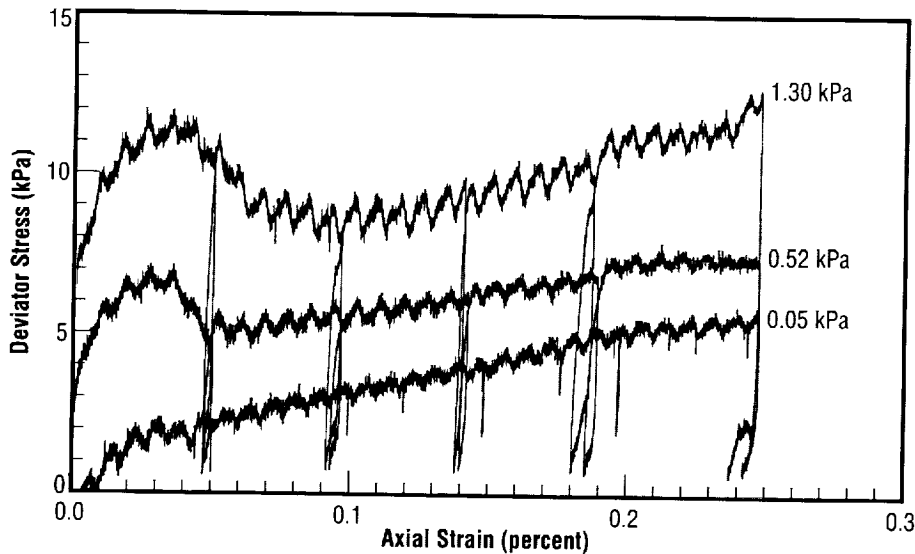


FIGURE 79.—Axial strain versus deviator stress relations of MGM experiments performed during the STS-79 mission.

while the overall stick-slip oscillations are very similar in all three cases. The 0.05 kPa confining pressure experiment shows continuous plastic hardening, and peak resistance, or

strength, at small strain (3 percent) is 2.0 kPa. The stress-strain response for the 0.52 kPa experiment shows much greater initial stiffness than the 0.05 kPa test, and a distinct peak

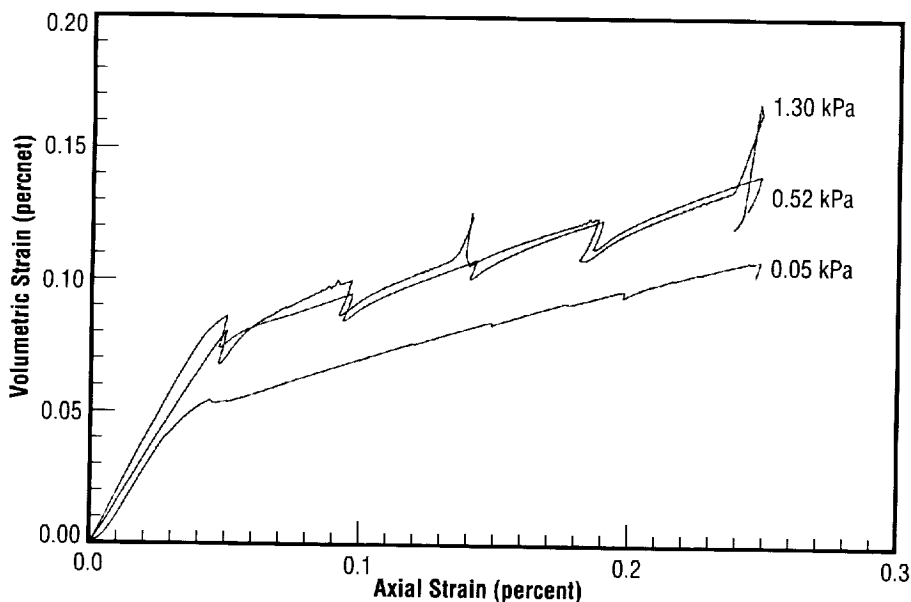


FIGURE 80.—Axial strain versus volumetric strain relations of MGM experiments performed during the STS-79 mission.

strength of 7.0 kPa is shown at 3 percent axial strain. The strain-softening phase is rather ductile and appears to be controlled without any local or global material instability. The response at the residual strength level is very similar to that observed in the 0.05 kPa test. The stress-strain response of the 1.30 kPa experiment shows initial stiffness behavior that is very similar to the 0.52 kPa test, whereas the stick-slip pattern is more pronounced and displays a similar period. The peak strength in this experiment is 12.0 kPa, also at 3 percent strain. The post-peak strain-softening proceeds at nearly the same rate as for the 0.52 kPa test. The residual level appears to remain quite stable. The peak friction angles observed for the three experiments are as follows: 75.1 degrees at 0.05 kPa, 58.5 degrees at 0.52 kPa, and 56.4 degrees at 1.30 kPa confining pressures. The observed angles of internal friction are unusually large for sand with initial relative density in the range of 85 percent. The friction angle for the same material at the same relative density, tested at 13.8 kPa and 34.5 kPa gives friction angles in the range of 38 to 41 degrees. There is a significant difference between the observed strength behavior at low- and high-stress levels. It appears that the relatively higher degree of mobilized resistance in the low confining stress experiments is a result of substantially different deformation mechanisms within the granular fabric, where more work-intensive modes of deformation involving extensive rotations rather than simple sliding are present and absorb more of the externally provided energy.

Figure 80 shows volumetric strain versus axial strain response diagrams

for the same three experiments. The initial responses appear to be very similar for the three experiments with initial dilatancy angles in the range of 12.2–14.6 degrees. There appears to be a significant departure from the initial, nearly linear, volumetric expansion at the 4 to 5 percent axial strain level. There the rate of expansion seems to be reduced by a factor of almost five, resulting in an average dilatancy angle of 3 to 4 degrees, which remains almost constant to the end of the experiments. None of the specimens displayed evidence of major shear-band formation or other forms of localized deformation. The volumetric changes were generally uniform and very diffuse, with extensive bulging at large axial strain levels.

The internal fabric of the tested specimens was examined by x-ray computed tomography (CT) scan techniques at Los Alamos National Laboratory. A reconstructed 1024×1024-pixel image was made every 1 mm along the height of the specimen for up to 120 images for each specimen. From these, three-dimensional volume renderings were built to investigate the internal structure. The CT data (fig. 81) reveal features unlike those present in ground-based tests. Cross sections have areas of generally uniform density outside of shear zones. Cross sections at right angles to the axis of compression show lower and higher density areas seeming to separate into radial streams, tied together toward the center of the specimen, and at right angles to the outer surface. In vertical sections, a shear cone and shear plane are visible. The shear cone appears to be in the center of the specimen indicating a “dead” space.

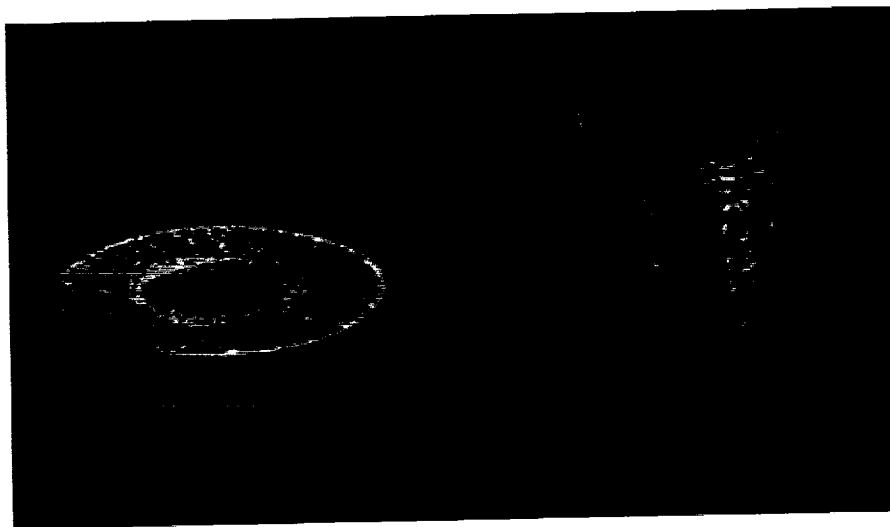


FIGURE 81.—Examples of CT scans of the specimens tested during the STS-79 mission.

Alshibli, K.A.; Costes, N.C.; and Sture, S.: “Behavior of Granular Materials Under Foundation Loading,” submitted to NASA Microgravity Materials Science Program in response to NRA-96-HEDS-02 announcement, 1997.

Alshibli, K.; Sture, S.; and Costes, N.C.: “Effect of Inclusions on Plane Strain Behavior of Sand,” accepted for publication at 12th ASCE Engineering Mechanics Conference, La Jolla, CA, May 17–20, 1998.

Costes, N.C.; and Sture, S.: “A Mobility Concept for Martian Exploration,” accepted for publication at Space 98: The 6th International Conference and Exposition on Engineering, Construction, and Operations in Space, Albuquerque, NM, April 26–30, 1998.

Costes, N.C.; and Alshibli, K.A.: “Behavior of Granular Materials

Under Foundation Loading,” submitted to the 1998 CDDF program, 1997.


Sture, S.; Costes, N.C.; and Alshibli, K.: “Penetration Resistance and Bearing Strength of Granular Materials in a Low-Gravity Environment,” submitted to the Glovebox Investigation, 1997.

Sture, S.; Costes, N.; Batiste, S.; Lankton, M.; Alshibli, K.; Jeremic, B.; and Swanson, R.: “Mechanics of Granular Materials at Low Effective Stresses,” accepted for publication, ASCE, *Journal of Aerospace Engineering*, 1998.

Sponsor: Office of Life and Microgravity Sciences and Applications

University Involvement: Dr. Khalid A. Alshibli is a research associate in the Department of Civil, Environmental, and Architectural Engineering,

University of Colorado at Boulder, and is currently working in MSFC's Space Sciences Laboratory to support the MGM experiment. The MGM principal investigator is Dr. Stein Sture, Department of Civil, Environmental and Architectural Engineering, University of Colorado at Boulder.

Biographical Sketch: Dr. Nicholas C. Costes is a senior research scientist in the Microgravity Science and Application Division, Space Sciences Laboratory, specializing in geotechnical engineering. He holds a Ph.D. in civil engineering from North Carolina State University. He is the coinvestigator on the Mechanics of Granular Materials Microgravity experiment. Costes was the principal investigator and coprincipal investigator on many Apollo mission lunar experiments and was a member of the Lunar Roving Vehicle design team. 

Modeling of Viscous Fluid Flow

Dr. Edwin C. Ethridge/ES75
256-544-7767
E-mail: edwin.ethridge@msfc.nasa.gov

Viscosity is an important thermophysical property that controls fluid flow in a liquid and is related to diffusion and the reorientational correlation time through the Stokes-Einstein and Debye-Stokes-Einstein relations. Viscosity appears in the classical equations for nucleation and crystal growth by aid of the Stokes-Einstein relation which inversely relates viscosity with the diffusion coefficient. A problem with crystallization calculations on undercooled liquids is that viscosity data do not exist between slightly above the glass transition temperature and just below the melting temperature for difficult glass formers due to the liquid crystallization. Over this temperature range the viscosity changes by as much as 10 orders of magnitude or more. Viscosity data can be fit with empirical equations but it is not known if it can be used to predict the viscosity in the undercooled region where viscosity normally cannot be measured. The theoretical viscosity models, used to interpolate between measured viscosity, vary by an order of magnitude and need scientific justification and testing in order to determine which are most suitable for modeling over the entire supercooled range from the melting temperature to glass transition. Without a knowledge of the viscosity of undercooled melts, one cannot accurately model undercooling, crystallization and glass formation. In order to develop a new method for determining the viscosity

of viscous undercooled melts, Dr. Edwin Ethridge at MSFC and Dr. Basil Antar at the University of Tennessee Space Institute undertook this fundamental fluid mechanical study to determine the viscosity of undercooled liquid using the phenomena of merging fluids.

The analytical formulation of the coalescence of two liquid masses has been completed. The mathematical model is based on the conservation of mass and momentum principles for fluid dynamics whose equations were solved numerically for the two-dimensional case. A computer code was developed based on the boundary element method (BEM) which solves the liquid coalescence problem for two cylindrical drops. The theoretical evolution of the shape as two liquid cylindrical drops, merging under the action of surface tension force in the absence of gravity force, can be compared with experimental results of actual merging experiments.

A set of low-gravity experiments were designed for the purpose of validating the merging results obtained with the numerical fluid dynamics model. The experiments were comprised of the merging together of two liquid drops of different diameters using four different liquids: glycerin, two silicone oils, and distilled water. The experiments were performed on board the NASA/KC-135 aircraft during the week of July 14, 1997, and lasted for 4 days. The merging process was visually recorded using a high-speed movie camera and film. Each merging test was performed during the low gravity portion of the flight parabola which nominally lasted for 20 sec. The data were analyzed by measuring the surface deformation during the

merging process. The low-gravity environment is necessary for these experiments in order to eliminate the deleterious effects of gravity on the merging process.

A means of quantitative comparison of theory with experiment is to use a plot of the ratio of the neck radius to the original drop radius versus the reduced time (fig. 82) of the experiment (fig. 83). A comparison of the variation of the contact radius with time as two glycerin spheres of equal diameter of 1.0 cm each merge in a low gravity environment was performed. Continuous curves in figure 84 represent the predictions from the numerical model for different liquid viscosities (for example, glycerin at temperatures: 20, 25, 30, 35, and 40 °C). Data points of the measured contact circle diameter from five consecutive film frames plot remarkably close to the 35 °C theoretical plot. Figure 84 shows excellent agreement between the low-gravity experiment and the calculated data for glycerin at 34 °C.

This initial success indicates that observation of the rate of merging behavior of fluid drops can be correlated with the viscosity of the liquid and may become a useful method for viscosity determination of undercooled liquids under containerless low-gravity conditions.

The results of this study will be used to propose critical measurements of the viscosity of a highly undercooled liquid to test the validity of viscosity theories. We are excited at the prospect of applying such a model to the measurement of the viscosity of highly undercooled liquid metals in the undercooled temperature range where

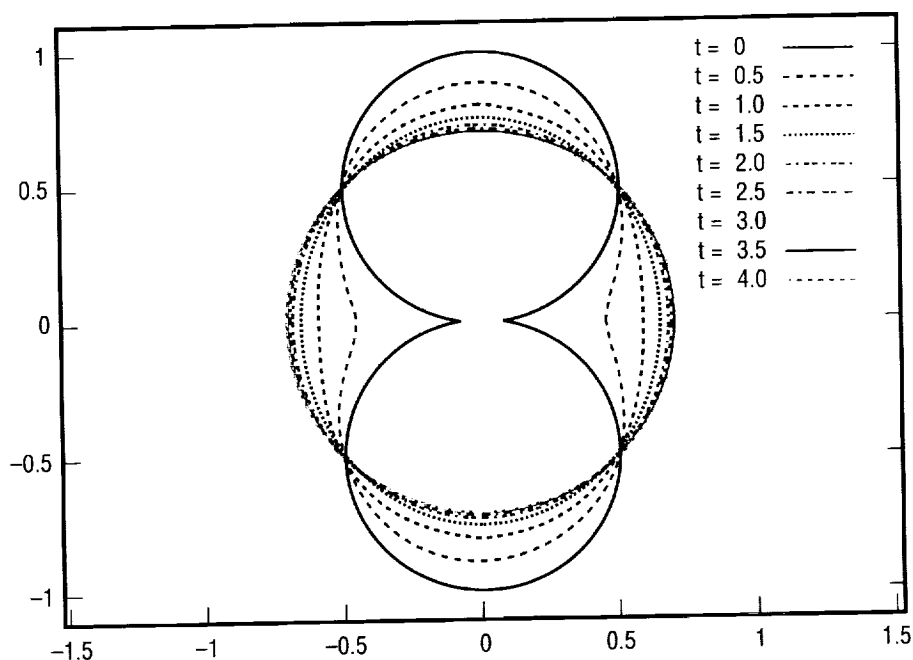


FIGURE 82.—Theoretical plot of the time evolution of geometry merging of two drops of glycerin.

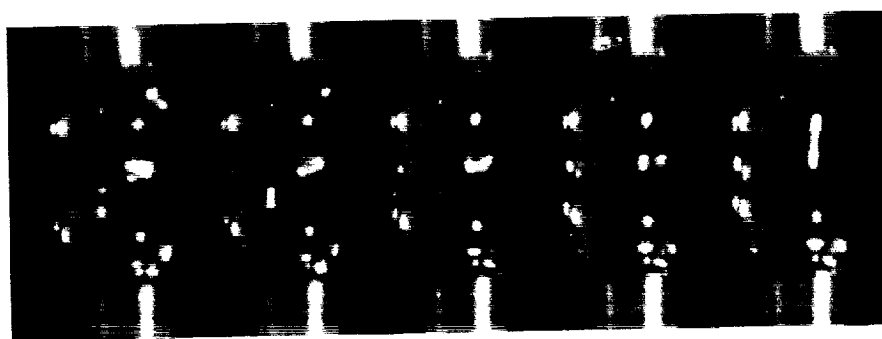


FIGURE 83.—Images of five consecutive frames from the high speed film of merging glycerin droplets.

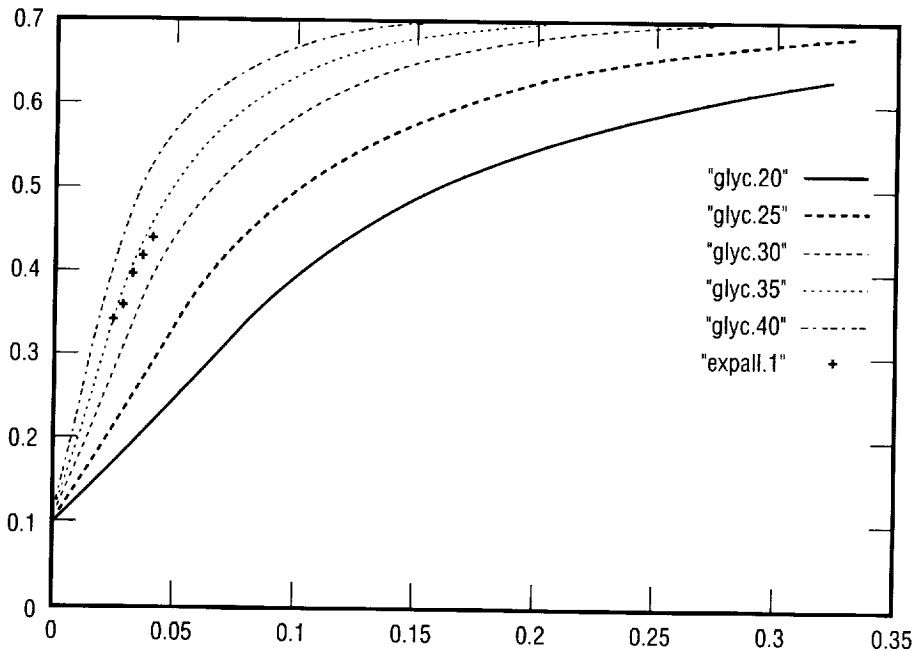


FIGURE 84.—Normalized neck diameter versus time calculated for glycerin at five different viscosities (temperatures) and five data points for experimental data.

viscosity cannot be measured at the present time. It is anticipated that this project could lead to the development of a space experiment to measure the viscosity of very “fragile” liquids in the region of rapidly changing viscosity.

Sponsor: Center Director’s Discretionary Fund

Biographical Sketch: Dr. Edwin Ethridge is a materials scientist, AST ceramics engineer, in the Space Sciences Laboratory. Ethridge is the principal investigator on the “Modeling of Viscous Fluid Flow” project. He has served as the assistant mission scientist on three Marshall-managed Spacelab missions and as assistant project scientist for the microgravity glovebox. Current research interests include modeling

viscosity of undercooled liquids, kinetics of glass formation, ZBLAN materials, and thermoelectric (Seebeck effects) during solidification. Ethridge received his Ph.D. in materials science and engineering from the University of Florida in 1977. ▀

The Solar Wind in the Inner Heliosphere

Dr. Steven T. Suess/ES82
256-544-7611
E-mail: steve.suess@msfc.nasa.gov

Coordinated observations with two deep space missions, Ulysses and the Solar Heliospheric Observatory (SOHO), are being used to construct a global description of the solar wind in the inner heliosphere and to isolate and enable research on problems in theoretical magnetohydrodynamics.

The Ulysses mission was specifically designed to map the global solar wind in the inner heliosphere—inside 5.5 astronomical units (AU) from the Sun. This has now been accomplished for the time of solar sunspot minimum in 1996¹ and is in progress for the next solar maximum, which will occur around the year 2001. The orbit of Ulysses is what allows it to carry out this mission. It is in a near polar orbit around the Sun that is inclined at 80 degrees to the Sun’s equator, and it ranges in distance from 1.34 AU at perihelion, to 2 AU over the poles of the Sun, to 5.4 AU at aphelion. Figure 85 shows this orbit, along with the initial transit from Earth to Jupiter, where the orbit was tilted from being in the ecliptic to being polar.

Solar wind arises in the solar corona, with high-speed solar wind (more than 600 km/sec) coming from coronal holes—dark regions of the corona as seen with x-ray telescopes. Low-speed wind comes from streamers, which are bright in x rays or during solar eclipse. At solar minimum, coronal holes lie at the north and south poles of the Sun and streamers are spread around the

equator. This relatively simple morphology is fully reflected in the resulting solar wind. Figure 86 shows the solar wind speed measured by the Solar Wind Observations Over the Poles of the Sun (SWOOPS) instrument on Ulysses between December 17, 1990, and March 2, 1996.² This figure, known as a "dial plot," shows how the solar wind speed varies as a function of solar latitude. The north and south poles are at the top and bottom of the figure and solar wind speed is plotted as a function of distance from the center—the scale is shown on the left. On the lower left are the measurements during the transit between Earth and Jupiter, and during the long passage from Jupiter to the south pole. Of main interest are the two quadrants on the right—the "fast latitude scan" between the two polar passages in September 1994 and July 1995. Over a period of less than 1 yr, Ulysses swept from the south to north poles, across the polar coronal holes and through the equatorial streamer belt. The solar wind speed was found to be remarkably uniform and always higher than 600 km/sec above 25 degrees latitude in both hemispheres. Then the speed fell precipitously to relatively low values in the streamer belt.

SOHO was launched in December 1995 and positioned at the L1 Lagrangian point between the Earth and the Sun in February 1996, as shown in the subpanel of figure 85. The L1 point is useful because it is a gravitationally stable location where a spacecraft can remain indefinitely with little or no orbital maneuvering. SOHO uses the L1 point to continuously observe the Sun from the plane of the ecliptic—essentially from the location of the Earth when considered

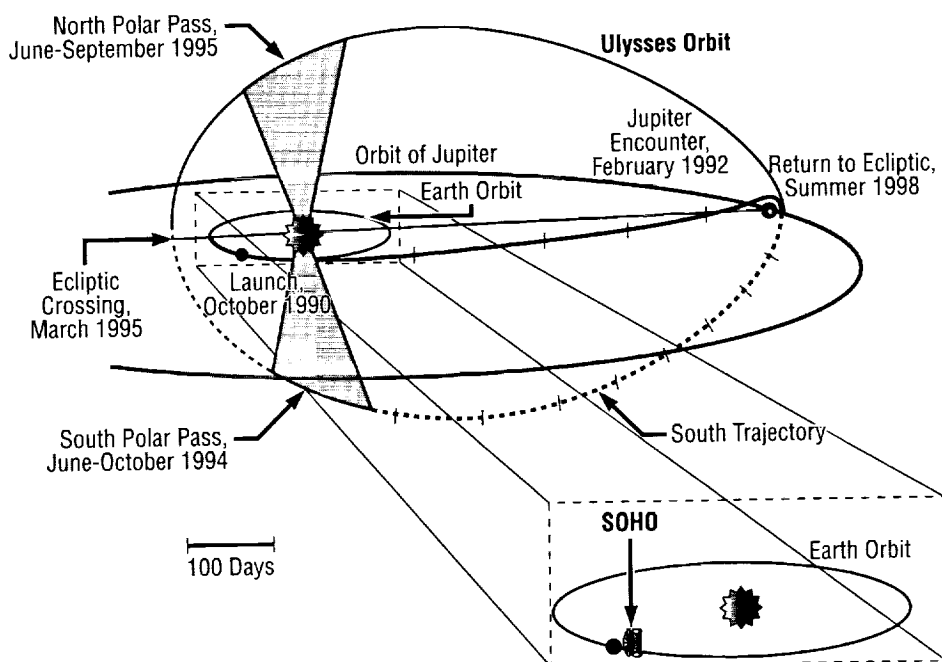


FIGURE 85.—Orbits of Ulysses and SOHO in relation to the orbits of Earth and Jupiter and to the Sun.

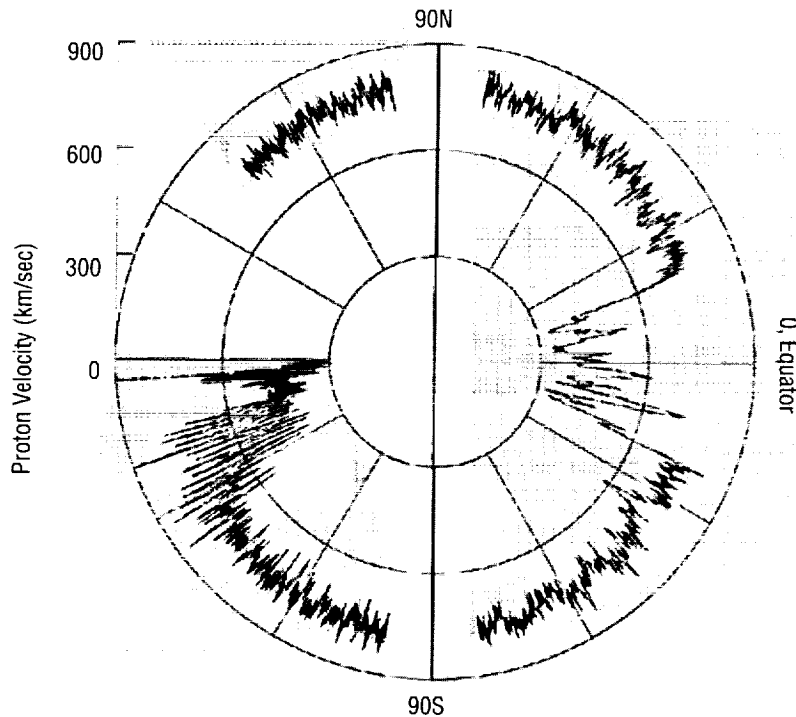
on scales the size of the solar system.

Since Ulysses and SOHO move in different orbits, they offer a variety of useful joint observing possibilities. For example in May 1997, Ulysses was directly off the left limb of the Sun as viewed from SOHO (and Earth) and slightly north of the equator. A CME was observed with SOHO, directed towards Ulysses, and it was rewarding that after a suitable elapsed time, almost 3 weeks in this case, a disturbance was detected at Ulysses. Similar joint observation opportunities occur at least twice a year. They supply data to analyze and model the striking uniformity of the high speed solar wind and the precipitous drop-off to low-speed solar wind shown in figure 86, and how the low-speed solar wind escapes from streamers. These modeling problems

are being solved within the Solar Science Branch of the Space Science Laboratory as part of our participation in both the Ulysses/SWOOPS and SOHO ultraviolet coronagraph spectrometer (UVCS) experiments.³

1. Suess, S.T.; Phillips, J.L.; McComas, D.J.; Goldstein, B.E.; Neugebauer, M.; and Nerney, S.: "The Solar Wind—Inner Heliosphere," *Advances in Space Research*, in press, 1998.
2. Phillips, J.L.; Bame, S.J.; Feldman, W.C.; Goldstein, B.E.; Gosling, J.T.; Hammond, C.M.; McComas, D.J.; Neugebauer, M.; Scime, E.E.; and Suess, S.T.: "Ulysses Solar Wind Plasma Observations at High Southerly Latitudes," *Science*, 268, p.1030, 1995.

July 31, 1995–March 2, 1996



December 17, 1990–September 13, 1994

FIGURE 86.—A solar wind dial plot shows how the solar wind speed varies as a function of heliographic (solar) latitude as measured by the SWOOPS solar wind plasma experiment on Ulysses.

3. Kohl, J.L. et al.: "The Ultraviolet Coronagraph Spectrometer for the Solar Heliospheric Observatory," *Solar Physics*, 162, p. 313, 1995.

Sponsor: Office of Space Science

University Involvement: University of California (Los Alamos National Laboratory); University of Alabama in Huntsville; University of Florence (Italy); Harvard University (Harvard-Smithsonian Center for Astrophysics)

Biographical Sketch: Dr. Steven T. Suess is an aerospace technician, Solar Studies. His duties include conducting research in theoretical magnetohydrodynamic modeling of space physics phenomena, advising NRC resident research associates, and collaborating with space scientists who are performing similar research within the Space Science Laboratory and at outside institutions. He received his A.B. degree at Berkeley in 1964 and his Ph.D. at UCLA in 1969. ▀

Time-Resolved Fluorescence in Crystallizing Protein Solutions

Dr. David D. Smith/ES76
256-544-7778
E-mail: david.d.smith@msfc.nasa.gov

September 13, 1994–July 31, 1995
The "Fast Latitude Scan"

The objective of this investigation is to apply time-resolved fluorescence techniques to study the gravitationally sensitive process of crystallization in protein solutions. The more general goal is to explore the dynamics of the formation of crystalline precipitates. This requires a very large macromolecule with many binding sites so that fluorescent chromophores may be easily added without affecting the reaction kinetics. Proteins are among the only macromolecules that can be derivatized without significantly changing the crystallization kinetics. More specifically, to determine the impact of the environment on the crystal growth of proteins, we will examine the effect of salt concentration, pH, and temperature on the protein crystal surface by analyzing fluorescence decay times. Furthermore, we will examine intermolecular and intramolecular energy transfer between labeled proteins to determine the aggregation requirements for crystal nucleation. Perhaps most important to determine is the correlation between aggregation and anisotropy. Larger aggregates have a longer rotational diffusion time which manifests itself in the anisotropy of the decay.

TABLE 5.—Lucifer yellow, EDANS, and cascade blue do not affect lysozyme crystallization. Oregon green, carboxyfluorescein, and pyreneacetic acid do hinder lysozyme crystallization.

Dye	Absorption Maximum (nm)	Emission Maximum (nm)
CB	400	420
LY	428	533
EDANS	335	440
OG	511	530
CF	492	518
PAA	340	376

We have identified the binding sites and derivatized lysozyme egg white protein with over 10 different fluorescent dyes. The derivatized proteins have been tested to observe the effect on their crystallization kinetics. Table 5 lists the absorption and emission maxima of some of the covalently attached dyes we have used. Lucifer yellow, EDANS, and cascade blue do not affect lysozyme crystallization. Oregon green, carboxyfluorescein, and pyreneacetic acid, on the other hand, hinder lysozyme crystallization. The fluorescence lifetimes may be determined by using time-correlated single-photon counting using the femtosecond output from a Ti:Sapphire laser. Single photon counting involves the measurement of the time delay between photons incident on a reference or trigger photomultiplier tube (PMT), and a signal or single photon PMT which records the fluorescence as shown in figure 87.¹ The signal PMT is desensitized so that a maximum of only one fluorescent photon per pulse is recorded. Discriminators are used to shape the trigger and signal pulses so that the delay does not depend on the pulse height. A time to amplitude

converter converts the time delay to a voltage by charging a capacitor at the initiation of the trigger pulse. A multichannel analyzer then produces a histogram of the time delays of the various fluorescent photons from the many pulses. The histogram represents the exponential or multi-exponential decay characteristic of the fluorescent chromophore (or fluorophore). Another technique for measuring lifetimes involves frequency modulation of the incident light. Each technique has its associated advantages. In our laboratory we are developing the capability to perform both these types of measurements.

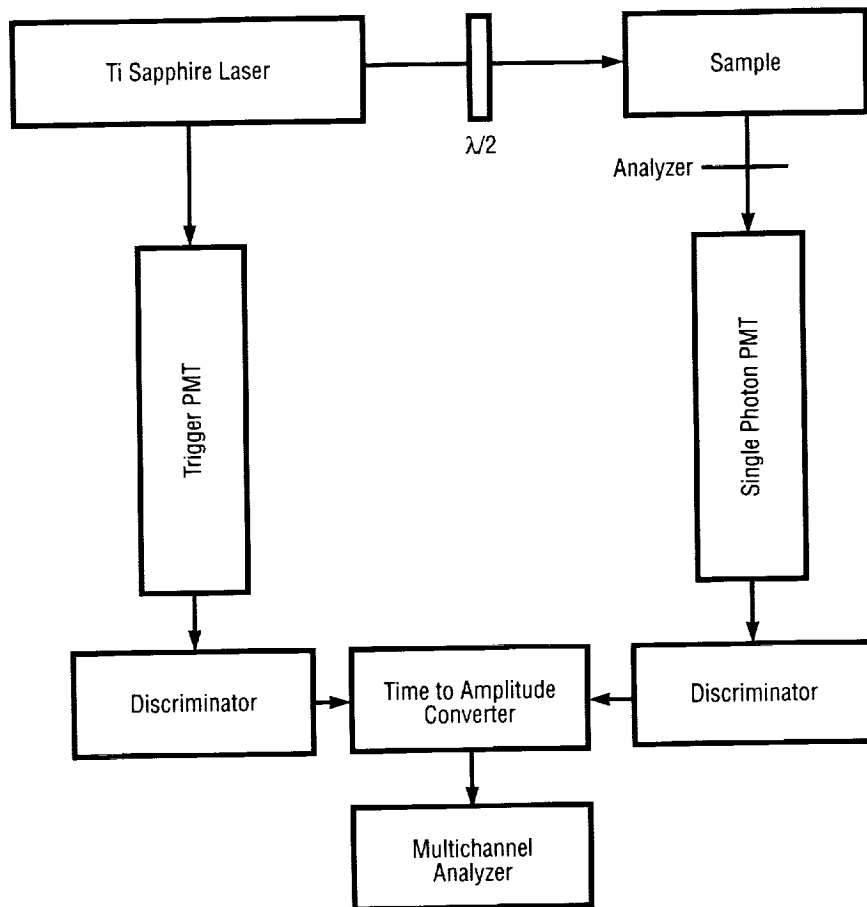


FIGURE 87.—Single photon counting system for determination of fluorescence decay.

Measurement of the anisotropy of the decay provides information on molecular rotation and flexibility. Free fluorophores become completely depolarized as the fluorescence decays. A restricted fluorophore however, never quite loses its anisotropy so that the fluorescent signal changes as the polarization analyzer is rotated. By measuring the fluorescence anisotropy we will determine if larger aggregates are restricted to a greater degree than smaller aggregates. We will also determine rotational restrictions imposed by the salt solution. Perhaps most importantly we will determine if aggregation may be monitored by the degree of rotational restriction imposed.

Initial fluorescence anisotropy measurements have been performed using both time- and frequency-modulated systems. The initial results have provided information necessary to modify the chemical synthesis of the lysozyme derivatives. We have found that in order to correlate anisotropy with aggregation, we need to select a fluorophore whose lifetime is comparable to the rotational diffusion time estimated from the Stokes relationship, or at least optimize the lifetime to diffusion time ratio to study different aggregate sizes.

1. *Topics in Fluorescence Spectroscopy, Vol. 1: Techniques*, ed. Jo Lakowicz, Plenum Press, 1991, New York.

Sponsor: MSFC Center Director's Discretionary Fund

University Involvement: Lloyd Davis, University of Tennessee Space Institute

Biographical Sketch: Dr. David D. Smith is a research scientist at the Marshall Center. He develops microgravity research programs by performing novel theoretical and experimental research in advanced materials. He also serves as project scientist for flight projects, promoting technology transfer of relevant research. Smith earned a B.S. in optics at the University of Rochester and a Ph.D. in physics at the University of Alabama in Huntsville. ■

Superconductor Interactions With Gravity

Ron Koczor/ES01
256-544-3078
E-mail: ron.koczor@msfc.nasa.gov

The Marshall Center is charged to investigate technologies and concepts that will result in future reductions in the cost of space travel. Among the areas of interest to these investigations are topics in breakthrough propulsion physics. These basic science investigations focus on ideas that are beyond our present capability to implement, yet offer some theoretical or experimental basis to warrant further research.

One of these ideas involves the reported interactions between high speed rotating superconductors, magnetic and electromagnetic fields, and the local gravity field. Published reports (Podkletnov, 1992) indicate a possible gravity shielding effect with such an apparatus. Podkletnov devised an experiment in which a large disk of high temperature ceramic superconducting material was magnetically levitated and rotated at high speed (up to several thousand rpm's in the presence of an external magnetic field. In the course of the tests he noted that objects above the rotating disk showed a variable but measurable loss in weight (variable from <0.5 percent to around 2 percent). The effect offers significant potential for space travel, if real.

An MSFC experimental team was created to develop methods to test the reported effect. In association with

researchers at the University of Alabama in Huntsville (UAH), the team developed a multipath approach to the investigation. First is material research that is investigating issues pertaining to the formulation and fabrication of high temperature ceramic superconductors. This research led to the successful fabrication of a large (30-cm-dia.) yttrium barium copper oxide (YBCO) superconducting disk. The disk is presently undergoing characterization of its superconducting performance and will be used in gravity tests in the near future. Second, the team developed several test devices to gather data to assist in understanding the interactions between these high temperature superconductors and a variety of electromagnetic and mechanical inputs. While our goal is to understand the effect that was reported, we have not exactly duplicated the apparatus which was used in the original experiments.

Third, it was decided early on that one of the most important requirements was to develop a measurement technique that would be able to repeatably and accurately measure a change in gravity. Several approaches were investigated, including optical interferometry, traditional balances and others. The most sensitive is a modified commercial LaCoste-Romberg gravimeter which reliably measures gravity field stability in the 1×10^{-6} cm/sec² range. The device is temperature and buoyancy compensated and the sensing element is isolated from the surrounding atmosphere.

We have reported (Li, 1997) results using this gravimeter to probe local gravity changes in the neighborhood

of large bulk-processed high-temperature superconductors. These static field tests were run at a number of temperatures between 30 K and 90 K. Tests included measurement of critical current and other disk parameters. The static field tests showed no gravitational field changes above the 1×10^{-6} cm/sec² level. Although many "signals" were seen, they were ultimately all attributed to explainable phenomena.

The original report (and subsequent conversations with the author) indicated that alternating AC fields play an essential role in their observed distortion of combined gravity and barometric pressure readings. In order to understand this role, we conducted experiments on large (15-cm-dia.) bulk YBCO ceramic superconductors placed in the core of a three-phase, AC motor stator. The applied rotating field produces a magnetic field having up to 60,000 rpm. The field intensity decays rapidly from the maximum at the outer diameter of the superconducting disk (~60 G) to the center (<10 G). This configuration was applied with and without a permanent DC magnetic field levitating the superconducting disk, with corresponding gravimeter readings indicating an apparent increase in observed gravity of less than 1×10^{-6} cm/sec², measured above the superconductor. No effect was noted (within the high precision of the observation) on the gravimeter readings of the rotating magnetic field or thermal environment or on rotating the superconducting disk.

Another essential component (as reported) to achieve anomalous gravity effects is an input in the form of radio-frequency (rf) electromagnetic fields. We conducted additional experiments

on rf-illuminated (1–15 MHz) superconducting disks. During these tests, gravity readings indicated an apparent increase in observed gravity of approximately $3\text{--}5 \times 10^{-5}$ cm/sec², above and to the side of the superconductor. In this preliminary study, rf-illumination is achieved using a 15-cm-dia. spiral antenna with rf power inputs on the order of 90 W. The gravitational modification range we observed is significantly lower than the 2.1 percent gravity modification reported by Podkletnov. However, our apparatus only partially simulated the apparatus reportedly used by Podkletnov. Further tests are underway with other rf-illumination techniques.

The error analyses of thermal and electromagnetic interference in a magnetically shielded gravimeter with vacuum enclosures, Faraday cages and shielded instrument leads, were performed both experimentally and theoretically. There is a nearly exact correspondence between the peak gravity effects reported by Podkletnov (3–4 MHz rf-excitation frequency) and the well-known peak in AC resistance in superconductors (2–7 MHz, owing to reverse Josephson quantum effects). This suggests that electrical resistance arises in this frequency range and subsequently any trapped magnetic fields in the superconductor may disperse partially into the measuring instrument's local environment.

Work continues with other experimental apparatus being prepared for tests in the coming year. These tests will include rotation of the disk in variable electromagnetic fields under AC levitation conditions. This project is being supported by Center Director Discretionary Funds and the Advanced Space Transportation Program (ASTP)

under its Breakthrough Propulsion Physics efforts.

Podkletnov, E.; and Niemanen, R.: "A Possibility of Gravitational Force Shielding by Bulk $\text{YBa}_2\text{Cu}_3\text{O}_{7-x}$ Superconductors," *Physica C* 203, pp. 441–444, 1992.

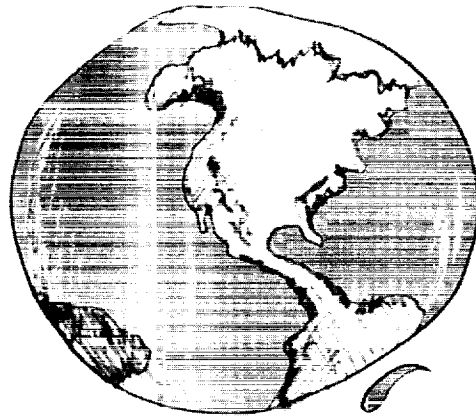
Li, N.; and Torr, D.G.: "Effects of a Gravitomagnetic Field on Pure Superconductors," *Physical Review D*, pp. 457–459, 1991.

Li, N.; and Noever, D., et al: "Static Test for a Gravitational Force Coupled to Type II YBCO Superconductors," *Physica C* 281, pp. 260–267, 1997.

Sponsor: Center Director's Discretionary Fund; the Advanced Space Transportation Projects Office

University Involvement: Cooperative research with UAH

Biographical Sketch: Ron Koczor is assistant director for Science and Technology in the Space Science Laboratory at MSFC. He has a degree in physics and has been with NASA for 10 years. **D**



space system concept studies

"The greatest gain from space travel consists in the extension of our knowledge. In a hundred years this newly won knowledge will pay huge and unexpected dividends."

—Wernher von Braun

Marshall Space Flight Center is dedicated to expanding our knowledge as we continually address issues that will yield benefits for future generations. We have learned to build on past successes by raising new questions which inspire new developments. The birth of technological wonder is how Marshall operates.

Program Development serves as the central focus within Marshall for conceptual definition and technical feasibility studies as well as related strategic planning that leads to the implementation of future programs. Our job is to look at the future. We are laying the foundation for new methods of space transportation and for new and exciting space science.

Since the day America's first satellite successfully orbited the Earth, we have been challenged to go further in our quest for solutions to scientific and technological issues. The work being conducted through Program Development will further extend our knowledge and reveal vital information which will be used in meeting tomorrow's exciting challenges in space exploration.

Axel Roth
Director
Program Development

Beamed Energy Research Program for Propulsion and Planetary Defense

Dr. Jonathan W. Campbell/PS02
256-544-7076
E-mail: jonathan.campbell@msfc.nasa.gov

Beamed energy may be accomplished at many different wavelengths including microwave, infrared, and the visible portions of the electromagnetic spectrum. Lasers are used in the infrared and visible regimes because of their low divergence over transmission ranges.

Laser technology is maturing rapidly. Atmospheric propagation problems such as thermal blooming and stimulated Raman scattering have been overcome by building lasers that operate at short pulse widths. New programs are on the horizon for using lasers in defensive roles. These include antimissile defenses on sea, air, and space-based platforms. Lasers may also be used to "push" orbital debris into the atmosphere for elimination as a space hazard (fig. 88). Developing laser systems to deal with the orbital debris problem would be a stepping stone to larger systems based on the laser/momentum transfer principle. These larger systems could potentially be used to deflect inbound asteroids and comets.

In addition to engaging noncooperative targets, lasers may also be used in a cooperative sense to propel specially configured launch vehicles both in the atmosphere and in space.

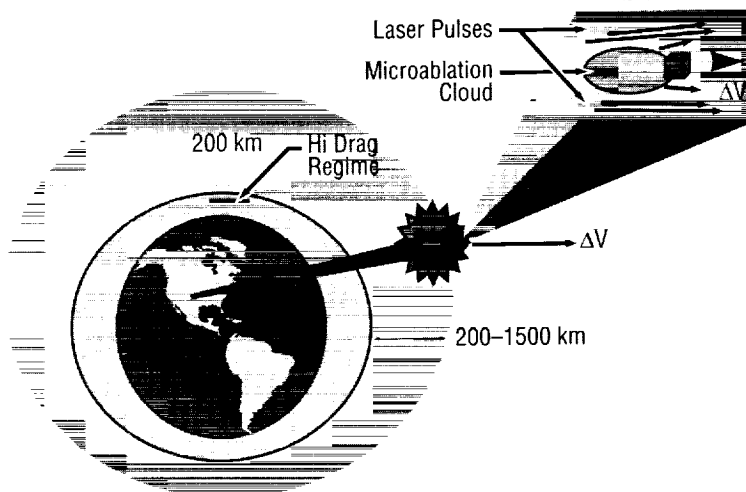


FIGURE 88.—Project ORION: Orbital debris removal using ground-based sensors and lasers.

During this past year we have made substantive progress on several technological fronts. In the area of orbital debris removal, we have demonstrated using a torsional pendulum suspended in vacuum that we can impart significant momentum to a target with a laser pulse. In fact, the preliminary outcome of these experiments has been to show that the effect is more pronounced than we thought. The implications of this finding if verified are that less intensity would be required on the target particle, hence adding technological margin to the mission concept. In other words, should the laser beam be degraded in transit to orbit, there should still be sufficient intensity to slow the particle down. This was a major breakthrough in developing this technology.

In addition, at White Sands we have achieved a major breakthrough in the application of using lasers to propel cooperative targets. In highly significant proof-of-principle joint United

States Air Force/NASA tests, we have demonstrated that we can leave the propulsion system on the ground and use the ambient air as a working medium to launch a payload (fig. 89). This opens a promising new chapter in propulsion technology.



FIGURE 89.—Night launch of a light craft capsule using a ground-based laser.

Biographical Sketch: Dr. Jonathan W. Campbell holds a Ph.D. in astrophysics and space science from the University of Alabama. In addition, he holds three master's degrees and a bachelor's in aerospace engineering from Auburn. He is a Colonel in the Air Force Reserve assigned to Air University and is an active Certified Instrument Instructor. During his career, he has worked for NASA, the Army Missiles and Space Intelligence Agency, the National Air Intelligence Agency, and Pratt and Whitney Aircraft. Currently, his primary research interests are in the areas of planetary defense, including orbital debris removal, gravitational breakthrough physics, and astrophysics. He has authored over 50 publications.

Sponsor: Advanced Space Transportation Programs Office

Other Involvement: United States Air Force **D**

Electrodynamic Tether Reboost of the *International Space Station*

Les Johnson/PS02
256-544-0614
E-mail: les.johnson@msfc.nasa.gov

The Marshall Space Flight Center is studying the feasibility of using electrical power to generate reboost thrust for the *International Space Station (ISS)* by means of a new type of electrodynamic tether attached to the Station, thus providing an alternative to chemical thruster reboost. A flexible system could be developed to generate an average thrust of 0.5–0.8 N for 5–10 kW of electrical power. By comparison, aerodynamic drag on *ISS* is expected to average from 0.3 to 1.1 N (depending upon the year and the prevailing solar conditions). The concept is illustrated in figure 90.

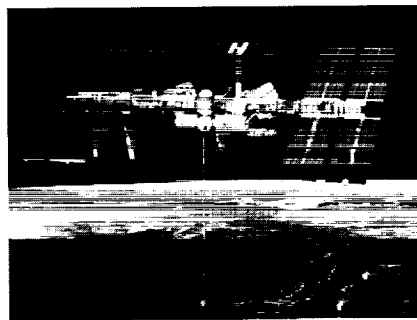


FIGURE 90.—Artist concept of an electrodynamic tether reboost system on the *International Space Station*.

The system being investigated uses a tether with a kilometers-long uninsulated bare segment capable of collecting currents greater than 10 A from the ionosphere. The new design exhibits a remarkable insensitivity to electron density variations, allowing it to operate efficiently even at night. A relatively short and light tether (10 km or less, weighing 200 kg) is required, thus minimizing the impact on the *ISS*. Such a system would cause a center of mass shift of less than 5 m.

An electrodynamic tether can work as a thruster because a magnetic field exerts a force on a current-carrying wire. This force is perpendicular to the wire and to the field vector. If the current flows downward through a tether connected to a spacecraft in Earth orbit, the force exerted by the geomagnetic field on the system has a component that accelerates the spacecraft along the direction in which it is already moving (fig. 91).

An orbiting system, by virtue of its motion through the Earth's magnetic field, experiences an electric field ($V \times B$) perpendicular to its direction of motion and the geomagnetic field vector. For an eastward-moving system, such as the *ISS*, the field is such that the electrical potential decreases with increasing altitude (at a rate of around 100 V/m for the *ISS* orbit). In order to drive a current down the tether, it is necessary to overcome this induced voltage. Thus, such a system requires a power supply and may be considered a type of electrical thruster.

The groundwork has been laid for a tether reboost system. NASA has developed tether technology for space

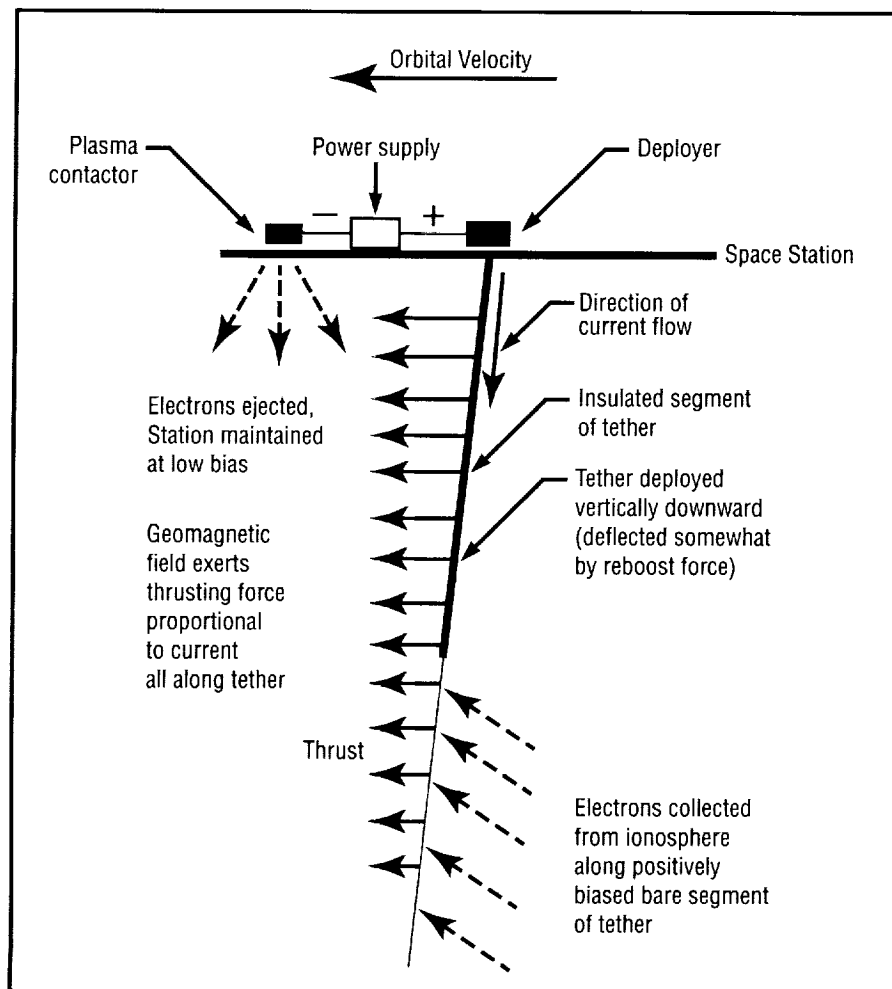


FIGURE 91.—Principles of operation for an electrodynamic tether reboost system on the International Space Station.

applications over the past several years. Important milestones include retrieval of a tether in space (tethered satellite system (TSS-I) mission, 1992), successful deployment of a 20-km-long tether in space (small expendable deployer system (SEDS-I) mission, 1993), and operation of an electrodynamic tether with tether current driven in both directions—power and thrust modes (plasma motor generator mission, 1994).

Most important for the reboost application, the TSS-I reflight mission recently drew currents on the order of 1 A, which corresponded to a magnetic force on the Shuttle-tether system of around 0.4 N (though as a drag rather than a thrust due to the direction of current flow in the tether). To summarize: the predicted behavior of tethered systems, dynamically and electrodynamically, has been confirmed in space.

A three-phase development approach leading to the implementation of an electrodynamic reboost system for the ISS is being considered. Phase 1 culminates with the flight of the propulsive small expendable deployer system (ProSEDS) experiment, and in the preliminary design of a prototype system for test on the ISS. Phase 2 results in the fabrication, integration and flight of the prototype system on the ISS and a system design for an operational ISS reboost system. Phase 3 concludes with the integration and use of the operational system on the ISS by 2004.

Sponsor: Advanced Space Transportation Programs Office

Industry Involvement: The Boeing Company; Tether Applications Company; Tethers Unlimited

Biographical Sketch: Les Johnson is the principal investigator for the Propulsive Small Expendable Deployer System flight experiment and the study manager for many of MSFC's future mission activities involving the use of space tethers. Prior to joining NASA in 1990, Johnson worked at General Research Corporation on the development of space-based neutral particle beam systems. He has a B.A. in chemistry and physics from Transylvania University, and an M.S. in physics from Vanderbilt University. He is a graduate of the International Space University Summer Session Program. ▀

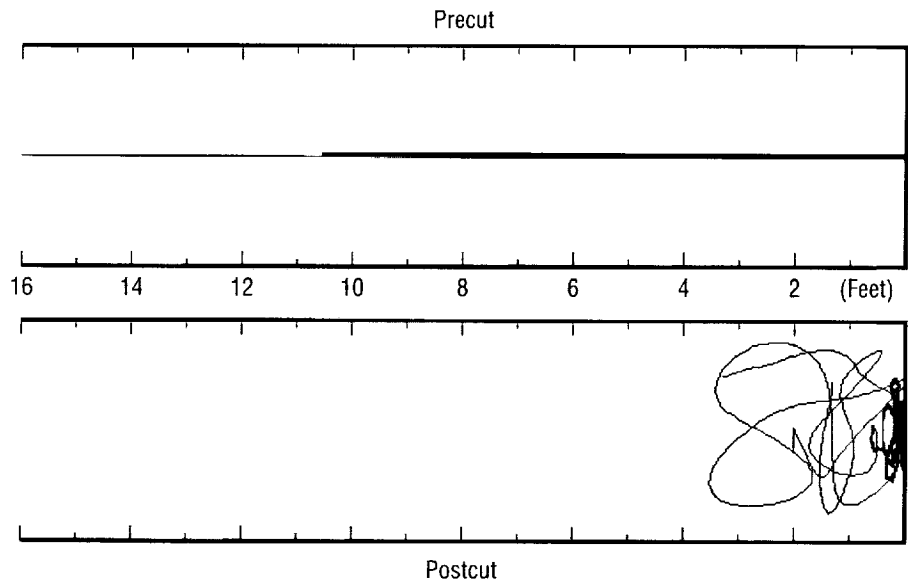
Improving the Safety of Space Tethers

Charles Rupp/PS04
256-544-0627
E-mail: Chris.Rupp@msfc.nasa.gov

“What happens if the tether breaks?” is often the first question asked when proposing tether applications on manned space flights. Even unmanned missions often require similar consideration in controlling tether recoil to prevent impacting other payloads. An SBIR contractor has performed preliminary tests on a technique to help control and contain slack tether if catastrophic damage occurs. But first, a brief explanation of what does happen if the tether breaks is in order.

If a space tether under tension is severed, a tension wave travels along the tether to spacecraft from which the tether has been deployed. The tether then moves to the spacecraft where it may gather and entangle parts of the spacecraft. Over time, the tether may redeploy under the effects of gravity gradient acceleration. This action has been simulated using numerical models of tether behavior in space and has been seen dramatically in pictures taken of the severed tether accident during the reflight of the tethered satellite system.

To help control the rebound of space tethers, it has been suggested that inserting a section of tether with different physical properties will cause traveling tension waves to be reflected. The effect has been demonstrated under laboratory conditions in work performed by the Michigan Technic



*Note—Shape of Microdyneema Fireline is only a representation of how the tether was generally collected and its overall dimensions. It is NOT an actual representation of its shape.

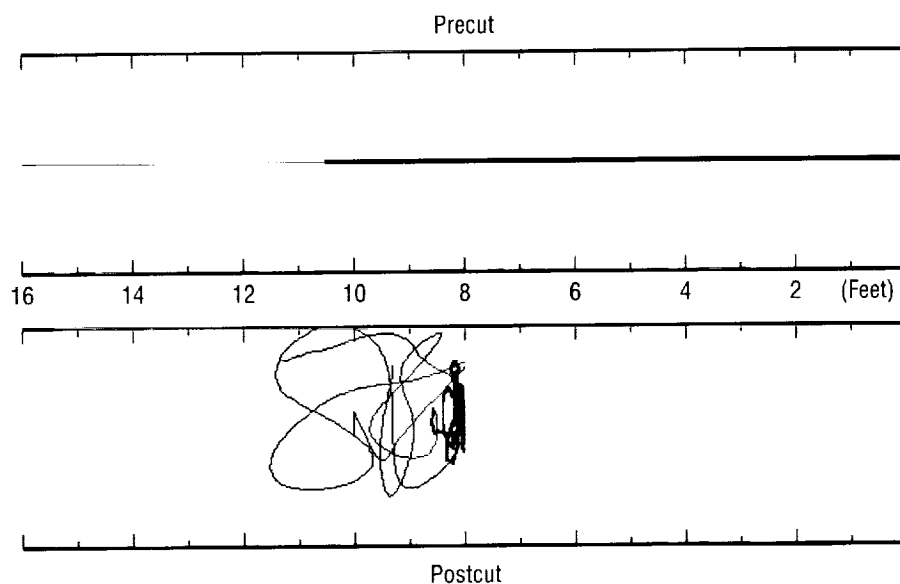
Legend

- 0.5 mm DIA Microdyneema Fireline Tether
- 2.25 mm DIA Spectra 1000 Braid/Yarn Filled Tether

FIGURE 92.— Traveling wave stops at the solder-filled tether splice and does not gather at the tether support.

Corporation in the SBIR Phase I contract “Safety Hazards and Emergency Deployment of a Tethered Satellite System.” The tether used in these experiments was a 10- and one-half-ft piece of 0.1-in.-dia. yarn-filled braided Spectra™ tether which is connected to a 5.5-ft piece of 0.02-in.-dia. commercially available Microdyneema Fireline™ fishing line. This combination was stretched

horizontally between two supports and then severed at the fishing line end. The resulting tether motion was video taped for subsequent analysis. Figure 92 shows the precut stretched configuration and then the postcut results. As can be seen, most of the tether rebounds back to the support even though the properties of the two tether sections are dissimilar.



*Note—Shape of Microdyneema Fireline is only a representation of how the tether was generally collected and its overall dimensions. It is NOT an actual representation of its shape.

FIGURE 93.—Tether moves and gathers at the tether support after being cut.

Figure 93 shows the dramatically different rebound when a 4-ft section of solder has been embedded in the Spectra™ section. As can be seen, the fishing line section has rebounded to the solder filled Spectra™ section, but the traveling wave stops there. The solder has added additional mass to the tether to further enhance the discontinuity in the tether properties between the two tether segments.

Future work will further quantify this preliminary finding and lead to simple modifications to existing tether designs which will greatly enhance tether safety.

Sponsor: NASA Small Business Innovative Research

Biographical Sketch: Charles Rupp began his employment at MSFC in 1966 working on the Skylab attitude control system. His interest in space tethers began in the late 70's when he developed a control law for stabilizing a tether system along local vertical. Rupp served as principal investigator for the Small Expendable Deployer System which successfully flew twice in the early 90's as a secondary payload on the Delta expendable launch vehicle. Rupp currently works in Program Development on the Propulsive Small Expendable Deployer System (ProSEDS) and other tether projects. ■

Space Tether Transportation System

Les Johnson/PS02
256-544-0614
E-mail: les.johnson@msfc.nasa.gov

A space-based spinning tether system can be used to boost payloads into higher orbits with a Hohmann-type transfer. The system would be anchored to a relatively large mass in LEO awaiting rendezvous with a payload delivered to orbit. The uplifted payload meets with the tether facility which then begins a slow spin-up using electrodynamic tethers (for propellantless operation) or another low-thrust, high specific impulse thruster. At the proper moment and tether system orientation, the payload is released into a transfer orbit—potentially to geostationary transfer orbit (GTO) or lunar transfer orbit. A network of such systems, using tether materials available today, could be developed to “hand off” a payload until it reaches the desired location. The approach is illustrated in figure 94.

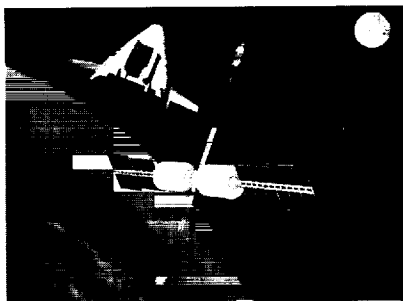


FIGURE 94.— Artist concept of a space-based momentum transfer tether transportation system for transferring payloads from low-Earth orbit to geostationary-Earth orbit and beyond.

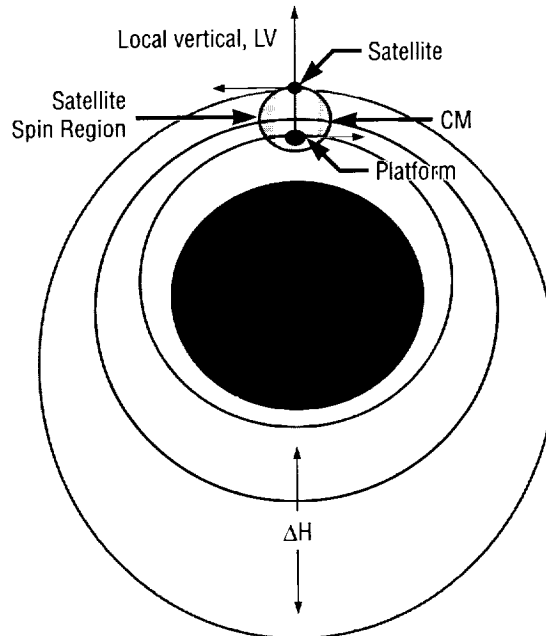


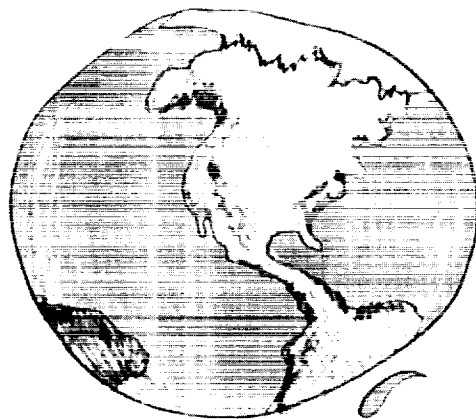
FIGURE 95.— Principle of operation for a rotating tether system used for orbit transfer.

The physics governing a rotating momentum exchange system is illustrated in figure 95. Following spin-up of the tether and satellite system, the payload is released at the local vertical. The satellite is injected into a higher orbit with perigee at the release location; the orbital tether platform is injected into a lower orbit with apogee at the release location. The satellite enters a GTO trajectory and accomplishes the transfer in as little as 5 to 16 hr, where the lower number applies to a single-stage and the higher number to a two-stage system. The platform then reboosts to its operational altitude using electric thrusters. The system thus achieves transfer times comparable to a chemical upper stage with the efficiencies of electric propulsion.

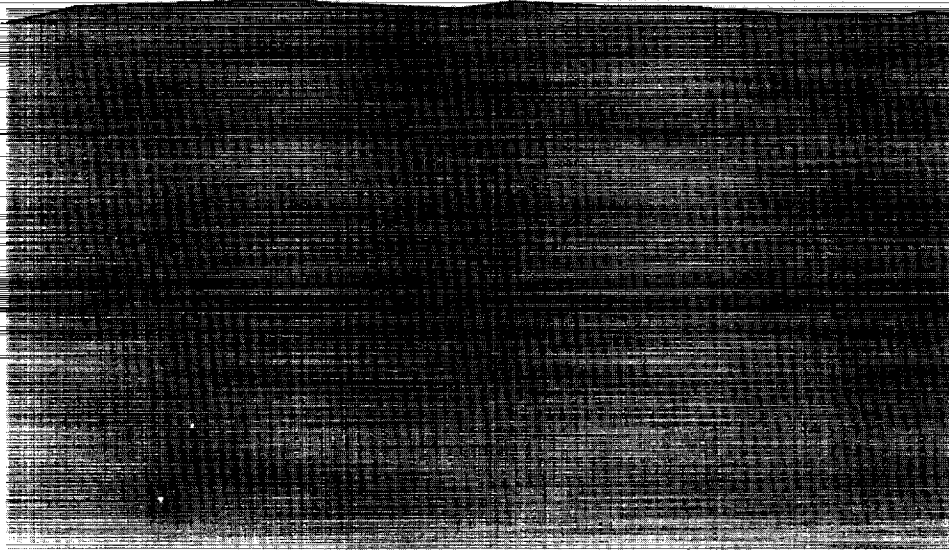
Sponsor: Advanced Space Transportation Programs Office

Industry Involvement: The Boeing Company

Biographical Sketch: Les Johnson is the principal investigator for the Propulsive Small Expendable Deployer System flight experiment and the study manager for many of MSFC's future mission activities involving the use of space tethers. Prior to joining NASA in 1990, Johnson worked at General Research Corporation on the development of space-based neutral particle beam systems. He has a B.A. in chemistry and physics from Transylvania University, and an M.S. in physics from Vanderbilt University. He is a graduate of the International Space University Summer Session Program.



technology transfer



"My friends, there was dancing here in the streets of Huntsville when our first satellite orbited the Earth. And, there was dancing again when the first Americans landed on the Moon. I'd like to ask you...don't hang up your dancing slippers."

— Dr. Werner von Braun

NASA's Marshall Space Flight Center has not hung up its dancing slippers. Today we continue to celebrate, dancing with partners that can benefit from the technologies derived from the space program to further enhance life on Earth.

This year the Technology Transfer Office at the Marshall Center launched a new initiative, coined "intentional serendipity," to promote partnerships with the non-aerospace community in utilizing NASA-based technological developments. Intentional serendipity stimulates the faster delivery of "spinoffs" by effectively leveraging talent and resources earlier in the technology development process.

New dual-use technology development partnerships are being formed with businesses, academia, and other government entities. These mutually beneficial partnerships are tailored to unite resources and enable NASA to assist businesses in overcoming significant technical obstacles. Intentional serendipity combined with the insertion of new technologies, technology reporting, invention disclosures and licensing of patents into the private and public sectors will allow us to succeed in making major new product developments, productivity enhancements, and health and social benefits in the daily lives of humans on Earth.

We are challenging scientists, technologists, entrepreneurs and industry to work together to improve our quality of life and enhance the future economic security of our nation. We continue to celebrate and dance because we realize that *"The technologies we need to reach the stars are the engines to drive America's future."*

Sally Little
Director
Technology Transfer Office

Marshall Center a Partner in High-Tech Business Incubator

Benita Hayes/C030
256-544-6539
E-mail: benita.hayes@msfc.nasa.gov

NASA's Marshall Center has partnered with Business Technology Development Center, Inc. (BizTech) to nurture small, high-technology oriented businesses through their vulnerable years.

BizTech, a not-for-profit business incubator, is supported by an alliance that provides matching funds to construct and operate the incubator. In addition to Marshall, other members of the alliance include the Tennessee Valley Authority (TVA), the State of Alabama Department of Economic and Community Development (ADECA), and the City of Huntsville.

Richard Reeves, chairman of the board, was a leader in getting the incubator incorporated and the temporary facility opened in August 1997. Joanne Randolph serves as the administrative director of BizTech.

BizTech, now located in their permanent facility in the Calhoun Community College Building on Wynn Drive, will eventually occupy 41,000 square feet of donated office and light manufacturing space.

Currently BizTech serves three budding Huntsville businesses, providing access to a computer resource library, workrooms, meeting rooms, mail room services and office equipment. The incubator beneficia-

ries are: QualTech, Inc., with a unique VCR product to index and catalog videotapes for use in education, training, teleconferences, and multimedia presentations; Banton Research, a software company specializing in Spatial Economics which can be used to solve problems in many disciplines including health care, politics, real estate and criminology; and Ublige, a software tool and programming services company which offers products and services in software code visualization, code analysis and code translation. Research and development in the hardware and sensor technologies is also available.

BizTech requires that businesses be high-technology oriented with good prospects of success, have a viable product and resources and a well developed business plan to qualify for acceptance into the incubator program. To achieve their goal of using client revenues to become self-sufficient, Biz Tech actively recruits new clients that have the ability to provide the required revenue and the potential to grow and create jobs.

Several other programs have been designed to benefit clients that do not require the full scope of the incubator. Clients that do not need office space may take advantage of all of BizTech's support resources through the nonresident program. A successful mentoring program has been established that has proven to be very beneficial to the local small business community. Successful entrepreneurs and senior business executives have volunteered to serve as advisors. BizTech matches the individual expertise of the advisor with the needs of the client. Networking clients with service providers such as lawyers, accountants, bookkeepers,

computer training centers and temporary employment services is another program available.

NASA's Marshall Center is helping to nourish and encourage the growth of new, high-technology firms in Huntsville and Madison County through its partnership and financial support of the small business incubator.

Sponsor: Office of Commercial Development and Technology Transfer

University Involvement: Calhoun Community College

Biographical Sketch: Benita C. Hayes is a technology manager for the Technology Transfer Office and is Marshall's representative for the state of Alabama. She received an undergraduate degree from the University of Kentucky and a master's from Penn State. She joined NASA in April 1980. ■

NASA Computer Imaging Technology Looks Into a Broad Range of Commercial Uses

Lisa Hediger/CO30
256-544-2544
E-mail: lisa.hediger@msfc.nasa.gov

The roots of computed tomography (CT) scanning go back to the 1960 Apollo space program and the field of medicine. The medical applications of the technology have benefited millions of people worldwide since its inception. Throughout the years, technological advances have made it possible for CT scanning to look into other important fields with a broad range of application possibilities.

NASA developed digital image processing in the 1980's when Bio-Imaging Research (BIR) of Lincolnshire, IL, created an industrial inspection system using CT technology to find imperfections in aerospace structures and components for the Marshall Center. The Advanced Computed Tomography Inspection System (ACTIS) helps NASA engineers characterize structural assemblies, reveals interface abnormalities that could result in mission failures, and detects flaws in turbine and valve castings. Since then, the system has been used to scan an entire automobile and large castings used in the automotive industry, a cruise missile jet engine, and a complete satellite.

By further refining the technology for broader commercial application, BIR



FIGURE 96.—Bio-Imaging Research, Inc., Waste Inspection Tomography mobile unit inspects drums of waste at a dump site.

has developed a small, PC-based unit called ACTIS+. Created for general industrial use, the ACTIS+ provides CT imaging capability at less than one third of the cost of current CT systems. Adding ACTIS+ to existing real-time radiography (RTR) using major RTR components eliminates the expense of an x-ray and detector system.

Charles Smith, BIR spokesperson, said "One of the most important commercial applications of the technology came when Marshall allowed us to scan a 55-gal drum containing cement, metal parts, liquids, and other materials. This allowed us to demonstrate to the U.S. Department of Energy (DOE) that computed tomography is much better at seeing what is inside drums of radioactive waste than any existing techniques."

Testing at Marshall led to the development of Waste Inspection Tomography (WIT), a trailer-mounted portable system (fig. 96) that can be taken to waste dump sites to identify the contents in drums found there. Custom software has been written that allows BIR to combine 3D x-ray CT images with 3D gamma-ray information. The system can identify the location of radioactivity in the drum, identify and measure the volume of potentially corrosive free liquids, determine how much the wall of the drum has thinned by corrosion, and identify the presence of objects that cannot legally be stored in drums.

Richard Bernardi, program manager for WIT, says "The mobile device has performed outstandingly at a number of DOE sites." BIR hopes to expand its services to more industries by building two additional trailers.

Dr. John F. Moore, president of BIR, points out that the technology developed for NASA has led to other products and services, created eight additional jobs at the plant, resulted in the marketing of two new products, and generated \$11 million in sales during the 6 years since the system has been in operation. Demand for the products has led BIR to a \$2 million capital investment to expand production.

Sponsor: Office of Commercial Development and Technology Transfer

Biographical Sketch: Lisa Hediger is team lead for the Nondestructive Evaluation Team in the Materials and Processes Laboratory at the Marshall Center. Hediger holds advanced degrees in engineering and mathematics. Over the past 15 years, she has made significant contributions to the field of quantitative nondestructive evaluation. She led the effort to design and build NASA's Advanced Computed Tomography System as well as several other large-scale, state-of-the-art systems. ▀

NASA "Smart Bolts" Likely to Revolutionize Some Industries

Helen Stinson/CO30
256-544-7239
E-mail: helen.stinson@msfc.nasa.gov

NASA needed an improved fastening technology for the critical-fastening appraisal and validation of spacecraft segments that are coupled together in space. In-orbit assembly requires both lightweight wrenches for enhanced robot-arm mobility as well as remote fastener-load inspection. Ultrafast, Inc. of Malvern, PA, proposed a solution under a NASA small business innovation research (SBIR) contract managed by the Marshall Center. The Ultrafast "intelligent bolt" developed for NASA promises to have many down-to-Earth, practical applications as well.

Because insufficient bolt preload is usually the root cause of joint failure resulting from joint separation, bolt loosening or fatigue, the Ultrafast intelligent bolt utilizes a piezoelectric, thin-film deposited directly on one end of the fastener. When electrically excited by an Ultrafast tool, tensile loads can be controlled accurately during the bolt-tightening process.

A bolt topped with the durable, thin-film—at a cost of just pennies per fastener—functions as a transducer for measuring and recording bolt tensile load. The technology uses the relationship between the speed of ultrasonic waves in a material and the stress applied to the material as its basis for


computing load measurements. The time of flight of the ultrasonic signal traveling in a fastener increases as the load on the fastener increases. The film is deposited on the bolt by sputtering, a vacuum process that has numerous practical applications ranging from integrated circuits to reflective coatings on glass or decorative coatings on plastic. The technology also eliminates the need of loosening fasteners and disturbing the joint during maintenance and inspection.

The automotive industry is particularly interested in the innovation. Safety-critical components such as powertrains, steering systems, and brakes can now be more reliable while minimizing service costs and other impacts related to joint failure. Joint assembly times—as well as costs—can be reduced by using high speed impact or impulse wrenches to improve joint integrity.

There are many other practical uses for the ultrasonic, thin-film fasteners ranging from computer disk drive assemblies to forklifts. Nuclear engineering uses range from small flanges to large pressure vessels. Chemical processing, critical-fastening applications include offshore platforms and pipes. The technology can also be applied in the construction of buildings and bridges.

Ultrafast sales are expected to exceed \$100 million in a few years. The company has licensed two major European tool companies to supply power tools for automotive assembly and is establishing worldwide fastener coating services through its Ultracoat subsidiaries.

Sponsor: Office of Aeronautics & Space Transportation Technology, Commercial Development and Technology Transfer Division

Biographical Sketch: Helen Stinson manages the SBIR and STTR programs for the Technology Transfer Office at the Marshall Center. She graduated from the University of Alabama in Birmingham with a degree in materials engineering. Her work assignments have included the Space Shuttle main engine and Spacelab payloads in the Structural Analysis division of the Structures and Dynamics Laboratory. She has received numerous awards including the NASA Exceptional Service Medal. 

Space Code Solves Industries' Identity Crisis

Bob Lessels/C030
256-544-6539
E-mail: bob.lessels@msfc.nasa.gov

Digital data matrix technologies developed at NASA's Marshall Center to identify the millions of parts that comprise Space Shuttles such as the Endeavour are helping to launch a new commercial endeavor.

Symbology Research Center, a partnership between CiMatrix Corp. of Massachusetts and NASA, began operations August 5 in Huntsville to

commercially market the new method of identifying products with invisible and virtually indestructible markings.

The laser-etched markings are seen as the next generation of product "bar codes," already familiar around the world. Traditional bar codes can only be used on paper or plastic packaging and are not tamper resistant. Digital data matrix codes are applied directly to the product (fig. 97). The markings can range from as small as $4\ \mu$ to as large as $2\ \text{ft}^2$.

Donald Roxby, director of Symbology Research Center, reports commercial interest in the new marking system ranging from electronic parts to pharmaceuticals to livestock. He sees a growing need for an identification



FIGURE 97.— Don Roxby, director of the new Symbology Research Center in Huntsville, AL, inspects a data matrix engraving on a piece of automotive glass.

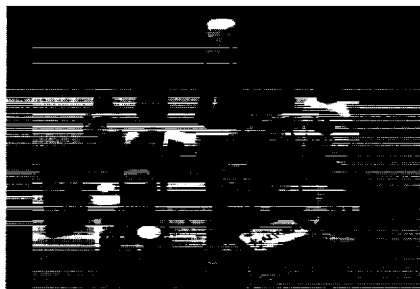


FIGURE 98.—A sample of commercial products using data matrix compassed symbology codes.

system that can be placed directly on a product while conforming to the product's shape, size, color and other properties (fig. 98). Paper bar coding, he said, will continue to have uses in many industries, but—where identification of a small part is essential or where the paper bar coding could deteriorate—digital data matrix technologies hold the solution. Roxby and his staff expect to handle up to 500 product marking problems each year. They also will be exploring more opportunities to use the new product coding system.

Working with Roxby has been NASA engineer Fred Schramm from the Marshall Center. "NASA began using paper bar coding technologies in 1983," Schramm said. "In 1986, the Marshall Center began examining the possibility of developing a paperless identification system. Problems had been experienced with the paper on which the code was imprinted separating from the part. When you consider the thousands and thousands of parts in something such as the Space Shuttle, this can be a huge problem. Another problem is the durability of paper bar codes. They cannot survive being placed on parts exposed to high heating, such as the thermal tiles on the orbiters during re-entry.

In 1991, Roxby said, NASA determined that converting to digital data matrix coding would save \$1 million a year on the orbiter fleet alone.

Proven in the demanding environment of space flight, the decision to commercialize the technology was a natural one. NASA agreed to partner with CiMatrix—a division of Robotic Vision Systems, Inc., (RVSI) of New York—to identify potential sites for the Symbology Research Center. CiMatrix has a strong track record in the bar coding industry, having manufactured labels and their readers and recorders since the early 1980's.

Roxby added that industries see the new system as a means of complying with new federal requirements to include more content information on labels. Where space is at a premium and bar coding the information onto the product is impractical, digital data matrix technologies offer a solution.

Many other industries are expressing interest in the new system, and—as industry's demands increase—the Huntsville center will serve as the prototype for additional centers across the country and around the world.

Sponsor: Office of Commercial Development and Technology Transfer

Biographical Sketch: Bob Lessels is the technical writer/editor (physical sciences) for the Technology Transfer Office at the Marshall Center. A graduate of the University of Nebraska, he has been a professional journalist for the past 30 years. He joined NASA in 1986. ▀

Small Vibrations In Space Lead To Earthshaking Technology

Dr. Mark Whorton/ED12
256-544-1435
E-mail: mark.whorton@msfc.nasa.gov

When it comes to space technology, size really doesn't matter. NASA's solution for reducing minor vibrations in space that affect delicate experiments is also effective in minimizing the devastating damage of major earthquakes.

Technologies developed at the Marshall Center to protect experiments such as crystal growth aboard the Space Shuttle are directly applicable to buildings and bridges during seismic events. Current work is focused on developing technological "tools" which architects and construction engineers can use when designing more earthquake-tolerant structures, and in enabling existing structures to better survive earthquakes.

The National Science Foundation program on Earthquake Hazards Mitigation in the Civil and Mechanical Systems Division is funding a major research program on structural control. The Georgia Institute of Technology and other universities are involved in various aspects of earthquake engineering such as developing better building materials, passive damping methods, and active vibration control.


Although there are several ways to reduce the effect of structural vibrations, lightweight but equally effective vibration mitigating alternatives were needed for applications in the space

program. These technologies were found to have down-to-Earth applications as well.

One way of countering structural vibrations caused by strong wind gusts or seismic ground motion is by placing sensors and force-producing devices called actuators at specific locations on buildings. The sensors in the system measure structure motion and the actuators apply force to counteract the vibrations. Placing adjustable tendons along the sides of a structure is one method of the force device system. In fractions of a second, sensors read the structural vibration patterns caused by earthquakes or high winds and adjust the tension on the appropriate tendons to reduce the excessive forces.

The active control technology for vibration isolation is mature and fully capable of doing the job. This is a technology ready now for commercial applications.

Sponsor: Office of Space Flight

Biographical Sketch: Mark S. Whorton is an aerospace engineer in the Precision Pointing Systems Branch of the Control Systems Division, NASA/Marshall. Whorton received B.S. (with honors) and M.S. degrees in aerospace engineering from The University of Alabama in 1987 and 1989 and a Ph.D. from The Georgia Institute of Technology in 1997. Dissertation research was in the area of robust control for flexible space structures. Recent work assignments have included control design and analysis for microgravity vibration isolation systems such as STABLE and the Boeing Active Rack Isolation System. 

NASA Technology Conserves Power and Generates a Successful New Business

William H. Nabors/CO30
256-544-0688
E-mail: william.h.nabors@msfc.nasa.gov

It is estimated that approximately one billion induction motors are in operation on a daily basis. Elevators, escalators, machine tools, compressors, pumps and conveyors are just some of the common applications for variable load motors. It is also estimated that these motors consume more than half of all the electricity generated in the United States. Unfortunately, a large percentage of the power being consumed is wasted because they are running at full mechanical load—even when idle. With this in mind, it is easy to understand the significance of the NASA-developed technology that reduces the energy consumption of electric motors.


The three-phase power factor controller with induced electromotive force (EMF) sensing was developed and patented in 1984 by Frank Nola, an engineer at the Marshall Center. The commercial impact of the electronic control boards led to the development of a new company, Power Efficiency Corporation of Hackensack, NJ, to manufacture and market products developed exclusively from NASA technology.

Power Efficiency manufactures three different motor controllers under the following brand names: Power Commander™, Performance

Controller™, and Energy Master™. The concept of the power factor motor controller is to reduce excessive energy waste in ac induction motors, by reducing voltage start, reducing energy consumption, and improving power factor. The device monitors the phase lag of the current-voltage relationship in motors operating at less than full mechanical load. The controller decreases the voltage to precisely what the motor requires to maintain the rated speed and torque under its present capacity. The power factor controller's ability to lower the amount of energy consumed results in lower monthly utility bills while extending the life of the motor.

In 1997, Power Efficiency Corporation filed for a new patent due to engineering changes that have occurred in the manufacture of ac induction motors. Nicholas Anderson, president of Power Efficiency says "The original NASA technology was excellent for the control of ac induction motors manufactured in prior years." The purpose of the new patent is specifically for controlling motors that were not in existence when Nola's patents were issued.

Sponsor: Office of Commercial Development and Technology Transfer

Biographical Sketch: William H. Nabors is a technology manager for the Technology Transfer Office and is Marshall's representative for the state of Kentucky. He received undergraduate and master's degrees from Auburn University. He joined NASA in February 1985. 

Hair Cleans Up Hairy Oil Spill Problem

Dr. Elizabeth Rodgers/CO30

256-544-2647

E-mail: Elizabeth.B.Rodgers@msfc.nasa.gov

Without question, oil spills present a hair-raising problem, but a Madison, AL, hairdresser may have found a way to quickly and efficiently clean up the oil—in a way that is economical and environmentally friendly—using hair.

While watching the 1989 clean up efforts of the Exxon Valdez oil spill in Prince William Sound, Phil McCrory noticed that otters' fur was heavily saturated with oil. He reasoned that if otter fur trapped oil, wouldn't human hair? To test his theory, he collected 5 lb of hair from the floor of the shop, placed it in a pair of his wife's pantyhose and put it into his son's wading pool which contained black motor oil. In less than 2 min, the oil in the pool was gone. Since this initial test, McCrory has learned that hair does not absorb oil, but rather adsorbs it. Each hair shaft is covered with thousands of tiny scales that the oil clings to, which is actually adsorption.

One current method for cleaning up spills uses bags with polypropylene strips inside that absorb the oil. A typical 1.5-lb bag picks up 7.6 lb of oil, but the process takes 24 to 48 hours and the bags can only be used once. McCrory says that similar-sized bags with hair would adsorb 9 lb of oil in approximately 2 min, and could be wrung out and reused multiple times.

McCrory received a patent for the idea in 1995, and testing is in progress

under a Space Act Agreement through the Marshall Center's Technology Transfer Office. Initial testing was done by Marshall contractor BAMSI, Inc., using a 55 gal drum containing 40 gal of water and 15 gal of oil. In a single pass of the hair, the water contained no more than 17 parts per million of oil. The U.S. Environmental Protection Agency allows discharge of water that has 15 parts per million of oil.

A more recent NASA test was performed to determine the best density of hair to use to adsorb oil. The experiment used 15 small (3 in. × 3 in.) pillows stuffed with hair, 3 each, at 5 densities of hair. The hair pillows were observed to rapidly take up clean, nondetergent motor oil when the pillows were vigorously agitated in a beaker of 1 L of water and 10 times the weight of the hair in oil. The results indicated simply by difference in weight of the packages before and after their vigorous contact with oil and water that hair is capable of rapidly (within 3 min) adsorbing approximately 5 or 6 times its weight in oil. There was no significant difference in the adsorptive capability among the five densities of hair.

A more definitive test, an oil-water extraction test, is currently underway. This experiment will determine whether the hair also picks up water and how much. Using the old adage that, "oil and water don't mix," and the current findings that oil is attracted to the great surface area of hair, it is believed that hair selectively adsorbs oil.

The tests being performed by NASA are simple, bench-scale, proof-of-concept tests. Many more tests are still

required on the process, but preliminary results indicate that hair is, indeed a very efficient adsorber of oil.

Sponsor: Office of Commercial Development and Technology Transfer

Biographical Sketch: Dr. Elizabeth Rodgers is a technology manager for the Technology Transfer Office and is Marshall's representative for the state of Georgia. She received an undergraduate degree from Brown University and a Ph.D. in biology from Washington University in St. Louis. She has worked at NASA since 1985. ■

NASA Sheds New Light on Cancer

Helen Stinson/C030
256-544-7239
E-mail: helen.stinson@msfc.nasa.gov

NASA lighting technology has created a new surgical procedure, photodynamic therapy (fig. 99), to remove cancerous tumors and offer new hope to victims of the disease.

The technology was originally used in NASA's second United States Microgravity Laboratory Spacelab mission in October 1995. In commercial plant growth experiments, tiny light emitting diodes (LED's) were used as a low-energy light source in the Astroculture Plant Growth Facility. Dr. Raymond J. Bula of the Wisconsin Center for Space Automation and Robotics, a NASA Commercial Space Center, led the experiment. The objective of NASA-supported Commercial Space Centers is to seek opportunities for technologies developed through space to benefit U. S. industry.

To demonstrate the feasibility of using LED's in cancer treatment, NASA funded the "Solid State Photon Emission Probe for Application with Photodynamic Therapy" contract through the Small Business Innovation Research (SBIR) Program. Through the Marshall managed contract, Quantum Devices, Inc. developed a 9-in. neural probe. In photodynamic therapy, the LED probe is used to activate light-sensitive, tumor-treating drugs.

The probe has several qualities that are proving superior to traditional laser



FIGURE 99.—Demonstration of photodynamic therapy.

methods. The LED probe illuminates all nearby tissues and can be used for hours at a time while remaining cool to the touch. The light source is compact—about one-half inch in diameter and consists of 144 tiny diodes. It is mechanically more reliable than lasers or other light sources used to treat cancer and can be purchased for a fraction of the cost of a laser. Lasers also have a limited color spectrum, are very expensive and lose power in their fiber optic cables.

Approval from the Food and Drug Administration to use the probe on a trial basis to remove children's brain tumors was granted to Dr. Harry Whelan, pediatric neurologist at the Children's Hospital of Wisconsin, and professor of neurology at the Medical College of Milwaukee, WI. In surgery, the patient is injected with a drug called Photofrin II which attaches to unwanted tissues leaving the surround-

ing tissues unaffected. Dr. Whelan then places the LED probe near the affected tissue to illuminate the tumor and activate the Photofrin II drug. Activation by the light allows the drug to destroy the tumor's cells, leaving the tender brain stem tissues virtually untouched.

"The LED technology developed by NASA offers new hope to children with cancer," Dr. Whelan said. Full approval is expected upon completion of the FDA clinical trials. Continuing research indicates that the combination of LED's and promising new drugs will lead to deeper tumor penetration, faster reaction times and shortened patient sensitivities to sunlight. "If it wasn't for the pre-existence of all that technology, it wouldn't have been possible for us to walk right in and use it to treat cancer," concludes Dr. Whelan.

NASA's Space Product Development Program in partnership with the scientific community and commercial industry supports 19 U.S. universities designated by NASA as Commercial Space Centers. The Space Products Development Office is part of the Microgravity Research Program at the Marshall Center.

Sponsor: Office of Aeronautics & Space Transportation Technology, Commercial Development and Technology Transfer Division

Biographical Sketch: Helen Stinson manages the SBIR and STTR programs for the Technology Transfer Office at Marshall Center. She graduated from the University of Alabama in Birmingham with a degree in materials engineering. Her work assignments have included the Space Shuttle main engine and Spacelab payloads in the Structural Analysis division of the Structures and Dynamics Laboratory. She has received numerous awards including the NASA Exceptional Service Medal. ▀

NASA-Designed Knee Brace Turns Rehabilitation Into a Moving Experience

Steve Jones/C030
256-544-4373
E-mail: steve.jones@msfc.nasa.gov

Applying the mechanisms and materials used in propulsion systems, five Marshall Center engineers have designed the Selectively Lockable Knee Brace (fig. 100).

Michael Shadoan, Neill Myers, John Forbes, Kevin Baker and Darron Rice spent 3 years designing the prototype. The unique aspect of the device is that

it allows a patient recovering from a knee injury or loss of muscle control to bend and use the knee as long as weight is not on the heel. Placing weight on the heel locks the brace into position. Until now, knee braces were designed to keep the knee locked in a rigid, straight-leg position. The Selectively Lockable Knee Brace attaches around the thigh with the lower part secured around the shoe by a stirrup. The brace offers patients freedom of movement making rehabilitation faster and less painful.


Horton's Orthotic Lab., Inc., of Little Rock, AR, assisted the Marshall team in field testing the brace in 1996 and 1997. After adjustments were made to the original design based on information from the tests, the device was



FIGURE 100.— A knee brace prototyping and fitting at Horton's Orthotic Lab, Inc., in Little Rock, AR.

licensed for commercial production. An exclusive licensing agreement has been signed by Horton's Orthotic Lab., Inc. to manufacture the improved version, and clinical trials have begun.

Sponsor: Office of Commercial Development and Technology Transfer

Biographical Sketch: Steve Jones is a technology manager for the Technology Transfer Office at the Marshall Center. A graduate of Auburn University, he is an electrical engineer with a background in digital and radio-frequency electronics. He left industry and joined NASA in 1985. 

NASA's Enlightening View on Veins

Dr. Elizabeth Rodgers/C030
256-544-2647
E-Mail: Elizabeth.B.Rodgers@msfc.nasa.gov


There is always a moment of apprehension as the medical professional begins to look for a good vein, and no matter which side of the needle you're on, missing the vein is a most unpleasant experience. By allowing a better view of the vein, NASA technology is helping eliminate multiple sticks of the needle.

NASA engineer Eric Corder of the Marshall Center Astrionics Laboratory, Electro Optics branch, assisted Frank Creaghan of Applied Biotech Products of Lafayette, LA, in improving the design of a tissue illuminating prototype called the Venoscope™ (fig. 101). The device emits a bright light that is reflected by tissue below the skin. Since veins absorb light rather than reflect it, they

appear as distinct dark lines under the Venoscope™. Marshall assisted Applied Biotech Products in determining a way to achieve the same light output with greater efficiency and increase visualization of blood vessels while making the device more compact.

Applied BioTech Products holds the design and technology patent for the Venoscope™ which is now moving into commercialization. The device may also travel on a future Space Shuttle mission to test its applicability in a microgravity environment.

Sponsor: Office of Commercial Development and Technology Transfer

Biographical Sketch: Dr. Elizabeth Rodgers is a technology manager for the Technology Transfer Office and is Marshall's representative for the state of Georgia. She received an undergraduate degree from Brown University and a Ph.D. in biology from Washington University in St. Louis. She has worked at NASA since 1985. 

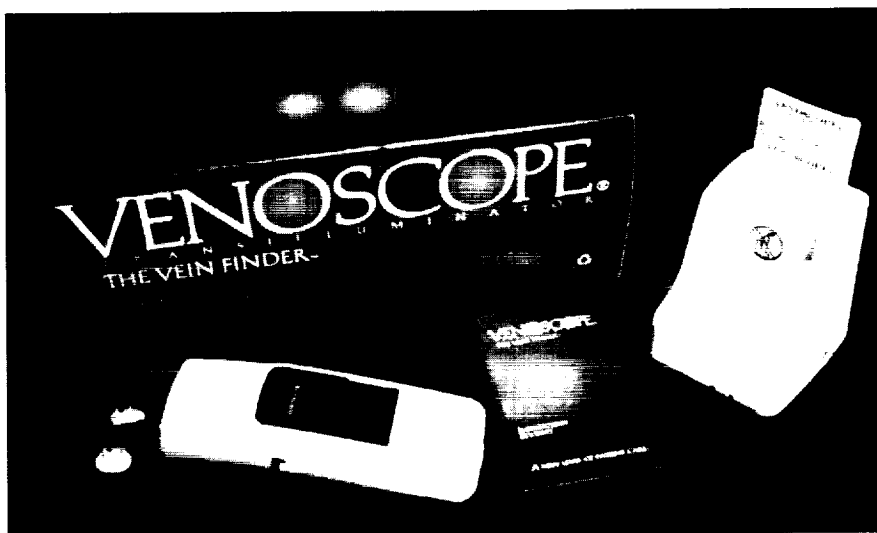


FIGURE 101.—The Venoscope

NASA Funnels Technology to Develop Tornado Warning System

Helen Stinson/LA02

256-544-7239

E-mail: helen.stinson@msfc.nasa.gov

Weather radar such as NEXRAD or Doppler can detect a tornadic vortex signature up to distances of 100 miles, but they cannot determine when a tornado has touched the ground. Information obtained through a completed Small Business Innovation Research (SBIR) project for the Marshall Center in 1991 is putting a new "twist" on twister detection. Wind noise from a tornado has often been described as "sounding like a train" and through NASA-based research, it may be possible to use the noise and turbulence to identify a tornado's distance, direction, and path up to 10 miles away.

Dr. Frank Tatom, president of Engineering Analysis, Inc. of Huntsville, AL, worked with Marshall to calculate the turbulent pressure fluctuations on the surface of the Space Shuttle during atmospheric flight. The fluctuations produce noise and vibrations inside the Space Shuttle. This research, along with a recently completed study for the Department of Commerce's National Oceanic and Atmospheric Administration, prompted Tatom to examine the possibility that turbulent pressure fluctuations within a tornado should produce seismic waves when in contact with the ground.

Earthquake studies have proven that seismic waves can travel long dis-



FIGURE 102.—Dr. Frank Tatom with the tornado sensor "snail."

tances and can be detected by seismometers. Tatom's theory was that tornadic vibrations should also be identifiable. He further reasoned that if the signature of vibrations from a tornado in contact with the ground could be isolated and identified, then a warning system would be feasible.


Tatom studied seismometers operated by the University of Memphis and the

University of Mississippi. The data recorded during tornadic activity clearly indicated that tornadic turbulence does create ground pressure fluctuations detectable by seismic sensors.

Using his own company's funds, Tatom has developed two concepts for warning devices (fig. 102): a network warning system with 20 or more sites,

each possessing one or more geophones, a microprocessor, a communications link, an independent power supply and a security system linked to city or county emergency centers as well as Doppler radar; and a residential model for homes and businesses linked to a home alarm system with a distinct warning signal. Dr. Tatom says this device "will make possible a truly accurate tornado warning system that should save countless lives, once it is in operation."

Sponsor: Office of Aeronautics and Space Transfer Transportation, Commercial Development and Technology Transfer Division

Biographical Sketch: Helen Stinson manages the SBIR and STTR programs for the Technology Transfer Office at Marshall Center. She graduated from the University of Alabama in Birmingham with a degree in materials engineering. Her work assignments have included the Space Shuttle main engine and Spacelab payloads in the Structural Analysis division of the Structures and Dynamics Laboratory. She has received numerous awards including the NASA Exceptional Service Medal. 

NASA Technology Helps Zap Mosquitoes Before They Zap You

Steve Jones/C030
256-544-4373
E-mail:steve.jones@msfc.nasa.gov

In 1995, Alvin Wilbanks of Environmental Products and Research, Inc. of Osceola, AR, developed an idea for a mosquito killing system. He contacted NASA for technologies that could be incorporated in designing the proposed product.

Engineers Jeff Martin and John Bush of Marshall's Astrionics Laboratory studied the concept and design, then recommended several modifications that would cut costs and improve efficiency which the firm adopted. The MSFC team also referred Wilbanks to a nonprofit agency that assisted him in rapidly producing molds used to manufacture the base and top structure of the new product.


The Mosquito Killing System (MKS) actually attracts mosquitoes. The patented device relies on the natural ability of the insect to sense heat and breathing to find its prey. A heat source with gentle air current to simulate breathing is used to provide an image to attract the insects. The system also uses a pheromone attractant to further lure the insects into the device. Mosquitoes are attracted over a one-acre area and are electrocuted upon entering the device's killing zone.

The MKS is equipped with secure mounting points, a tip-over safety switch, and an energy-conserving

photoelectric cell used to activate the machine at dusk and turn it off at dawn. The device is self-cleaning and environmentally friendly, using no chemicals to destroy the pests. It uses 110 V alternating current and is expected to cost about \$6 per month to operate.

Environmental Products and Research, Inc., estimates that municipalities using MKS could entirely eliminate mosquito spraying and recoup costs in 5 years. The mosquito control device is another example of ways in which technologies from the nation's space program can be applied to solving down-to-Earth problems.

Sponsor: Office of Aeronautics and Space Transfer Technology, Commercial Development and Technology Transfer Division

Biographical Sketch: Steve Jones is a technology manager for the Technology Transfer Office at the Marshall Center. A graduate of Auburn University, he is an electrical engineer with a background in digital and radio-frequency electronics. He left industry and joined NASA in 1985. 

NASA, USBI Technology Make A Triple Play

Vernotto McMillan/C030
256-544-2615
E-mail: vernotto.mcmillan@msfc.nasa.gov

Convergent Spray Technologies™ (CST™) spray process was originally developed by USBI for Marshall to apply heat-resistant coatings to the Space Shuttle's solid rocket boosters. The technology was then successfully adapted to quickly apply a skid-resistant coating to roadways and bridges. Now the same technology is being used to recoat metal roofs.

The newest application is a result of a recently completed Marshall Center/USBI project that demonstrated the feasibility of reusing their space-age technology to benefit the roofing industry. The concept uses an environmentally compliant coating made up of recycled materials, a CST™ spray process portable application cart, and a hand-held applicator with a CST™ spray process nozzle.

The first phase of the project involved conducting a survey of the roofing industry to determine their needs. In the second phase, tests were performed on paints, coatings, filler materials, hand mixes, sprays and various supplemental materials. Two base coatings were selected and the spray process was refined. The third phase consisted of applying the selected coatings in two field demonstrations, which were funded by the Environmental Protection Agency under the Environmental Technology Initiative. In 1996 a certification test demonstrating the process and coating of choice was applied to a roof at the

Marshall Center. The coating was both galvanized steel/aluminum-painted substrate and a foam insulation surface. In 1997, a section of a second Marshall Center building roof was coated. Real-time wear, performance, durability, and resistance to weather of the coatings are being monitored.

The two base coatings that were selected and tested used a filler material made from finely ground rubber tires. This is the third time NASA has found uses for wornout tires. The Stennis Space Center in Mississippi developed a cryogenic recycling process to convert thousands of wornout tires into road paving material and garden hoses.

Researchers hope their work would result in a fast, easy, environmentally friendly spray-on coating process for the roofing industry. Preliminary tests indicate that the coating has a satisfactory moisture resistance, adhesion properties, tensile strength, flexibility, resistance to water vapor penetration, and resistance to the cyclic effects of aging, rain, dew and ultraviolet radiation.

Sponsor: Office of Commercial Development and Technology Transfer

Biographical Sketch: Vernotto McMillan is a technical manager for the Technology Transfer Office at the Marshall Center. He is a graduate of The University of Alabama School System (B.S.M.T.E.) and Florida Institute of Technology (M.S.). He has more than 17 years of diverse experience ranging from materials development to propulsion system development. He joined NASA in 1983. ▀

NASA Spinoff Helps Golfers Get More Spin on the Ball

Fred Schramm/C030
256-544-0823
E-mail: harry.f.schramm@msfc.nasa.gov

Technology developed for NASA by Memry® Corporation of Brookfield, CT, has links to a number of commercial applications, including golf clubs that offer golfers more control on the links.

The Marshall Center contracted with Memry Corporation to investigate shape memory effect (SME) and materials for the Space Station. SME is a property of certain metal alloys that can change from shape to shape depending on temperature fluctuations. The NASA-based technology has led Memry Corporation to create a line of home and industrial safety products as well as an alloy specifically for the golf industry.

Zeemet® is a high proprietary, high-damping shape memory alloy. The Nicklaus Golf Equipment Company of West Palm Beach, FL, is using Zeemet inserts in a new line of golf clubs. The super-elastic, high-damping inserts allow golfers to get more spin on the ball, greater control and a solid feel. In the memory alloy design, as the club makes contact with the ball, the insert undergoes a split second change in metallurgical structure. The elastic property keeps the ball on the club face longer giving it more spin while not affecting distance.


Memry Corporation has used the science of shape memory to create a

wide range of products. MemrySafe® is an antiscald device that instantly restricts water flow before scalding. Using a patented valve that reacts to temperature rather than pressure and a memory metal alloy, the unit senses dangerously high temperatures and reduces the flow of hot water. The unit automatically resumes normal flow when a safe temperature is attained. UltraValve® is another type of antiscald device. Preselected water temperature can be turned on or off with the push button system and a control panel continually displays exact water temperature. FireCheck® is a reusable fire safety valve for industrial facilities, such as petrochemical, chemical, semiconductor, pharmaceutical and large oil and gas fired boilers. The device can be applied to any pneumatically-operated process valve and is designed to sense excessive heat, immediately venting the pneumatic actuator pressure which closes the supply line.

McDonnell Douglas of St. Louis, MO, has signed a contract with Memry to design and manufacture a unique control surface for helicopter blades. Small microprocessor-controlled tabs for the trailing edges of the blades will enable a pilot to fine tune each blade for improved performance and reduced vibration.

Memry's Super-Elastic Nitinol is proving very beneficial to the medical equipment industry for use as catheter guide wires, lesion localizers, suture anchors and dental arch wires. Nitinol is a binary nickel-titanium alloy that withstands being distorted by heavy pressure then springs back to its original shape.

Sponsor: Office of Aeronautics & Space Transportation Technology, Commercial Development and Technology Transfer Division

Biographical Sketch: Fred Schramm is a technology manager for the Technology Transfer Office at the Marshall Center. A graduate of Tennessee Technological University and the University of Tennessee, he is an industrial engineer with a background in production technology. He left industry and joined NASA in 1981. 

NASA Deep-Space Communications Technology Now Used at NASCAR Race Tracks

Bob Lessels/C030
256-544-6539
E-mail: bob.lessels@msfc.nasa.gov

A technology developed by NASA to better interpret signals sent from spacecraft great distances from Earth, and later adapted to mark parts of the Space Shuttle's main engines, has been adapted to develop an inventory control system for parts used in NASCAR racing.

BSR Products, Inc., of Charlotte, NC, sells off-the-shelf and custom-made automotive products directly to race teams from mobile parts vans at the race tracks. The company contacted CiMatrix, the Canton, MA, firm partnered with the U.S. space Agency to seek commercial applications of the NASA-developed compressed symbology data matrix concept.

BSR had used a manual parts checkout system. Inventories were troublesome to update and billing problems occasionally occurred. The automated system developed by CiMatrix uses the firm's HT-100 Handheld Image Reader. The unit accelerates high-speed sorting and quality-control inspections by tracking critical information from receiving, work-in-process and manufacturing, through finished good inventory.

With BSR Products, it is to be used to perform automatic billing and inventory updates. Race teams' mechanics present identification badges at the

point of sale. The parts being purchased are then scanned. The team's sales record is updated, and a bill showing total purchases is mailed at the end of each month. The BSR inventory control system is being phased in with the identification of parts in inventory. It will be expanded to include over-the-counter, mail order, and on-site sales at race tracks. BSR will initially mark its products with labels, then transition into direct-parts marking. Teams currently considering using the new symbology parts identification system include that of Ricky Rudd.

The data-matrix system offers another significant advantage. Earlier systems printed parts coding information on the packaging. The data-matrix system prints the code directly onto the part (fig. 103). Butch Stevens, president of BSR Products, said the adoption of the data-matrix symbology system for his company's products will greatly enhance the firm's ability to relate parts to their use history, a critical factor in the racing industry. Race car parts typically last for 5 to 10 races. Ideally, racing teams would like to scan each part as it is installed in the vehicle, entering the information directly into a database. After a race, when the car is disassembled for inspection and repairs, parts which have been used in five races can be identified and retired.

The principal innovators behind NASCAR's new technology are NASA engineer Fred Schramm at the Marshall Center and Donald Roxby, director of the Symbology Research Center. In 1989, the pair worked to adapt the space signal interpretation technology into a system that could be used to identify the myriad of parts

used in the Space Shuttle's main rocket engines.

The center is a partnership between CiMatrix Corp. of Massachusetts and NASA. It began operations August 5 in Huntsville to commercially market the new method of identifying products with virtually indestructible markings. Schramm recently received the Federal Laboratory Consortium Southeast Region Award of Excellence for his efforts in developing the new system.

The laser-etched markings are seen as the next generation of product "bar codes." Traditional bar codes are applied to product packaging and are not tamper resistant. Digital data matrix codes are applied directly to the product. The markings can range from as small as 4 μ to as large as 2 ft².



FIGURE 103.—BSR Products show data matrix compressed symbology squares imprinted on the product.

The compressed symbology marking system has found a number of commercial applications. Dozens of everyday items including electronic parts, livestock, and mouthwash bottles carry the data-matrix product codes. Roxby reports interest in the new marking system from a broad range of commercial interests, and

expects to handle up to 500 product-marking problems each year. Racing teams are studying the system's applicability to reduce the instance of counterfeit souvenirs and items bearing the various trademarked insignia.

For more information on the new data-matrix technology, contact CiMatrix at 5 Shawmut Road, Canton, MA 02021 or phone 1-800-646-6664 or 781-821-0830. CiMatrix is a division of Robotic Vision Systems, Inc., (RSVI) of Hauppauge, NY.

Sponsor: Office of Commercial Development and Technology Transfer

Biographical Sketch: Bob Lessels is the technical writer/editor (physical sciences) for the Technology Transfer Office at the Marshall Center. A graduate of the University of Nebraska, he has been a professional journalist for the past 30 years. He joined NASA in 1986. ■

Abbreviations and Acronyms

2D	two dimensional	DLC	DuPont Lanxide composites
3D	three-dimensional	DOE	Department of Energy
ACG/P	automatic cylindrical grinder/polisher	DOE	diffractive optical element
ACTIS	Advanced Computed Tomography Inspection System	ECO	engine cutoff
ADECA	Alabama Department of Economic and Community Development	EMF	electromotive force
Ag	silver	EPFM	elastic-plastic fracture mechanics
AIAA	American Institute of Aeronautics and Astronautics	ESI	Engineering Sciences, Inc.
AITP	Aerospace Industry Technology Program	ET	external tank
Al-Cu	aluminum-copper	FAD	failure assessment diagram
Al-Si	aluminum silicon	FDNS	Finite-Difference Navier-Stokes (code)
APT	Advanced Propulsion Technology	Fe	iron
AR&C	autonomous rendezvous and capture	FFT	fast Fourier transform
ASME	American Society of Mechanical Engineers	fig.	Figure
ASTP	Advanced Space Transportation Programs Office	FMLI	foam/multilayer insulation
ATD	Advanced Technology Development	ft	foot
ATP	alternate turbopump	GaAs	gallium arsenide
AU	astronomical units	GOES	Geostationary Operational Environmental Satellite
AXAF	Advanced X-Ray Astrophysics Facility	GPS	global positioning system
B	boron	GTO	geostationary transfer orbit
Ba	barium	HeNe	helium-neon
BaO	barium oxide	HPD	half-power diameter
BATSE	Burst And Transient Source Experiment	HPFTP	high-pressure fuel turbopump
BEM	boundary element method	in	inch
BPM	beam propagation method	IRFOT	infrared fiber-optic thermography
Btu	British thermal unit	I_{sp}	specific impulse
C*	combustion efficiency	<i>ISS</i>	<i>International Space Station</i>
CCD	charged coupled device	J-T	Joule-Thompson
CCI	Ceramic Composites Incorporated	keV	kiloelectronvolt
CDDF	Center Director Discretionary Funds	kG	kilogauss
CDF	cumulative distribution function	kg	kilogram
CFC	chlorofluorocarbon	kPa	kilopascal
CFD	computational fluid dynamic	KSC	Kennedy Space Center
CGH	computer generated holography	LAD	liquid acquisition device
CGRO	Compton Gamma-Ray Observatory	lb	pound
cm	centimeter	LCBT	Low-Cost Boost Technology (program)
CMG	controlled moment gyroscope	LED	light emitting diode
CPU	central processing unit	LEO	low Earth orbit
CST	Convergent Spay Technologies	LeRC	Lewis Research Center
CT	computed tomography	LH ₂	liquid hydrogen
Cu	copper	Li	lithium
CuO	copper oxide	LIMB	laser induced momentum balance
CVD	chemical vapor deposition	lox	liquid oxygen
CXM	Constellation X-Ray Mission	LVLH	local vertical-local horizontal
dia.	diameter	m	meter
		m ³	cubic meter
		MAPO	magnetically actuated propellant orientation
		MCP	microchannel plate

Mg	magnesium	SEDS	Small Expendable Deployer System
MGM	Mechanics of Granular Materials	SFL	solid film lubricant
MHD	magnetohydrodynamics	SIMD	single instruction multiple data
MHTB	multipurpose hydrogen test-bed	SINDA	Systems Improved Numerical Differencing Analyzer
min	minute	SMA	structural module assembly
MKS	Mosquito Killing System	SMA	structural module assembly
MLI	multilayer insulation	SME	shape memory effect
MLP	mobile launch platform	Sn	tin
mm	millimeter	SOFI	spray-on foam insulation
Mn	manganese	SRB	solid rocket booster
MOPA	master oscillator and power amplifier	SSC	Stennis Space Center
MSFC	Marshall Space Flight Center	SSE	Shooting Star Experiment
ND	neodymium	SSME	Space Shuttle main engine
NDE	nondestructive evaluation	STICS	Scanning Thermal Ion Composition Spectrometer
nm	nanometer	STP	solar thermal propulsion
ns	nanosecond	STUSTD	Solar thermal Upper Stage Demonstrator
NSOM	near-field scanning optical microscope	SWOOPS	Solar Wind Observations Over the Poles of the Sun
O	oxygen	SXI	Solar X-Ray Imager
obj.	object	SXT	soft x-ray telescope
ODC	ozone depleting chemical	T/W	thrust to weight
OMS	Orbital Maneuvering System	TAI	transverse accelerated ion
ORNL	Oak Ridge National Laboratory	TCA	tetrachloroethane
OTA	optical telescope assembly	TCS	thermal control system
Pa	Pascal	TEC	thermoelectric coolers
PCAP	pressure controlled atomization process	Ti	titanium
PCG	protein crystal growth	TSS	tethered satellite system
PE	processing element	TVA	Tennessee Valley Authority
pf	picofarad	TVS	thermodynamic vent system
PI	principal investigator	UAH	University of Alabama in Huntsville
PMD	propellant management devices	UAHCAO	University of Alabama in Huntsville Center of Applied Optics
PMMA	polymethylmeth-acrylate	UV	ultraviolet
PMT	photomultiplier tube	UV	ultraviolet
ppi	pores per inch	UVCS	ultraviolet coronagraph spectrometer
ProSEDS	Propulsive Small Expendable Deployer System	V	vanadium
PSC	propulsion system controller	VGS	video guidance sensor
PSF	point spread function	VME	Versa Module Eurocard
psi	pounds per square inch	W	watt
PSU	Pennsylvania State University	WTMM	wavelet transform modulus maxima
PTA1	propulsion test article one	XRCF	X-Ray Calibration Facility
PTE	pump test equipment	Y	yttrium
Re	rhodium	YBCO	yttrium barium copper oxide
RLV	reusable launch vehicle	Zn	zinc
RMS	remote manipulator system	°C	degree Celsius
rms	root mean square	°K	degree Kelvin
RP-1	rocket propellant fuel		
RVSI	Robotic Vision Systems, Inc.		
SBIR	Small Business Innovative Research		
sec	second		

Index of Contacts

Ballance, Judy	Propulsive Small Expendable Deployer System (ProSEDS)	13
Beabout, Brent L.	Diffraction Optics by Direct Write Electron Beam Lithography	77
Beshears, Dr. Ron	Comparison of Computed Tomography Data to Actual Physical Density Data for Composite Materials	37
Beshears, Dr. Ron	Computed Tomography System Upgrade Provides Improved Imaging Capability	38
Brown, Dr. Andrew M.	Combining Loads From Random and Sine Excitation Using Monte Carlo Techniques	20
Bryan, Don	Infrared Fiber Optic Thermographic Sensor for High Temperature Applications	32
Campbell, Dr. Jonathan	Beamed Energy Research Program for Propulsion and Planetary Defense	114
Clinton, Dr. Raymond G.	Material Robustness Testing and Nondestructive Evaluation Methodology Assessment for Liquid Rocket Engine Composite Nozzles—Phase I Results	45
Coffey, Victoria	Characteristics of Thermal Ions in the Topside Auroral Zone as Observed by TOPAZ3/STICS	89
Cole, Dr. Helen J.	Rapid Prototyping of Diffraction Optics by Excimer Laser Micromachining	63
Costes, Dr. Nicholas C.	Mechanics of Granular Materials Under Very Low Effective Stresses	100
Dabney, Richard	Automated Rendezvous and Capture Technology Description	31
Denniston, Charles L.	Elastic-Plastic Proof Test Philosophy for Metallic Structures	17
Dewberry, Brandon S.	Electrical Impedance Spectrometer Development and Analysis	76
Ding, Jeff	Friction Stir Welding Process Development	39
Edwards, David	Space Environmental Effects on Transparent Polymer Lenses for Inflatable and Rigid Space Structures	49
Eng, Ron	Space-Borne Solar Vector Magnetograph Optical Design	70
Engberg, Robert C.	Interdisciplinary Testing of Inflatable Structures for the Shooting Star Experiment	26
Etheridge, Dr. Edwin C.	Modeling of Viscous Fluid Flow	103
Garcia, Roberto	Unshrouded Impeller Technology Development	23
Hagyard, Dr. Mona J.	Large-Scale Organization of Active Region Magnetic Fields	99
Hall, Phillip	Development of Environmentally Compatible Solid Film Lubricants	35
Hastings, Leon J.	Cryogenic Fluid Management for the Aerospace Industry Technology Program	2

Hastings, Leon J.	Multipurpose Hydrogen Test-Bed Thermal Control Subsystem Testing	6
Hastings, Leon J.	Spray-Bar Zero Gravity Cryogenic Vent System Test	11
Hayes, Benita	Marshall Center a Partner in High-Tech Business Incubator	122
Hediger, Lisa	NASA Computer Imaging Technology Looks Into a Broad Range of Commercial Uses	123
Herren, Kenneth	Determining the Fractal Dimension of an Image Using Wavelet Analysis	58
Herren, Kenneth	Phase Correction in a Semiconductor Amplifier Array Using Fiber Optics	65
Hill, Scott A.	Solar Thermal Upper Stage/Shooting Star Experiment	25
Howard, Ricky	Video Guidance Sensor—Flight Proven	54
Huegele, Vinson B.	Composite Fresnel Lens for Solar Concentration and Alignment	62
Jett, Tim	Effect of Bearing Cleaning on Long-Term Bearing Life	36
Johnson, Les	Electrodynamic Tether Reboost of the <i>International</i> Space Station	115
Johnson, Les	Space Tether Transportation System	119
Jones, Steve	NASA-Designed Knee Brace Turns Rehabilitation Into a Moving Experience	130
Jones, Steve	NASA Technology Helps Zap Mosquitoes Before They Zap You	133
Jones, William D.	Replicated X-Ray Optics Development	80
Kegley, Jeffrey R.	Interdisciplinary Testing of Inflatable Structures for the Shooting Star Experiment	26
Keys, Andrew S.	Modeling Optical Pulse Propagation Using Parallel Processing	74
Koczor, Ron	Superconductor Interactions with Gravity	109
Lassiter, John O.	Interdisciplinary Testing of Inflatable Structures for the Shooting Star Experiment	26
Lawless, Kirby	Automated Measurement of Weld Shrinkage Recovery	41
Lee, Jonathan A.	High-Strength Aluminum Casting Alloy for Automotive Applications	42
Leslie, Dr. Fred W.	Gradient Forming With Magnetic Fluids	95
Lessels, Bob	Space Code Solves Industries' Identity Crisis	125
Lessels, Bob	NASA Deep-Space Communications Technology Now Used at NASCAR Race Tracks	135
McMillan, Vernotto	NASA, USBI Technology Make a Triple Play	134
Martin, Jim	Magnetically Actuated Propellant Orientation	4

McNichol, Randal S.	Signal Conditioning Electronics for Discrete Capacitive Level Sensor Introduction	56
Min, Dr. James B.	Life Prediction of Composite Structures Based on Progressive Damage Analysis	18
Moore, Dr. Ronald L.	Coronal Heating	91
Moore, Dr. Ronald L.	Solar Flares and Coronal Mass Ejections	93
Nabors, William H.	NASA Technology Conserves Power and Generates a Successful New Business	127
Olsen, Carrie D.	Development of Elliptic Orbit Rendezvous Analytical and Operational Techniques	15
Redmon, John W.	Lightweight Nickel Alloy Mirrors for the Next Generation Space Telescope	68
Robertson, Tony	Hot Pressing Yttrium, Copper, and Barium Oxides to Form Bulk-Shaped $\text{YBa}_2\text{Cu}_3\text{O}_{7-x}$ Ceramic Superconductors	50
Robertson, Tony	Pressure Controlled Atomization Process (PCAP) for Permanent Magnet Fabrication	51
Rodgers, Dr. Elizabeth	Hair Cleans Up Hairy Oil Spill Problem	128
Rodgers, Dr. Elizabeth	NASA's Enlightening View on Veins	131
Rupp, Charles	Improving the Safety of Space Tethers	117
Russell, Carolyn	Weld Filler Wire Development for Aluminum Lithium 2195 Alloy	43
Russell, Kevin	Solar X-Ray Imager (SXI) X-Ray Detector Calibration	67
Russell, Kevin	Solar X-Ray Imager Alignment and Focus	72
Schramm, Fred	NASA Spinoff Helps Golfers Get More Spin on the Ball	134
Schunk, R. Gregory	Interdisciplinary Testing of Inflatable Structures for the Shooting Star Experiment	26
Smith, Brett H.	Tooling Foam for Structural Composite Applications	47
Smith, Dr. David D.	Time-Resolved Fluorescence in Crystallizing Protein Solutions	107
Smith, Dr. David D.	Incorporation of Metal Nanoparticles Into Aerogels for Catalysis Applications	97
Smith, Dennis A.	Signal Conditioning Electronics for Discrete Capacitive Level Sensor Introduction	56
Smithers, Dr. Martin E.	Solar X-Ray Imager Alignment and Focus	72
Spann, Dr. James F.	A Laboratory Study of the Interaction of Charged Particles With Electron Beams and Ultraviolet Radiation	84
Stinson, Helen	NASA "Smart Bolts" Likely to Revolutionize Some Industries	124
Stinson, Helen	NASA Sheds New Light on Cancer	129
Stinson, Helen	NASA Funnels Technology to Develop Tornado Warning System	132

Suess, Dr. Steven T.	The Solar Wind in the Inner Heliosphere	105
Swords, Kenneth L.	Signal Conditioning Electronics for Discrete Capacitive Level Sensor Introduction	56
Tinker, Dr. Michael L.	Interdisciplinary Testing of Inflatable Structures for the Shooting Star Experiment	26
Trinh, Huu P.	Injector Technology for Orbital Maneuvering System (OMS) Engine Upgrade	3
Tucker, Stephen	Shooting Star Solar Thermal Propulsion System	9
Vaughn, Jason A.	Laser Induced Impulse on Debris Materials	34
Wang, Ten-See	Multidisciplinary Thermal-Fluid Design Optimization Tool	21
Whorton, Dr. Mark	On-Orbit Controller Tuning for Robust Pointing Control	28
Whorton, Dr. Mark	Microgravity Vibration Control and Civil Applications	29
Whorton, Dr. Mark	Small Vibrations in Space Lead to Earthshaking Technology	126
Wilson, Dr. Robert B.	BATSE Observations of Accreting Pulsars	87
Witherow, William K.	A New Ultra-High Resolution Near-Field Microscope for Observation of Protein Crystal Growth	85
Zimmerman, Frank	Vacuum Plasma Spray Forming of Propulsion Components	44

Index of Key Words

3D reconstruction	38	effective medium theory	100
accretion	89	elastic-plastic fracture mechanics	17
actuator	127	electric motors	127
aerogels	99	electrical impedance spectrometry	77
aggregation	109	electricity	127
alignment	62, 72	electrodynamic tethers	13
aluminum lithium	43	electron beam lithography	78
aluminum-lithium alloy 2195	39	elliptic orbit	15
anisotropy	109	environment	49, 133, 134
automated rendezvous	55	environmentally compatible	35
automation	41	external tank	39
automotive	136	FAD's	17
autonomous docking	32	failure criteria	19
bar codes	126, 136	failure mode	19
bearings	36	fast Fourier transform	74
bicentrifugal coaxial swirler	3	fasteners	124
blood samples	131	FDNS	21
Boosterlube™	35	FFT	74
business incubator	122	fiber optics	65
calibration	67	filler wire	43
cancer	124	fluid dynamics	97
capacitive sensors	57	fluorescence	88, 109, 110
carbon-carbon	45	focus	72
catalysis	99	fractal dimension	60
ceramic matrix	47	fresnel	62
CFD	21	friction stir welding	39
cleaners	36	gamma ray	89
coatings application	134	genetic algorithms	15
composite materials	38	golf	134
composites	18	granular materials	102
computed tomography	37, 38, 123	gravity shielding	111
controller tuning	28	grease	36
core magnetic field	94	grid generation	23
coronal heating	93	ground vibrations	132
coronal mass	95	harmonic	20
cryogenic fluid management	2	high temperature superconductors	112
cryogenic insulation	6	high vacuum	36
damping	132	hydrocarbon engine emissions	42
data matrix	135	hypereutectic aluminum-silicon alloy	42
debris	34	image processing	59
density profile measurements	38	impact damage	19
diffractive optics	78	impeller	23
digital data	126, 136	incubator	127
diode lasers	67	inflatable structure	25, 26
docking	31	infrared thermography	32
dynamic response	20	interferometers	66
earthquake engineering	29	interplanetary dust	86
earthquakes	126	inventory control	136

ion heating	91
ionosphere	91
J-Integral	17
J-R curves	17
jobs	122
KC-135	105
knee brace	125
laser	34, 114, 136
LED's	129
light emitting diodes	129
lightweight optics	69
magnetic activity	93
magnetic explosion	95
magnetic helicity	101
magnetohydrodynamics	107
MARCORE™	47
MasPar	74
material degradation	19
medical	124, 129, 130, 131
microgravity	97, 102
microlens	78
microscopy	87
mirrors	68
mobile	123
momentum exchange	121
Monte Carlo	20
mosquitoes	133
multilayer insulation	6
NASCAR	135
NDE	46
neural networks	32
neutron star	89
nondestructive evaluation	45
nondestructive testing	128
oil spill cleanup	128
oils	37
optical design	71
optics	80
orbital debris removal	116
orientation	4
ozone depleting chemicals	36
parallel	21
parallel processing	74
parallel resonant circuit	58
parameter identification	77
parts identification	136
Perma-Slik RMG™	35
permanent magnets	51

phase corrections	65
phase modulators	66
pintle injectors	3
piston	42
planishing	41
plasma	91
platelet technology	4
plating	81
pointing control	28
polyimide	64
polymer	49
power beaming	65
pressure controlled atomization	51
proof test	17
propellant	4
propulsion	116
prosthetics	130
protein	109, 110
protein crystal growth	87
protein fluorescence	109
pulsars	89
pulse propagation	74
racing	136
random	20
reboost	117
rendezvous	15, 31
resolution	68
retractable pin-tool	40
rhodium	44
road resurfacing	134
robust control	29
roofing	136
seismic	132
sensors	41, 54
shipyard	135
Shooting Star Experiment	9, 26
Silastic-E	47
silver nanoparticles	99
SINDA	21
SOHO	107
solar concentrators	62
solar flares	95
solar magnetic fields	102
solar thermal propulsion	9
solar thermal propulsion engines	44
solar thermal upper stage	25
solar vector magnetograph	70
solar wind	107

solid film lubricants	35
space environment	49
space propulsion systems	13
Space Station	117
space telescopes	69
space transportation	6
splash plate injector	3
stability	103
stage loading	23
stray capacitance	57
stress calculations	19
Sun	107
superconductors	50
SXI	67, 72
symbology	126, 136
synthetic aperture	65
system identification	28
tapered fiber probe	87
telescope	68, 72
tether	117, 119, 121
thermal deflections	27
thermal spray	44
thin layers	51
thin-film	124
three-dimensional magnetic field	96
tooling foam	47
tooling technology applications	47
tornado	132
traxial tests	102
tungsten	44
turbopump	23
Ulysses	107
undercooling	105
vector magnetograph	101
vibration isolation	30
video guidance sensor	54
viscosity	105
wavelets	60
welding	41, 43
x ray	67, 72, 81
YBCO	51
zero gravity pressure control	11

